



The
University
Of
Sheffield.

Department
Of
Mechanical
Engineering

**Non-Conventional Pollutant Species Measurement and Prediction
from a Gas Turbine**

By

Emamode Akpofure Ubogu

Supervisors

Dr Bhupendra Khandelwal

Dr Simon Blakey

Department of Mechanical Engineering

A thesis submitted to the Department of Mechanical Engineering
in partial fulfilment of the requirements for the degree of

"Doctorate of Philosophy"

Department of Mechanical Engineering

Sheffield, United Kingdom

March, 2016

© Emamode A Ubogu 2016

UNIVERSITY OF SHEFFIELD
RESEARCH AND INNOVATION SERVICES

The undersigned certify that they have read, and recommend to Research and Innovation Services for acceptance, a thesis entitled “*Non-Conventional Pollutant Species Measurement and Prediction from a Gas Turbine*” submitted by Emamode Akpofure Ubogu in partial fulfilment of the requirements of the degree of “Doctorate of Philosophy”.

Supervisor, Bhupendra Khandelwal, Mechanical Engineering

Supervisor, Simon Blakely, Mechanical Engineering

11/03/2016

Date

Abstract

There is increased interest in particulate matter (PM) measurement – driven by the contribution to air quality degradation and potential to cause harm to both health and environment. Despite technological advances in the PM emissions measurement instrumentation, the gravimetric method widely acknowledged to be prone to uncertainties is the regulatory measure for ground based gas turbine PM emissions. Thus, the focus of this research was to develop correlations between established as well as newly developed particle instruments and a reference gravimetric protocol for particle emissions from a gas turbine.

The following instruments; Atrium extractive Laser Induced Incandescence (LII300), Cambustion differential mobility spectrometer (DMS500), CPMA, DMA, CPC were selected to develop correlations with the filterable particulate matter fraction as defined by US EPA regulatory method 5I. In addition, a Fourier Transform Infrared (FTIR) and flame ionisation detection (FID) were selected to attempt correlations with the condensable particulate matter fraction as measured using the US EPA regulatory method 202.

Firstly experiments were performed using surrogate fuels on a small scale premix burner and alternative fuels to investigate the impact of aromatic on the physical characteristics of PM emissions. The results showed that type of aromatic present in the fuel impacts on the emitted PM mass concentration and physical characteristics. This facilitated the selection of fuels needed to generate a range of PM emission mass concentration from a single test that best represent PM emissions from gas turbine in the industry.

Particulate emissions were sampled from an aircraft auxiliary power unit and simultaneously distributed to the instrument from a single extraction probe. The result shows a near 1:1 correlation between the filterable PM fractions of regulatory gravimetric method and the DMS500 mass concentration measurement. Although there was no correlation between the condensable PM fraction and FTIR, the CPM organic fraction shows good correlation at certain engine power condition with the FID instrument.

Acknowledgement

I wish to express my sincere appreciation to my supervisors, Late Professor Chris Wilson and Prof Yang Zang, Dr. Simon Blakey and Dr Bhupendra Khandelwal for their patience, guidance, and support through my time at the University of Sheffield. I appreciate the opportunities they provided for me to be involved in a number of frontier research projects and international academic conferences. I have learned a lot from them both academically and personally. I also acknowledge the support of the staff of Rolls Royce Canada (Now Siemens Canada) for their support - Patrick Batchelor, Gilles Bourque, Louis-Marie Kamoso and Kevin Cuddihy.

I would like to acknowledge the Low Carbon Combustion Centre (LCCC) team; Tim Haycock – Facility Manager; Roy Swapneel – Research Assistant for his support with the experiments; technicians Del Delorenzi, Sam Chapman, Andy Hemstock and Tony Swift for their help with the rig setup and modifications and Dave Dustan for help with fuel supply.

I extend my profound appreciation to my lovely wife, Blessing Tosin Ubogu and my son, Mitchell Emeoghene Ubogu. I would not be able complete my PhD study without her support and understanding all these years in Sheffield. I also would like to thank my parents, Sir and Lady J E Ubogu, for their support as always. My sincere thanks to my brother and his spouse Barr Enifome Ubogu and Vuslat Uren, my sisters and their spouses, Dr and Mrs Onohwakpo; Mr and Mrs Oduma; Mr and Mrs Ejakpovi; and Mr and Mrs Oruah. Special thanks to their children; the Onohwakpo's - Faith, Ese and Riwo; Dora Ubogu; the Oduma's - Tejiri, Uruemu, Okeoghene, Oghenewegba; Segburuemu Ejakpovi; the Oruahs – Nathan, Ethan and Evan. My cousin Oghogho Ubogu.

Thank you to the best father and mother in-law; Mr and Mrs Richard Ofolu and their children Faith and Miracle. My friend and his lovely wife Mr and Mrs Jude Akporubere; Mr Edwin Owhofaria and his wife; Dr Ife Fayajuola and his girlfriend Rebecca Hardy, Mr and Mrs Anthony Anju. To my house mates; Oku Nyong, David Akindele, Ayotunde Ojo, Benjamin Oluwadare, Ebyte Bejor, Mayowa Famuyiwa, Godstime Onwuemene and Dr Stephen Temitope. Thanks to members of Light House Christian International – Rev and Lady Pastor D Adagbe, Mr and Mrs Krako, Rev Ebenezer Benti, Reginald Cole and Natasha.

Table of Contents

Acknowledgement.....	iii
Table of Contents	v
Table of Figures	xiii
List of Tables.....	xx
Nomenclature	xxiv
List of Publications.....	xxviii
1 Background Information.....	1
1.1 PM Health Effect.....	2
1.2 Environmental impact	4
1.3 Regulatory Drivers	4
1.4 Overview of Particulate Emissions	7
1.4.1 Non-volatile PM	7
1.4.2 Volatile PM	8
1.4.3 Primary and Secondary PM	8
1.4.4 Particle size.....	9
1.4.5 Particle Size Distribution (PSD).....	11
1.5 Research Objectives	12
1.6 Thesis Outline	12
2 Gas Turbine PM Properties and Aerosol Measurement Instruments	17
2.1 Formation of PM in a Gas Turbine	17
2.1.1 Formation of Particulate from Fuel Molecule Reaction.....	18
2.1.1.1 Impact of Gas Turbine Combustor Design	19
2.1.1.2 Fuel Characteristics.....	20
2.1.2 PM Emitted at the Exhaust Exit and Further Reaction.....	21
2.2 Gas Turbine PM Physical Characteristics	22
2.3 Land Based Gas Turbine PM Emission Measurement Reference Methods	25
2.3.1 Issues with the Gravimetric Protocols for Gas Turbine PM Measurement	28

2.3.1.1	Filterable PM	29
2.3.1.2	Condensable PM.....	31
2.3.1.3	Measurement Time	33
2.4	Requirements for New Gas turbine PM Measurement Instruments	33
2.4.1	Correlation to Gravimetric Method.....	33
2.4.2	Response Time	34
2.4.3	Lower Detection Limit (LDL) and Minimum Upper Range (MUR).....	34
2.4.4	Particle Cut-off Size.....	35
2.4.5	Traceable Measurement	35
2.5	Fast PM Instruments for PM Emissions	36
2.5.1	Automated Filter Based Instruments Measuring Mass Concentration.....	37
2.5.2	Particle size resolved Instruments.....	38
2.5.3	Chemical Speciation Instruments	43
2.5.3.1	Carbon Speciation instruments.....	43
2.5.3.1.1	Carbon Burn-off Analysers	43
2.5.3.1.2	Filter-Based Elemental Carbon Analysers	44
2.5.3.1.3	Non-Filter Based Elemental Carbon Analysers	46
2.5.3.2	Continuous Multi-Component Analyser	47
2.6	Research Hypotheses	49
2.7	Sampling System for Instrument Correlations	50
2.7.1	Extraction of Representative Sample.....	50
2.7.1.1	Dealing With Exhaust Sample Conditions and Instrument Requirements	51
2.8	Real-time Instrument Correlation with Gravimetric Reference Methods	53
2.8.1	LII Correlation with Filterable Fraction of Gravimetric Measurement.....	53
2.8.2	PSD Derived Mass Concentration Correlation with Filterable Fraction of Gravimetric Measurement	54
2.8.2.1	PM Density.....	55
2.8.3	PSD Mass Concentration Using Experimentally Derived Density.....	57
2.8.4	Smoke Number Comparison with Soot Mass Correlation.....	58
2.9	Recommended Instruments for PM Mass Correlation	60

2.10	Summary of Knowledge Gaps	61
3	Design of Experimental Set-up.....	65
3.1	Instrumentation.....	65
3.1.1	US EPA Method 5 and Method 202 Sampling System.....	66
3.1.1.1	Modular Sample Case Components	67
3.1.1.2	Source Sampler Console	69
3.1.1.3	Calibration.....	70
3.1.2	Laser Induced Incandescence	71
3.1.3	NIOSH 5040 SETUP	72
3.1.4	DMS500	73
3.1.5	SAE Smoke Number	75
3.1.6	Fourier Transform Infrared (FTIR)	76
3.1.7	Gas Analysers	77
3.1.7.1	Calibration.....	79
3.2	Exhaust Gas Distribution System.....	83
3.2.1	Description of the Sampling System	83
3.2.2	Sampling Probe	87
3.2.3	Heated Sample Lines	88
3.2.4	Splitters	88
3.2.5	Cyclones	89
3.2.6	Nafion Dryer.....	90
3.3	The Gas turbine Test Engine	90
3.4	Summary	91
4	Preparatory Tests	93
4.1	Engine Performance and Certification Gas Emissions	93
4.1.1	Exhaust Sample Transfer Line	94
4.1.2	Data logging and Processing	95
4.1.2.1	Engine Performance	95
4.1.2.2	Gas Analysers	96
4.1.3	The Test Fuels	97
4.1.4	Results	97
4.1.4.1	APU Performance	97
4.1.4.2	Gaseous Emissions.....	98
4.1.4.3	Combustion Efficiency	100

4.2	Traverse Test	101
4.2.1	Traverse Test Results	102
4.3	Test Engine PM Emission Concentration Correlation with Fuel Aromatic Content	104
4.3.1	Test Fuels	105
4.3.2	Engine Operating Condition	106
4.3.3	Sampling System and Instrumentation	106
4.3.4	Results	107
4.3.5	Discussion	109
4.4	Characteristics of Particulate Emission from Different Aromatic Species	110
4.4.1	Experimental Details	110
4.4.1.1	The Premix Burner	110
4.4.1.2	Test Fuels	112
4.4.1.3	Burner Settings and Sampling System	113
4.4.2	Results	114
4.4.2.1	Soot mass concentration	114
4.4.2.2	Soot particle size	116
4.4.3	Discussion	117
4.5	The APU PM Size Verification	118
4.5.1	Experimental Details	118
4.5.1.1	Instrumentation	118
4.5.1.2	Sampling System	119
4.5.1.3	Experiment Procedure	120
4.5.1.4	Results and Discussion	120
4.6	Chapter Summary	123
5	Test Matrix, Fuel Composition and Density Functions of the Particle Emissions from the APU Burning the Test Fuels	125
5.1	Test Matrix	125
5.2	Fuel Composition	126
5.3	Effective Density Functions of the Particle Emissions from the APU Burning the Intended Test Fuels	126
5.3.1	Instrumentation	127
5.3.1.1	Differential Mobility Analyser (DMA)	127
5.3.1.2	Centrifugal Particle Mass Analyser (CPMA)	128

5.3.1.3	Condensation Particle Counter (CPC)	128
5.3.2	Sample System	129
5.3.2.1	Experiment Procedure	130
5.3.2.2	Test Fuels and Engine Power Settings	131
5.3.3	Results and Discussion	131
5.4	Chapter Summary	134
6	Experimental Procedure	135
6.1	Equipment Configuration	135
6.1.1	Laser-Induced Incandescence	135
6.1.2	Fourier Transform Infrared Spectrometer	136
6.1.3	DMS500	136
6.1.4	Gravimetric Sample Train	137
6.1.5	Smoke Meter	137
6.1.6	NIOSH 5040	137
6.2	Pre-test Procedures	138
6.2.1	Sampling Media Preparation	138
6.2.1.1	Preparation of Gravimetric Sampling Train	138
6.2.1.2	Preparation of Smoke Meter and NIOSH 5040 Filters	139
6.2.2	Equipment start-up	139
6.2.3	Sample Acquisition	140
6.2.3.1	Sample Acquisition Duration	141
6.3	Sample Recovery, Preservation and Transportation	143
6.3.1	Method 202 Liquid Content Recovery	143
6.3.2	Transportation	144
6.4	Post-Test Laboratory Procedures	144
6.4.1	PM Gravimetric Analysis	144
6.4.2	Analysis of Organic and Elemental Carbon	144
6.4.3	Smoke Number	145
6.5	Data Post Processing	145
6.5.1	Method 5I and Method 202	146
6.5.2	NIOSH 5040	147
6.5.3	DMS500 Data Analysis	148
6.5.4	Laser-Induced Incandescence Measurements	148
6.5.5	Fourier Transform Infrared Spectrometry	148

6.5.6	Smoke Number	149
6.6	Calculation of Data Quality Indicator.....	149
6.7	Chapter Summary	149
7	Results and Discussions	151
7.1	Summary of Tests Completed	151
7.2	Result	152
7.2.1	Method 5I.....	152
7.2.2	Method 202	153
7.2.3	Laser-Induced Incandescence	154
7.2.4	NIOSH 5040 EC/OC.....	154
7.2.5	Differential Mobility Spectrometer DMS500	155
7.2.6	Smoke Meter	159
7.2.7	FTIR.....	159
7.3	Repeatability of Engine Operating Conditions and Corresponding Emissions	159
7.3.1	Engine operating point check.....	159
7.3.2	Variability of Engine Operating Parameters and Gaseous Emissions	161
7.3.3	PM Instrument Repeatability of the Engine PM Emissions	162
7.4	Validity of the PM Instruments Measurements	164
7.5	Correlation between FPM Instruments	166
7.5.1	NIOSH 5040 Comparison.....	166
7.5.1.1	Discussion - NIOSH 5040 Comparison	169
7.5.2	DMS500 Comparisons	169
7.5.2.1	Unit Density Derived Mass Concentration without Nafion Dryer in Place	169
7.5.2.2	DMA/CPMA/CPC Density Derived Mass Concentration without Nafion Dryer in Place.....	171
7.5.3	DMS500 with Nafion Dryer	173
7.5.4	Comparisons between the Various DMS500 Mass Concentration.....	175
7.6	Smoke Number Comparisons	178
7.7	Condensable PM Data	180
7.7.1	Method 202 Data.....	180
7.7.2	FTIR and FID Data	182
7.7.3	Correlation between Method 202, FTIR and FID.....	183

7.8 Chapter Summary.....	188
8 Conclusions and Future Work	189
8.1 Contribution to Knowledge	189
8.2 Future Work	192
9 References.....	193
Appendix A: Analysers Interference analysis.....	209
Appendix B: Full details of Engine Gaseous Emission concentration	210
Appendix C: Speciation Analysis of Main Hydrocarbon Types	212
Appendix D: Method 202 Sample Processing Flow Chart	213

Table of Figures

Figure 1-1:	Overview of the complex interactions among air pollutants and effects of exposures on cardiovascular health in a multi-pollutant context [13].....	3
Figure 1-2:	Secondary particle formation pathway [7]	9
Figure 1-3:	Idealised exhaust particle number and mass weighted size distributions [30, 31]	10
Figure 2-1:	Basic schematic of soot formation for combustion of fuel [34]	18
Figure 2-2:	Main Components of a Conventional Combustor [36]	19
Figure 2-3:	Tendency to soot (TSI) for hydrocarbons [37]	20
Figure 2-4:	Photomicrographs of soot particles extracted from exhaust of an aircraft engine at different power conditions from different fuels[42]	23
Figure 2-5:	Particle Size Distribution for and aircraft Auxiliary Power Unit (APU) Burning : JP8 Fuel [43].....	24
Figure 2-6:	Schematic of Method 5I [25].....	26
Figure 2-7:	Schematic of EPA Method 202 PM Sampling Train [28].....	27
Figure 2-8:	Uncertainties' of stack test data (EPA Methods 201/201A and 202) for combustion turbines and engines [40]	28
Figure 2-9:	A photograph to demonstrate poor filter handling	31
Figure 2-10:	Schematic of differential mobility analyser (DMA) and an impactor [65, 66]	39
Figure 2-11:	Schematic of light scattering technique [71]	42
Figure 2-12:	A schematic diagram of the commercially available Aerodyne Aerosol Time of Flight Mass Spectrometer (ATOFMS) [86].....	48
Figure 2-13:	Chart Showing How Correlations between Real-Time Instrument Gravimetric Methods were studied	49
Figure 2-14:	A Schematic of a Nafion Dryer [90]	52

Figure 2-15: Comparison of SMPS to Gravimetric Mass Concentration [92]	54
Figure 2-16: Literature correlations relating soot mass and smoke numbers [125]	59
Figure 3-1: Picture of Gravimetric Sampling Kit	67
Figure 3-2: Picture of the method 5I filter holder	68
Figure 3-3: Picture of Method 202 components and water content of the US EPA gravimetric method	69
Figure 3-4: Model XC-522 Source Sampler Console Front Panel [132]	70
Figure 3-5: The experimental set-up for an LII device [133]	71
Figure 3-6: Picture of the NIOSH 5040 Filter Paper Holder	73
Figure 3-7: Schematic of a DMS500 [101]	74
Figure 3-8: Smoke measurement by SAE/ARP 1179D [81, 135]	76
Figure 3-9: Schematic of A Fourier Transform Infrared [136]	77
Figure 3-10: Zero and span calibration	80
Figure 3-11: Schematic of the experimental setup	84
Figure 3-12: USA EPA Method 5I Probe	87
Figure 3-13: Photograph of 3/8" 2 way splitter and manufactured splitters [45]	89
Figure 3-14: Photograph of Mexa Labs specially made to order PM1.0 sharp cut cyclone [45]	89
Figure 3-15: PD-Series Nafion dryer	90
Figure 3-16: Schematic of the HoneyWell GTCP85 series gas turbine [141]	91
Figure 4-1: Picture of the test engine showing the bleed and air inlet	94
Figure 4-2: Picture of the exhaust gas extraction probe	95
Figure 4-3: Schematic of the data logging system for APU performance monitoring	96

Figure 4-4:	LCCC Gaseous Emission Analysers, Data Acquisition Snapshot	97
Figure 4-5:	APU engine performance	98
Figure 4-6:	THC, CO and NO _x Emission Indices and NO/NO _x Ratio	99
Figure 4-7:	Combustion efficiency of test fuels versus EGT	101
Figure 4-8:	Traverse probe positions.....	102
Figure 4-9:	Total number concentration at traversed points	103
Figure 4-10:	Total mass concentration at traversed points.....	104
Figure 4-11:	DMS 500 heated sample block.....	106
Figure 4-12:	Particle number concentration for fuels 2 - 7 and Jet A-1.....	107
Figure 4-13:	SAE smoke number for fuels 2-7 and Jet A-1.....	108
Figure 4-14:	Geometric mean diameter for fuels 2-7 and Jet A-1	109
Figure 4-15:	Schematic of Premixed Burner Assembly – 1, burner globe with side arm; 2, flame jet; 3, gas mixing baffle; 4, vaporisation chamber; 5, secondary air entrainment port; 6, fuel injector; air via ‘A’, test fuel via ‘B’, 7, test fuel capillary [148]	111
Figure 4-16:	Gas chromatography and mass spectroscopy comparing diesel and the multicomponent surrogate fuel [150].	113
Figure 4-17:	The premixed burner schematic [151].....	114
Figure 4-18:	Soot mass concentration of the 100% surrogate fuel and Jet A-1	115
Figure 4-19:	Soot mass concentrations emitted from blends of the surrogate fuel with aromatic blends	115
Figure 4-20:	Mean primary particle diameter emitted by blends of the surrogate fuel and aromatic specie	116
Figure 4-21:	Laser measuring chamber of the optical particle counter.....	119
Figure 4-22:	The design for the OPC sampling system	120

Figure 4-23:	Particle number distribution for NL engine power setting burning diesel.....	121
Figure 4-24:	Particle number distribution for ECS engine power setting burning diesel.....	121
Figure 4-25:	Particle number distribution for MES engine power setting burning diesel 50.5	122
Figure 4-26:	Cumulative Mass undersize plots for OPC data	122
Figure 5-1:	Schematic of A Differential Mobility Analyser [45]	127
Figure 5-2:	Schematic of A Centrifugal Particle Mass Analyser [106].....	128
Figure 5-3:	Schematic of a Condensation Particle Counter (CPC)	129
Figure 5-4:	Schematic of Sampling System	130
Figure 5-5:	Power law trend lines of the effective densities and the corresponding mobility diameter.	132
Figure 6-1:	Illustration of a thermogram for filter sample containing organic carbon (OC), carbonate carbon (CC), and elemental carbon (EC) [59].....	145
Figure 7-1:	Examples of Method 5I filter samples. Picture A – engine run with LACF fuel at MES power setting and picture B – engine run with diesel fuel at MES power setting.	153
Figure 7-2:	Examples of Method 202 filter samples. Picture A – engine run with LACF fuel at MES power setting and picture B – engine run with diesel fuel at MES power setting.....	153
Figure 7-3:	LII mass concentration measurement for Test point 15.....	154
Figure 7-4:	Example of sample deposits for NIOSH 5040. Picture A – engine run with diesel fuel at MES power setting and picture B – engine run with LACF fuel at MES power setting.....	154
Figure 7-5:	DMS500 three dimensional animation spectrum.....	155
Figure 7-6:	Showing the DMS500 size distribution for the engine power setting for Jet A-1.....	155

Figure 7-7:	DMS500 size distribution of the test fuels at the MES engine condition for the three test fuels	156
Figure 7-8:	Un-normalised DMS500 size distribution of the test fuels at the MES engine condition for the three test fuels	157
Figure 7-9:	Geometric mean particle diameter.....	158
Figure 7-10:	Geometric standard deviation.....	158
Figure 7-11:	Example of sample deposits for Smoke Meter filter papers. Picture A – engine run with LACF fuel (Test 4) and picture B – engine run with diesel fuel (Test 17).	159
Figure 7-12:	Correlation between fuel consumption and the engine exhaust gas temperature.	161
Figure 7-13:	Relative standard deviation of the engine parameters and gaseous emissions for Jet A-1	162
Figure 7-14:	Relative standard deviation of the engine parameters and gaseous emissions for diesel.....	162
Figure 7-15:	Relative standard deviation of the engine parameters / gaseous emissions for Jet A-1	163
Figure 7-16:	Relative standard deviation of the engine parameters / gaseous emissions for diesel.....	164
Figure 7-17:	Absolute values of total mass and total carbon concentration measured using method 5I and NIOSH 5040 respectively	165
Figure 7-18:	Absolute values of elemental carbon concentration measured using NIOSH 5040 and LII300.	165
Figure 7-19:	Correlation between LII300 and NIOSH 5040 EC	167
Figure 7-20:	Correlation between Method 5I and NIOSH 5040 TC	168
Figure 7-21:	Correlation between Method 5I and NIOSH 5040 TC showing the fuel data separately.....	168
Figure 7-22:	Correlation between DMS500 mass concentration [No Nafion Dryer (Unit Density)] and Method 5I.....	170
Figure 7-23:	Correlation between NIOSH 5040 TC and DMS500 mass concentration [No Nafion Dryer (Unit Density)]	171

Figure 7-24: Correlation between DMS500 mass concentration [No Nafion Dryer (DMA/CPMA/CPC Density)] and Method 5I	172
Figure 7-25: Correlation between DMS500 mass concentration [No Nafion Dryer (DMA/CPMA/CPC Density)] and NIOSH 5040 TC.....	173
Figure 7-26: Correlation between DMS500 mass concentration [Nafion Dryer (DMA/CPMA/CPC Density)] and Method 5I.....	174
Figure 7-27: Correlation between NIOSH 5040 TC and DMS500 mass concentration [Nafion Dryer (DMA/CPMA/CPC Density)]	175
Figure 7-28: DMS 500 mass concentrations without Nafion dryer, derived from experimental density function and unit density	176
Figure 7-29: DMS 500 mass concentrations derived from experimental density function with and without Nafion dryer in place	176
Figure 7-30: Particle size distribution of LACF at MES engine power setting with and without Nafion dryer	177
Figure 7-31: Black carbon mass concentration versus SAE Smoke number, comparing literature correlations with the data recorded in this study	179
Figure 7-32: Method 202 data for Jet A-1 and diesel at the NL, ECS and MES gas turbine engine power settings.	181
Figure 7-33: Method 202 data for the Van engine test at idle condition	182
Figure 7-34: FTIR and FID THC emissions	183
Figure 7-35: Correlation between Method 202 inorganic mass concentration and FTIR inorganic gas data	184
Figure 7-36: Correlation between Method 202 organic mass concentration and FTIR THC concentration.....	185
Figure 7-37: Correlation between Method 202 organic mass concentration and FID THC concentration.....	186
Figure 7-38: Correlation between Method 202 organic mass concentration and FID organic gas emission for 3 engine power settings	187

List of Tables

Table 1-1 Summary Table of Air Quality Requirements [17]5

Table 2-1 Stack Sampling Gravimetric Methods25

Table 2-2	A summary of factors affecting the reliability of filter weighing as the basis for determining PM [50].....	30
Table 2-3	Summary of Fast Particulate Measurement Instrument [7, 58].....	36
Table 2-4:	Summary of previous work on PM instrument correlation and knowledge gap	62
Table 2-5:	Summary of Previous Work on Impact of Aromatics on Soot Characteristics	64
Table 3-1	PM Instrumentation	65
Table 3-2	Gaseous Emission Analysers.....	78
Table 3-3:	Calibration gases	80
Table 3-4	Analyser calibration range and full scale error.....	82
Table 4-1:	Nominal Fuel Composition	97
Table 4-2:	Selected specification of the test fuels.....	105
Table 4-3	Properties of Aromatics used in Experiments	113
Table 5-1	Experimental test points	125
Table 5-2	Selected Fuel Properties	126
Table 5-3	Nominal APU Operating Conditions.....	131
Table 5-4	Results of effective densities of the same particle sizes from diesel and LACF	133
Table 5-5	Power law functions for all the test points including the overall functions for the test fuels at NL and the overall function for Jet A-1 at NL and BL.	133
Table 6-1	Test duration for four sample concentration levels	142
Table 6-2	Sampling times for a flow rate of 50lpm across the gravimetric and EC/OC filters Error! Bookmark not defined.	
Table 7-1	Available Data	152
Table 7-2:	Average APU parameters	160

Table 7-3:	Multiple linear regression analysis of the relation between NIOSH5040 Elemental Carbon and LII mass concentrations.	166
Table 7-4:	Multiple linear regression analysis of the relation between NIOSH5040 Total Carbon and Method 5I mass concentrations.	167
Table 7-5:	Multiple linear regression analysis of the relation between DMS500 mass concentration [No Nafion Dryer (Unit Density)] and Method 5I mass concentrations.....	170
Table 7-6:	Multiple linear regression analysis of the relation between NIOSH 5040 TC and DMS500 mass concentration [No Nafion Dryer (Unit Density)] mass concentrations.	170
Table 7-7:	Multiple linear regression analysis of the relation between DMS500 mass concentration [No Nafion Dryer (DMA/CPMA/CPC Density)] and Method 5I mass concentrations.	172
Table 7-8:	Multiple linear regression analysis of the relation between DMS500 mass concentration [No Nafion Dryer (DMA/CPMA/CPC Density)] and NIOSH 5040 TC mass concentrations.	172
Table 7-9:	Multiple linear regression analysis of the relation between DMS500 mass concentration [Nafion Dryer (DMA/CPMA/CPC Density)] and Method 5I mass concentrations.	174
Table 7-10:	Multiple linear regression analysis of the relation between NIOSH 5040 TC and DMS500 mass concentration [Nafion Dryer (DMA/CPMA/CPC Density)] mass concentrations.	174
Table 7-11:	Multiple linear regression analysis of the relation between Method 202 inorganic mass concentration and FTIR inorganic concentrations.	183
Table 7-12:	Multiple linear regression analysis of the relation between Method 202 organic mass concentration and FTIR THC concentrations.	184
Table 7-13:	Multiple linear regression analysis of the relation between Method 202 organic mass concentration and FID THC concentration.	186

Table 7-14: Regression statistics of the relation between Method 202 organic mass concentration and FID organic gas emission for 3 engine power settings.....	187
---	-----

Nomenclature

AAFEX	Alternative Aviation Fuel Experiment
ACS	Acute Coronary Syndrome
AMS	Aerosol Mass spectrometer
APMA	Aerosol Particle Mass Analyser

APS	Aerosol Particle Sizer
APU	Auxiliary Power Unit
AQHI	Air Quality Health Index
ATOFMS	Aerodyne Aerosol Time of Flight Mass Spectrometer
BACT	Best Available Control Technology
BAT	Best available techniques
BC	Black Carbon
BSI	British Standards Institution
C Fraction	Carbon Fraction
CEMS	Continuous emission monitoring systems
COPD	Chronic obstructive pulmonary disease
CPC	Condensation Particle Counter
CPM	Condensable Particulate Matter
CPMA	Centrifugal Particle Mass Analyser
CV	Cardiovascular
DGM	Dry Gas Meter
DMA	Differential Mobility Analyser
DMM	Dekati Mass Monitor
EC	Elemental Carbon
ECS	Environmental Cooling System
EEPS	Engine Exhaust Particle Sizer
EGT	Exhaust Gas Temperature
EHS	Environmental, Health, and Safety
ELPI	Electrical Low Pressure Impactor
FAA	Federal Aviation Administration
FAPES	Fast Aerosol Particle Emission Sizer
FID	Flame Ionisation Detection
FOA3	First Order Approximation version 3
FPM	Filterable Particulate Matter
FTIR	Fourier Transform Infrared
GDI	Gasoline Direct Injection
GMD	Geometric Mean Diameter
GSD	Geometric Standard Deviation
GtL	Gas to Liquid
HC	Hydrocarbon
HEFA	Hydrogenated Esters and Fatty Acids
HES	Hot End Simulator
HT-ELPI	High Temperature Electrical Low Pressure Impactor
ICAO	International Civil Aviation Organisation
IED	Industrial Emissions Directive
LACF	Low Aromatic Content Fuel
LAER	Lowest Achievable Emission Rate
LCCC	Low Carbon Combustion Centre
LCPD	Large Combustion Plant Directive
LHV	Lower Heating Value
LII	Laser-Induced Incandescence
LDL	Lower Detection Limit
LTO	Landing and Take-off
M.W	Molecular Weight

MAAP	Multi-angle absorption photometry
MEL	Mobile emission laboratory
MES	Main Engine Start
MFC	Mass Flow Controller
MSS	Micro Soot Sensor
MUR	Minimum Upper Range
NAAQS	National Ambient Air Quality Standard
NDIR	Non-dispersive infrared
NIOSH	National Institute for Occupational Safety and Health
NL	No Load
NPL	National Physics Laboratory
NSCR	Non-selective catalytic reduction
NSR	New source review
OC	Organic Carbon
OPC	Optical Particle Counter
PAT	Performance Acceptance Tests
PM	Particle Matter
PSD	Particle Size Distribution
PSD	Prevention of Significant Deterioration
PSL	Polystyrene Latex
RPM	Revolution per Minute
RSD	Relative Standard Deviation
SCR	Selective Catalytic Reduction
SMPS	Scanning Mobility Particle Sizer
SN	Smoke Number
SN'	Individual Smoke Number
SPK	Synthesized Paraffinic Kerosene
Stk	Stokes number
SVOC	Semi volatile organic compounds
TC	Total Carbon
TEM	Transmission Electron Microscope
TEOM	Tapered Element Oscillating Microbalance
THC	Total Hydro Carbon
TOF-AMS	Time-of-Flight Aerosol Mass Spectrometer
TSI	Threshold Sooting Index
TSP	Total Suspended Particulate
US EPA	United States Environmental Protection Agency (EPA)
WHO	World Health Organisation
YDI	Yield Sooting Index

Chemical Abbreviations

CO	Carbon monoxide;
CO ₂	Carbon dioxide
H ₂ O	Vapour/Water
H ₂ SO ₄	Sulphuric acid
NaCl	Sodium chloride

NH_4HSO_4	Ammonium bisulphate
NH_4NO_3	Ammonium nitrate
NO_x	Oxides of nitrogen
O_3	Ozone
SO_2	Sulphur dioxide
SO_3	Sulphur trioxide
SO_x	Oxides of sulphur

List of Publications

- B. Khandelwal, E. Ubogu, M. Akram, S. Blakey, and C. W. Wilson, "Experimental analysis on emission production and performance of stressed 100% SPK, stressed Fully Formulated Synthetic Jet Fuel and Jet A-1 in a small gas turbine engine," in *Proceedings of the 11th International Energy Conversion Engineering Conference, San Jose, CA, USA, 2013*, pp. 14-17.

In Preparation

- E.A. Ubogu, B. Khandelwal and S. Roy, “Effective Density and Fractal Dimensions of Gas Turbine Particulate Matter Emissions From Different Fuels,”(*in prep*), 2016
- E.A. Ubogu, C. Qian and B. Khandelwal, “Investigation of the Effects of Aromatic on Seal Swell against Black Carbon Emission Physical Characteristics,”(*in prep*), 2016
- E.A. Ubogu, B. Khandelwal, “An Aircraft Auxiliary Power Unit Smoke Number Correlation with Black Carbon Mass Concentration,”(*in prep*), 2016
- E.A. Ubogu, B. Khandelwal, “Relationship between Aromatic Volume Contents and Particulate Emission Characteristics of Novel Fuel Blends Compared to Approved Jet Fuels,”(*in prep*), 2016

Reports

- E.A. Ubogu, B. Khandelwal and S. Blakey, “Review of Particle Emissions Measurement Instruments for Gas Turbines (Project Number R/134029),” 2015
- E.A. Ubogu, B. Khandelwal and S. Blakey, “The Impact of Aromatic Species on Particulate Emissions Characteristics from Gas Turbine Liquid Fuels (Project Number R/134029)”2015
- E.A. Ubogu, B. Khandelwal and S. Blakey, “Experimental Set-up for Particulate Sampling and Measurement, From a Gas Turbine (Project Number R/134029)”2014
- E.A. Ubogu, B. Khandelwal and S. Blakey, “Assessment of a Newly Installed APU for PM Emissions Measurement Campaign (Project Number R/134029)”2013

1 Background Information

Gas turbine emitted particulate matter (PM) is a complex air pollutant made up of mixtures of solid particles of different particle sizes and shapes and with different chemical composition. In the atmosphere, the emission contributes to the degradation of air quality thus posing serious danger to both health and the environment. To mitigate the impact of the pollutant most countries and relevant international organisations have air quality standards stating the maximum acceptable levels of particulate in the atmosphere over a period. Though, the degradation of visibility was the most observable aspect of the air pollutant to the public that prompted regulation of PM levels in the atmosphere, the increasing recognition of the effects of PM emission on human health and the environment continue to drive regular revision of the standards. The regular revision of PM air quality standards which are often based on research of the health and environmental impacts continue to drive the study of PM emissions from combustion sources. One of the several knowledge gaps in PM study is the measurement and quantification of the pollutant emitted by gas turbine. The big question is: how do you measure and quantify PM emission from a source which some would argue produces negligible PM.

Presently, mass concentration is the regulatory measure of gas turbine particulate matter emissions for compliance assessment for industrial gas turbines and health and environmental impact analysis for all turbines (aero and industrial). The rationale is that, mass is one of the few particle measurements parameter that is traceable to national standards. In brief, to take this measurement, a steady flow of the exhaust sample is passed through a filter with the impregnated filter weighed before and at the end of the test under controlled temperature and relative humidity conditions. However, this measurement technique known as the gravimetric technique was developed many years ago for use on high-emission sources such as coal-fired power plant. Despite reviews and subsequent modifications to improve the gravimetric method to meet the lower and possibly negligible PM emissions from gas turbine, concern remains for most of the sampling and measurement [1] techniques/protocols. These concerns include;

- Interference that cause negative and positive bias and introduce substantial uncertainties in the measurement.
- Manual handling which could have a huge impact on the repeatability and invalidate measurements.
- Slow response time as manual handling is at the core of the process, thus making the protocol unsuitable to capture PM emission at engine transient conditions.

There are real-time instruments currently applied in the monitoring of ambient particles and emissions from petrol and diesel engine emissions. These may have the appropriate level of sophistication and sensitivity to measure the particle emission mass concentration from gas turbines. Thus, the aim of this thesis is to investigate the potential use of established as well as newly developed particle instrument by developing correlations to a reference gravimetric protocol on particle emissions from a gas turbine for predictive purposes.

1.1 PM Health Effect

In the atmosphere PM emissions contribute significantly to poor visibility especially when it combines with fog to form smog. An air pollution event in history that demonstrates the impact of PM emission on visibility is the London smog which lasted five days. It caused disruption to travel as visibility of less than three metres [2] was reported in parts of London. Over 4000 deaths were attributed to the smog episode at the time, making the impacts of pollution to human health a major subject worldwide [2].

Studies [3-5] have shown correlations between particulate emissions and alterations in morbidity and mortality indices. It is suggested that the correlations may have been boosted by respiratory and cardiac effects within susceptible groups including the elderly [6] as studies have also shown that a link does exist with the increasing asthmatic cases and hospital admissions [7]. Hence, the accepted view that PM emission has serious negative health effects ranging from the aggravation of respiratory related ailments to cardiopulmonary disease (Figure 1-1) [8, 9].

The most concerning category of particulate matter to health, are the ultrafine particles (see section 1.4.4) which have the potential to deposit in the gas-exchange region of the lungs, when inhaled. Oberdörster et.al [10] in his experimentation of the effects of PM to exposed animals over a period, attributed the observed health effect to ultrafine particle and concluded that ultrafine particle matter are pathogenic. However, a better understanding relies on the knowledge of which is still a subject of continued research. What happens when the particles get deposited in the respiratory system is believed to be related to the chemical and toxic properties of the particulate matter [11]. Nevertheless, it is established the deeper in the respiratory tree these particles can reach; the longer they settle in the body; and how they interact with the body when they deposit, depends on their size, shape and density [12].

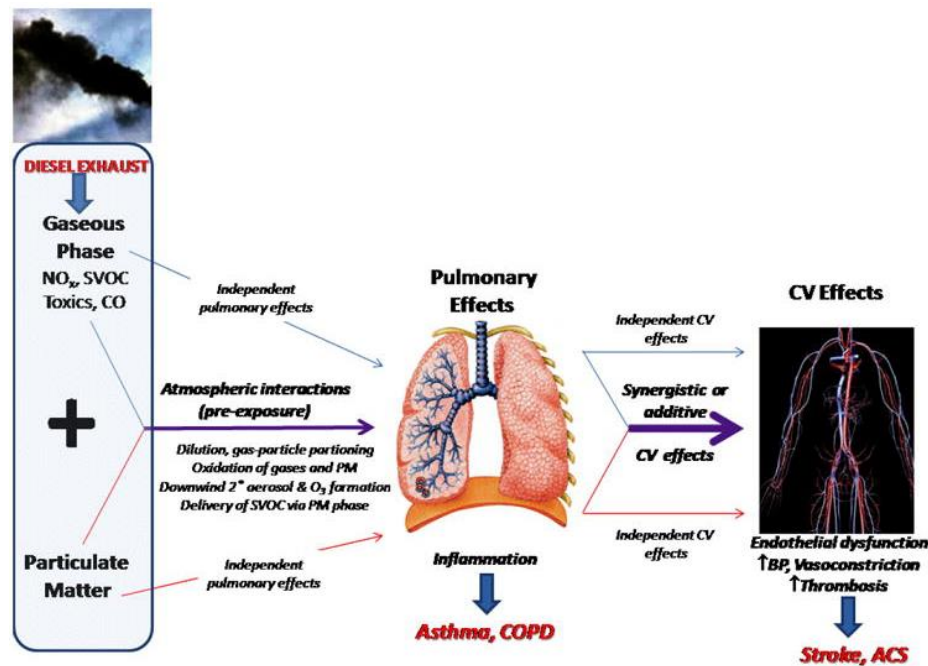


Figure 1-1: Overview of the complex interactions among air pollutants and effects of exposures on cardiovascular health in a multi-pollutant context [13]. NO_x, indicates nitrogen oxides; SVOC, semivolatile organic compounds; CO, carbon monoxide; O₃, ozone; PM, particulate matter; COPD, chronic obstructive pulmonary disease; CV, cardiovascular; ↑BP, increased blood pressure; 2°, secondary; and ACS, acute coronary syndrome

The occupational health community thus classifies PM size fractions into three categories; inhalable, thoracic, and respirable, to describe their entrance into various compartments of the respiratory system. The inhalable refers to particles

that end-up in the respiratory tract, beginning with the head airways. Thoracic particles end –up in the lung airways and possibly in the gas-exchange regions of the lung while respirable particles define particles with a greater probability of ending up in the gas-exchange region of the lung. Out of the three classifications, the respirable particles are considered ultrafine particles. The danger posed by particle deposited in the gas exchange region is high as they can diffuse deep into the lungs with the possibility of entering into the blood stream. If not, they can accumulate in the alveoli lung epithelium and subsequently engulfed in the intracellular space, thus increasing the potential of pulmonary disease and eventual lung damage.

1.2 Environmental impact

Particulate emissions play a role in the environmental effects of combustion of fossil fuels. Deposition on plant and material surfaces [14] remains one of the clear evidences of particulate emission impacts on the environment. When particulate matter in the atmosphere finally succumbs to gravity, it settles on surfaces including plants. This can physically deform the plant in addition to affecting its chemical structure depending on the chemical composition of the particles [15]. The most recorded toxic effects of particles on plants relate to acidity, metal content, nutrient, surface properties and salinity [15]. Similarly, many construction materials and paints can be greatly affected while in agricultural and natural ecosystems its effects can include interruption of nutrient cycles [15, 16] and reduced productivity.

1.3 Regulatory Drivers

PM air quality standards are the foundation on which PM policies applied to land based gas turbine are formed. Gas turbine emission might not be directly regulated as they are considered clean burning sources, however with established air quality standards for matter particulate which are continuously reviewed, the subject cannot be ignored by both users and manufacturers. The PM standards or guidelines state the PM thresholds not to be exceeded over a short-term (24-hour) or long-term (annual mean). Mostly expressed in terms of either total suspended particulate matter (TSP), mass of suspended particulate matter less than 10 μm or 2.5 μm in size, Table 1-1 is an overview of the PM air quality standard for some

countries and the world health organisation (WHO). To demonstrate the importance government authorities have placed on particle pollution through these thresholds, some countries have incorporated PM data in their Air Quality Health Index (AQHI) reports. Also, some countries have a set time table in which ambient PM concentration is to be achieved below the acceptable levels [17]. Consequently, efforts to make an area meet the air quality standards can result in stricter regulations of emissions from a PM emission source including gas turbines which implies that the PM emissions must be measured.

Table 1-1 Summary Table of Air Quality Requirements [17]

Country	PM Type	Time	Value($\mu\text{g}/\text{m}^3$)	Comments
Australia	PM10	24 hours	50	
Canada	PM2.5	24 hours	30	Federal Guideline
Brazil	PM10	24 hours	150	
		Annual	50	
China	Total Suspended Particles	Annual	800	Sensitive Areas
			200	Residential Areas
			300	Industrial Areas
		Daily	120	Sensitive Areas
			300	Residential Areas
			500	Industrial Areas
	PM10	Annual	40	Sensitive Areas
			100	Residential Areas
		Daily	150	Industrial Areas
			50	Sensitive Areas
European Union	PM2.5	Annual	25	
	PM10	24 hours	50	
		Annual	40	
India	Total Suspended Particles	24 hours	100	Sensitive Areas
			200	Residential Areas
			500	Industrial Areas
		Annual	70	Sensitive Areas
			140	Residential Areas
			360	Industrial Areas
	PM10	24 hours	75	Sensitive Areas
			100	Residential Areas
			150	Industrial Areas
		Annual	50	Sensitive Areas
60	Residential Areas			
120	Industrial Areas			
Japan	PM10	24 hours	100	

Mexico	PM2.5	24 hours	65	
		Annual	15	
	PM10	24 hours	120	
		Annual	50	
Philippines	TSP	24 hours	250	
USA	PM2.5	24 hours	35	PM10 annual limit revoked in 2006 due to lack of evidence of a link between long term PM10 exposure and health effects
		Annual	12	
	PM10	24 hours	150	
WHO	PM2.5	24 hours	25	
		Annual	10	
	PM10	24 hours	50	
		Annual	20	

In the United States the air quality of power plant site compared to the National Ambient Air Quality Standard (NAAQS) determines policies implemented on a new power plant project or modification of an existing plant or repairs. For instance an application for a new source review (NSR) or Prevention of Significant Deterioration (PSD) permitting process can trigger the application of rules such Best Available Control Technology (BACT) or the Lowest Achievable Emission Rate (LAER) to control the emissions depending of the air quality assessment of the area. In Europe, there is the Large Combustion Plant Directive (LCPD) (2001/80/EC) [18], which controls emissions of sulphur dioxide, nitrogen oxides and particulate matter from combustion plants with a thermal input of 50MW and greater. There are PM limits in the document, but the LCPD exempts gas turbines from these limits. However, the directive also allows member states to set more stringent regulations. The LCPD is supported with the Industrial Emissions Directive (IED) 2010/75/EU [19] which sets out the main principles for the permitting and control of installations based on an integrated approach and the application of best available techniques (BAT). *"BAT is the most effective techniques to achieve a high level of environmental protection, taking into account the costs and benefits"*. For countries requiring financial support from the world bank to execute power plant projects the International Finance Corporation of the World Bank policy document titled "General Environmental, Health, and Safety (EHS) Guidelines, " for thermal power plants [20, 21] may apply. The

documents state limits for PM emissions from gas turbines firing fuels other than natural gas.

1.4 Overview of Particulate Emissions

Particle emissions, widely known as particulate matter (PM), refers to solids or liquids present in the effluent gas after combustion. The particles can include carbonaceous particles, inorganic acids (and their corresponding salts, such as nitrates and sulphates), abraded metals, as well as PM present in the ambient air due to natural sources, such as soil or dust particles [22]. In effect, the PM emission is a makeup of individual particles with irregular shapes, sizes and chemical composition. Thus, a robust description of PM emissions would account for the chemical composition, morphology [23], as well as the relative abundance of each particle type as a function of particle size [23, 24]. Consequently to properly describe particle emissions, various terms and definitions are often used for operational, regulatory and research purposes. The most common terminologies are volatile and non-volatile PM.

1.4.1 Non-volatile PM

Non-volatile particles are particles that are in solid form at the exit plane of the engine exhaust and remain in a condensed phase even when ambient conditions vary widely. They largely consist of carbonaceous materials frequently referred to as soot emissions, or smoke from combustion sources. Soot is often used interchangeably with black, elemental or refractory carbon depending on the property used to identify it. Black carbon is mostly used when identified and quantified through its optical property. Similarly, the term elemental carbon is used when detected through its thermal property while the terminology refractory carbon is used when it is identified and quantified using its incandescence property. Also, closely related to the non-volatile terminology is the term filterable PM. Filterable PM (FPM) is mostly used by the United States Environmental Protection Agency (EPA) to define particles that are emitted directly from a source as a solid or liquid at stack or release conditions and can be captured on a filter, during stack testing [25-27].

1.4.2 Volatile PM

Volatile particles, describe particles that change their state under ambient conditions. Since the exhaust gas temperature of a gas turbine is at a very high temperature, some of the gaseous emissions would condense to particulate emission when cooled in the atmosphere. The transformations of such gaseous emissions depend on their vapour pressure as well as the ambient conditions such as temperature and relative humidity. The volatile PM definition also fits the condensable PM (CPM) terminology mostly used by the EPA. Condensable PM (CPM), are vapour phase at stack conditions, but condense and/or reacts upon cooling and dilution in the ambient air to form solid or liquid PM immediately after discharge from a stack [28]. The vapour phase materials either condense on existing solid particles or nucleate to form new particles.

1.4.3 Primary and Secondary PM

The primary and secondary terminology is used to describe the state of the particle on entry into the atmosphere. Primary particles refer to those particles that enter the atmosphere in a particulate form as a direct emission from its source. As a result, on entering the atmosphere, these sets of particles are ready for dispersion and transport and/or physical and chemical processes simultaneously, which determines their residence time in the atmosphere. This definition is also expanded to include nucleation fractions which are quickly (within approximately one minute of exiting the stack) formed from precursor gases on mixing with the atmosphere [7]. In contrast the term secondary particle refers to particles not emitted directly into the atmosphere, but as a result of transformation of precursor gases or breakdown of the primary particle. They are produced from gases by chemical and physical processes in the atmosphere after release. The formation depends on the atmospheric conditions and the presence of other particles and the precursor gases can be sensitive to changes in temperature and the surrounding gas concentrations. Some of the several formation pathways through which they form, are depicted in Figure 1-2 below.

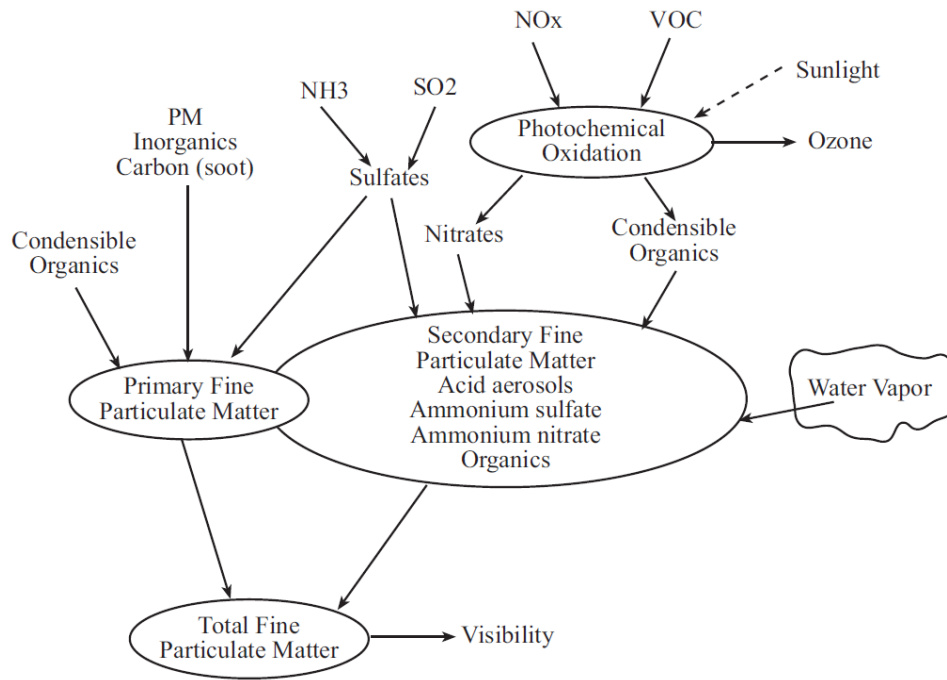


Figure 1-2: Secondary particle formation pathway [7]

1.4.4 Particle size

Gas turbine particulate matter emission can be described as polydisperse in terms of mass and size, meaning they are a makeup of many single particles of various sizes, geometry and mass that may be coagulated, agglomerated, or remain as a single particle. Thus, it is difficult to describe the PM emission sizes with a single parameter as a result of the irregular shapes [24]. Consequently, exhaust particles sizes are often indexed in equivalent diameter [29]. This is the diameter of a spherical particle, exhibiting the same particle behaviour when subjected to similar conditions. For instance, the electrical mobility equivalent diameter is the diameter of a sphere that has the same electrical mobility as the particle in question while the aerodynamic equivalent diameter is the diameter of a unit density sphere which settles at the same speed as the particle.

Using this idea, over the years, various size categorisation techniques for particle emission have emerged. These are coarse, fine and more recently ultrafine particles. Shown in Figure 1-3 is an idealised particle number, surface area and mass weighted size distributions highlighting the particle classes.

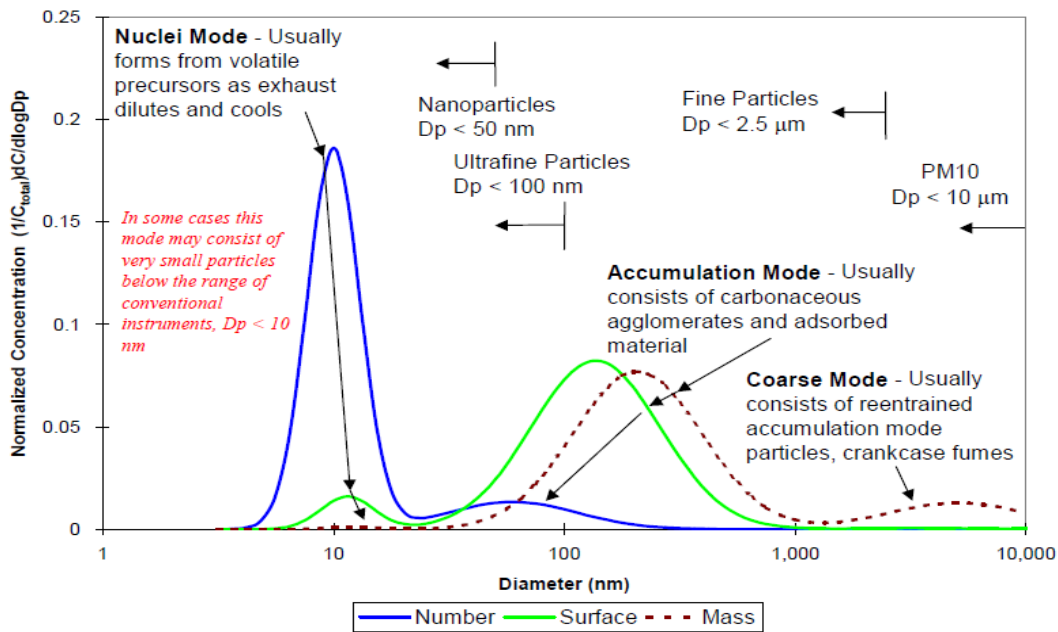


Figure 1-3: Idealised exhaust particle number and mass weighted size distributions [30, 31]

Coarse particles are those particles smaller than $10 \mu\text{m}$ but larger than about $2.5 \mu\text{m}$. Fine particles are particles less than $2.5 \mu\text{m}$ while ultrafine particles, refer to particles below $0.1 \mu\text{m}$ and represented by the acronym, $\text{PM}_{0.1}$. Similarly, acronyms are used to denote particles smaller than $10 \mu\text{m}$ and $2.5 \mu\text{m}$, represented by the terms PM_{10} and $\text{PM}_{2.5}$ respectively. One of the categories often used in the early stages of particle research not shown in Figure 1-3, is the total suspended particulate” (TSP). It refers to the PM up to a nominal size of 25 to $45 \mu\text{m}$.

Also shown in Figure 1-3 are categories used to describe the particles primarily in terms of their formation mechanisms in relations with particle sizes, referred to as modes as first proposed by Whitby [32]. The nuclei mode describes newly formed particles which have little chance to grow by condensation or coagulation. It typically consists of volatile organic and sulphur compounds that form during exhaust dilution and cooling, and may also contain solid carbon and metal compounds. The accumulation mode term is used to acknowledge the growth of particles by coagulation and condensation on a particle. As a result, it contains non-volatile PM which have agglomerated and volatile material which have condensed on the non-volatile fraction. This is where soot and associated

adsorbed materials exist [24]. The third mode in this size category is the coarse mode which consists of re-entrained accumulation mode particles.

1.4.5 Particle Size Distribution (PSD)

Since PM emission contains several orders of magnitude in particle size, it is often a common practice to present the particle sizes in the form of a distribution expressed in terms of the logarithm of the particle diameter on the *X-axis* and the measured number concentrations on the *Y-axis*. This is represented in the form of either a frequency distribution curve, or a cumulative distribution curve. Thus the area under such distribution curve represents the total of the property that the particle sizes have been weighed against. The *Y-axis* parameters are usually particle number, surface area, volume and mass distribution. These, distributions are mathematically linked as shown in equations 1-1 to 1-4. Thus, assuming the particles are spherical, with a number distribution measurement, the surface area and volume size distribution can be derived using equation 1-2 and 1-3 respectively. Equation 1-4, makes it possible to derive the particle mass concentration as required for PM engine certification to be calculated from the particle size distribution instruments; however a density value would be required to be assumed constant across different sizes of PM.

$$dN = N(d_p)dD_p \quad \mathbf{1-1}$$

$$dA = dN \times \pi D_p^2 \quad \mathbf{1-2}$$

$$dV = dN \times \pi/6 D_p^3 \quad \mathbf{1-3}$$

$$dM = \rho(d_p)dV \quad \mathbf{1-4}$$

Where;

- N = Number
- A = Surface Area
- V = volume
- M = Mass
- D_p = particle diameter

1.5 Research Objectives

Several key objectives to be achieved to attain to the research aim are:

- To identify the most widely used standards for industrial gas turbine PM compliance testing.
- To identify well established real-time PM measurement instruments available off the shelf
- To identify new/emerging instruments and techniques
- Select some of the identified instruments based on the maturity of the technology used, measurement frequency, detection limit and precision accuracy
- Define a reference standard to be used for experiment to develop correlation.
- To generate PM emissions from a small scale gas turbine to be measured using the selected instruments.
- To design a sampling system that would enable the distribution of the extracted sample at the exhaust plane to comparing instruments simultaneously.
- To investigate how different particle mass concentrations equivalent to the mass concentration obtainable from industrial gas turbine can be generated using a test gas turbine to create multiple data points.
- To present the PM emission results for the test points for the instruments.
- To produce correlations between the filterable PM derived using gravimetric techniques and real-time non-volatile particle measurement instrumentations.
- To critically appraise the repeatability of the condensable gravimetric method based on the experiments observations.
- To suggest future works.

1.6 Thesis Outline

This thesis is divided into three main parts; the introductory part, the main (body) part and the concluding part. The main part of the thesis is contained in chapters two to six inclusive with one and seven the introductory and conclusive chapters. An insight into topics covered in the chapters is summarised as follows;

- **Chapter 1** - This chapter begins by giving an insight into the issues with measuring PM emission from a gas turbine, thus emphasising the importance of this study. Next, it gives an overview of the health, environmental concerns associated with the PM. Following the health and environment section are details of regulatory policies linked to gas turbine PM emission from different countries with the PM air quality thresholds of some countries are tabulated. Also covered in the chapter are the basic terminologies and definitions associated with PM studies to familiarise the reader with the inter relationship and interchangeable use of the terms. Detailed objectives along with the structure of the thesis make up the ending sections of the chapter.

- **Chapter 2** - To justify the need for this thesis, this chapter provides a comprehensive literature review of various real-time PM measurements from which instruments to be compared with a standardised PM measurement method is selected. The literature review also identifies the knowledge gaps that demonstrate the importance of the study. Consequently, an overview of conventional stationary source testing methods and associated sampling issues are first highlighted thus justifying the follow-up section on the requirements for a robust PM measurement of gas turbine emissions. Fast particle measurement instruments are then introduced, categorised and summarised. Next, is an overview of the working principles and a match of how their specification with gas turbine PM measurement requirement. Based on this information a theory of how the instruments could correlate with the gravimetric reference method is developed. This leads to a review of studies that have conducted correlations between PM instruments. First, the experimental method is reviewed to justify the design of experimental setup developed in chapter three. Then, correlation results involving the instrument in the hypothesis with gravimetric method from any combustion sources are reviewed to identify the trends, data and knowledge gaps that can advance PM research studies in relation to this thesis. This chapter ends with a summary of the knowledge gaps the thesis aims to fill.

- **Chapter 3** - Details about the experimental setup are presented in this chapter. How the constraints in the design of the sampling system were considered is explained in detail. Accordingly, the chapter covers a detailed description of the functions of each component part of the sampling system. Also contained in the chapter is a description of the working principles and working procedure of the instruments selected in chapter two.
- **Chapter 4** - This chapter covers preparatory tests needed to refine the experimental design and develop a test procedure experiments. Thus, the preparatory tests are aimed at resolving issues with sampling and engine data representativeness. Below is a list of the tests.
 - Engine performance and certification gas emissions
 - Traverse test to determine the best position of the exhaust sampling probe.
 - PM emission concentration correlation with fuel aromatic content
 - Investigation of the characteristics of particulate emission from different aromatic species.
 - Verification of the particle size distribution
- **Chapter 5** – This chapter presents the test matrix which lists the fuel burnt and the engine power settings conducted during the experiment. Accordingly, the properties of the fuels tested are presented. Also described in the chapter, is the experiment performed to determine the equations that defines the individual particle mass and size relationship required to convert particle number concentration measurement to mass concentration. Also covered in the chapter is the result analysis and discussion of the experiment.
- **Chapter 6** – This chapter documents the experimental procedure and data collection procedure. The operating procedure developed to obtain samples for the filter methods and to collect data in real-time from the fast PM instruments is presented. Analysis conducted to arrive at a considerable sample acquisition test time is described. In addition a detailed analysis of the impact of the sample acquisition test time on the precision of data

obtained from the real-time instrument is analysed. Also documented in the chapter is the post processing procedure of the data from each of the instruments each which include the corrections conducted. The chapter ends with an analysis of the data quality indicators including the accuracy of the results.

- **Chapter 7** - This chapter presents the PM results obtained from different gas turbine operating conditions and the fuels used to generate different particle concentrations. Gaseous emission results are also presented. The chapter begins by confirming the gas turbine test engine operating conditions by showing the variability of the engine. Likewise a repeatability analysis is performed using selected data points for the real-time instruments and the gravimetric reference method. The next section focuses on the particle size instrument data. It includes the analyses of the particulates measured at the different conditions which the exhaust sample was subjected prior to the heated sample line directly connected to the instrument. The next section investigates the relationship between the smoke number and particulate emission sizes. The last section presents and discusses the correlations between the real-time particle sizing instrument and the filterable fraction of the gravimetric method.

- **Chapter 8** Summary of recommendations for future test programs. Solid conclusions are drawn based on the results and discussions in previous chapters. This chapter also provides recommendations for the future work in this area. The final chapter summarises the key finding of this PhD and introduces recommendations for future work.

2 Gas Turbine PM Properties and Aerosol Measurement Instruments

This chapter reviews the performance of various real-time PM instruments and evaluates their suitability for the measurement of particle emissions from gas turbines. It investigates how the real-time instruments compare with the gravimetric technique. Thus details of the gravimetric reference methods used for industrial gas turbine PM emission compliance testing are reported and reviewed. It details the issues with gravimetric measurement reference methods and then defines the requirements for real-time mass concentration readout measurements of gas turbine PM emissions. First the chapter looks at the sources of PM, chemical and physical processes that occur in the combustor leading to the formation of particulate matter and particulate matter and further reaction at the engine exhaust exit of a gas turbine before detailing the characteristics of PM from a gas turbine.

2.1 Formation of PM in a Gas Turbine

The source of particulate matter in a gas turbine combustion process is from inorganic and organic materials drawn in with the fuel or air or from the reaction of the fuel itself or both. The engine lubrication oil has also been shown to be a potential source of PM emission especially when it leaks into the combustor or the exhaust gas pathway. Other possible sources include the precipitation of solids from steam if injected into the turbine for the control of oxides of nitrogen (NO_x), metallic erosion from the interior surfaces exposed to the exhaust flow path. Inorganic materials, if introduced into the gas turbine combustion process either through the fuel flow or air stream may be altered chemically and physically due to the high energy density environment experienced in the combustor. The extent to which the materials changes depend on the properties but at the exhaust exit they constitute the non-volatile inorganic fraction of the PM emitted. Likely changes include a reduction in the particle size or some degree of oxidation if not in its highest oxidation state. Inorganic materials introduced with fuel are more prevalent in heavy liquid fuels compared to gaseous fuels. In addition to the inorganic materials in fuel organometallics may be present in the fuel, particularly

as additive substances. These species are oxidised in the flame and the metal component appears as an inorganic oxide or salt in the post flame gases.

2.1.1 Formation of Particulate from Fuel Molecule Reaction

Particulate matter from the reactions of the fuel molecules is usually the dominant source and responsible for the production of soot or black/elemental carbon (see section 1.4.1) that is visible when captured on a filter paper. The process of particle formation from fuel molecules during combustion is still a subject of research but a widely accepted formation process has been developed over the years from laboratory flame studies [33]. The evolution of the fuel molecules from liquid or vapour phase hydrocarbons to solid soot particles inside the combustor is currently described in five processes: pyrolysis, nucleation, coalescence/surface growth, agglomeration and oxidation which usually occur simultaneously with other processes.

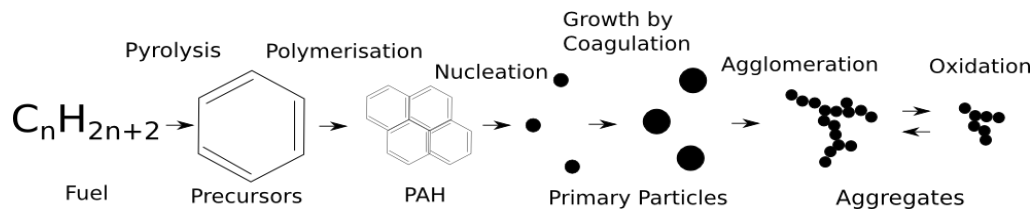


Figure 2-1: Basic schematic of soot formation for combustion of fuel [34]

It begins with the formation of unsaturated hydrocarbons and aromatic compounds that form soot precursor particles. Oxidation and pyrolysis of combusting fuel, results in small fragments that form into an aromatic ring - benzene or phenyl radical [35]. The continued growth and carbonization of the rings leads to recognizable primary particles as outlined in Figure 2-1 followed by the coagulation and surface growth steps. Coagulation is the result of colliding macromolecules/nanoparticles to produce new spherical structures while surface growth is the outcome of chemical reactions, involving molecules in the gas phase and on the surface of the particle, such as adsorption and desorption processes. The last step of soot formation is the agglomeration which produces clusters or chain-like agglomerates.

2.1.1.1 Impact of Gas Turbine Combustor Design

As noted in the previous section, pyrolytic reactions promoted by fuel rich reactions are central to the formation of soot. The combustion process characteristics affecting the formation of combustion particulates and influenced by the combustor design are:

- Combustion zone temperature
- Residence time in the combustion zone
- Mixing efficiency between air and fuel
- Air to fuel ratio (engine operating condition)

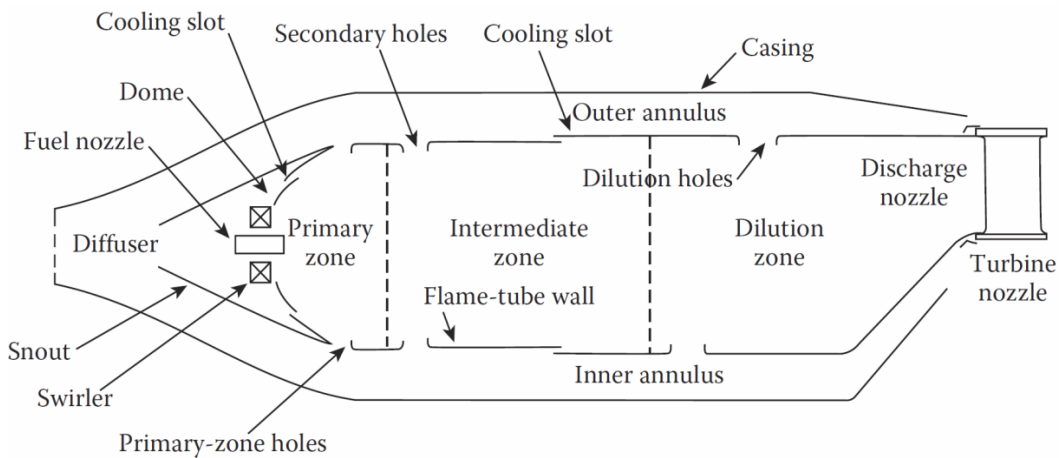


Figure 2-2: Main Components of a Conventional Combustor [36]

A basic gas turbine combustor design (Figure 2-2) is divided into three zones namely; the primary, intermediate and the dilution zone. In the basic combustor design the fuel-rich regions occur in the primary zone of the combustor which is very close to fuel spray. This can be attributed to the movement upstream toward the fuel injector of recirculating burned products thus creating local pockets of fuel vapour enveloped in oxygen-deficient gases at high temperature. Therefore an increase in the fuel in the combustor which is basically the resultant of an increased engine operating condition would result in more local fuel rich condition in the combustor. Some of the PM formed in the primary zone eventually gets oxidized in the dilution zone with the remainder going through the expansion process in the turbine and exiting as solid particles. Consequently, the primary zone governs the rate of PM formation while the dilution zone determines the rate of soot consumption [36].

In summary, the control of the PM emission from a gas turbine through the combustor design is within the manufacturers control during design. The engine operator only has control of the PM the engine emits through a change in the engine operation conditions which is normally in response to engine load demand.

2.1.1.2 Fuel Characteristics

The type of fuel burnt in a gas turbine has a huge impact on PM emissions it produces. This is evident when the PM emissions from two extreme gas turbine fuels are brought into perspective. Methane on one extreme tends to produce low levels of soot, while heavy distillate on the opposite end produce large amount of soot emission. Work conducted by Calcote et al [37] and McEnally et al [38] which introduced threshold sooting index (TSI) and yield sooting index (YSI) respectively, the aromatic content of a fuel is largely responsible for its sooting tendency. As shown in Figure 2-3, the TSI ranks hydrocarbons sooting tendencies on a scale 0-100 with 1-methyl naphthalene assigned 100 at the top end and n-hexane assigned a TSI of 2 at the bottom. Thus, perhaps in agreement with the formation mechanism detailed in section 2.1.1.1 the presence of aromatic in gas turbine fuel speed up the formation of “seed” molecules that contribute to the formation of soot nuclei during combustion in as gas turbine [36].

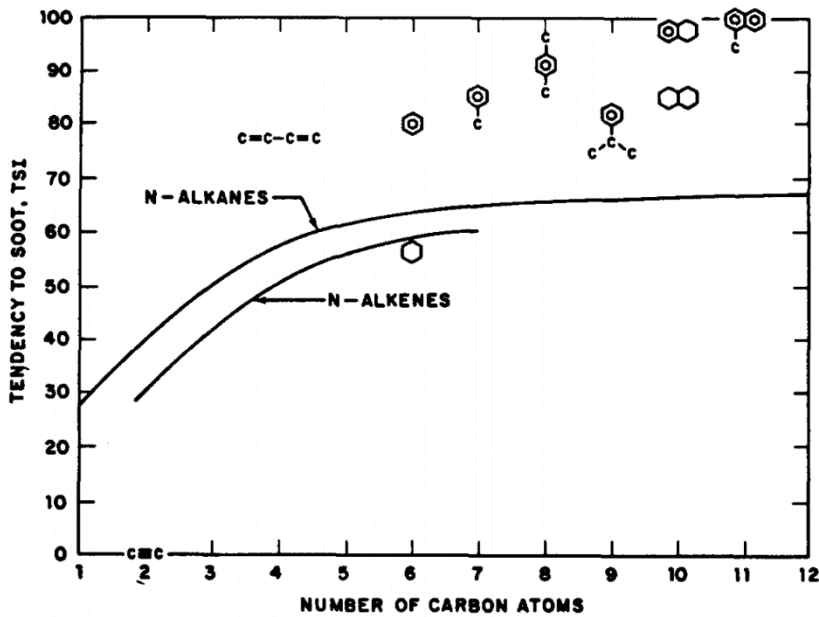


Figure 2-3: Tendency to soot (TSI) for hydrocarbons [37]

Despite the high sooting characteristics of aromatics none of the studies investigated the impact of aromatic species on PM particle size. As detailed in section 1.1, there is a relationship between PM particle sizes and possible health effects thus a similar ranking of the aromatic species PM emitted would be of valuable knowledge to PM research. A recent finding by Botero et al [39] confirms the variability of PM sizes with aromatic species but interestingly do not correspond with the assigned TSI and YSI developed by Calcote [37] and McEnally [38]. Using a wick-fed diffusion flame to compare the soot sizes from five aromatic species, toluene and 1,2,4-Trimethylbenzene produced the largest soot particles while tetralin, butylbenzene and phenylcyclohexane showed the lowest soot particles. This is contrary to the high sooting tendency ranking for tetralin compared to toluene and 1,2,4-trimethylbenzene. Thus, it suggests the effect of the hydrocarbon molecular structure as it relates to incipient soot formation is different for soot growth.

2.1.2 PM Emitted at the Exhaust Exit and Further Reaction

The particulate emitted from a gas turbine are either filterable or condensed as a combination of the two mass fractions form the total particle concentration emitted from a turbine source. The percentage composition of each of the fraction significantly varies as they are both dependent on the post combustion emission control technique in place in addition to the fuel composition and engine operating condition. The filterable fraction of the PM emission can account for 11 – 74 percent of the total PM [40] while the condensable fraction ranges from 26 – 89 percent [40] of the total PM. The filterable particulate emissions from a gas turbine are mainly composed of black carbon (elemental carbon/soot – see section 1.4.1) which can make up to 95% of the mass fraction as demonstrated by Timiko [41]. Accordingly, the remaining components are inorganic non-volatile materials if CPM is not captured as part of the filterable particulate matter.

The CPM fraction is composed of organic or inorganic materials. They are basically low vapour pressure organic and inorganic gases emitted above their dew point and as a result condense when under atmospheric conditions. Though a detailed profile of the organic and inorganic species that form the CPM is still a

subject of continued research, the CPM organic fractions are broadly organic acids, aromatics and heavy aliphatic formed from unburnt hydrocarbon and possibly lubricating oil [41]. The inorganic fractions are mainly composed of nitrate and sulphates and can be traced to the nitrogen and sulphur content of the combusting air and fuel mixture. Thus, the precursor gases of the inorganic fraction of the CPM are mainly the oxides of nitrogen and sulphur in the exhaust gas. Ammonia is also a precursor gas but mainly present when selective catalytic reduction (SCR) or non-selective catalytic reduction (NSCR) NO_x abatement strategies have been deployed.

Most of the combustion related CPM are found as sulphuric acid (H_2SO_4) from oxides of sulphur, ammonium bisulphate (NH_4HSO_4), and ammonium sulphate ($(\text{NH}_4)_2\text{SO}_4$) from oxides of sulphur and ammonia gas, and ammonium nitrate (NH_4NO_3) from oxides of nitrogen and ammonia gas. How these particulates form is greatly determined by the gas phase chemical pathway involved, with the hydroxyl pathway the main pathway [7]. For example, the formation of sulphuric acid droplets from gas turbine effluent gas in the atmosphere starts with the reaction of sulphur dioxide with hydroxyl radical to form hydrogen sulphide. Hydrogen sulphide then rapidly reacts with oxygen to SO_3 which further reacts with small amounts of water vapour to become sulphuric acid gas. Sulphuric acid has a low gas pressure thus condenses on existing particles or nucleates at high relative humidity to form sulphuric acid droplets which is typically neutralised by ammonia if available. In a similar fashion hydroxyl is the favoured pathway for nitrate to transit from nitrogen oxide. However, sulphates are better detected in the atmosphere as a CPM because nitric acids are more volatile than sulphuric acid [7].

2.2 Gas Turbine PM Physical Characteristics

Presently, gas turbine PM is described as a makeup of compact aggregates in which the particles can be highly fused or discrete but tend to be smaller and less highly coagulated than the chain aggregates that are typical of diesel engine PM [36, 37]. This understanding of gas turbine PM emission morphology is based on the work by Vander Wal [42] whom studied photomicrographs of a High

Resolution Transmission Electron Microscope (TEM) of PM emission from an aero gas turbine. The study highlighted that the morphology of the soot particles changes with engine operating conditions (Figure 2-4). With increasing power, single primary particles, which are difficult to recognise at idle setting become increasingly apparent. They are clearly separate and distinct at the higher power levels resulting in a higher particle size. Also, there is a progressive increase in nano structure order with increasing power. At idle or close to idle power setting nearly amorphous nano structure can be observed while an extended lamella organized into parallel stacks is observed at high power.

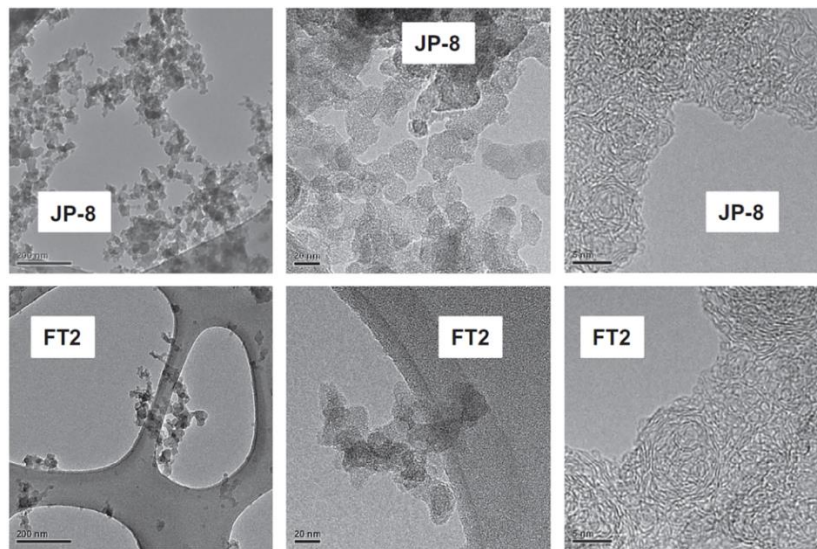


Figure 2-4: Photomicrographs of soot particles extracted from exhaust of an aircraft engine at different power conditions from different fuels[42]

The single particle sizes or aggregates found in the PM emission of the gas turbine are believed to be less than one micron in size. Kinsey et al [43] under the Alternative Aviation Fuel Experiment (AAFEX) programme analysed the particle size distribution (PSD) of the PM emissions from a Honeywell (formerly Garrett) Model GTCP85-98CK auxiliary power unit burning jet 8 fuel. As presented in Figure 2-5 the observed particles are between 5 and 200nm, far less than one micron. Similarly, Corporan et al [44] particle size distribution data show a single mode lognormal, between 5nm and less 200nm for a CFM56-2C1 gas-turbine engine. Crayford et al [45] work during the Studying, sAmpling and Measuring of aircraft ParticuLate Emissions III (SAMPLE III) made similar observations with

PW4000 engine series and CFM56 engine. Marsh et al [46] investigation of a commercial Roll-Royce Large Modern Civil Aero Engine not mentioned as a result of confidentiality, noted that the majority of the particles were counted in the less than 1000 *nm* range. These results are well within the expectations of current scientific opinion (within SAE E31) which suggests that all aero exhaust PM is in the range of 1- 1000 *nm*.

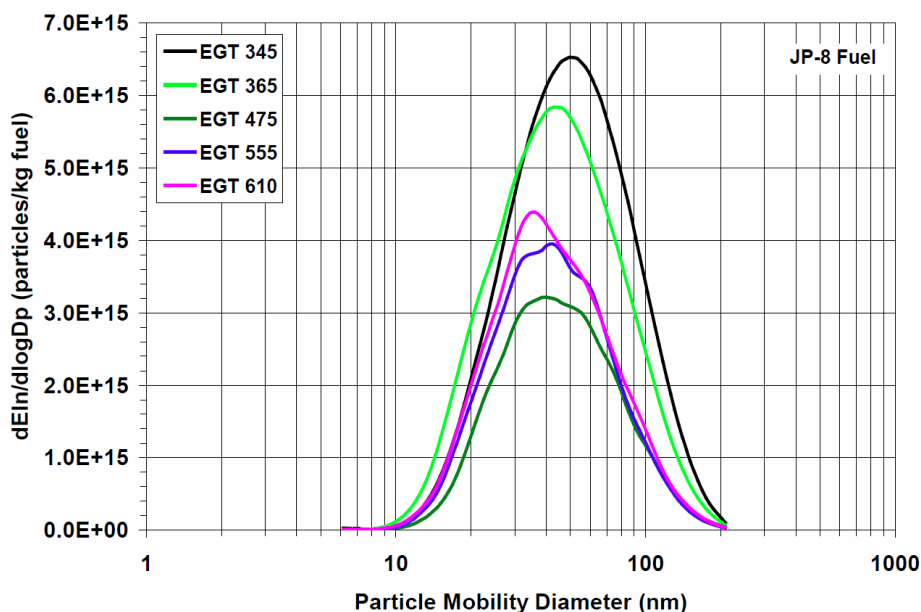


Figure 2-5: Particle Size Distribution for and aircraft Auxiliary Power Unit (APU) Burning : JP8 Fuel [43]

Apart from the Marsh et al [46] study, which used an instrument with the capacity to detect particles up to 32 microns in size, the other studies mentioned used instruments with the capacity to detect only particles below 1 micron. Thus, a one micron cut-off sizer (cyclone or an impactor) was deployed upstream of the analysers to ensure that particles getting to the sensing zones were within the instrument requirement. This creates some element of doubt, given that the PM emitted is not only a function of the fuel, but also a function of the age and the atmospheric particle. Meaning that, if it is assumed that all the carbonaceous non-volatile particle resulting from hydrocarbon reactions in the combustor are less than one micron that position cannot be asserted for the other types of solid particle that may result from the engine and expected to be quantified as particulate using gravimetric measurement methods.

2.3 Land Based Gas Turbine PM Emission Measurement Reference Methods

For regulatory purposes, exhaust particle emissions measurements are based on filtration and gravimetric determination of the mass of the filter substrate. The mass is simply derived by weighing the filter before and after loading under controlled temperature and relative humidity conditions. The total exhaust volume through filter is recorded at the end of the sampling to calculate the mass concentration of the filter catch per volume. This is basically the case for filterable particles. Table 2-1 contains a list of some of the widely used particle emission measurement reference methods applicable to ground based gas turbine PM emissions.

Table 2-1 Stack Sampling Gravimetric Methods

Sampling Method	Sample Collection Point	PM Sample Collected	References
US EPA Method 5	Outside Stack	Filterable	[25]
US EPA Method 5I	Outside Stack	Filterable	[27]
US EPA Method 17	Inside Stack	Filterable	[26][20]
US EPA Method 201	Outside Stack with a size selective inlet	Filterable	[47]
US EPA Method 202	Outside Stack	Condensable	[28]
BS ISO 11042-1	Inside Stack/Outside Stack	Filterable	[48]

For this research work, the US EPA method 5I and method 202 is the reference baseline for filterable and condensable particulate measurement respectively. The rationale for US EPA method 5I as baseline reference is based on the fact that it has been developed for performing correlation of manual PM measurements to PM continuous emission monitoring systems (CEMS) as compared to the other (US EPA 5,17, 201, BSI 11042) reference methods. For U.S. EPA Method 202, it is the only available standard for the measurement of condensable PM in the U.S and it is widely used worldwide as the standard if condensable PM measurement is required.

Figure 2-6 shows the key components of the Method 5I sampling train. Basically, it consists of a gooseneck nozzle through which exhaust samples are continuously drawn from the turbine exhaust stream and transported via a short heated sample line (probe in the figure), to a filter holder kept inside a heated box. With a filter in the filter holder the exhaust sample is stripped of all the containing solid particles. An impinger arrangement directly behind the filter holder as the exhaust exits the filter holder is used to determine the moisture content of the exhaust gas as the weight gain in the impingers. The other reference test methods for measuring FPM have similar configurations. The common differences between these references usually have to do with the sample collection temperature, the location of the filter and having a selective inlet upstream of the filter if particles below a specific size are of interest. As a result of the crossovers between the references methods, the gravimetric kits are mostly made of modular components that can be arranged and re-arranged to perform multiple reference methods. The exact steps to conduct this type of sampling are spelt out as referenced in Table 2-1.

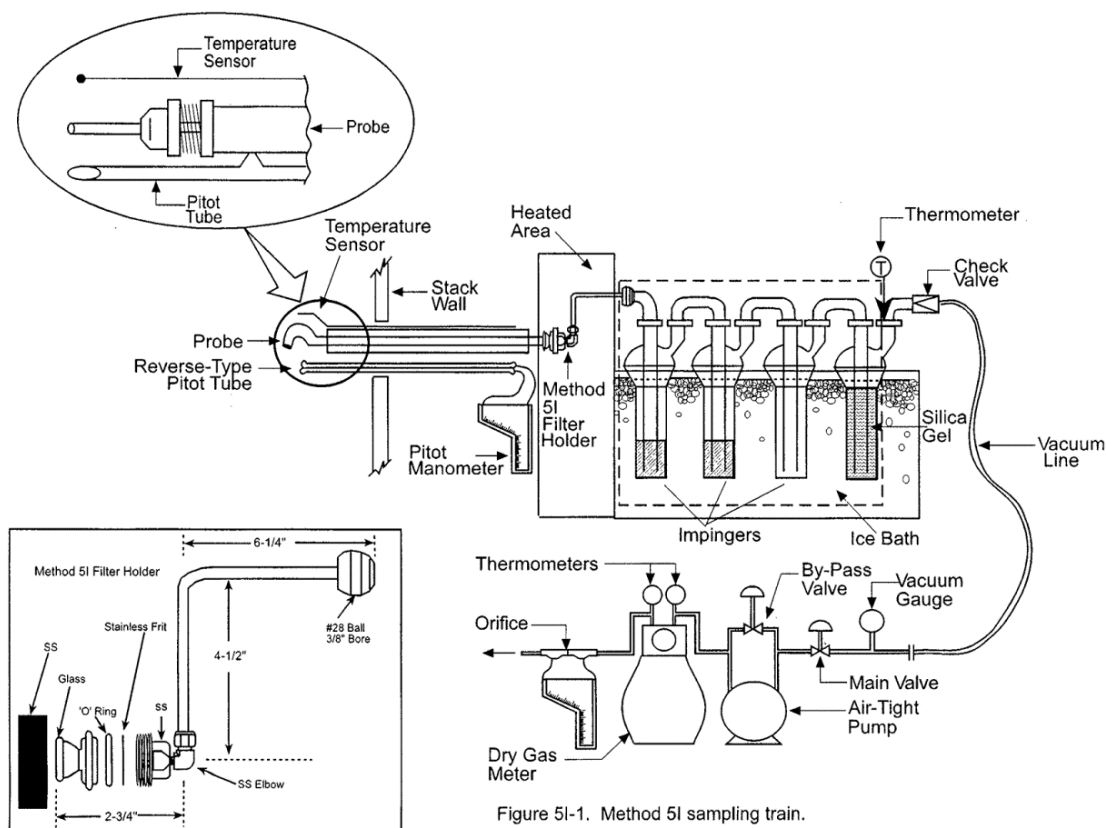


Figure 2-6: Schematic of Method 5I [25]

Figure 2-7 shows schematic of the condensable PM arrangement as placed in series with any of the FPM methods. It is an arrangement downstream of the filterable filter reference methods designed to capture all vapour phase materials that condense at a temperature below the filterable fraction filter temperature and above an exit temperature of 20 °C, thus, often referred to as the back half of filterable PM. The arrangement is quite different to the arrangement used to determine the water content in any of the FPM gravimetric methods. It consists of a condenser, a short stem dry impinger, a long stem dry impinger placed in a water bath to keep the temperature between 20 °C and 30 °C and a condensable filter in the stated order, The sample deposit from the condenser down to the condensable filter front cover are recovered by rinsing with water into a bottle as the aqueous collection followed by acetone and hexane rinses into a separate bottle marked as organic rinse. The CPM filter with the organic and aqueous fractions is then processed as described in the standard. Usually, this is performed in an off-site laboratory to determine the inorganic content and the organic CPM fraction from the aqueous and organics rinses respectively, which are summed up to give total CPM. Behind the condensable filter are two more impingers, the first contains 100 g of water and the follow-up impinger filled with 200 g of silicon. The purpose of the impingers downstream of the method 202 section is to evaluate the water content of the exhaust.

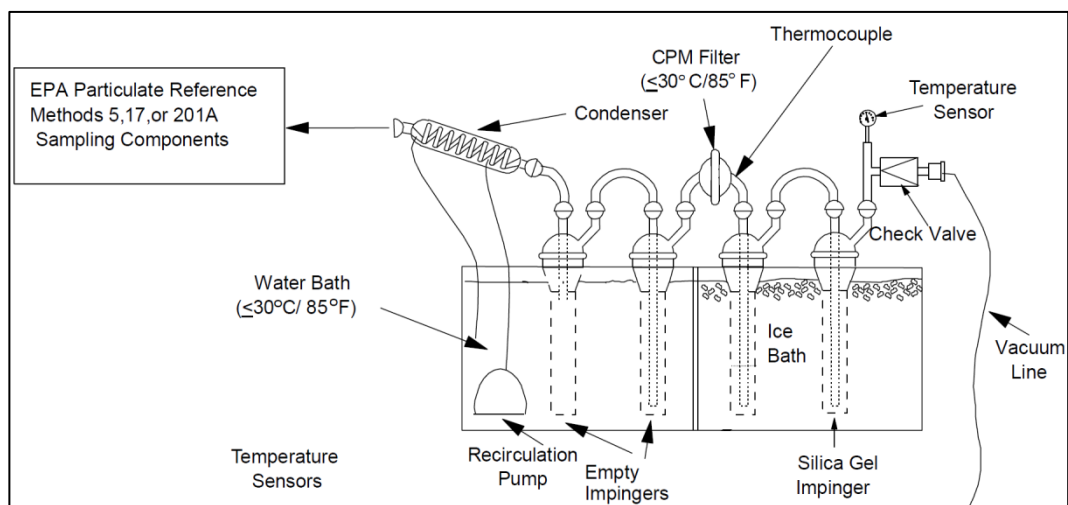


Figure 2-7: Schematic of EPA Method 202 PM Sampling Train [28]

2.3.1 Issues with the Gravimetric Protocols for Gas Turbine PM Measurement

The gravimetric reference method 5I is described as a simple, reliable, easy to maintain and relatively inexpensive method [49]. However the concerns are accuracy, repeatability and measurement time [50]. It is difficult to determine the accuracy, repeatability and reproducibility of the gravimetric method as there is no reference material, unlike gaseous instruments where certified span and zero gases traceable to a national standard are used for these checks. At best, repeatable and reproducible results are dependent on the accuracy of sample collection components (e.g., flow control, inlet aspiration, cut size, timer, etc.) and the filter weighing scale. This explains why regulators ensure that the sampling kit design and the sampling recovery steps as defined in the standards are implemented in order to ensure the quality of the results. In summary, the gravimetric techniques are defined with the consistency of the step involved rather than with the accuracy of the true mass concentration measurement in mind [51].

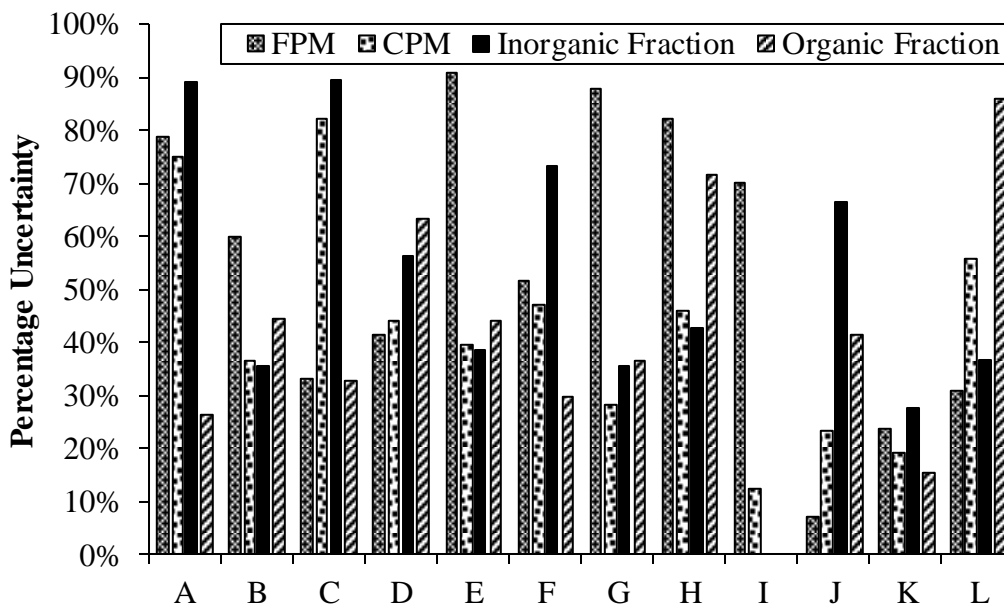


Figure 2-8: Uncertainties' of stack test data (EPA Methods 201/201A and 202) for combustion turbines and engines [40]

Label	Source	Operation Description	Heat Input (mmBtu/hr)	Fuel
A	Lakewood Cogeneration LP Cogen.	CT #1 ^a	1063	NG
B	Lakewood Cogeneration LP Cogen.	CT #2 ^a	972	NG
C	Lakewood Cogeneration LP Cogen.	CT #1 ^a	1091	#2 Oil
D	Lakewood Cogeneration LP Cogen.	CT #2 ^a	969	#2 Oil
E	Kamine Milford LP Cogen.	CT(SI on)/ WHRB off	407	NG
F	Kamine Milford LP Cogen.	CT(SI off)/ WHRB off	386	NG
G	Kamine Milford LP Cogen.	CT(SI on)/ WHRB on	433	NG
H	Kamine Milford LP Cogen.	CT(SI off)/ WHRB on	422	NG/NG
I	Bristol-Myers Squibb Cogen.	CT/HRSG on ^{a,b}	85	NG/NG
J	Bristol-Myers Squibb Cogen.	CT/HRSG off ^{a,b}	48	K
K	Trigen-Trenton Energy Cogen ^c	Engine#1/WHRB#1	204	DF/NG
L	Trigen-Trenton Energy Cogen. ^d	Engine#2/WHRB#2	215	DF/NG

Legend: NG = natural gas; K = kerosene; SI = steam injection; WHRB = waste heat recovery boiler; CPM = condensable particulate matter; CT = combustion turbine; HRSG = heat recovery steam generator; DF = dual fuel; and NA = not available.^a*Facility uses selective catalytic reduction technology for NO control.*^b*Cogeneration facility consists of one combustion turbine and a heat recovery steam generator with a duct burner.*^c*Cogeneration unit consisting of Engine No. 1 (#2 oil- and natural gas-fired) and Waste Heat Recovery Boiler No.1 (natural gas-fired).*^d*Cogeneration unit consisting of Engine No. 2 (#2 oil- and natural gas-fired) and Waste Heat Recovery Boiler No. 2 (natural gas-fired).*

Despite consistency checks of the gravimetric set-up, the associated variation from repeated measurement from the same engine diminish the validity of the measurements obtained using the instruments. As shown in Figure 2-8 the variability of up to 80 and 90 percent was observed for FPM and CPM respectively for three repeated test run of an engine under similar atmospheric condition. It can be argued that the atmospheric conditions influence combustion, thus the same amount of sample cannot be said to be captured within the same period at different times. A counter argument would be that the measurements are corrected to standard temperature and pressure and at worst a moderate variability should be observed. Again, this raises the question if the variability arises from the method's associated artefacts or engine related. In any case it again re-echoes the need for a reference material and automation of the process.

2.3.1.1 Filterable PM

Apart from the solid particles which the filter is intended to capture with a high degree of efficiency, some of the condensable precursor gases get trapped with the

filterable portion or in the filter membranes. Table 2-2 is a summary of factors affecting the reliability of filter weighing as the basis for determining PM.

Table 2-2 A summary of factors affecting the reliability of filter weighing as the basis for determining PM [50]

Effects causing the undesirable filter mass increase	Effects causing undesirable filter mass decrease
Absorption of water vapour by the filter material over time (highly dependent on filter material)	Physical loss of filter material, especially fibres, or PM due to poor handling
Absorption of reactive gases by the filter material or PM on the filter during sampling	Excessive loss of semi-volatile PM due to overheating of the filter during sampling
Filter conditioning at the post-sampling weighing being carried out at a higher end of the allowed range for temperature or relative humidity	Filter conditioning at the post-sampling weighing being carried out at a lower end of the allowed range for temperature or relative humidity

Turpin et al., [52] noted the adsorption of CPM precursor gases (e.g. ammonium nitrate, organics) onto filters is a source of bias during and/or after sample collection. The quartz filters as specified by the gravimetric reference methods to a greater extent eliminates nitrate and sulphate artefacts, but organic gases are still known to cause interference on this filter material [49]. Likewise, there is the possibility of sample contamination from atmospheric materials that can deposit on the filter when exposed. Negative bias, is also of great concern during sampling and removal of the filter from the housing as a result volatilisation of some of the adsorbed components. In addition, sample losses from poor handling are also a common occurrence [49]. An illustration of poor handling showing losses of captured PM emission is the tweezer markings as highlighted in Figure 2-9. Katz et al [53], Wang et al [54], noted that there are two scenarios that can cause volatilisation during sampling; (1) as a result of pressure reductions as the filter captures particle thus creating upset in the equilibrium between the deposited particles and the vapour in the exhaust; (2) from changes in temperature, relative humidity or composition of the incoming particulate during sampling. In a bid to eliminate bias associated with the removal of the filters, one

modification introduced in US EPA method 5I requires that the entire housing is weighed. This modification is difficult to implement as it increases the cost of obtaining duplicate samples which is typically employed unless the laboratory for filter post sampling and conditioning is located on test site which is rarely obtainable.



Figure 2-9: A photograph to demonstrate poor filter handling

2.3.1.2 Condensable PM

Though there has been a change in the method 202 to tackle its associated false positive bias, the improvements cannot be said to have totally eliminated its associated artefacts. In 2010, US EPA updated its 1991 version of Method 202. The key changes were the replacement of the water-filled impinger with dry impingers which still have to be placed in a water bath and the addition of a condenser and a CPM filter (see Figure 2-7). The issues that necessitated the update of the 1991 version were that it significantly over-stated the actual emissions of CPM as a result of the water in the impingers.

By bubbling the exhaust sample through the water-filled impingers, intense gas-liquid mixing is achieved, making it efficient at condensing and collecting CPM species [55]. This is a deviation from the way the condensable species coalesce into particles in the atmosphere. In the atmosphere CPM is formed by condensation, but in the 1991 version of method 202 is collected by both

condensation and scrubbing in the sample train CPM. However, it only covers the effects of cooling and totally neglects the dilution effects in the ambient air [55]. So, some of the exhaust components that would remain in the gaseous state in the atmosphere are forced into the condensed state.

As factors like photo-chemical reactions can affect the concentration of the precursor gases determine the condensable particulate, the final CPM concentration under ambient conditions does not necessarily correlate with the precursor gases source emission rate. From the CPM precursor gases (SO_x , NO_x , and soluble organic) sulphur dioxide (SO_2) was recognised as the CPM component causing problems under the 1991 version because of its high rate of reaction in liquid phase compared to gas phase. A portion of SO_2 which is not condensable oxidizes in the impinger water during sampling, converting to H_2SO_4 , which is a condensable particulate species. Aqueous transformation rates of sulphur dioxide to sulphate are 10 to 100 times as fast as gas-phase rates [7]. Richards et al [56] analysis of atmospheric reactivity studies summarized in the final edition of the Particulate Matter Air Quality Criteria Document [24], estimate the aqueous phase conversion rates of sulphur dioxide in the water filled impingers to be 2% to 6% per hour compared to 1% to 3% per hour conversion rate observed for dry, gas phase reactions. Thus, confirming that the reaction mechanisms for converting dissolved sulphur dioxide (sulphite ion) to sulphuric acid is different from the dry gas phase reaction that occurs under ambient conditions.

With the introduction of dry impingers, contact with water is substantially reduced except the exhaust water content. With this approach up to a 33% reduction of sulphate is achieved compared with the 1991 version of method 202 [56]. The results are very similar to artefact formation rates calculated based on sulphur dioxide solubility and a 4% per hour oxidation rate in solution. Despite these positives, the method still does not reflect the dilution effect that takes place in the atmosphere and as such the tendency to measure CPM that does not reflect the CPM levels from a source in the atmosphere cannot be categorically dismissed. However, method 202 remains the only standardised method for condensable

particulates and therefore is a reference for real-time instruments for CPM measurement.

2.3.1.3 Measurement Time

To ensure that the results are reliable and repeatable a minimum or target catch at a concentration or amount sufficiently larger than the minimum detection limits of the weighing scale is usually recommended. For instance, the US EPA method 5I [27] recommends the target catch must be no less than 3 mg . Thus, PM sources with very low particulate matter concentration in the stack would require a very large sample volume of the exhaust gas which leads to unacceptably long sampling times. The volume of effluent gas collected can generally be controlled by increasing the sampling time or by increasing the rate at which sample is collected. Consequently, the time required to acquire measurements for gravimetric filters is a function of the concentration and flow rate over the filters. If there is a reasonable estimate of the PM concentration from the source the target catch is collected by sampling the appropriate gas volume. Thus, a gas turbine source with an estimated PM emission mass concentration of 0.05 mg/m^3 targeting a catch of 3 mg of mass on the filter would require 20 hours of sampling time, if the exhaust gas is extracted from the effluent gas at a flow rate of 50slpm - a typical flow rate of the method 5 capacity. Adding the time for offline filter weighing, this can run into days if the laboratory for filter weighing is off site. Then, if repeat testing is required the whole measurement process can easily run into weeks and months.

2.4 Requirements for New Gas turbine PM Measurement Instruments

2.4.1 Correlation to Gravimetric Method

Presently, the ultimate goal for any candidate particle instrument for gas turbine PM emission is to correlate with the total PM measurements from a reference gravimetric protocol since they actually define the PM. Though application of any of the reference methods is dependent on the local country legislation, the most frequent request for guarantees is for total PM. It is therefore important that the instruments can make measurements at the temperatures that define filterable and condensable PM emissions of gas turbine. Thus it is important for the temperature

conditions of the sensing zones of the real-time PM be the same as temperature conditions of the heated box for the filterable fraction of the PM and the impingers' temperatures for the condensable PM. The reference gravimetric protocols generally implemented for filterable PM measurement from gas turbine mostly specify the sample collection temperature to be less than 170 °C but greater than 100 °C. This is also the standard line temperature for continuous emission monitoring systems (CEMS) for gaseous emission, thus making integration with PM emission sampling system a possibility. This would be beneficial as it would help reduce the operating cost of emission measurement from a gas turbine.

2.4.2 Response Time

A desired PM measurement for stationary gas turbines should have a quick time response in order to capture fluctuations or events that offline methods might miss. Gravimetrically determined PM mass concentration method has been criticised for the amount of time required (usually in the region of hours) to obtain enough samples for analysis from a very low PM emitting engine. Currently, the engine stabilization time during engine testing for steady state measurements from idle to base load with minimal impact to Performance Acceptance Tests (PAT) schedule is 10 minutes, therefore any additional stabilization time could potentially result in significant additional test costs. As such, transient measurements from light-up to base load and from base load to engine shutdown could be made which would enable a better understanding of the time dependent performance of engines and emission control systems. This would give engine manufacturers the necessary engine PM emission data to provide accurate PM emissions measurements for developing accurate start-up and shut down emission guarantees.

2.4.3 Lower Detection Limit (LDL) and Minimum Upper Range (MUR)

Sensitivity, of the real-time instrument is another important factor that must be considered for real-time PM instruments to meet the PM measurement needs of gas turbine engines. Balances with +100 µg sensitivities are adequate for high filter catch, but special electro-balances with sensitivities as low as ±1 µg are

needed for a low PM catch. The instrument should be sensitive enough to measure PM emissions of particle mass concentrations of $100 \mu\text{g}$ or less [57]. Likewise, with technological advancement in engine, fuel and emission control all aimed towards a zero emission guarantee, lower detection limits of the order of $1 \mu\text{g}/\text{m}^3$ is desired. The LDL range of interest envisions future PM emissions limits on natural gas would be lower than the current emissions PM guarantee practice. At the upper end, a minimum upper range of $500 \text{mg}/\text{m}^3$ is desired to allow PM measurement within the US EPA's upper allowable limit for TSP (for inlet PM measurements).

2.4.4 Particle Cut-off Size

Assuming land based gas turbine have similar emission performance to aero gas turbine, at the very least the new PM measurement instrument should be able to measure particles that are less than one micron in size. Ideally, the instrument should not have a particle cut-off limit as TSP is still a regulated/permited cut-off limit in some jurisdictions. However, it is imperative that the instrument can measure particles that are 10 micron or less and 2.5 micron or less, as these particle cut off sizes are the widely regulated /permited cut-off limits, as a minimum.

2.4.5 Traceable Measurement

Traceability refers to the ability to calibrate the system to a primary standard, which makes it possible to determine the repeatability, reproducibility and accuracy of the instrument. Unfortunately, no standard reference calibration material or procedure has been developed for particulate from combustion sources. Therefore, it is essential at the very least that the instrument has a manufacturer/internal calibration protocol as it is compulsory that all instrumentation must have a minimum of a manufacturer's calibration protocol [57]. Otherwise, ideally it should have a traceable calibration protocol to an industry standard.

2.5 Fast PM Instruments for PM Emissions

In general, the working principle of the fast PM instruments is based on passing the emission samples to be evaluated through the instrument sensing zone to generate a signal that is captured by a detector which relates to the corresponding properties of the particles analysed. Table 2-3 presents a summary of the established as well as recent instruments in the field of particle emission measurement. These instruments have been classified into three categories based on the measurement technique and the parameters measured.

1. Automated filter based instrument for mass concentration measurement
2. Particle size-resolved instruments
3. Chemical-speciation instrument

Table 2-3 Summary of Fast Particulate Measurement Instrument [7, 58]

Measurement Instrument	Principle	Measured Property	Response Time	Range
<i>Automated Filter Based Instruments For Mass Concentration Measurement</i>				
Tapered Element Oscillating Microbalance	oscillatory inertial microbalance	Mass	2sec	$5\mu\text{g}/\text{m}^3$ to mg/m^3
Beta Guage	Beta attenuation	Mass	1min	0.1 - 10mg
Piezoelectric Microbalance	Resonance frequency	Mass	1	
<i>Particle size-resolved measurements</i>				
Scanning mobility particle sizer (SMPS)	Electric mobility, Condensation particle counting,	Size, Number	16sec	$<1\mu\text{m}$
Cambustion DMS500	Electric mobility, Electrical detection	Size, Number	200ms	$<1\mu\text{m}$

Dekati ELPI	Impactor principle, Electrical detection	Size, Number	1sec	<10 μ m
Dekati Mass Monitor	Electric mobility, Impaction, Electrical detection	Size, Number, Density	2sec	0 – 1.2 μ m
Optical Particle Counter	Light Scattering	Size, Number	secs	0.2 to 30 μ m
Aerodynamic Particle Sizer® Spectrometer	Time of Flight	Size, Number	secs	0.3 - 20 μ m
<i>Chemical-Speciation/Specific Monitors</i>				
Micro Soot Sensor (MSS)	Photoacoustic absorption	Soot	1sec	0.001 - 50mg/m ³
Laser-Induced Incandescence	Laser-induced incandescence	Refractory Carbon	0.05sec	0.2 - 20 μ g/m ³
Multi-angle absorption photometry	Absorption photometry	Black Carbon	2min	<100ng/c m ³
SAE Smoke Meter	Light extinction and opacimeter	Soot	mins	N = 0 .. 100
Fourier Transform Infrared (FTIR)	Absorption spectra	Precursor Gas Speciation	Sec to Min	
NIOSH 5040 [59]	In-Situ Thermal/Optical Carbon Analyser	Organic & elemental carbon of FPM	5min - 2 hours	~ 0.2 μ g/m ³

2.5.1 Automated Filter Based Instruments Measuring Mass Concentration

The methods described here have similar features to the reference gravimetric method as particles from the exhaust gas stream for analysis are collected on a filter which is weighed beforehand and afterwards except that the process is automated with faster time-resolved mass measurements. In Beta gauges the filter

is placed between a β -emitter (e.g. ^{85}Kr) and a radiation detector. As particles deposit on the filter an increase in absorption of the radiation experience from which the measure of the mass of particles is evaluated [60]. The BAM-1020 manufactured Met One Instruments is an example of an off the shelf instrument implementing this measurement principle. In Piezo-balance the particles are collected on the surface of oscillating quartz crystal with the corresponding change in resonant frequency measured and related to the particle mass [61].

The other instrument under this category is the Tapered Element Oscillating Microbalance (TEOM) now manufactured by Thermo Scientific, [62]. Particles are deposited on a filter which is placed on the narrow end of the tapered tube, which is free to oscillate. The tube frequency of oscillation changes as particle materials deposit on the filter from which the particle mass deposit is evaluated.

The basic issue applying these instruments for gas turbine PM measurement is the temperature at which the gas turbine PM sample is collected. The instruments are limited in their sample temperature operating range. With the TEOM the detecting resonance frequency is distorted above 50 °C, likewise the absorbed radiation of the Beta gauge. This is contrary to the 160 °C specified for gas turbine PM sampling. However, they have been shown to correlate with atmospheric aerosol measurement determined gravimetrically thus their acceptance as equivalent methods for measuring atmospheric PM10 and PM2.5 mass concentration [63, 64].

2.5.2 Particle size resolved Instruments

The particle size and number instruments as listed in Table 2-3 can be classified into three groups based on the measurement principle combined as follows;

1. Optical Particle Counter (OPC) and the Aerosol Particle Sizer (APS) – This class of instrument apply a single technique to simultaneously measure particle size and count the respective number in each size class.
2. SMPS, DMS500 and Delkati ELPI – These instrument combine two measurement principles; one for particle size classification and the other principle for particle counting.

3. Dekati Mass Monitor (DMM) – This instrument combines three measurement principles; two different principles for particle size classification from which particle densities are evaluated in real-time and the third measurement principle for particle count.

The combining measurement principles can exist as stand-alone instruments. Figure 2-10a, is a schematic of a differential mobility analyser (DMA) that is a stand-alone instrument used for particle classification based on the widely used electrical mobility technique and Figure 2-10b is a representation of a cascade impactor that classifies particles into sizes using the principle of inertial collection by impaction. For particle number count, the condensation particle counter (CPC) and electrometer are the two widely used techniques that also exist as stand-alone instruments.

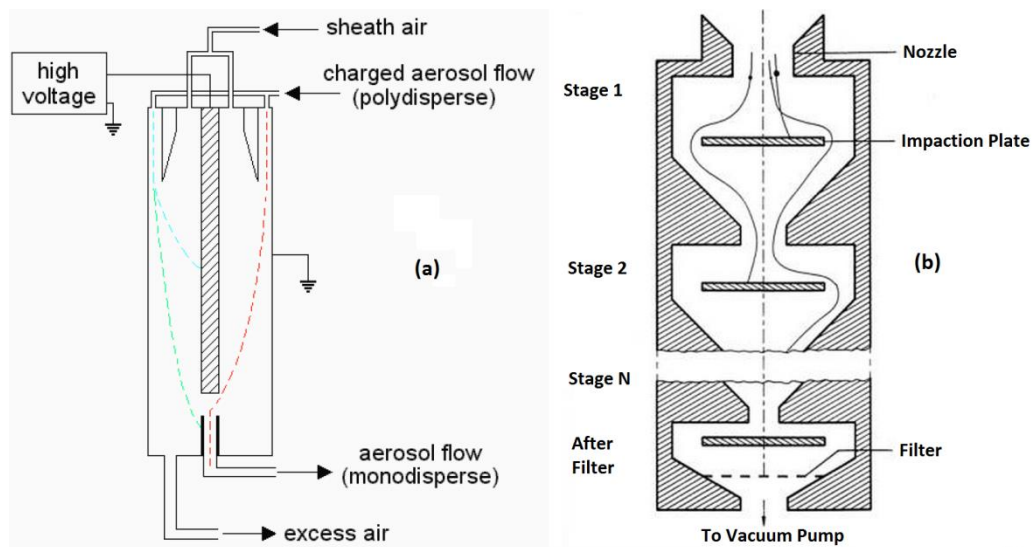


Figure 2-10: Schematic of differential mobility analyser (DMA) and an impactor [65, 66]

Electrical mobility sizing is applicable to particles smaller than one micron as the particles need to be charged before being separated based on electrical mobility. Insufficient charge is highly feasible for particles greater than one micron, thus they cannot be classified correctly [45] using this technique. To implement this technique, the major components are; 1) a charger to impart an electric charges to the particles 2) a classifier that separates the particles by acting on their electrical charge and mass. In the electric field of the DMA schematic shown in Figure

2-10a sheath air flows down the column acting as a barrier through which only particles with a balanced electrostatic force and drag forces can pass particles. These are highlighted by the red dashed line cross into the outlet tube in the chamber [29, 67]. By placing a CPC or an electrometer downstream of the classifier the monodisperse concentration is be counted. This combination of the DMA with the CPC forms the widely known Scanning Mobility Particle Sizer (SMPS). It is the first particle sizing instrument using the electrical mobility principle and as such it is used as a reference for other particle sizes. Thus, to have a wide range of particle size information the electrode voltage is adjusted to select different particles of different mobility to exit the classifier. Consequently, the SMPS has a time resolution of 16 seconds to scan for a selected size thus 1-5 minutes to scan for a series of sizes to generate an adequate data set for analysis.

Instruments applying the electrical mobility principle with better time resolution have been developed in recent years. Common in this group is the Engine Exhaust Particle Sizer (EEPS) manufactured by TSI, Differential Mobility Spectrometer (DMS500) manufactured by Cambustion, Fast Aerosol Particle Emission Sizer (FAPES) manufactured by GRIMM. DMS500 and EEPS can be described as a large DMA, but instead of ramping the voltage, it has a fixed voltage and a series of electrometer rings on one of the electrodes to count different particle classes simultaneously. FAPES is basically multiple SMPS setup with each SMPS dedicated to a particle size scan. A fundamental difference to the SMPS is the charging of the particles. The DMS500 and the EEPS use a corona discharge, while the SMPS uses a Kr-85 radioactive source to neutralise the charge. With the Kr-85 radioactive source the charge distribution (i.e. the percentage of particles charged as a function of size) is very well defined however, the majority of the particles carry zero charge. In contrast corona charger charges are distributed as a function of size, thus particles with lower electrical mobility can travel farther than those with higher electrical mobility. Thus, the EEPS and the DMS500 use this idea to stack up a series of electrometers in the travel path of the particles so that they deposit on the electrometers according to their sizes.

Impactors use the principle of inertia to retain and/or separate particles from an aerosol stream on an impaction plate according to their aerodynamic diameter. Impactors comprise of a set of jets (circular or rectangular) well placed above a stack of impaction plates that are vertically spaced. The plates are arranged in a vertical order, such that when the exhaust gas flows into the devices, particles of lower aerodynamic size are able to follow the streamline flow around the plates while the larger particles collect on the impaction plates. It is the fundamental technique applied in the newly developed High Temperature Electrical Low Pressure Impactor (HT-ELPI) and the DMM, manufactured by Dekati, to generate a particle size distribution. In brief, the particles entering the instrument are first charged and then separated by impaction on the vertically spaced impaction plates which also doubles as electrometers to frequently count the particles collected over a defined period.

The CPC and the electrometer are well established for counting aerosol particles in real-time and at high time resolution. The CPC counts particles by condensing butanol droplet on the particles in the supersaturated environment to make them swell to optically detectable sizes by light scattering when passed through a beam of light. Several models are available which detect particles as small as 3 nm model (TSI 3025A, TSI Inc., Shoreview, MN, USA) with a response time of less than 5 seconds. Meanwhile, electrometers are used to measure the number concentration of monodisperse aerosol by using the change in the electrical current, of a collection of charged particles on an electrically-isolated; high-efficiency filter that relates to the number of particle deposit.

The commonly used measurement principles that simultaneously measure the particle size and number density are light scattering [68] and the time of flight [69, 70]. The optical particle counter (OPC) is a typical example that illustrates the application of light scattering. The light scattering technique as represented in Figure 2-11 is based on theory that the intensity of light scattered when passed through a light beam, relates to the particle size while the number pulses detected equates to the number of particles of the analysed sample. With light scattering a wide particle range of particle size usually in the region of 0.2 to 30 μm can be

detected. An example of an OPC found off the shelf is the GRIMM miniWRAS, Airing, Germany.

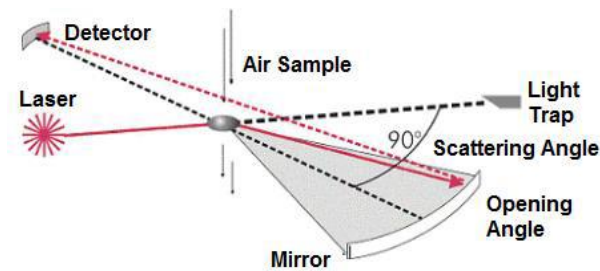


Figure 2-11: Schematic of light scattering technique [71]

For the time-off-flight measurement technique, it is based on the fact that the rate particles gain speed when in a vacuum is related to the particle size. Thus in practice the particle size is determined from the time of flight over two detectors usually light beams positioned over a distance in the vacuum. Thus, the particle count is determined from the number of pulses received by the detectors. A common example is the Aerosol Particle Sizer (APS) [70] manufactured by TSI.

A match of the instruments of the instrument specifications with the desired requirements for gas turbine PM measurements give an indication that all the particle-size resolved instrument are sensitive enough to measure concentration as $1 \mu\text{g}/\text{m}^3$ [71]. EEPS, DMS500 and ELPI can measure samples in an exhaust stream at the temperature required for filterable fractions of gas turbine PM particulates (between 150°C and 180°C). The HT-ELPI, APS and OPC can detect an upper particle size equal and greater than $10 \mu\text{m}$ and all the instruments can detect particle of approximately 5 nm in size. The instruments are usually calibrated against traceable monodisperse distribution of polystyrene latex spheres and/or other monodisperse particle from a combustion source as measured by a standard reference instrument. After years of research the procedure for calibrating electrical mobility instrument has only been recently documented as standard practices using the DMA and electrometer (faraday cup aerosol electrometer) as the reference instruments for calibration [72]. In summary the CPC is traceable [73, 74] to a standardised electrometer while the electrometers are traceable to electric current calibrations.

However, the issue with the entire particle size resolved instruments is restriction placed as a result of the specification which is determined by the limitation of the measurement principle they deploy. Thus, dilution is often required to reduce the PM emission concentration to meet the instrument specifications. For instruments like the SMPS, APS and OPC the fundamental purpose is to reduce the sample temperature while for the EEPS, DMS500 and ELPI it's to avoid water condensing inside the instrument. Also for combustion sources with the potential of high particle concentration dilution is recommended to reduce the frequency of instrument maintenance. Another issue with these set of instrumentations is that their direct read-out is not quoted in particle mass concentration a preferred parameter for gas turbine PM measurement. To facilitate these instruments generating mass from particle size distribution measurement a density of the particle is required.

2.5.3 Chemical Speciation Instruments

As listed in the Table 2-3, this section covers instrument with the capacity to measure individual components of the total particulate emission. However the review is limited to instruments which measure soot - the major component of PM emission and instruments that can simultaneously detect and measure a range of inorganic and organic components of the CPM.

2.5.3.1 Carbon Speciation instruments

2.5.3.1.1 Carbon Burn-off Analysers

This technique is used to partition the carbon content of particulate into elemental and organic carbon. An example of a widely used instrument in this category is the Model-4 Semi-Continuous OC-EC Field Analysers manufactured by Sunset Laboratory. This instrument speciate sample collected on a quartz fibre filter into organic and elemental carbon using a thermal-optical technique in a semi continuous manner. It proceeds in two stages using temperature, atmospheric control, and continuous monitoring of filter transmittance to distinguish between organic and elemental carbon. The first stage determines organic carbon. The filter sample is placed in an oven where it is simultaneously subjected to helium gas with an increase in the oven temperature to 850 °C. The vapour generated is

channelled through a manganese oxide bed heated to 1000 °C to oxidize the evolved carbon to carbon dioxide (CO₂) and transferred into a self-contained non-dispersive infrared (NDIR) detector. The second stage to determine the elemental carbon then follows. It begins with a reduction of the sample oven temperature for the introduction of an oxygen-helium mix before an increase in the temperature to 940°C and then the process is repeated with a new set of sample. This method can also be carried out off-line using the NIOSH 5040 [59] standard. In this case, the quartz filter sample is transferred to a laboratory where the same approach as with the semi continuous measurement is carried out using the Sunset Model-4 Semi-Continuous OC-EC Field analysers.

This class of instrument or measurement procedure meets the desired requirements for real-time particulate measurement from a gas turbine. The instrument results are traceable as CO₂ gas standards are used to calibrate the detector. Further calibration checks are achieved using filter blanks and various concentrations of traceable sucrose. They have a minimum quantifiable level of 0.5 µgC/m³ each for OC and EC. The procedure also has steps in place to ensure that there is no interference between the portioned components. To deal with this, light transmission through the filter is used to correct for charring (pyrolysis) of OC which may occur during the first analysis step. Also an identical quartz-fibre filter is exposed behind an absolute particle filter, allowing a correction for the adsorbed OC vapour artefact. Despite these positives that favour its application for gas turbine carbonaceous component of a gas turbine, its response makes it unattractive as gas turbine transient PM measurement cannot be observed as the response time could run into days if the offline approach is adopted. However, recent researches are aimed at taking advantage of its accuracy and repeatability to make it a calibration standard for other real-time elemental carbon analysers. Therefore, it is an important instrument for gas turbine particle research.

2.5.3.1.2 Filter-Based Elemental Carbon Analysers

This group of instruments evaluates particulate emissions based on the blackness of a filter onto which particles have been deposited. These tests measure the reduced filter reflectance using optical procedures to determine the absorption of

the blackened filter paper acknowledged to be the primary effect of the black carbon deposits. Evidence that these instruments quantify only black carbon can be found in Rye et al. [75] and Northrop et al. [76]. The two main examples of continuous measurement instruments implementing this absorption detection technique with the parameter read out as mass per unit volume are the “aethalometer” and the “multi angle soot sensor (MAAP)”. The “aethalometer” measures blackening in a continuous manner from the light attenuation through a quartz fibre filter [77]. For the MAAP [78, 79], the filter samples are continuously determined at several angles by simultaneously measuring optical absorption and scattering of light. The detection limits for the multi-angle absorption photometer can be as low as low as 100 ng/m^3 for a 2-minute sample and 20 ng/m^3 for a 30-minute sample [80]. Despite its fast response time when matched against an average PAT schedule of 10 minutes [57] it would be difficult to obtain statistically reliable data during mid to high power engine testing conditions. In addition these instruments are not suited for engine transient conditions.

Though the focus here is on continuous measurement instruments, it is worth mentioning that filter blackening technique has traditionally been used to regulate PM emissions by measuring the absorption on an empirical scale. For example, commercial aircraft have to report their smoke emissions based on the Society of Automotive Engineers (SAE) Smoke Number (SN) standard, ARP1179D [81], which states the filter deposit absorptions on an empirical scale of 0 to 100. In a similar fashion the Bacharach number which has a scale of 0 to 9 is contained in the International Standard Organisation standards for emission measurement from industrial gas turbines 11042 – 1:1996 [48]. These two procedures require the filter deposit to be analysed offline with a Reflectometer to determine the reflectance of the filter paper before and after deposit have been collected in the case of the SAE standard. For the Bacharach number, the filter deposit is visually compared to a grey scale to resolve the smoke number. This creates room for errors since the measurement is based purely on human judgement; hence the testing encourages a large number of samples to minimise error in measurement [63].

The SAE SN is considered a relevant technique since it is still a basic standard implemented in the aviation industry and most gas turbine producers and users have these instrument facilities on site. Meanwhile, it is the basis of the approved method by International Civil Aviation Organisation (ICAO) and the Federal Aviation Administration [82] to estimate mass emissions of soot from aircraft engines. Thus driven by these factors and that smoke number only provides empirical information on soot particulates, researchers have conducted a variety of studies to relate SN data to soot mass concentration. Details of these studies are contained in sections 2.8.4 of this thesis.

2.5.3.1.3 Non-Filter Based Elemental Carbon Analysers

Laser induced incandescence (LII) and the use of acoustic signals are common measurement principle under this instrument category. The laser-induced incandescence (LII) technique measures only the non-volatile fraction of PM emission by evaluating the incandescent [83] from the particles when heated using pulsed laser [84]. The heating temperature is high enough to separate the volatile particle components as they will be evaporated while the non-carbonated particles would undergo sublimation or evaporation. Sublimation/ evaporation leads to underestimation of mass therefore flux needs to be timed to source. With acoustic sensor, the measurement principle is based on the resulting sound wave produced by the surrounding exhaust gas of the elemental carbon when it absorbs light. By focusing a chopped light beam on an exhaust sample gas in a gas cell the elemental carbon absorbs some of the beam thus producing heat which results in a pressure pulse that is detected with a microphone and relates to the mass of the absorbing carbon. For optimum sensitivity the measurement cell and the chopper frequency are synchronized so that the sound wave resonates with the chopper frequency to produce a standing wave.

Examples of instruments that apply these techniques are the LII 200 and 300, manufactured by Atrium and Micro Soot Sensor (MSS) manufactured by AVL. They have a detection limit of less than $1\mu\text{g}/\text{m}^3$ and measure particulate samples in an exhaust stream with a temperature above 150°C . Also, with a response time of less than a second the instruments can potentially be applied for elemental

carbon measurement of transient conditions of an engine. These instruments have been extensively researched on aero engines over the past 5 years, with studies now focused on having a standardised calibration process using the NIOSH 5040 standard.

2.5.3.2 Continuous Multi-Component Analyser

The focus of the instruments under this category is the volatile components of the particulate emissions. The two attractive continuous measurement techniques are the Fourier Transforms Infrared (FTIR) spectroscopy and the Aerosol Mass Spectrometer. FTIR is a technique that is based on interaction between infrared radiation and a sample that is solid, liquid or gas. The Aerosol Mass spectrometer (AMS) approach basically involves vaporisation and ionisation of the particles from which the various species in the particle sample are detected based on their mass charge ratio. The mass charged ratio are further analysed to detect the different species with their mass concentration evaluated. Both the FTIR and the mass spectrometry are certified techniques for simultaneously detecting and measuring chemical components at the temperature presently implemented gravimetrically to measure condensable particulate. However, these instruments are mostly used for research studies as regulators have been slow to adopt them either as a result of their bulk size or the amount of time it requires to analyse the mass spectra to minimise uncertainties. This ultimately translates to huge financial commitments.

Each pure chemical component has a unique IR absorption in the frequency range of the infrared spectrum thus infrared in simple terms is a fingerprint for detecting compounds. Miller et al [85] demonstrated the unique IR of a range of inorganic compounds including nitrates and sulphates. To simultaneously detect and quantify multiple components in a sample the FTIR instrument encodes all, the frequency of the infrared spectrum using an interferometer into a single beam before passing it through a gas sample. The signals are then unbundled and decoded using the well-known mathematical technique called the Fourier transformation. The next step is to compare the transmitted or absorbed spectra of the sample with the various transmission or absorbed spectra of the pure

components of interest to determine the concentration of the component in the sample. One of the primary advantages of the FTIR technique is that infrared spectroscopy causes no damage to the sample. However, the common challenge using the FTIR is the interference that could occur when components having similar transmission and absorption are present in the sample. Thus, it requires very sensitive and properly tuned instruments to differentiate the interfering components which escalate expenses, and time and labour.

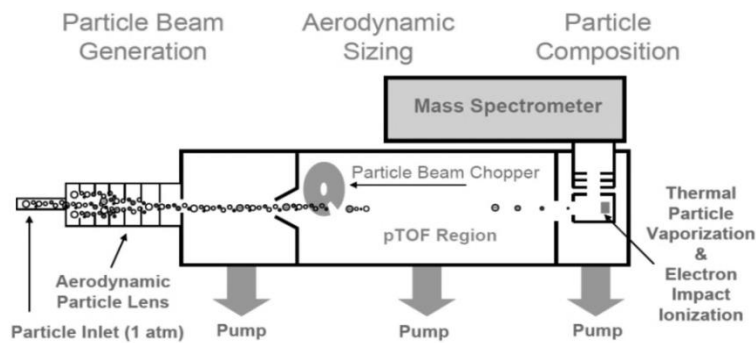


Figure 2-12: A schematic diagram of the commercially available Aerodyne Aerosol Time of Flight Mass Spectrometer (AATOFMS) [86]

An example of instrument applying the aerosol mass spectrometer is the Aerodyne Time-of-Flight Aerosol Mass Spectrometer (TOF-AMS) models manufactured by Aerodyne. The basic concepts of the operation can be classified into five discrete stages which include: sample introduction, time-of-flight principle for particle size measurement, vaporisation, ionisation and mass spectrometry which largely determines how the instrument operates. Sample introduction into the instrument is a crucial aspect of the instrument measurement process as it is important to have the particle in the exhaust particle entering into the instrument as a particle beam. This is achieved using aerodynamic lens systems [86] after which the exhaust sample undergoes supersonic expansion where particles move out of the gas stream to form particle beam as a result of their greater mass. Then similar to the APS, the particle sizes are determined using two photomultipliers to in a vacuum to determine their time of flight. The next stage is the vaporisation and ionisation stage. The TOF-AMS employs thermal vaporisation and 70eV electron impact for ionisation. With a synchronised chopper, pulse of ions is generated for continuous measurement.

2.6 Research Hypotheses

From the highlighted instruments in Table 2-3 with the subsequent details contained in the subsections of section 2.5, it is evident that there is no single instrument that can measure both filterable and condensable PM emissions of gas turbine. However, the need to have the instrument data readout as mass concentrations coupled with an overview of the gas turbine PM characteristics and the desire to have the instruments analyse samples continuously, unfolds how correlations with the total PM mass concentration measured by the gravimetric compliance method can be developed. Figure 2-13 illustrates this hypothesis.

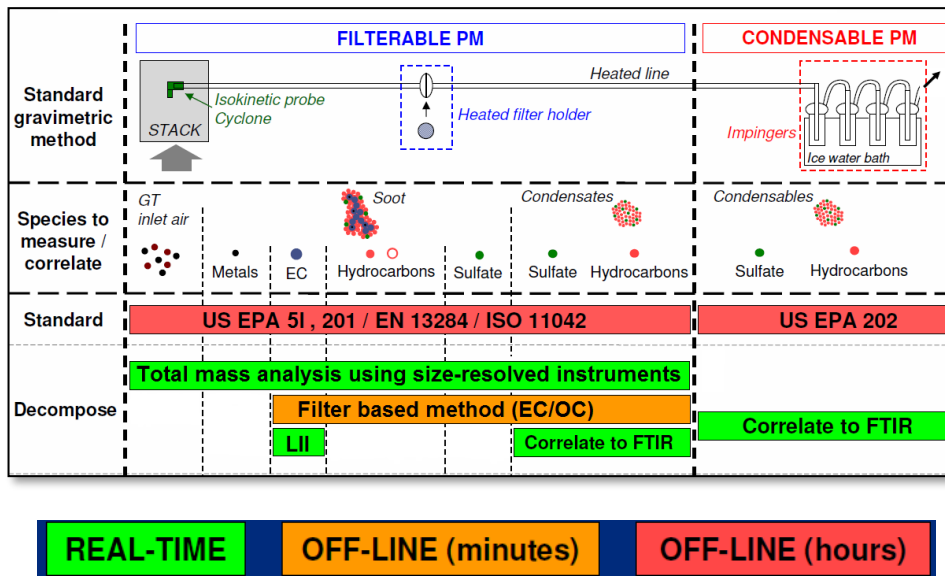


Figure 2-13: Chart Showing How Correlations between Real-Time Instrument Gravimetric Methods were studied

A recap of the characteristics of the gas turbine particulate shows that the chemical composition of the filterable particle emission is mainly carbonaceous with a small fraction of various metals. Similarly, the condensable PM has been shown to contain many chemical components that can be classified into three main groups; organic carbons, sulphates, ammonia nitrates or nitric acids. With respect to the physical characteristics of the PM they contain particles of different sizes and shapes. Consequently, the proposed approach as illustrated in Figure 2-13 is to use instruments that measure different components of the total PM, which can be summed up and then correlated to the TPM from gravimetric. Therefore the summation of measurements from instruments that measure

different components of the filterable portion should correlate with the gravimetric filterable measured, likewise the condensable PM.

2.7 Sampling System for Instrument Correlations

Like the gravimetric reference protocols, the continuous PM instrument summarised in Table 2-3 rely on the extraction of representative exhaust samples and a gas sampling system for continuous supply of exhaust sample during testing. It has been shown that the sampling system is of great importance as it can have a big impact on the exhaust samples that reach the instrument. Thus, it is important that the exhaust sample from the combustion source is extracted and distributed to the comparing instrument simultaneously, so that the instrument particles analysed must have been subjected to the same physical conditions. Therefore, this section details and reviews sampling system related sampling systems found in the literature for instrument comparisons which have thus guided the decision making of the sampling system design for this study.

2.7.1 Extraction of Representative Sample

The first crucial step in the particulate emission measurement and analysis is the continuous extraction of a representative particulate sample. Particle transformation can occur through volatilisation or crystallisation, which can be misleading about original particles at the sampling point. To avoid altering the physical and chemical state of the PM in the exhaust gas at the extraction point, the continuous pulling out of samples from the exhaust stream has to be done in a way that do not disturb the dynamics of the exhaust flow. This is important given that the inertia of particle in exhaust stream differ from that of the exhaust fluid. As a result, one of the basic requirements when implementing a gravimetric protocol is the emphasis on isokinetic extraction. This simply means that PM emissions and the exhaust flow in which they are entrained should not be changed in velocity or direction at the point of extraction into the sampling system. However, the need to monitor the extraction velocity to ensure isokinetic extraction as required by the gravimetric protocols has is downplayed at the engine exhaust plane considering the Stokes number of sub-micron particles in exhaust flow of the magnitude from gas turbine engines [87].

The tendency of submicron particles to maintain the streamline path entry into the extraction nozzle is negligible given that the Stokes number is far less than one [87]. Stokes number (Stk), characterises the curvilinear motion (bending of streamlines due to curved tube flow, flow around obstacles or bends) of particles suspended in a fluid flow. Low Stokes number means that particles maintain a streamline path, and not adhere to tube walls while the high Stokes number describes particles that do not change direction, consequently in bends in transport tubes, such particles more likely to impact with tube walls, rather than streamlines at bends. Thus, maintaining best practices for the probe is enough to extract samples isokinetically [87]. First, the geometry of the extraction nozzle tip is important as it should be shaped to prevent particles from being deflected from their actual path. The nozzle tip must be pointed directly in the upstream direction, in order not to perturb the streamlines in which the particulates are entrained. In this manner, particulate extracted remains representative considering the fact that instantaneous velocity fluctuations in the turbulent flow of gas turbine exhaust are generally within a tenth of the mean, which averages to zero [29, 87].

2.7.1.1 Dealing With Exhaust Sample Conditions and Instrument Requirements

Another important factor that must be considered when measuring PM with the continuous instruments is the need to ensure that the exhaust sample condition is within the instrument requirements, otherwise there would be a risk of instrument damage. The exhaust sample conditions of concern to the instruments are one or all of the following; (1) exhaust temperature, (2) exhaust water content and (3) high particle concentration. Studies have shown that dilution with a preheated inert dry gas as rapidly as possible is the best approach to address the concerns. It controls the condensation and nucleation processes which can occur if left to cool [88]. Thus, when comparing real-time instruments with these restrictions with a reference gravimetric method, the common approach found in literature [45, 46, 89] is to dilute the exhaust sample before distributing to the instruments. The negatives of this approach on an exhaust stream with very low particle concentration is the resulting expense with respect to the amount of time required to collect a significant amount of particle that could be weighed with a high

degree of confidence with the gravimetric method. Moreover, it does not adhere to the gravimetric protocols which discourage dilution of the exhaust sample in any form.

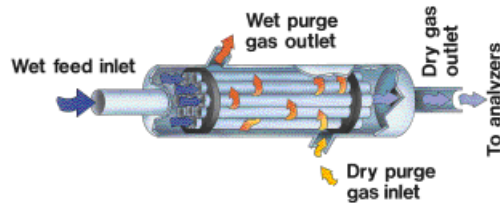


Figure 2-14: A Schematic of a Nafion Dryer [90]

An alternative to dilution where temperature and the exhaust water content are the only concern using a real-time PM instrument is to reduce the water concentration of the exhaust gas. A widely used device is the trademarked Nafion dryer [90] which operates like a shell-and-tube heat exchanger (Figure 2-14) to reduce the water content in an exhaust sample. The Nafion tube is made of a copolymer material made of tetrafluoroethylene and perfluoro-3, 6-dioxa-4-methyl-7-octene-sulfonic acid. Exhaust sample is passed through the Nafion tube to a counter-flowing purge gas – compressed nitrogen. Water molecules permeate through the Nafion tube wall, evaporating into the purge gas stream. The water concentration differential between the two gas streams drives this reaction, quickly drying the exhaust gas.

The working temperature condition of the Nafion dryer goes up to 150 °C Celsius within the range specified for gravimetric testing, for gas turbine particulates. However, the immediate concerns having this device upstream of a gas particle size-number distribution instrument is the possibility of particle losses and transformation inside the shell tubes. Johansson [91], investigation into particulates from a GDI-engine operating at low load showed that the sample loses within a Nafion dryer are negligible. Despite this observation, there is need to investigate this result for gas turbine particulate as more studies is also necessary to verify this observation.

2.8 Real-time Instrument Correlation with Gravimetric Reference Methods

This section reviews study aimed to correlate the hypothesised instruments detailed in section 2.6 and as illustrated in the Figure 2-13. Firstly, there are no studies to the knowledge of the author that have compared real-time CPM fraction measurement instruments with US EPA method 202. So, this section focuses more on the review of the FPM fraction as the CPM correlation study is an entirely new area of study.

2.8.1 LII Correlation with Filterable Fraction of Gravimetric Measurement

LII measures only refractory black carbon as detailed in section 2.5.3.1.3. The instruments still fall short of the PM measurement requirements because they are unable to quantify the metallic particles if present and the volatile organics portion of the PM emitted [1]. In addition the instrument is calibrated using a black body to measure absolute incandescence intensity and an extended source of known radiance to interpret the measured LII signals instead of particles with known soot volume fraction. Nevertheless, the instruments have shown precision in measuring the carbonaceous non-volatile organics [83, 84]. The extent to which it underestimates gravimetric measurement thus depends on the ratio of the black carbon composition of the particle matter emitted as demonstrated by Smallwood [92] and Petzold et al [46]. Smallwood et al [92] reports a ratio of 0.83 between the LII mass and gravimetric mass for a methane generated PM using an inverted flame burner set at EC levels > 83%. The ratio significantly increases to 0.98 between LII mass concentration and the EC fraction of NIOSH 5040 consistent with the EC level setting of the inverted flame burner. Meanwhile, Petzold et al [46] using a Hot End Simulator (HES) to mimic the behaviour of a turbine section in a gas turbine observed a ratio of 0.24 between the LII black carbon mass concentration and the total carbon fraction of NIOSH 5040 against the 0.54 – 0.85 EC levels settings for the HES. However, the low ratios were possibly from super-micron particles from random shedding (sampling artefacts) reportedly detected and known to add to discrepancy between filters and real-time analysers [46].

2.8.2 PSD Derived Mass Concentration Correlation with Filterable Fraction of Gravimetric Measurement

To determine the mass concentration from particle size resolved measurements [41], the density of the particulates is important. Until recently, researchers have often justified their assumptions of a unit density [43, 80, 93, 94] or the bulk density of carbon (1500–1900 kg/m^3) [95, 96] to calculate the particle mass concentrations. The implication of this assumption is that it ignores the poly disperse nature (with respect to size and mass of single particles) of gas turbine particulate emissions as it suggest that the particles are all solid spheres or that they are completely solid carbon structure [97].

Particle mass concentration obtained using these hypothesis have often been criticised with 50% and 35% overestimations and underestimations quoted when compared against conventional gravimetric or against optical techniques that measure black carbon. Figure 2-15 is an example of a very good quality of fit when comparing SMPS mass concentration derived using a density of 1.2 g/cm^3 with a mass concentration determined using a US EPA method 5I gravimetric method [92].

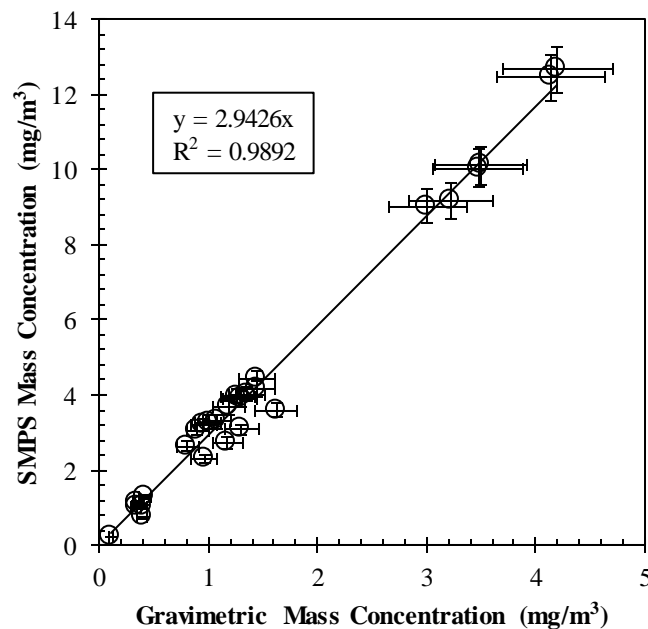


Figure 2-15: Comparison of SMPS to Gravimetric Mass Concentration [92]

Despite the very good quality fit, the SMPS values are almost thrice the values of the US EPA method 5I. Kelly et al [98] noted that by assuming a uniform particle density the chemical composition of the PM samples is ignored. Zhu et al. [99] and Wichmann [4] also noted that as particles in combustion exhaust are non-spherical and follow a fractal-like relationship that makes the density a function of the particle size.

2.8.2.1 PM Density

A better density evaluation that recognizes the particle structures would be to use the effective density of the particles. The effective density is a parameter derived from the combination of two particulate measurement [100]. Using this approach, the effective density of soot agglomerates have been reported to decrease with increasing particle size. Also, using an experimentally derived effective density rather than a uniform density, reasonable agreement with gravimetric data [101, 102] has been observed from the PM size distributions of motor vehicle. Therefore, it can be adapted for gas turbine PM measurements where similar challenges emerge at ultra-low PM mass emissions.

To determine the effective density distribution of a statistically significant number of particles, a measure of the density of a large number of the single particles would be ideal. Still an area of active research, various concepts have been developed to determine effective densities of a significant number particle sizes in a particle sample. Frequently used concepts involve one of the following combinations: mobility size – aerodynamic size, mobility size – particle mass or aerodynamic size – particle mass. Another frequently used concept is based on the ratio of gravimetrically derived mass to mobility equivalent volume. This concept was used by Li-Jones et al. [103] at idle conditions of T700-GE-700 helicopter engine and Timiko et al. [41] at various engine conditions of a PW308 turbine engine using gravimetric filters and multi angle absorption photometer (MAAP) (see section 2.5.3.1.2) respectively to evaluate the particulate masses in both studies respectively and the particle volume calculated using SMPS. An average effective density of 1000 kg/m^3 was observed for the T700-GE-700 while values

ranging between 400 to 820 kg/m^3 were observed for the PW308 depending on the type of fuel used and the engine thrust.

The electrical mobility size – aerodynamic size relationship can be realised using, Aerosol Particle Sizer (APS) and Scanning Mobility Particle Sizer (SMPS) in parallel or differential mobility analyser (DMA) and multi stage impactor as incorporated in the newly developed Dekati Mass Monitor (DMM) for real time evaluation of the particle mass concentration. Combining an aerosol mass spectrometer (AMS) and a SMPS, Timko et al. [41] also evaluated the effective density the PW308 engine and reported a density range of 710 – 840 kg/m^3 which depended on the fuel type and engine thrust. Similarly, Onasch et al. [104] deployed the same concept to investigate the densities of a CFM56-2-C1 at full throttle and reported an average density of 1000 kg/m^3 .

With the development of a particle mass classifier, the concept of mobility size and particle mass has become an attractive concept. This technique introduced by McMurry et al. [97], is implemented by combining a DMA and either an Aerosol Particle Mass Analyser (APMA; by Kenomax) developed by Ehara et al. [105] or a Centrifugal Particle Mass Analyser (CPMA; by Cambustion) developed by Olfert et al. [106] downstream. The APMA and CPMA are instruments that use the mass charge ratio to classify particles based on their mass. Thus, the idea of the concept is to classify the particles based on their sizes using a DMA and further classify them based on their mass using the APMA or CPMA, with a CPC or electrometer downstream acting as a detector. An alternative approach is to have the CPMA placed upstream of a modified fast particle analyser like the DMS500 or EEPS. With this approach the mass mobility exponent (fractal dimension), D_m , which relates the particle mass, m , to its mobility diameter, D_p , is determined. The fractal dimension is significant as it gives information about the structure with respect to the extent of void within the particle. To achieve this, several size-mass classifications is performed to have enough data set to generate their power law relationship from which the mass mobility exponent can be established as shown in equation 2-1.

$$m = C \cdot D_p^{D_m} \quad 2-1$$

$$\rho_{eff} = C \cdot \frac{6}{\pi} \cdot \frac{m}{D_p^3} \quad 2-2$$

$$\rho_{eff} = k \cdot D_p^{D_m-3} \quad 2-3$$

This relationship can be expressed to define the effective density, ρ_{eff} , as shown in equation 2-3 [107-109]. Where C is a scaling constant, k is the mass-mobility prefactor ($k=6C/\pi$). With this approach, Durdina et al [110] reported a mean effective density within 10% of the unit density (1000 kg/m^3) for a commercial turbofan engine CFM56-7B26/3 from an undiluted exhaust sample with Nafion dryer (see section 2.7.1.1) up stream of the DMA-CPMA-CPC instrumentation. Using a CPMA and a modified DMS500, Johnson et al [111] reported a varied density of 600 to 1250 kg/m^3 for CFM56-5B4/2P, CFM56-7B26/3, and PW4000-100 gas turbines. The variation was attributed to the sample conditions studied which included; with or without a catalytic stripper and with or without dilution which have determined the presence of semi volatile material on the particles. Also, it was reported that the largest variability was observed for the undiluted sample without a catalytic stripper an indication that the relative amount of semi volatile material produced was engine thrust dependent.

2.8.3 PSD Mass Concentration Using Experimentally Derived Density

There are limited studies that have compared real-time particulate instruments with a gravimetric reference method. Most recent PM instrument comparison studies [110-112] on gas turbine PM emission have been focused on demonstrating particle size distribution instrument as an applicable instrument for real-time measurement of non-volatile mass concentration measurements. Nevertheless studies have been performed on laboratory generated flames, light duty vehicle and diesel engines. Li et al [102] reports an underestimation of the gravimetric mass concentration by 37% from particle size distribution measurement using EEPS a light duty vehicle PM emissions. Park et al [113] found that the DMA-APM mass concentration measurements for laboratory-generated NaCl aerosols agreed with values determined gravimetrically from filters to within 15–20%.

Liu et al [114] reports an increased ratio of 0.99 ± 0.04 to filter mass concentration using SMPS with experimentally derived effective density for diesel engine PM. This shows that particle size distribution when converted using an effective density is a promising method to correlate gravimetric measurement for gas turbine PM. However, there are significant differences which affect the accuracies between the experimental method implemented by Liu et al [114] compared to the gravimetric procedure implemented for gas turbine PM measurement. Firstly, unlike method 5I the exhaust sample were diluted and the temperature lowered to 47 ± 5 °C contrary to the undiluted sampling and sample temperature maintained at 160 °C. Also 47 mm Teflon filters papers were used against the quartz filter papers recommended for US EPA method 5I.

2.8.4 Smoke Number Comparison with Soot Mass Correlation

Notwithstanding previous researches aimed towards quantitatively understanding the empirical smoke number there are still uncertainties associated with the relationship developed between smoke number and soot mass concentration. Nevertheless aircraft engines PM are still regulated by the International Civil Aviation Organization (ICAO) using the SAE smoke number (SN) [82]. Cappa et al. [115] reports that the uncertainties are associated with increased absorption of light experienced by captured sample in the presences of volatile organic aerosol. However, the work done by Rye et al. [75] and Northrop et al. [76] rules out the influence of semi volatile material thus increasing the suggestion that the uncertainties can be ascribed to the structure of the deposits. The rationale for the suggestion that the particle structure can be linked to the uncertainties can be understood given that a variation in particle sizes have been observed from studies that have compared gravimetrically derived soot mass with the smoke number.

Champagne [116] measuring soot from a General Electric J79 engine exhaust gas reported a geometric mean particle diameter (GMD) of $\sim 550nm$, which differed from Stockham et al [117] report a GMD of $\sim 100nm$ from the same engine. Meanwhile Girling et al. [118] study of soot generated by a smoke generator showed a geometric mean diameter (GMD) between 80 and 100 nm. However, despite these variations the correlation of the smoke number from the studies cited

above were within ~10% of the black carbon concentration of size meter. It is on this basis that the ICAO [119] and the Federal Aviation Administration [120] estimate mass emissions of BC from SN of aircraft engines during the landing and take-off (LTO) cycle, named the First Order Approximation version 3 (FOA3). In the United States it is the FOA3 that is used to estimate the public health impacts [121-124] of aircraft LTO PM emissions. A more recent literature by Stettler et al [125] using a combustor rig to generate soot from propane reported that the relationship between the smoke number and soot mass concentration is dependent on the particle mobility diameter.

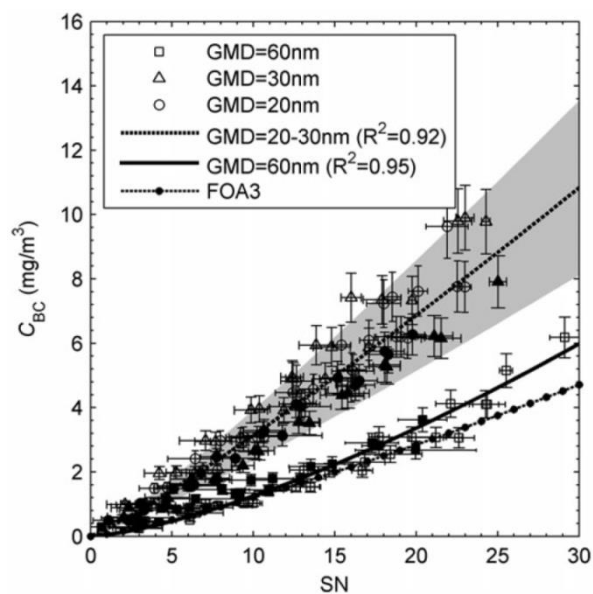


Figure 2-16: Literature correlations relating soot mass and smoke numbers [125]

Figure 2-16 above is a graph of reported correlations that was developed. Though the soot mass concentration was determined using a particle sizing instrument, a DMA-CPMA-CPC was used to measure the mass concentration and was confirmed to be between within 10 percent of the gravimetric determined soot mass concentration. However, the study was restricted to only particle sizes between 20 and 30 nm, and 60 nm. In contrast current aircraft engines have been shown to produce particle emissions characterized as having a lognormal PSD with GMD in the range 20 –140 nm [126]. Therefore, the FOA3 SN – black carbon correlation, based on ~100 nm, 20 – 30 nm and 60 nm BC, is not totally representative of the observed size distribution of aircraft-generated BC.

2.9 Recommended Instruments for PM Mass Correlation

The review of the direct reading instruments presented, shows how their limitations complement each other as a 'perfect' single instrument that measures total PM mass represented as particle mass concentration per unit volume is not yet available. The existing real-time instruments, mass based as well as non-mass-based systems have been shown to achieve a lower limit of detection and better repeatability than the gravimetric filter method. Thus, the complexity of the particulate content means the best approach presently to develop correlations to the gravimetric reference method requires a combination of direct reading instruments as hypothesised in section 2.6.

Among the real-time non-volatile instruments, the LII and MSS in addition to showing good correlations with the elemental portion of gravimetric standards is robust and fast. For instance, the multi angle absorption photometry (MAAP) which has equally shown good correlation with the elemental portion of gravimetric standards requires the advancement of its filter paper after each condition, making it unsuitable to measure PM emission during transient. Between the size-number distribution instruments, though the SMPS is recognised as a standardized instrument for particle size-number distribution, when compared with other available size-number instruments - DMS500, HT-ELPI and the EEPS, it is slow and its sampling conditions does not match up with the required conditions for PM emission sampling from a gas turbine. DMS500, HT-ELPI and EEPS can analyse the exhaust particulate at temperatures greater than 150°C, while the HT-ELPI can detect up to 10 micron sized particles. However, these instruments need a tandem connection of DMA-CPMA-CPC/electrometer for a direct out of the measurement in mass concentration. With the condensable PM, no reference literature comparing method 202 reading with the multi component analyser has been identified. However in theory, if the FTIR is tuned to the sampling conditions required for method 202, comparable results are likely. Nevertheless, the Time of Flight Aerosol Mass Spectrometers is also an interesting instrument to research but it is not as more established compared with the FTIR techniques as studies research efforts on achieving better time resolution analysis are still ongoing [127].

Consequently, this review recommends the use of LII, DMS500 for correlating real-time measurement instruments to the filterable fraction particle mass measured determined using US EPA method 5I for gas turbine particle emissions. It also recommends the use of a tandem connection of a DMA-CPMA-CPC/electrometer combination to ascertain the effective density of the particle emission sizes to help minimize uncertainties introduced in converting size-number distribution measurements to mass per unit volume metric. Also recommended, is a smoke meter instrument based on its availability on site as it is an opportunity to advance the knowledge and understanding of particle size relationship and smoke number reading. FTIR instrumentation is recommended for correlation with the condensable fraction of method 202. However, the implementation of this process during the course of this study is subject to the details contained in chapter 3 describing the FTIR. It finally recommends that OPC be deployed to confirm that the particle emissions from the gas turbine that would be used for this study are largely less than one micron for the engine conditions and fuels tested.

2.10 Summary of Knowledge Gaps

Table 2-4 is a summary of previous work on PM instrument correlation, impact of aromatics species in fuel on PM emission and PM emissions from gas turbine alternative fuels. In addition to the knowledge gap correlating real-time instruments to the US EPA methods 5I and method 202 the summary gives a number of data gaps the research would fill. Firstly, as demonstrated in the table experiments that have implemented method 5I and method 202 are scarce and thus, this research provides valuable method 5I and method 202 data as a reference for gravimetrically determined PM mass concentration data from a gas turbine for future research.

There is no information on the particle emission density of PM emissions from the test engine for this research. Again, this would be a major addition to knowledge as the test engine is widely used in aircraft as APU particularly as PM emissions from aircraft related activities is been heavily researched presently. Thus, in addition, this research aims to expand the knowledge of the DMA-CPMA-CPC

approach by evaluating the particle emission density from a gas turbine engine. Unlike recently published articles that have placed a Nafion dryer prior to the DMA-CPMA-CPC instruments this thesis has justified the need to exclude the Nafion dryer (details in chapter 4). Therefore, this study offers a different perspective of the measurement of particle density with a DMA-CPMA-CPC connection.

Table 2-4: Summary of previous work on PM instrument correlation and knowledge gap

Instruments	Components	APU	Diesel	Jet A-1	LACF	FPM	CPM	Glass Probe	dilution	no dilution	nafion dryer	NIOSH EC	35-50nm & <1µm	Ref
Particle Size Instrument	Effective Density	✗	✗	✓	✗	✗	*	✗	✗	✓	✓	✓	✓	[110, 112]
	Unit Density	✓	✓	✓	✗	✗	*	✗	✗	✓	✓	✓	✓	[43, 80]
NIOSH 5040	EC	✗	✗	✓	✗	✓	*	✗	✓	✓	*	✓	✗	[80, 92]
	OC	✗	✗	✓	✗	✓	*	✗	✓	✓	✓	✓	*	[45, 92]
LII	EC	✓	✓	✓	✗	✗	*	✗	✓	✓	✗	✓	✗	[128]
FTIR	THC	✓	✓	✓	✗	*	✗	✗	*	*	*	*	*	[129]
	Inorganic gases	✗	✓	✓	✗	*	✗	✗	*	✗	*	✓	*	[129]
FID	THC	✓	✓	✓	✗	*	✗	✗	*	✗	*	*	*	[130]
SAE AIR6241		✓	✗	✓	✗	✓	✗	✗	✓	✓	✓	*	✓	[45]
Smoke Number		✓	✓	✓	✓	✓	*	✗	✓	✓	✗	✓	✗	[75, 130]
OPC		✗	✗	✓	✗	✗	✗	✗	✓	✓	✗	✗	✗	[46]
Method 51/202		✗	✗	✗	✗	✓	✓	✓	✗	✓	*	✓	✗	[92]
APU		*	✓	✓	✗	✗	✗	✗	✓	✓	*	✗	✓	[43]

Note: ✓In the literature; ✗Data gap; *Not Applicable

One of the data gaps that must also be addressed is the assumption that the particle size distribution of aero gas turbine engines are less than one micron which may not necessarily be the case for land based gas turbines and aircraft APU. While the assumption that PM emissions sizes from gas turbine may not be entirely unreasonable, it would be preferable to have data which support the assumption. Therefore, it is important to have evidence that the particle emission from this research test engine is less than one micron as the test engine (details in section 3.3) is widely used in the aero industry and for industrial applications. As identified in section 2.2 only one study [46] have used a particle size instrument capable of measuring particle sizes greater than one micron PM size studies from a gas turbine. Though the literature reports that the PM sizes that more of this testing need to be performed to confirm this assumption and advance studies focused on gas turbine PM emission size studies.

Pertaining the sampling system, the issue of diluting the exhaust sample or the use of Nafion dryer so that the instrument specifications is not exceeded while also meeting the US EPA method 5I requirement need to be resolved. The recommended instruments measure different particle parameters and most importantly have their specifications which must not be exceeded to avoid instrument damage. Though, there are studies that have used multiple PM instruments for PM emission research from a single gas source as detailed in section 2.7, none has used the US EPA method 5I and method 202 as a framework and reference for the design of their PM sampling system. The information gained from these literatures [45, 80] includes details of the sample line diameter, material and maximum length from the engine exhaust exit plane to the instruments for minimum particle transformation to occur in the sample line. This information is now specified in SAE AIR 6421 [131] and ARP 1179D [81].

Furthermore, in contrast with the US EPA method 5I and method 202 gravimetric requirements, the studies which have compared some real-time instruments with a gravimetric protocol have diluted the exhaust sample prior to the distribution of the exhaust samples instruments. Therefore, how the instrument would compare with gravimetric results of an undiluted exhaust sample remains unknown. On the

other hand, studies which have opted for the use of a Nafion dryer against dilution for the purpose of reducing the exhaust water content, have only compared the non-volatile measurement capacity of particle size distribution instruments with real-time soot measurement instruments. There is no report about the influence of the Nafion dryer on the particle emissions measured. Consequently, a knowledge gap which this research seeks to address is to understand the impacts of the dilution and the use of the Nafion dryer in correlating a particle size instrument with undiluted exhaust samples measured gravimetrically.

The PM levels from industrial gas turbines is reported to be now largely less than 10 mg/m^3 with concentration levels less than 1 mg/m^3 easily obtained with new technologies implemented on new liquid fuel turbines or from turbines burning natural gas. It is thus imperative that particle concentration between 0.5 mg/m^3 and 10 mg/m^3 is achieved with the research test engine. In addition to changing the engine operating condition, the particle mass concentration is also largely determined by the aromatic content of the fuel been combusted. Using this knowledge, the best approach to generate various PM mass concentrations from a single engine source would be to start with a fuel that has no aromatic content and subsequently dope the fuel with aromatic. The follow-up question becomes how to choose the aromatic specie and the various percentage content of the fuel that should be aromatic. However, from a different perspective the extent to which each aromatic species impact on the soot physical characteristics emitted is a subject of interest. Thus, summarised in in Table 2-5 are the previous work and gaps with respect to aromatic species and soot emission.

Table 2-5: Summary of Previous Work on Impact of Aromatics on Soot Characteristics

Aromatic Specie	Aromatic Blends		100% Aromatic Specie	Particle Size	Sooting Tendency	Ref
	15%	8%				
Benzene	×	×	×	✓	✓	[37, 38]
Ethylbenzene	×	×	×	✓	✓	
m-Xylene	×	×	×	✓	✓	
Tetralin	×	×	✓	✓	✓	[37-39]

Note: ✓ in the literature; × Data gap; * Not Applicable.

3 Design of Experimental Set-up

This chapter covers the experimental hardware and sampling system design but first, is a detailed description of the recommended instruments. These instruments have different metric output including; particle number, PM size distribution, elemental PM mass and total PM mass. Thus, details of the instruments described include calibration and technical specification. The chapter then proceeds with the description of the sampling system and covers a detailed description of the sampling system components and the test gas turbine.

3.1 Instrumentation

As recommended in chapter two, a summary of the PM measurement instrument techniques and the models of the instruments and manufacturers for the study are listed on Table 3-1. Also included are gaseous measurements techniques sanctioned by SAE E31 for commercial engine certification measurements which have been deployed to for gaseous emission monitoring in this study.

Table 3-1 PM Instrumentation

Measurement Method	Parameters	Instrument
Gravimetric Analysis	Total particulate mass	Method 51&202
Filter Blackening	SAE Smoke Number	Smoke Meter
Laser Induced Incandescence	Black Carbon	Atrium 300
Carbon Burn-off	Total Carbon	NIOSH 5040
Fourier Transform Infra-Red	Volatile Particulates	Thermo Scientific Antaris Industrial Gas Analyser
Electrical Mobility	Size/Number Distribution	DMS500

3.1.1 US EPA Method 5 and Method 202 Sampling System

The hardware of the gravimetric particulate sample train consists of five (5) main components (Figure 3-1). These include the:

1. **Source Sampler Console** which houses the controls of the instrument. The controls include a dual column manometer for monitoring exhaust flow rate, sample flow control valves, dry gas meter with calibrated Orifice Tube located on the outlet, and temperature controls and monitors.
2. **Vacuum Pump** including hoses with quick-connect fittings and lubricator. This is a rotary vane pumps with a maximum relative vacuum capacity of 25.5 inches of Hg (86.35 kPa) and a maximum flow of 87.78 lpm (0.088 m³/min) at 1 inch Hg (3.39 kPa) and 42.46 lpm (0.042 m³/min) at 15 inches Hg (50.80 kPa).
3. **Heated Sample Line** –The heated sample line is self-regulated through which exhaust sample is delivered to filter holder contained in the modular sample casing. The heated line head is fitted with a #28 glass filled PTFE unground ball fitting to connect a corresponding #28 unground socket of the filter holder described in the next subsection.
4. **Modular Sample Case** includes hot box for filter assembly, cold box for impinger glassware, and electrical connections.
5. **Umbilical Cable** includes electrical and pneumatic lines to connect corresponding plugs between the modular sample case, sample pump and source sampler console.

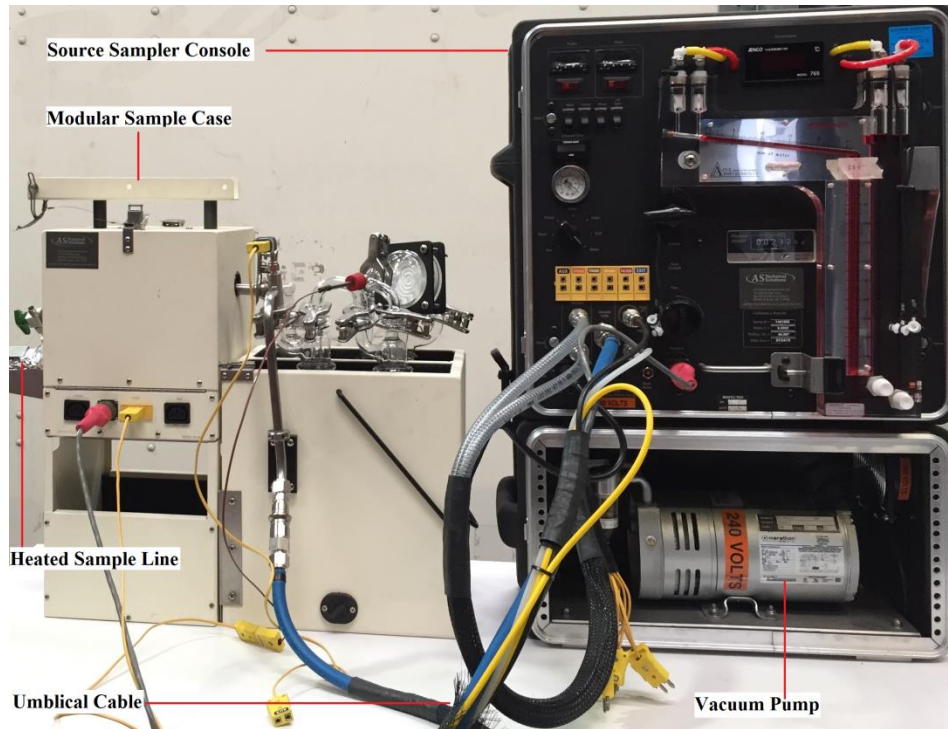


Figure 3-1: Picture of Gravimetric Sampling Kit

3.1.1.1 Modular Sample Case Components

Method 51 Filter Holder

Designed for a 47 mm diameter filter, the components of the filter holder can be divided into two parts; a front half and a back half. The component of the front half includes a borosilicate glass front cover with #28 socket, wafer-thin stainless steel filter support, an O-Ring and a Teflon seal. All three components are important to prevent leakages from outside or around the filter. The back half includes a filter wafer-thin stainless steel filter mesh and a stainless steel filter holder which is fastened to an outlet stainless steel tube that has two 45 degree bends with a #28 ball adapter. Figure 3-2 is a picture of the filter holder as a single unit.



Figure 3-2: Picture of the method 5I filter holder

Method 202 Section

Figure 3-3 is a picture of the assembled component parts that collect the method 202 samples and exhaust water content analysis. The components are made of borosilicate glass ware with the appropriate #28 balls and sockets inlets or outlets. These include a spiral condenser labelled 1 in the Figure 3-3 with #28 ball and socket inlet and outlet. To help induce condensation, the spiral condenser has water jacket hose barbs through which water is circulated with the aid of a pump around the spiral tube of the condenser. The other components are impingers with #28 ball inlets and outlets as follows; a short stem dry impinger (knockout impinger), labelled 2; a long stem dry impinger (backup impinger), labelled 3; and the front of the CPM filter housing with a #28 socket, labelled 4. The CPM filter holder is designed for an 83 *mm* diameter filter. L-tube and U-tube with #28 sockets are used to connect the impingers and the method 5I section.

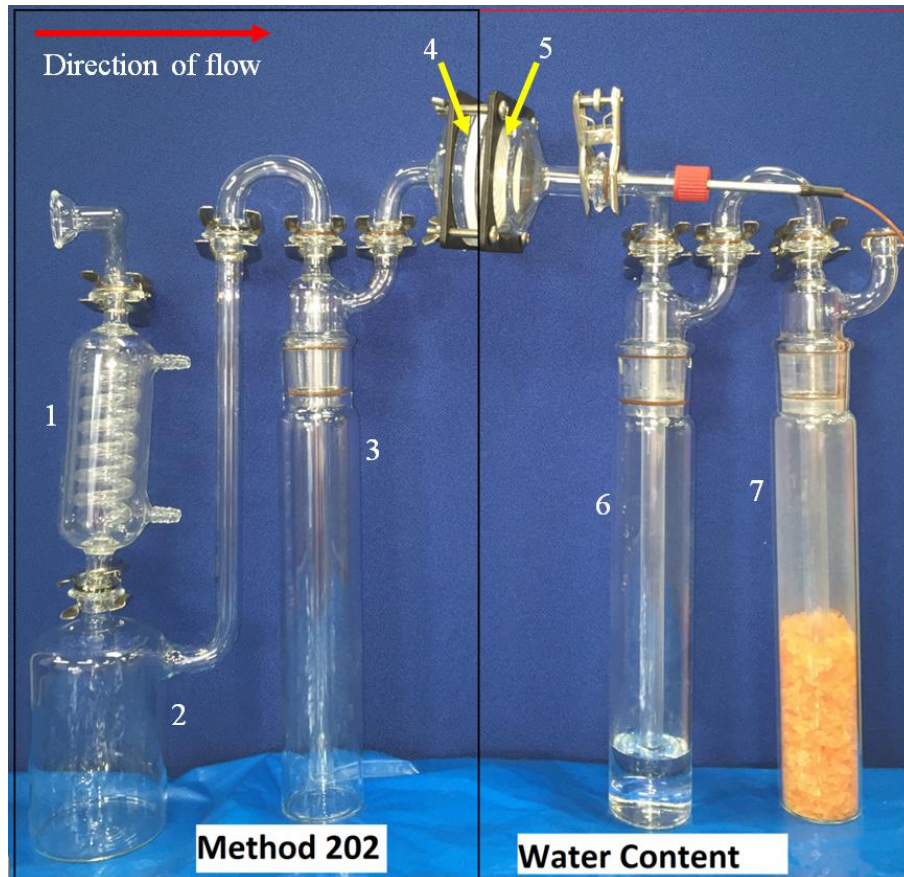


Figure 3-3: Picture of Method 202 components and water content of the US EPA gravimetric method

Exhaust Sample Water Content Section

The exhaust water content collection apparatus include the components behind the CPM filter up to the outlet of the impinger labelled 7 in Figure 3-3. These include; the plastic mesh which supports the CPM filter; the back housing (labelled 5 in Figure 3-3) of the filter holder; and a double “L” connector with a Type-K temperature control assembly that has a screw cap and silicone seal. Directly connected with the double L connector is the impinger labelled 6 which is filled with 100 g of water. The next impinger labelled 7 is filled with 200 g of silica gel to strip the exhaust gas of its water content.

3.1.1.2 Source Sampler Console

The Source Sampler Console is the operator’s control station from which the exhaust gas velocity and temperatures of the gravimetric setup can be monitored and controlled. Figure 3-4 illustrates the Apex Instruments Model XC-522 Source

Sampler Console's front panel which have been deployed for this purpose. It is full featured manual meter console with a dual column manometer, sample flow control valves with orifice flow meter, dry gas meter, and electrical controls.

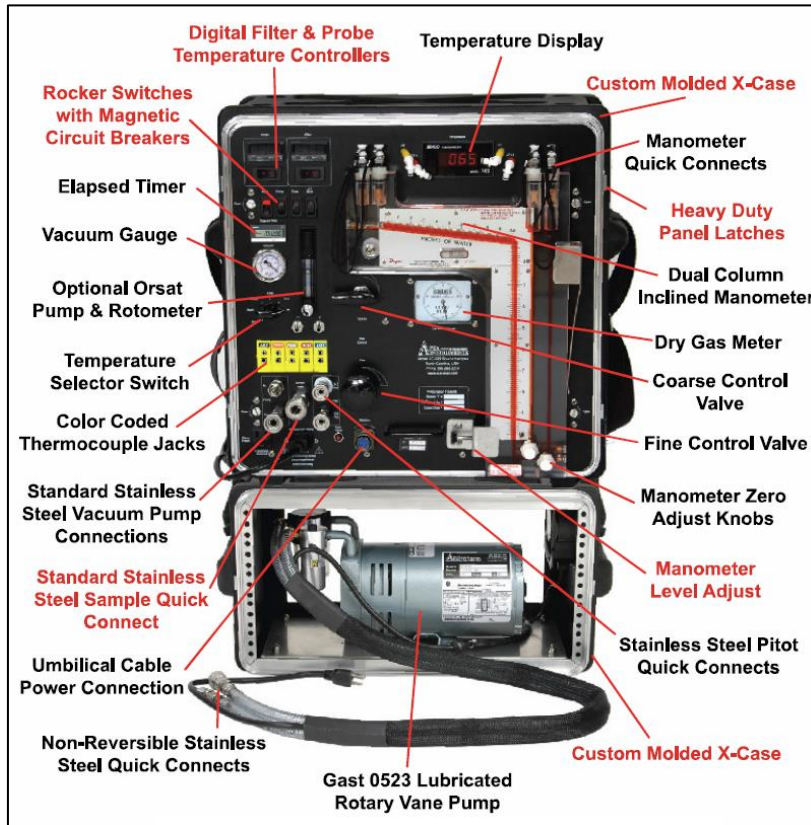


Figure 3-4: Model XC-522 Source Sampler Console Front Panel [132]

3.1.1.3 Calibration

As noted in section 2.3.1, the accuracy of the method 5I and method 202 sampling test is dependent on the accuracy of sample collection components. Components of the particulate sampling system which required calibration are:

1. Dry Gas Meter (DGM) which was calibrated using a traceable wet test meter secondary reference DGM with a correction factor (dimensionless) subsequently derived and applied to the data as detailed in equation 6-3.
2. Thermocouples (filter box, impinger exit, and dry gas meter) and Digital Temperature Indicator which were calibrated against a certified Hg-in-glass thermometer in ice slush and boiling water to within $\pm 3^{\circ}\text{C}$.

Overall the calibration the components are recommended for calibration semi-annually and with the next calibration scheduled for 24 January, 2015.

3.1.2 Laser Induced Incandescence

The laser-induced incandescence (LII) technique deployed for a direct readout of the elemental carbon fraction of the exhaust samples is a LII300 model manufactured by Atrium. A schematic of the internal structure of the instrument is shown in Figure 3-5. As detailed in section 2.3, the LII measurement theory is based on incandescence of soot generated when heated up using a laser beam. The Atrium LII300 uses a neodymium-doped yttrium aluminium garnet (Nd:Y₃Al₅O₁₂; Nd:YAG) set-up to produce laser pulses with 60 *mJ/pulse* at 20 *Hz* and 1064*nm*. The laser is refined using beam shaping optics and directed using a series of mirrors to the sample cell where its fluence profile is imaged at the sample volume. On contact with the laser light beam, the soot particles in the sample cell get heated to temperatures at which their thermal emission is detectable. For maximum signal and to avoid any sample losses the soot temperature is kept from soot sublimation temperature but high at 3400 to 3800 °K for a stable incandescence.

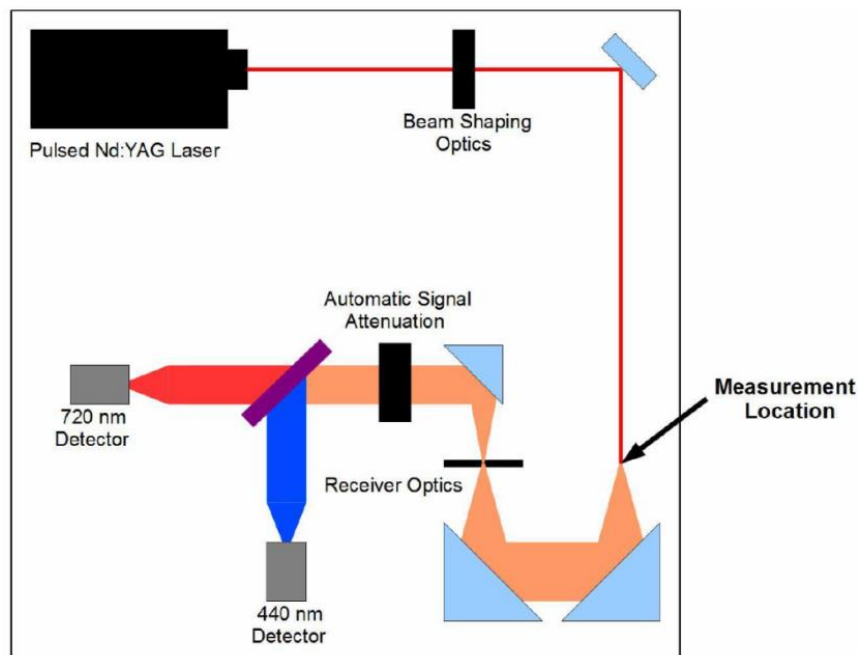


Figure 3-5: The experimental set-up for an LII device [133]

Two independent photomultipliers are employed to ensure that the incandescence signal is reliable. To achieve this, the photomultipliers are tuned to detect specific wavelength of the incandescence signal, precisely 440 *nm* and 720 *nm*. Thus the soot incandescence directed towards the photomultiplier is first beamed on a

narrowband interference filters which filters and direct the wavelength to the corresponding photomultipliers. The signal on the photodetectors is converted to voltage to provide the temperature of the soot particles and the absolute signal intensity at a specific temperature used to measure the soot volume (or mass) fraction. The rate of decay of the soot temperature has been suggested to relate with the primary particle size [134]. However the particle sizes established using this relationship has been acknowledged to be an effective or apparent size as the instrument treats the particles as individual mono-sized particles, not accounting for the effects of size distribution and aggregation. Nevertheless, the results are repeatable and gives a picture of the soot particle sizes even though it's measurement are reported to be considerably larger than soot particle sizes from the same source measured using transmission electron microscopy (TEM) [134]. Consequently, the measured LII particle sizes have not been analysed for the correlative part of this thesis.

The Atrium LII300 calibration was performed by the instrument manufacturer using the signals and absolute intensities of incandescent at specific temperatures on 8 May, 2014 with the next calibration scheduled for the 16 May, 2016. The calibration was conducted using a NIST traceable spectral radiance source at a known temperature from which correction factors that associates measured signal to absolute intensities is established. Thus, the traceable calibration source travels through the same optical path including windows, lenses, mirrors, filters and photodetectors that incandescent light from the particles navigate. Therefore no further step is needed or assumed as the measured signal from the incandescent light is directly related to the absolute intensity of the traceable calibration source.

3.1.3 NIOSH 5040 SETUP

Due to unavailability of the Sunset EC/OC analyser, the NIOSH 5040 [59] method approach was adopted for this study. The set-up included a filter holder, a flow meter to control the flow through the filter, a pump to pull exhaust samples through the filter. The filter holder is designed to house a 47 mm diameter filter with a sample area of 11.95 cm². Supplied by Sierra CP Engineering, it is made of 316L Stainless Steel material. To ensure an even spread of the particulate captured

by the filter, the inlet and outlet holder are tapered inlet section with an angle of less than 12.5 degree. To help regulate the temperature of the filter during sampling, the filter is housed in a heated box which was kept at 160°C with the k type thermocouple for temperature regulation. The electronic mass flow controller used was an AALBORG Model GFC-1133 and confirmed traceable to a Gilibrator reference flow meter with bubble generators. Figure 3-6 is a picture of the filter holder.



Figure 3-6: Picture of the NIOSH 5040 Filter Paper Holder

3.1.4 DMS500

For particle size distribution measurement a DMS500 Mk II instrument have been deployed for the experiment. Manufactured by Cambustion it measures only particles less than one micrometre. As discussed in chapter 2, it has the capacity to detect particle in a sample gas of upto 800 °C and has a time resolution of 200 ms. It uses a high sample flow rate of 8 litres per minute and sheath flows in the charger to guard against diffusion losses. Figure 3-7 is a schematic of the instrument classifier. From the instrument sample inlet, the exhaust sample is directed through a corona discharge charger where the particle gain charges according to their sizes and transported to a classifier. The components of the classifier include a centrally placed high voltage electrode and in an annular cylinder with twenty two ringed electrometer. A sheath air flow enters the

classifier at the same time with the exhaust sample surrounding the sample thus separating it from the electrometers.

On application of high voltage to the central electrode, the charged particles are deflected towards the electrometer rings. Particles with a higher charge / lower drag will be deflected more, and will land on an electrometer ring closer to the sample inlet. As charged particles land on the metal electrometer rings (22 bins, in number), their charge flows to ground, via an electrometer amplifier. This amplifier is capable of measuring the small currents (femto Ampere) caused by groups of particles landing on the metal rings, and this forms the basis of particle detection. The average number-weighted particle mobility diameter (D_p) distribution, $n(D_p) = dN/d\log D_p$, for each size bin recorded is used to generate a particle size distribution which is then integrated to produce the total number concentration per volume of the exhaust.

The instrument is sent to the manufacturer – Cambustion annually for calibration. It is calibrated for nucleated aerosols, agglomerate and non-agglomerate aerosols. National Institute of Standards and Technology (NIST) traceable polystyrene latex (PSL) spheres were used to calibrate the instrument for non-agglomerate aerosols for particle sizes as follows; $50 \text{ nm} \leq D \leq 900 \text{ nm}$. Calibration for nucleation aerosols was achieved using DMA size selected re-nucleated sulphuric acid [101] and sodium chloride which included particle sizes as stated; $5 \text{ nm} < D < 50 \text{ nm}$. While a DMA size selected soot from a soot generator, have been used to calibrate the device for agglomerate aerosols.

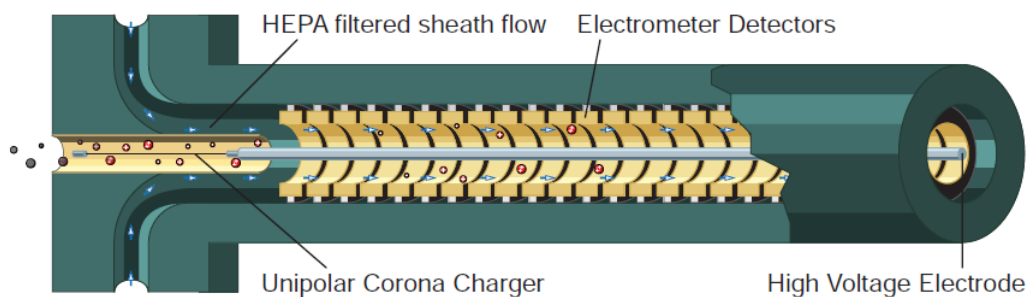


Figure 3-7: Schematic of a DMS500 [101]

3.1.5 SAE Smoke Number

The smoke number analysis was carried out according to the SAE ARP1179D which specifies the design parameters for the filter holder and the sample control. The working principle is based on the reduction of the reflectance of a white filter paper which captures the particulate matter from a $16.2 \text{ kg exhaust gas/m}^2$ of filter area. This was achieved using a Richard Oliver Smoke meter to collect samples on a Whatman #4 filter paper and an EEL043M Smokestain Reflectometer manufactured by Diffusion Systems Limited to determine the filter paper reflectance before and after sample collection. The reflectometer conforms to the ANSI PH 2.17 [81] as required by the SAE document.

The Richard Oliver smoke meter is designed to automate the sample system as specified in the SAE ARP1179 document. Therefore, the internal flow system of the Richard Oliver smoke meter consist of a bypass loop through which flow is directed when not passing through the heated filter holder. Thus, with a solenoid the instrument automatically directs the exhaust sample flow between the bypass loop and the filter block. Basically, when the instrument is switched to collect sample the solenoid channels the flow to the bypass loop through which it is dumped to the atmosphere when sufficient sample have been collected to allow for a change of the filter or and end of the experiment. Figure 3-8, is a picture of the Richard Oliver Smoke Meter with control appropriately labelled.

Volume measurement of the Richard Oliver Smoke Meter and other checks including cleanliness, temperature controls and leak test were performed before testing. The volume measurement was calibrated against a dry gas meter while the linearity of the reflectometer was checked prior to usage using reflectance standards traceable to NPL. The instrument response was less than 2% of the expected values.

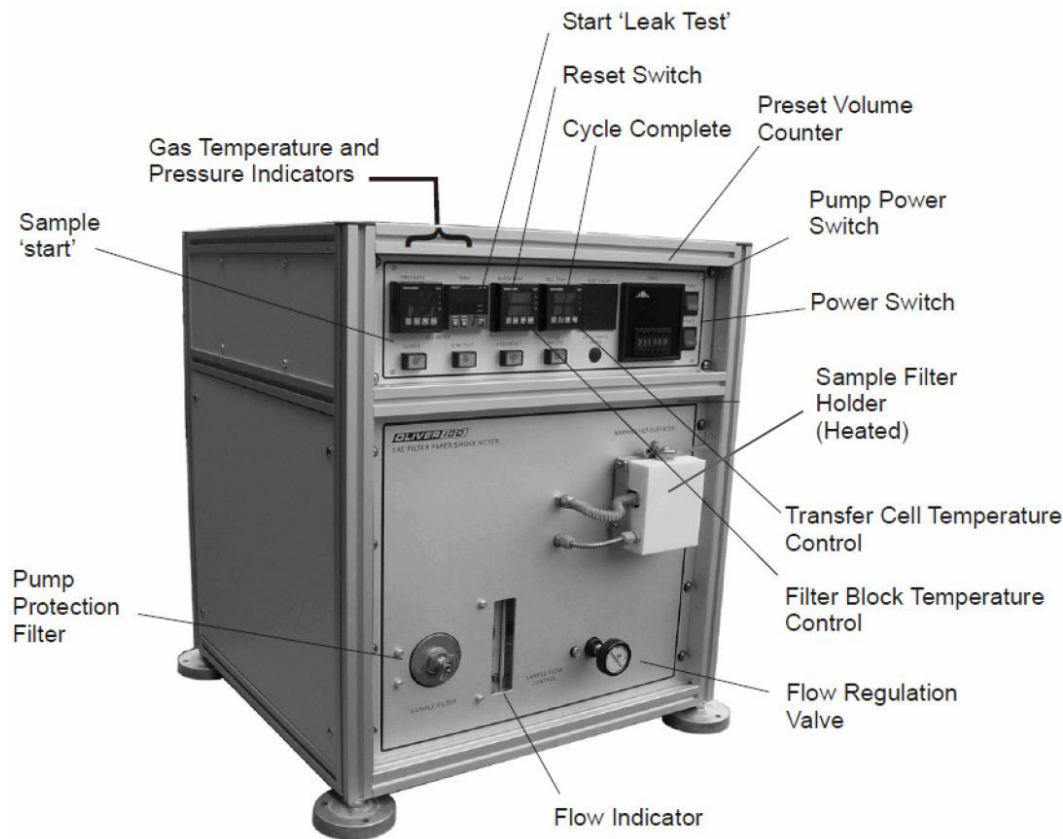


Figure 3-8: Smoke measurement by SAE/ARP 1179D [81, 135]

3.1.6 Fourier Transform Infrared (FTIR)

The FTIR system used for this experiment is a Thermo Scientific Antaris Industrial Gas Analyser. Figure 3-9 shows a schematic of the internal structure of the instruments. Typical of FTIR instruments, it consists of an infrared source with the light beam directed into an interferometer where all the frequencies in the beam are combined into one signal called interferogram. In the interferometer this is achieved using a fixed mirror, a moving mirror and a beam splitter. Upon transmission out of the interferometer, the interferogram is then directed using a number of mirrors into a two metre gas cell path where infra-red absorption by the sample gas occurs and the transmitted beam directed to a detector. The ensuing electrical signal is then sent to the computer software for processing. To ensure that the mirrors are always in position, a laser beam of a known and constant emitted light frequency is deployed as an internal calibrator. The instrument uses a mercury cadmium telluride (MCT) detector with the capacity to detect wave

numbers between $11,700\text{ cm}^{-1}$ and 600 cm^{-1} and wavelengths of 855 nm to 16667 nm . The detector requires liquid nitrogen for cooling during sampling.

The instrument has the capacity to measure gases from ambient temperature to up to $185\text{ }^{\circ}\text{C}$ and have been factory calibrated to measure 19 gas species and calculate the THC and NO_x . It was decided against calibrating the instrument for specific inorganic and organic fractions of interest after consultation with the instrument manufacturer as it required an experienced personnel and as such, too costly to implement. Consequently, the correlation with the condensable fraction of the gravimetric method was limited to comparing the organic fractions of both instruments. More information about the FTIR settings and procedure for the experiment is contained in chapter 6.

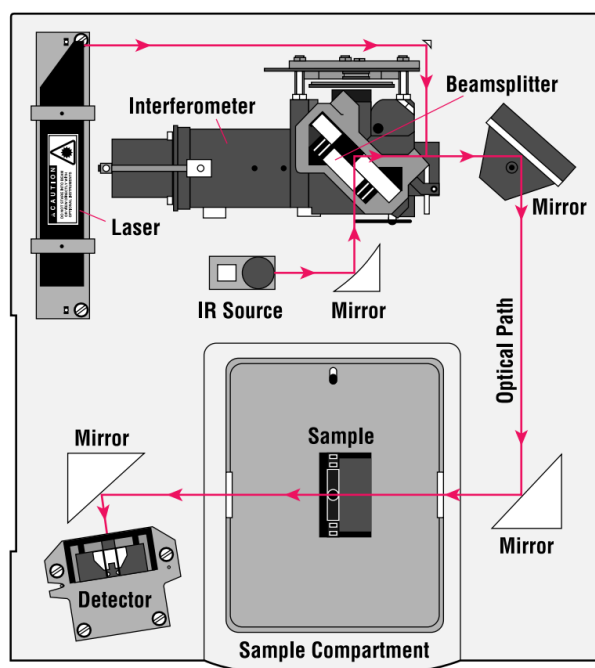


Figure 3-9: Schematic of A Fourier Transform Infrared [136]

3.1.7 Gas Analysers

The gas analysers deployed for this research, provided for the measurement of carbon monoxide (CO), carbon dioxide (CO_2), oxides of nitrogen (NO_x), unburned hydrocarbon content (UHC), and oxygen (O_2) within the exhaust gases. Table 3-2 is a list of the gas instrument models used to measure the gas species in the exhaust sample gas. These instruments are housed in a cabin known as the

mobile emission laboratory (MEL) with a single exhaust sample inlet into the cabin from which sample is distributed to the instruments [137]. Below is a summary of the operational principle of each instrument.

Table 3-2 Gaseous Emission Analysers

Instrument	Species	Technique
Signal 3000HM	THC	FID
EcoPhysics CLD 700 EL ht	NO _x	Chemiluminescence
Signal MGA	CO CO ₂	Dual Channel - Non Dispersive Infra-Red
	O ₂	Paramagnetic Cell
NDIR Rosemount Binos 1000	CO CO ₂	Dual Channel - Non Dispersive Infra-Red
ADC (MAG) Oxygen Analyser	O ₂	Paramagnetic Cell

The total hydrocarbon content of the exhaust stream was measured using a Signal 3000HM analyser which employs flame ionization detection (FID). The flame ionization detection system works using the theory that ions produced when the exhaust sample is burned in a hydrogen flame is proportional to the carbon atoms in the sample gas. The signals are then amplified to evaluate the total hydrocarbon content of the exhaust sample. For NO_x concentration, the measurement was made from the chemiluminescence property of the exhaust stream at 160°C using an EcoPhysics CLD 700 EL ht - NO_x analyser. The chemiluminescence property is the light emitted as a result of the reaction of the nitric oxide (NO) content of the exhaust with ozone (O₃). Therefore, to determine the NO_x concentration the nitrogen dioxide (NO₂) content of the exhaust is first converted to the NO by passing the exhaust sample through the a catalysed thermal reaction ($2\text{NO}_2 \rightarrow 2\text{NO} + \text{O}_2$).

The Signal 9000 MGA and the Binos 1000 analyser where used to characterise the concentration of CO and CO₂. The Binos 1000 analyser was used for the

preparatory experiments (chapter 4) but was replaced due to breakdown with a Signal 9000 analyser. The Signal 9000 is a multi-gas analyser and measure the oxygen content of the exhaust in addition to CO and CO₂ characterisation. Both analysers employ a dual channel non dispersive infra-red (NDIR) technique to quantify CO and CO₂ while it uses a paramagnetic cell to detect the oxygen content in a gas sample. The dual channel non dispersive infra-red (NDIR) technique for CO and CO₂ detection and measurement is based on the reduction of the intensity of the wavelength in the infrared spectrum that uniquely identifies these gases. For CO, there is an overlap in the infrared spectrum with the wavelength H₂O, thus a chiller is installed upstream of the analyser to reduce the dew point temperature of the exhaust to approximately 3°C before entering in to instrument. To measure the oxygen (O₂) content of the exhaust prior to the installation of the Signal 9000 analyser, an ADC MAG oxygen analyser was used in for O₂ analysis in the preparatory experiments (chapter 4). The oxygen chamber of the Signal 9000MGA analyser and the ADC MAG oxygen use the paramagnetic property of oxygen gas for analysis. They achieve this by exposing the sample gas to a magnetic field thereby causing the oxygen content to gravitate in the direction of higher field strength, thus causing a diamagnetic body suspended in the field to respond to the turning force.

3.1.7.1 Calibration

Each of the gaseous analysers is calibrated using a certified zero gas and a span gas to internally adjust the zero and span points of each detector. With the zero gas, the instrument baseline is set after which the span gas is used to set a point of known concentration as shown in Figure 3-10. The certified and traceable zero gas and span gas mixtures are also used for routine verification and adjustment of analyser response. The set point provides a straight line graph which the instrument output are mapped against either internally or through the Labview software interface developed to simultaneously log data from the analysers [137]. Details of the Labview software user interface are contained in chapter 4.

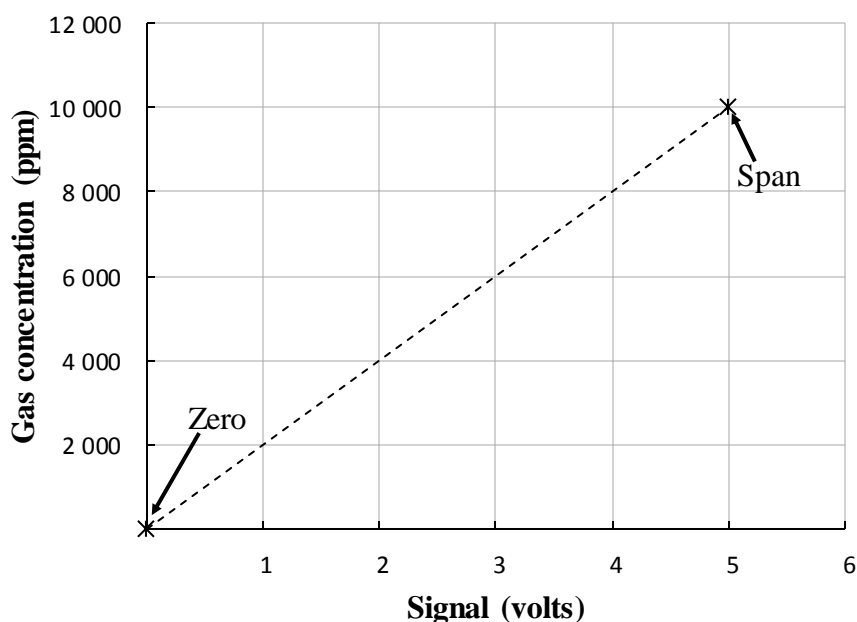


Figure 3-10: Zero and span calibration

Table 3-3 details the zero and span gases used to calibrate the analysers. To calibrate the zero baselines for the analysers, zero grade nitrogen (99.998% purity) was used except for the FID analyser which requires zero grade air and hydrogen-helium fuel supply. Zero grade nitrogen gas is not suitable for the calibration of the zero point of an FID. It creates an uncontrolled calibration because it changes the ionisation flame's fuel-air ratio. The zero grade as supplied by BOC is certified to contain less than 0.1 *ppmv* of hydrocarbons and NO_x ; less than 1 *ppmv* of CO_2 and less than 2 *ppmv* of H_2O while the ratio of hydrogen-helium gas mixture was 40-60% (2:3).

Table 3-3: Calibration gases

Instrument	Zero Gases	Span Gases
Signal 3000HM	40% H_2 /bal. He zero grade air	100 ppm C_3H_8 (bal. zero grade air)
Eco Physics CLD	N_2	100 <i>ppm</i> NO (bal. N_2)
Signal MGA	N_2	5% CO_2 / 1000 <i>ppm</i> CO (bal. N_2)

	-	zero grade air (for the oxygen chamber)
Binos 1000	N ₂	5% CO ₂ / 1000 ppm CO (Bal. N ₂)
ADC (MAG)	-	zero grade air

As shown in Table 3-3 the span gases are blends of the desired concentration of the calibration gases with nitrogen gas used as a balance to fill up the gas cylinders. This applies to CO, CO₂ analysers and the NO_x analyser. On a different note the span gas for the FID is propane with zero grade air used as a balance. The span concentrations were chosen to be similar to the expected gas concentration from the test engine. The span gases were supplied by BOC and comes with a BOC B certificate which specifies a concentration certified uncertainty of $\pm 2\%$. However this uncertainty is not critical with respect to this research as the purpose is not to certify the combustion performance of test fuels.

Table 3-4 shows the selected measurement range used for this study and the corresponding full scale error. The full scale error is the reading error of the instrument on the measured concentration and it is based on the upper range value. Therefore, accurate selection of the required instrument range is important to reduce the full error of the instrument on the measured value. The range selected was based on the span concentration and should ideally match the expected maximum concentration of the gas in the exhaust. For instance the full scale error of $\pm 0.5\%$ on a selected range of 1000 ppm is ± 5 ppm. Therefore, if the 1000 ppm range is selected for an expected sample concentration of 10 ppm the uncertainty of this value is ± 5 ppm in contrast to measurements close to the 1000 ppm. The instrument linearity (R^2) for the selected ranges was checked as during the commissioning of the MEL [137] and included in Table 3-4. The instrument linearity (R^2) for the selected ranges was checked in accordance with ARP1256D [138] and thus performed for 0, 30%, 60%, 90% and 100% of the span gases. The result showed that the instrument for the selected ranges are linear as R^2 values of approximately one was observed.

Table 3-4 Analyser calibration range and full scale error

Analyser	Species	Range (ppm)	Full Scale error	Linearity(R2)
Binos 1000 (NDIR)	CO	0-1000	±1.2%	0.9999
	CO ₂	0-5%	±1.3%	0.9999
Signal 3000 (FID)	THC	0-100	±0.5%	1
Eco physics (CLD)	NO (NO _x)	0-100	±0.7%	0.9999 0.9999
ADC (MAG)	O ₂	0-25%	-	0.9999
Signal MGA	CO	0-1000	±0.5%	0.9999
	CO ₂	0-5%	±0.5%	0.9999
	O ₂	0-25%	-	0.9999

Another important aspect of the calibration of the gas analysers is the need to maintain the same pressure at which exhaust sample are analysed for both zero and span points. It is important because using a higher pressure span point setting means a higher concentration which results in inaccurate calibration. The effect in the case of overpressure would result in analyser output readings less than the actual exhaust sample concentration. With regulators installed in the exhaust sample line in the MEL [137] and calibration cylinders a constant calibration and sampling pressure operation of 5 *psi* (34.47 *kPa*) is maintained.

Despite calibration of the instrument and all the care taken to ensure accurate gas concentration measurement, correction of the analyser output result is still necessary as important as a result of interference. The gas analysers respond to presence of components other than the gas that is to be measured. During recommissioning of the MEL [137], the interference effect factors were determined through laboratory measurement according to the Audit Procedures for Gas Analysis Instruments as contained in the Aerospace Recommended Practice SAE 1256C [138, 139]. Appendix A provides the interference correction factors obtained from laboratory experiments during the recommissioning of the MEL.

3.2 Exhaust Gas Distribution System

The aim of the exhaust gas distribution system is to deliver representative particulate emission from the gas turbine engine exhaust to the instruments without diluting the exhaust sample as expected by the reference gravimetric method (US EPA Method 5I and 202). Therefore the objectives are:

1. To isokinetically extract the sample from the exhaust.
2. To prevent particle transformation or nucleation inside the transporting lines before entering the instruments without diluting the exhaust sample.

Given the above listed objectives, the following factors were considered:

1. Distance from the extraction source to the instruments.
2. Limitations of the instruments.

Based on the above stated objectives and design factors, the design was largely developed based on the SAE Aerospace Information Report (AIR) 6421 [131] which recommends a framework for the distribution for particulate matter to multiple instruments from a single source. It recommends that instruments must be located no more than 35 *m* from the exhaust extraction point and heated so that the internal temperature is maintained at $160\text{ }^{\circ}\text{C} \pm 15\text{ }^{\circ}\text{C}$ to minimise particle transformation inside the heated sample lines for the sample collection section and specified at $60\text{ }^{\circ}\text{C}$ after dilution.

3.2.1 Description of the Sampling System

First and foremost, the exhaust sample extraction probe nozzle is positioned behind the exhaust exit plane and no further than half the exhaust diameter behind the engine exhaust plane as specified by Aerospace Recommended Practices 1256D [138] and 1533B [140]. This is contrary to the location of at least eight stack or duct diameters downstream and two diameters upstream from any flow disturbance such as a bend, expansion, or contraction in the stack as contained in US EPA method 5I. The US EPA method 5I exhaust extraction probe nozzle location point was not possible for the test engine given its location and the tending space required for the multiple instrument sampling.

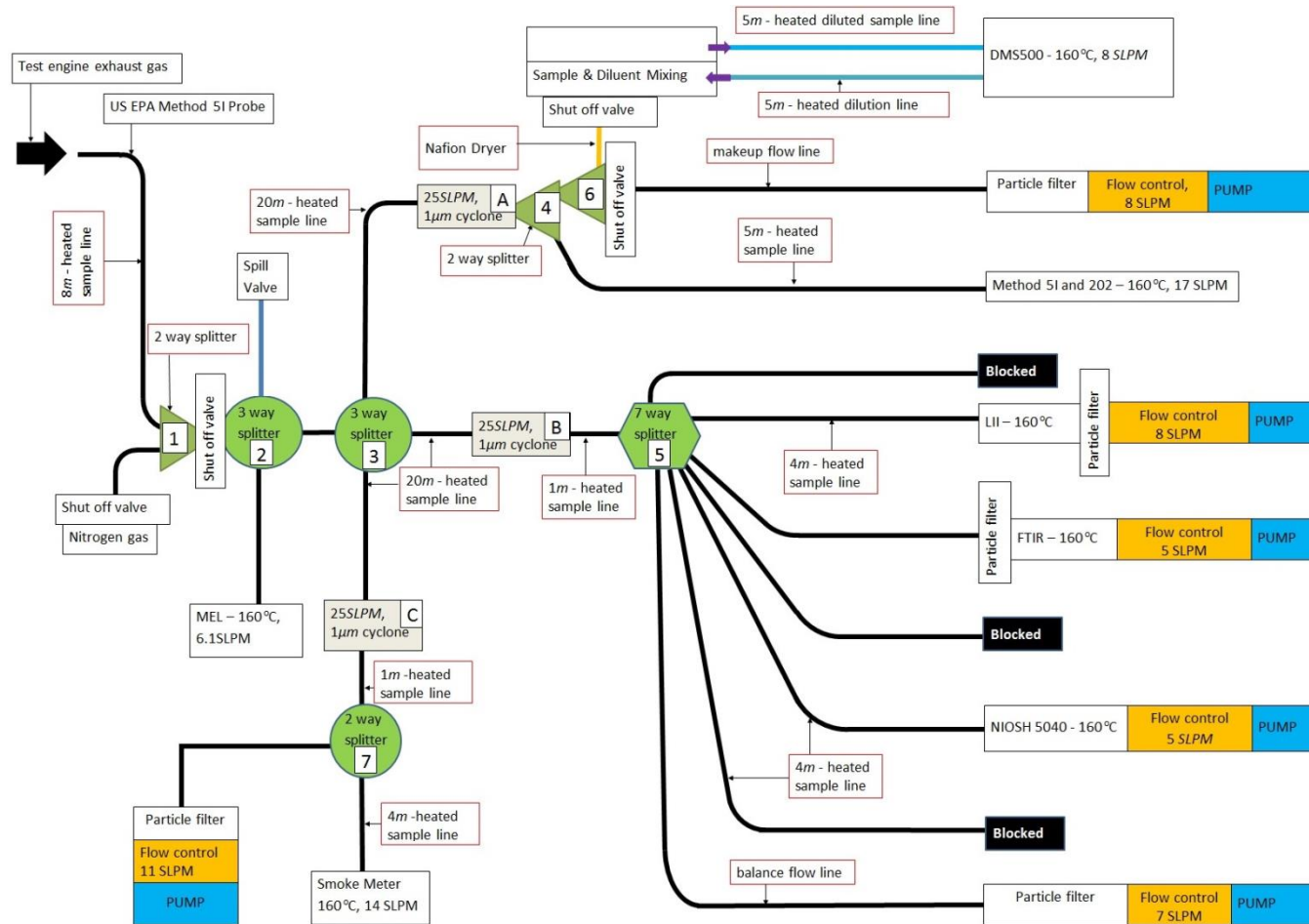


Figure 3-11: Schematic of the experimental setup

A method 5I extraction nozzle (probe) was selected to extract the sample in from the engine exhaust plane. The US EPA method 5I specifies that the integrity of the exhaust sample needs to be preserved during extraction. That is, the exhaust gas sample must be extracted isokinetically, thus the method 5I procedure defines a method for monitoring the isokinetic sampling. However, it was determined as reviewed in section 2.7.1 that the method 5I probe nozzle design is enough to guarantee isokinetic sampling when placed directly behind the exhaust plane of the laboratory gas turbine test engine. Full details and a picture of the probe is presented in section 3.2.2.

Working with the 35 *m* heated sample line framework, the method 5I sample probe nozzle is attached to an 8 *m* heated sample line to form the primary extraction and distribution line to all the instruments. The sample extraction line is connected to a two way flow splitter '1', which is coupled to a shut off valves linking a purge gas line and a three way flow splitter '2' respectively (refer to Figure 3-11 for numbers in parentheses). Hence, prior to engine start the 8 *m* heated sample line with the probe nozzle can be isolated with a valve and then purged to avoid exhaust build up in the sample system. The flow splitter '2' distributes exhaust sample to the gas analysers in the MEL through a 5 *m* heated sample line; a second three way flow splitter '3', through a 1 *m* heated sample line; and the third split connected to a spill valve.

The first instrument limitation which had to be considered is the particle size restriction of the DMS500. It is important that the particle analysed by the instrument are less than one micron otherwise it can result in the instrument damage. Thus, it is necessary to include a cyclone of a 1 micron diameter cut-off upstream of all the PM instruments to ensure uniformity in particle been analysed. Consequently, the designed sampling system has focused on correlating particle emissions between the instruments, of less than or equal to one micron PM size. Accordingly, one micron cyclones have been employed to achieve the defined PM size targets. Therefore, connected to the flow splitter '3', are three one micron cyclones labelled A, B and C in Figure 3-11. Between, the flow splitter '3', and the cyclones are 20 *m* heated sample line each.

The mass flow restrictions of the three cyclones are 25 *lpm*. In contrast the total mass flow required by all the instruments downstream is 56 *lpm*. Normally, the sampling duration of US EPA method 5I and 202 protocols is dependent on the flow rate of the exhaust flow through it and as such can be up to 50*lpm*. Therefore, with the experience from Smallwood et al [92] experiment and the need to achieve the best possible reduced time duration the DMS500 and the method 5I and 202 were assigned to the cyclone labelled A, as shown in Figure 3-11. As the exhaust sample exits cyclone A, a two way splitter, '4', distributes the exhaust sample to the US EPA method 5I at 17 *lpm* via a 5 m heated sample line. The second flow exit from splitter '4' is further split into using a two way splitter, '6'. Splitter '6' is linked via a Nafion dryer and a 5 m heated sample line to deliver exhaust sample flow at 8 *lpm* to the DMS500. The remaining splitter '6' exit is connected to a shut off valve, a flowmeter set at 8 *lpm* and a rotary vane pump.

The rationale for connecting a pump downstream a flowmeter set at 8 *lpm* is to compare the use of a Nafion dryer and dilution to address the issue of water condensation inside the DMS500. Water vapour is a known constituent of gas turbine exhaust and it can lead to damage the DMS500 if it condenses into liquid inside the instrument. Though, preliminary investigation of the technique [91] suggests the dryer has no impact on the characteristics of combustion particles, further investigation to evaluate the impact of the Nafion dryer on the DMS500 results is important. Meanwhile, the dilution head operated by the DMS500 with is located upstream of the 5 m heated sample line connected to the DMS500. Inside the DMS500 further dilution can be carried out as it comes with a rotary disc diluter. In total a dilution ratio of up to 3000 can be achieved.

The one micron cyclone labelled B, distributes exhaust sample to the FTIR, LII and NIOSH 5040 filter holder through a seven way flow splitter, '5'. The essence of a seven way splitter is to create room for the addition other instrument if the need arose. Since, the seven ways flow splitter supplies only three instruments, three of the flow exits is blocked off while the remaining one is connected to a particle filter, a flow controller and a pump in series. The particle

filter, flow control and a pump connection, allow regulation of the deficient flow needed by the cyclone for efficient particle size cut off. Meanwhile, to ensure that the heated sample line length between cyclones and the instruments are the same, the seven way flow splitter is first connected to the cyclone with a one metre heated sample line and the instruments connected to the seven way splitter are all linked with a 4 m heated sample line each.

The third cyclone labelled C in the sample distribution schematic, delivers samples to the Richard Oliver smoke meter through a two way flow splitter '7' and a pumping system for a balance flow to maintain the 25 lpm required by the cyclone. Connecting the two way flow splitter and the cyclone is a one metre heated line likewise; a 4 m heated sample line connects the two way flow splitter and the smoke meter.

3.2.2 Sampling Probe

Figure 3-12 shows a picture of the exhaust extraction probe. It is as specified by the US EPA method 5I for exhaust sampling from engines with low particle emissions. It is made of a quartz glass material to prevent the reaction of the probe material with the exhaust sample and design to a button-hook shape. It is a single point sampling probe of 14.1 mm OD (8 mm ID) with a vertical length of 10 cm before attaching to the heated probe sample line. The inlet of the probe is grounded to a sharp, tapered leading edge to enhance isokinetic sampling by maintaining the exhaust sample stream lines as they enter into the probe. The angle of taper is less than 30°, with the taper on the outside to preserve a constant internal diameter.



Figure 3-12: USA EPA Method 5I Probe

3.2.3 Heated Sample Lines

All the PM instruments used in the experimental setup rely on a sampling system to deliver exhaust gas to the analyser. The SAE AIR 6241 [131], recommends that the sample line diameters should have an internal diameter of between 7.59 and 8.15 mm which corresponds to nominal line outer diameter dimensions of 3/8 inch, 7/16 inch, and 10 mm. Consequently the 3/8 inch dimension was selected. To prevent any step change in the sampling system, the sample line internal diameters and the connection fitting have the same internal diameters. Where bending or shaping of the sample lines is required the sample lines was subjected to bending radius greater than 10 times [81] the inside diameter of the line to minimize particle deposition in the sample lines. The heated sample lines used where self-regulated but the internal temperature was monitored using K-type thermocouples to ensure that the temperature reading where $160\text{ }^{\circ}\text{C} \pm 15\text{ }^{\circ}\text{C}$ within the sample temperature limitations of EPA Method 5I protocol.

3.2.4 Splitters

As shown in the experiment schematic (Figure 3-11), a number of splitters are required to distribute the PM sample to the PM measurement instruments. The splitters includes; two way splitters, three way splitters and a seven way splitter. To ensure that the flow to each system is uniform the splitters were designed as specified in SAE AIR 6241 [131]. The SAE AIR 6241 recommends that the flow angle between the split flows is small as practically possible but should not exceed 35 degrees. The flow splitters are made of stainless steel and where machined with internal shoulder equal to the wall thickness of the stainless steel tubing, thus making the internal diameters of the tubes and splitter fit without any shoulders. Figure 3-13 show a picture of the three and two way splitters used. The splitters were wrapped with controlled heating tapes and insulation to ensure that the internal temperature inside the tube were the same ($160\text{ }^{\circ}\text{C}$) as the heated sample lines.



Figure 3-13: Photograph of $\frac{3}{8}$ " 2 way splitter and manufactured splitters [45]

3.2.5 Cyclones

The cyclones are sharp cut cyclone designed and specially made to order by Mexas Laboratory in the United States. It was first specified by Greg Smallwood at National Research Council (NRC) Canada and Mexas Laboratory has allocated the part number BGI 3800 NRC Canada. This cyclone achieves the one micron size cut-off at a flow rate of 25 litres per minute. A picture of the cyclone is shown in Figure 3-14 below. The cyclone is designed with $\frac{3}{8}$ " inlets and outlets thus ensuring no shoulders are witnessed when connecting to imperial sample lines before or after the cyclone.



Figure 3-14: Photograph of Mexa Labs specially made to order PM1.0 sharp cut cyclone [45]

3.2.6 Nafion Dryer

Figure 3-15, is a picture of the Nafion dryer located upstream of the DMS500. It is of the PD series gas dryers manufactured by perma pure which contains a hundred 0.030" O.D. Nafion tubes arranged in parallel housed within a single large tube shell. For reference, the manufacturer model number is PD-100T. As Nafion dryer selection is based on the sample flow rate across the tubes dryer and dew point, the choice of the PD-100T model is determined by the 8 *lpm* at which the DMS500 receives sample gas.



Figure 3-15: PD-Series Nafion dryer

3.3 The Gas turbine Test Engine

The gas turbine test engine is a GTCP85CK series (Figure 3-16) Auxiliary Power Unit (APU), manufactured by Honeywell with a 32 *kW* electricity generator attached. The GTCP in the code means a gas turbine compressor unit with shaft power capabilities. It is widely used in the aviation industry commonly in aircraft for the purposes of providing power for stand-alone, ground-based operation of an aircraft and its compressor flow can be split between the combustor and other aircraft functions, like, the aeroplane environmental control and main engine start. The gas turbine engine is comprised of a two-stage centrifugal compressor with a compression pressure ratio of approximately 5:1, a single-can combustor, and a single stage radial inflow turbine. The engine is rated to produce bleed air flow of 58 *kg/min* at 220 °C exhaust gas temperature (EGT) and 0 *kW* shaft work; a maximum shaft work of 149.2 *kW*; and a maximum EGT of 621 °C.

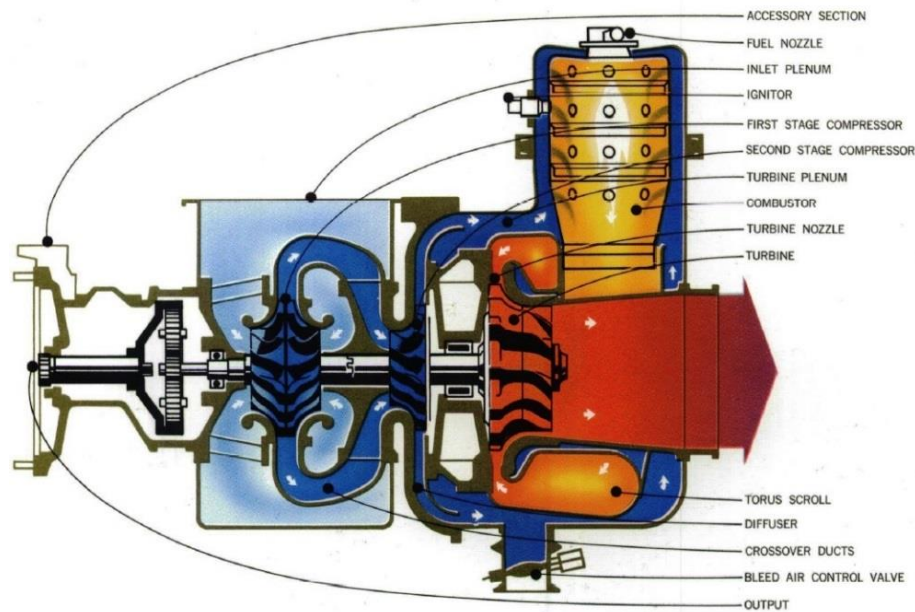


Figure 3-16: Schematic of the HoneyWell GTCP85 series gas turbine [141]

As a laboratory test engine in the University of Sheffield Low Carbon Combustion Centre, it is mounted on a test bed with various pressure transducers and thermocouples to monitor the performance of the engine. The engine test bed facility provides an ideal experimental platform to simulate engine performance and emissions of various liquid fuels on a modern gas turbine engine. The rig fits in the range of possible combustion analysis between laboratory bench scale testing of fuels, of the order of a litre of fuel, and full engine tests, requiring thousands of litres. This has advantages in sourcing sufficient quantities of fuel for testing and the possibility of running several fuels back to back, through one test engine.

3.4 Summary

This chapter details the PM instruments used in this research to generate correlations with the US EPA method 5I. Thus, considering the fact that the instruments have different specification the chapter covered the following;

- Specification of the instruments and their operating principle. It also covered the instrument calibrations.
- The gaseous instruments employed for this study were also presented, describing their operating principle and calibration procedures adopted.

- A description of the exhaust sample distribution system design. It detailed the sampling constraint considered including; the instrument specification; space; and the requirement of the gravimetric reference method.
- Details of the components parts of the sampling system have also been described in detail with their respective functions.

4 Preparatory Tests

This chapter covers various preparatory experiments that were carried out to acquire information necessary for the sample design as described in chapter 3 and to decide on the best approach to generate PM mass concentrations representative of industrial gas turbine from the test engine. An overview of the experiments is as follows:

1. Engine performance and certification gas emissions
2. Traverse test
3. Test Engine PM Emission Concentration Correlation with Fuel Aromatic Content
4. Characteristics of particulate emission from different aromatic species
5. Verification of test engine particle size distribution.

4.1 Engine Performance and Certification Gas Emissions

This section describes tests to ascertain the performance of the test engine. The test focused on the engine stability at selected engine operating conditions and the conventional gaseous emissions. Three operating modes, each representing a specific load on the APU [43, 89]: no-load (NL); ECS (all air conditioning [A/C] packs operating); and main engine start (MES) were selected to conduct the test. In a laboratory, the ECS conditions would ideally be simulated using a load bank of different electrical capacity, resulting in a change in fuel flow to the combustion chamber. However, efforts to use a load bank on the APU have shown no corresponding changes in fuel flow to the combustion chamber and exhaust gas temperature. This has been attributed to the high amount of energy going into the installed 32 kW generator on the APU. Thus, the power set points were achieved by varying the air-fuel ratio in the combustion chamber by regulating the bleed flow bleed flow valve while using the exhaust gas temperature as an indication of change in engine power to simulate the ECS and MES engine condition. Figure 4-1 is a picture of the engine showing the bleed

valve and the bleed exit from the engine. Care was taken to make sure that the engine had reached a steady operating condition before the data was recorded.

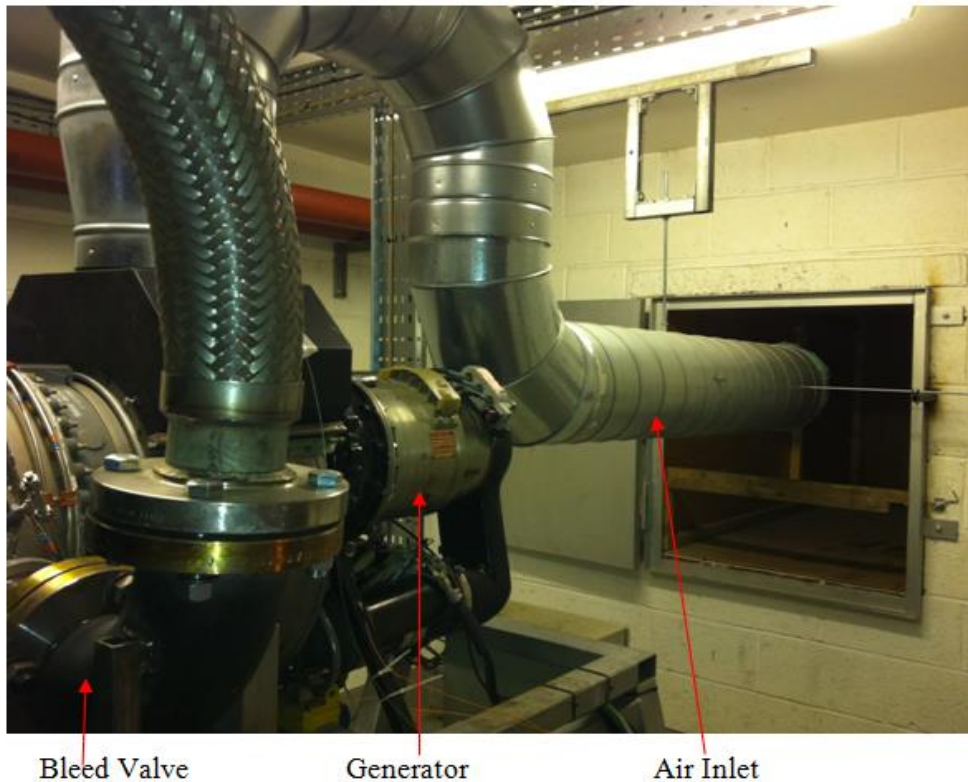


Figure 4-1: Picture of the test engine showing the bleed and air inlet

4.1.1 Exhaust Sample Transfer Line

The gaseous emissions were sampled from the APU exhaust as per the Aerospace Recommended Practice [81, 138, 139]. Figure 4-2 shows a picture of the sample probe used to extract exhaust gas samples to the gas analysers in the MEL. The probe tube used is of a quarter inch outer diameter made of a non-reactive material – in this case stainless steel. Positioned behind the APU exhaust at no further than half the exhaust nozzle diameter of the engine, the exhaust blockage was no more than 5% of the exhaust exit plane. The probes have been used in previous measurement campaigns [142] to extract PM and gas samples from a gas turbine engine which was satisfied to meet the relevant SAE Aerospace Recommended Practices.

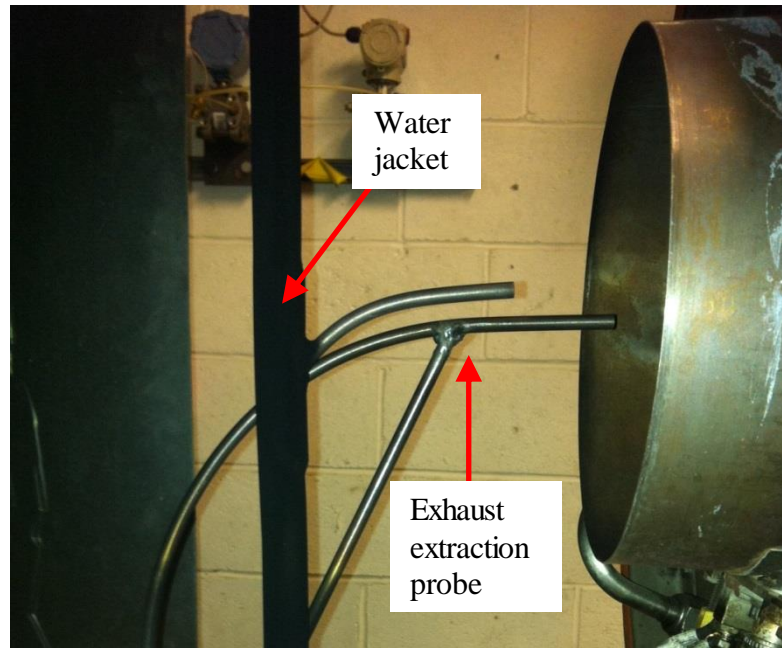


Figure 4-2: Picture of the exhaust gas extraction probe

Temperature conditioning was in place to ensure that water vapour in the sampled exhaust gas did not condense in the sample system. Thus, the probe was actively cooled to avoid overheating and to maintain the sample temperature at no less than 150 °C. The sampled exhaust gas extracted at the probe tip travels 38 mm (1.5”) through the length of the probe tube before entering a 16 m (50 ft) long heated sample line used to transport the exhaust sample to the MEL. Also, to ensure a steady flow of the exhaust through the heated sample line it was laid with a minimum bend radius of ten times the inner diameter of the line.

4.1.2 Data logging and Processing

4.1.2.1 Engine Performance

A data acquisition system was used to log a complete set of engine operating parameters. The data logging system as shown in Figure 4-3 provides the measurement of key engines operating parameters including, spool speed, fuel flow and exhaust gas temperature with a timely response of 50 ms. The logging system also records the engine pressure and temperature distribution at selected location, including the inlet air stream and within the fuel and oil systems of the

APU. Boolean data are also logged, which details the status of the ignition, fuel and oil systems mainly used for operator feedback.

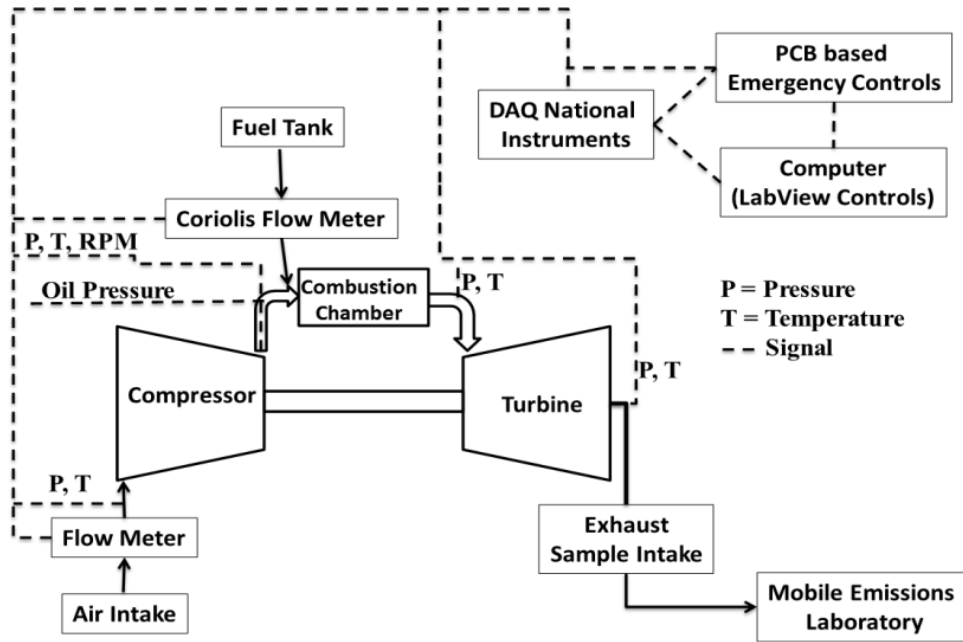


Figure 4-3: Schematic of the data logging system for APU performance monitoring

4.1.2.2 Gas Analysers

The gas analysers in the MEL are all linked to a data logging software. Figure 4-4 is a snap shot of the user interface. The software has been programmed to generate dry emission results and corrected emission indices at standard temperature (273.15 K) and pressure (101.325 kPa) for each pollutant using the equations outlined in SAE ARP 1533B [140]. The emissions index of constituent Z, EI_Z , is the ratio of the mass of constituent Z to 1000 mass units of fuel consumed. It is expressed mathematically as follows:

$$EI_Z = \left[\frac{\text{mass rate of Z}}{\text{mass rate of fuel}} \right] \times 1000 \quad 4.1$$

The software is programmed to log in sample concentrations in percentage and parts per million (ppm) every second depending on the analyser. These logged data is averaged over a period as determined by the operator during which the dry emission index is generated. The dry emission index (EI) results are presented in

this section to maintain consistency with emission measurement in literature [143]. Full details of the wet and dry concentration are contained in Appendix B.

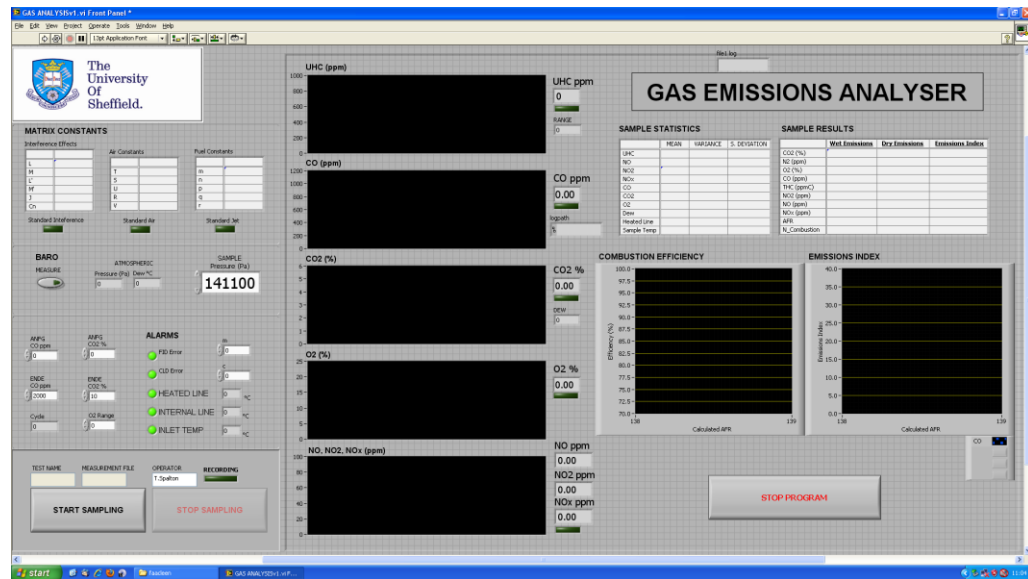


Figure 4-4: LCCC Gaseous Emission Analysers, Data Acquisition Snapshot

4.1.3 The Test Fuels

The APU is designed to burn jet fuels and petroleum diesel thus the two fuels selected to conduct the test includes: Jet A-1 and petroleum diesel. Selected fuel properties are presented in Table 4-1. Data for Jet A-1 have been provided from laboratory measurement, while the diesel fuel properties were taken from EN590:2009 [144] except otherwise referenced.

Table 4-1: Nominal Fuel Composition

Fuels	Density	LHV	C Fraction	HC Ratio	M.W	Aromatic
	kg/m^3	MJ/kg	wt/wt	mol/mol	g/mol	$\%v/v$
Jet A-1	801.9	43.21	0.861	1.899	151.715	18.5
Diesel	827.1	42.7	-	1.797	157.700	24.4

4.1.4 Results

4.1.4.1 APU Performance

Figure 4-5 shows the engine power cycle matrix represented by the exhaust gas temperature (EGT), fuel flow rate and RPM against time for the test fuels used in this study. The graphs indicate that the fuel flow rate and exhaust gas

temperatures for the test fuels are approximately the same. It shows that the target power settings were maintained in the course of the experiment. Furthermore, the reproducibility of the engine is evidenced as the engine achieved the same RPM, fuel flow rate and EGT values for the NL engine set point for diesel prior to shut down. The high RPM shown by diesel fuel compared against the Jet A-1 is the resultant of the higher density of diesel over Jet A-1.

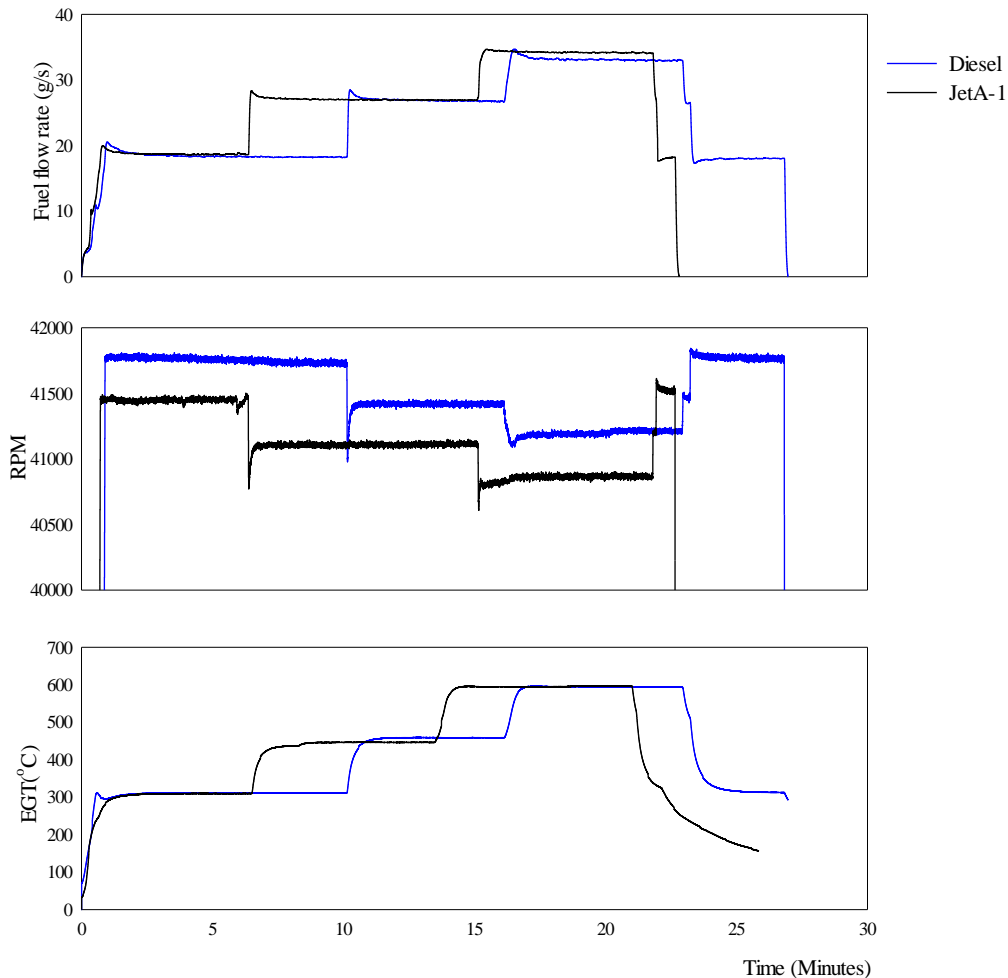


Figure 4-5: APU engine performance

4.1.4.2 Gaseous Emissions

The APU emission indices for total hydrocarbons (THC) presented in methane equivalent, carbon monoxide (CO) and nitrogen oxides (NOx) have been plotted against the engine operating conditions of the APU represented by the exhaust gas temperature. Results for each pollutant are grouped on the same graph for the tests

fuel as shown in Figure 4-6. The observed emission trends are similar with GTCP85 APU emissions presented in literature [143] where similar fuel hydrogen and aromatic content fuel were used for the same engine operating conditions.

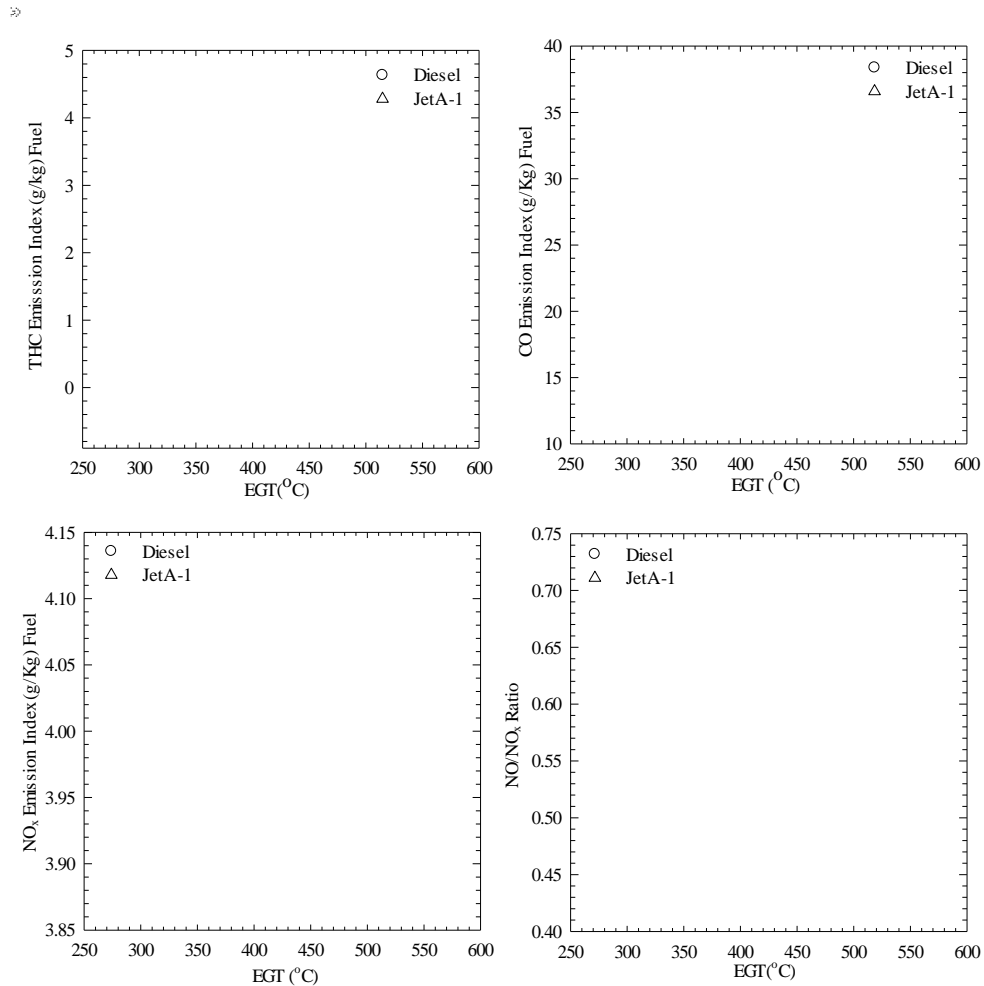


Figure 4-6: THC, CO and NO_x Emission Indices and NO/NO_x Ratio

The emissions index decreases with increasing engine set points for the THC and CO emissions while it increases with NO_x emissions for both fuels with respect to the engine set points. Total hydrocarbons (THC) emissions, like carbon monoxide, are associated with combustion inefficiency and as such are dependent on the loading of the gas turbine. For example, a gas turbine that operates under a full load will experience greater combustion efficiencies and a reduced formation of carbon monoxide when compared with a no load set point for the engine. Thus, the total hydrocarbon emissions from a gas turbine show the same trend as the carbon monoxide. The THC emission levels for Jet A-1 and diesel are less than 5

g/kg of fuel with maximum values of 4.52 *g/kg* and 4.28 *g/kg* at the NL engine set point for both fuels respectively. Similarly, CO emissions can be observed to have 37.4 *g/kg* and 34.9 *g/kg* of fuel for diesel and Jet A-1 respectively. CO and THC emissions are lowest at the MES engine set points.

The principal mechanism for the formations of NO_x emission from a gas turbine is thermal NO_x, which arises from the thermal dissociation and subsequent reaction of nitrogen (N₂) and oxygen (O₂) molecules in the combustion air. On the average the NO_x emission index, for all the engine test points is 4 *g/kg* of fuel ranging between 3.86 *g/kg* and 4.1 *g/kg* of fuel. Meanwhile the ratio of NO to NO_x is 0.73 for the Jet A-1 and 0.72 for diesel for the MES operating condition, thus an indication that the NO_x analyser was without problems during testing as noted in the SAE ARP 1533B [140].

4.1.4.3 Combustion Efficiency

The combustion efficiency as contained in the SAE ARP 1533B [140] is also programmed in the gas analyser data logging software and as such presented in Figure 4-7 for the three engine operating conditions for the two fuels. The combustion efficiency, η_b , is determined based on enthalpy by subtracting the inefficiencies as a result of unburned hydrocarbon and CO from 100%.

$$\eta_b = \left[1.00 - 10109 \frac{EI_{CO}}{H_c} - \frac{EI_{C_xH_y}}{1000} \right] \cdot 100 \quad 4-2$$

Where:

H_c = Net heat of combustion of fuel in *J/kg*

Overall the combustion efficiency is greater than 98.6% with efficiencies above 99.5% recorded for both fuels at the MES engine power setting. Higher combustion efficiencies are generally observed for the Jet A-1 fuel compared to the diesel fuel at all the engine power conditions tested.

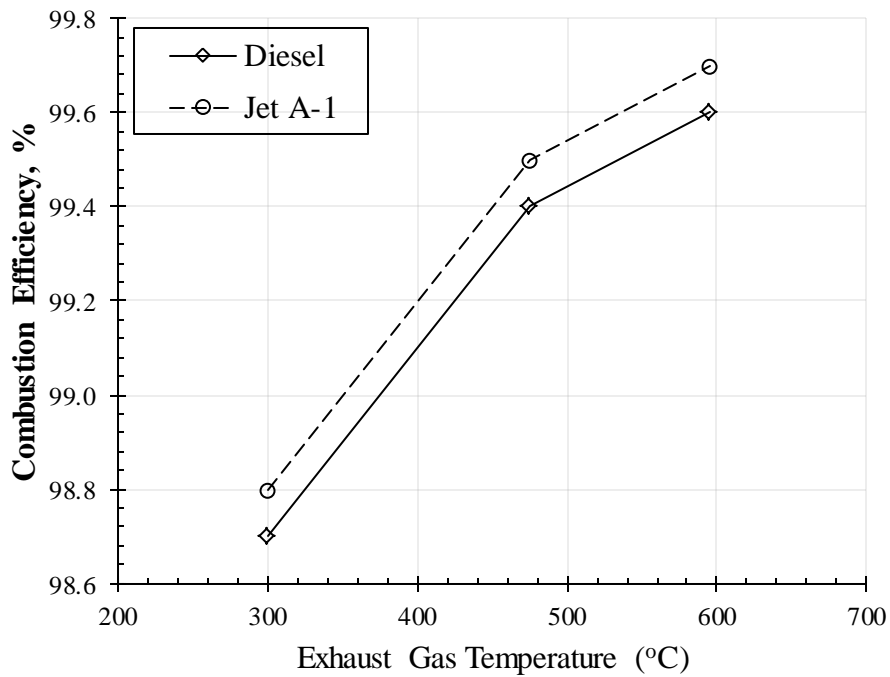


Figure 4-7: Combustion efficiency of test fuels versus EGT

4.2 Traverse Test

Emissions from gas turbine engines cannot be assumed azimuthally symmetric, in which case spatially resolved measurements across the engine exit plane are necessary at several steady state power settings to represent overall emissions from the engine [145]. Thus, a study of the particulate emission profile of the APU exhaust plane was necessary, to identify the probe position that best represents the engine particle emissions. A detailed mapping of the exhaust exit plane was achieved using a single probe mounted to a 2-dimensional traverse mechanism which allows sequential measurements at a number of spatial locations distributed across the exhaust plane.

No special rake design criteria other than extending spatially across the exhaust plane and sufficient structural integrity for the expected flow-field properties as defined by the exhaust temperature, pressure and gas velocity was required. Thus, the traverse system included a slide table attached to a linear worm drive turned by a computer controlled stepper motor that allowed remote positioning of the probe at discrete locations across the engine exhaust nozzle. Spatial mapping measurements was thus performed by first locating the probe at the centreline of

the exhaust nozzle ($x=0$ inches) after which the probe was stepped 75 mm (3.0 inches) from centreline along the horizontal axis and repeated for the opposite side of the exhaust nozzle centre line. Figure 4-8 shows the probe position investigated as identified in the picture as points A, B and C. The exhaust samples extracted with the probe were transported through a 5 m heated sample line to a DMS500 instruments which was employed for this investigation. The exhaust sample was diluted by a ratio of 57 prior to analysis by the DMS500.

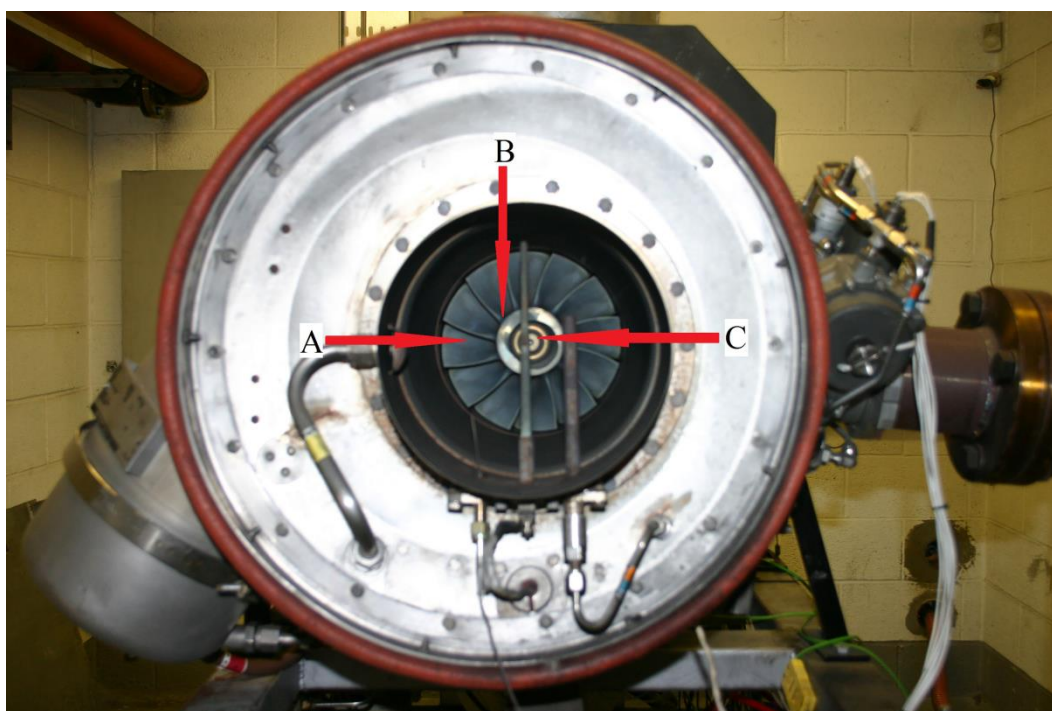


Figure 4-8: Traverse probe positions

4.2.1 Traverse Test Results

The total number and mass concentration for each sample extraction point and engine set point is shown in Figure 4-9 and Figure 4-10 respectively. The mass concentration was evaluated by assuming a unit density. As the purpose was to determine the variation of the mass concentration across the exhaust it was not critical to use an assumed uniform effective density to evaluate the mass concentration from the number size distribution of the DMS500. Measurement uncertainties highlighted using error bars were calculated using 1σ standard deviation of the averaged data.

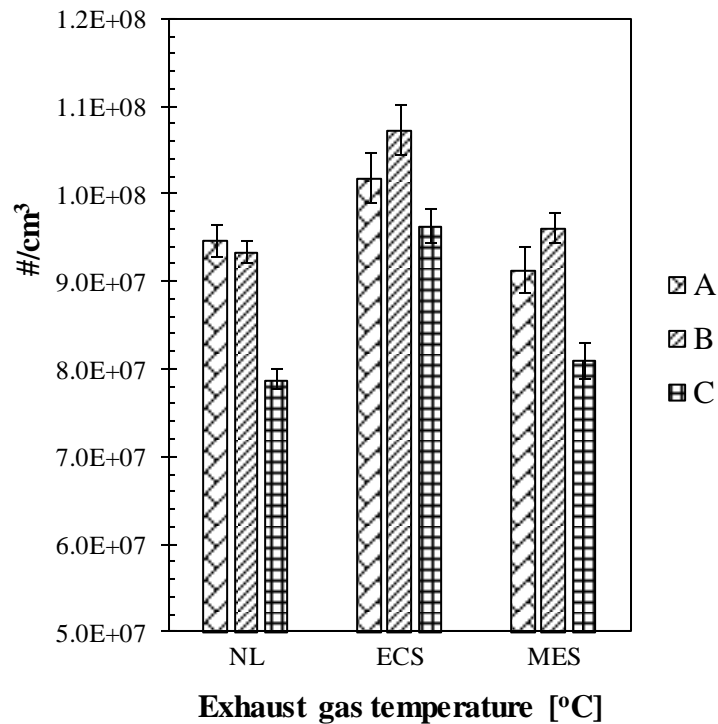


Figure 4-9: Total number concentration at traversed points

Figures Figure 4-9 and Figure 4-10 show that there is a significant spatial variation in the number and mass concentrations across the exhaust exit plane between point B and C. The number concentration is lowest at position C and varies from B by a factor of 10 from the number concentrations at position B. In a similar fashion the highest mass concentration occurs at position C and differs from the mass concentration at position B by a factor of 11. Thus the higher mass concentration and low number concentration observed at position C shows that larger particles are being found. As observed in Figure 4-8, the probe position C is at the centreline of the exhaust nozzle where the exhaust gas temperature and pressure sensors are located. Meanwhile, the errors bars of the number concentration and mass concentration at position A and B overlap therefore can be considered the same at best suited for the engine PM emission study.

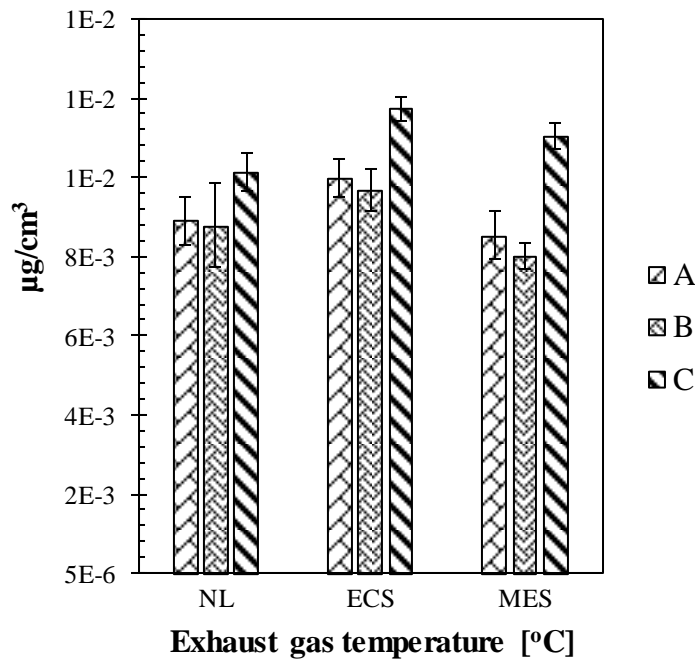


Figure 4-10: Total mass concentration at traversed points

4.3 Test Engine PM Emission Concentration Correlation with Fuel Aromatic Content

This section describes the test performed to assess the impact of the aromatic content by volume and aromatic species on the PM emissions of the engine. Industrial gas turbine fuels are largely petroleum based liquids and natural gas, with natural gas powered gas turbine power plants experiencing tremendous growth since the 1970s [135]. With natural gas the PM emission concentrations are in the region of $1 \text{ mg}/\text{m}^3$ [57]. This low level would be hard to achieve with the GTCP85CK engine even when operated at its most combustion efficient conditions as it is designed for Jet and petroleum diesel fuels.

To achieve this objective, alternative fuels from novel feedstock and production process pathway with different percentage aromatic volume content have been tested. Also tested are fuel blends of Jet A-1/ hydrogenated esters and fatty acids (HEFA) in addition to 100% HEFA and conventional Jet A-1 at three APU operating conditions. The compositions of alternative fuels especially with minimum aromatic content fall outside the current envelope of approved jet fuels which is largely due to the feedstock and production pathway processes. The novel blends contain synthetic aromatics of varying types and levels which is a

dimension of novelty and divergence from currently approved products for aviation gas turbines [146].

4.3.1 Test Fuels

A total of seven fuels were tested is summarised in Table 4-2. The fuel mixes include two blends of conventional Jet A-1 and synthesized paraffinic kerosene (SPK) - blending components from hydrogenated esters and fatty acids (HEFA); novel single processed fuel including alcohol to Jet A-1 and catalytic hydrothermolysis processes; two novel blends of gas to liquid (GtL)/sugar bioforming and cellulose aromatic/SPK .

Table 4-2: Selected specification of the test fuels

	Fuel Description				
	Fuel ID	Fuel Type and Description		Aromatic content	Density
Baseline blends	Jet A-1	Jet A-1	Conventional	17.3%	801.9
	Fuel 2	Jet A-1 + HEFA (50/50)	ASTM 7566 type Blend	8.6%	781.9
	Fuel 3	HEFA	ASTM 7566 type SPK	0.1%	761.7
Novel fuels	Fuel 4	Alcohol to Jet	Novel Single Process	9.4	791
	Fuel 5	GtL + Sugar Bioforming	Novel Blend	13.4	756.2
	Fuel 6	Cellulose - Aromatic +SPK	Novel Blend	19.7	782.5
	Fuel 7	Catalytic Hydrothermolysis	Novel Single Process	15.8	804.4

A detailed speciation of the fuels was carried out using a combination of gas chromatography and mass spectroscopy [147]. Overall all the fuels contain the same molecular types as conventional fuels but in some cases very different levels and ratios. Speciation of Fuel 2 which is a blend of conventional Jet A-1/HEFA shows the typical broad spread of n-, iso- and cyclo paraffins and also the range of single and multi-ring aromatic (see Appendix C for a detailed hydrocarbon analysis). For the novel fuels the aromatic content are synthetic and fall within the

narrow range specified by ASTM D7566 [146]. Fuel 4 and Fuel 7 contain both alkyl benzene and benzocycloparaffins while Fuel 5 and Fuel 6 are composed of only alkyl benzenes.

4.3.2 Engine Operating Condition

Three operating conditions for the GTCP85 APU were selected to conduct the test: no load (NL), environmental control systems (ECS), and main engine start (MES). Overall, the APU was very stable at each operating condition, and the reproducibility of the parameters during the study was very good. The APU was started and put through a warm up sequence before stabilising at the first condition. The test matrix followed a step up from NL to ECS to MES which represented 1 test cycle for each fuel evaluated.

4.3.3 Sampling System and Instrumentation

A DMS500 and Richard Oliver smoke meter was deployed for the PM emission analysis. Two separate single point probe placed within half a nozzle diameter of the APU exit plane and side by side were used to continuously extract exhaust sample to the analyser. To extract and transfer sample to the smoke meter the earlier described probe in section 4.2 was deployed. For the DMS500 the probe is 30mm long tube with a quarter inch outer diameter made of a non-reactive material – stainless steel. The probe was directly connected to a heated sample block (see - Figure 4-11) where a first phase dilution and pre classification using a one micron cyclone occurred.

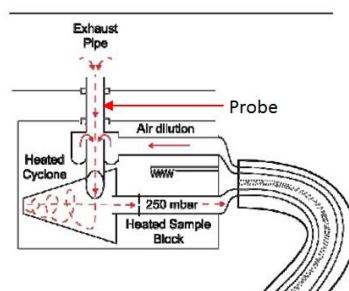


Figure 4-11: DMS 500 heated sample block

In the dilution chamber the exhaust gas was diluted with nitrogen prior to the one micron cyclone which ensured that only particles equal to or less than one micron are transported to the analyser. The diluted sample was then transported through a

5m heated sample line to the analyser where the exhaust sample was further diluted. The total dilution ratio which is a product of the first and second dilutions was on the average 200 ± 5 as calculated by the DMS500 control interface.

4.3.4 Results

Figure 4-12 shows a plot of the PM number concentration against the percentage fuel aromatic content for the test fuels for the three engine operating conditions. The results confirm the influence of aromatic contents on soot emissions from gas turbines. Overall the particle number concentration is highest at the ECS engine power setting with the exception of Fuel 3 where concentrations for ECS and the NL engine power settings are statistically equal. Meanwhile the NL engine power setting shows the lowest particle number concentration with the exceptions for Fuel 3, Fuel 2 and Fuel 5 which all indicate that the MES engine power setting emits the lowest particle number concentration. Similar trend can be observed with the SAE smoke number measure taken alongside the particle number concentration as shown in Figure 4-13.

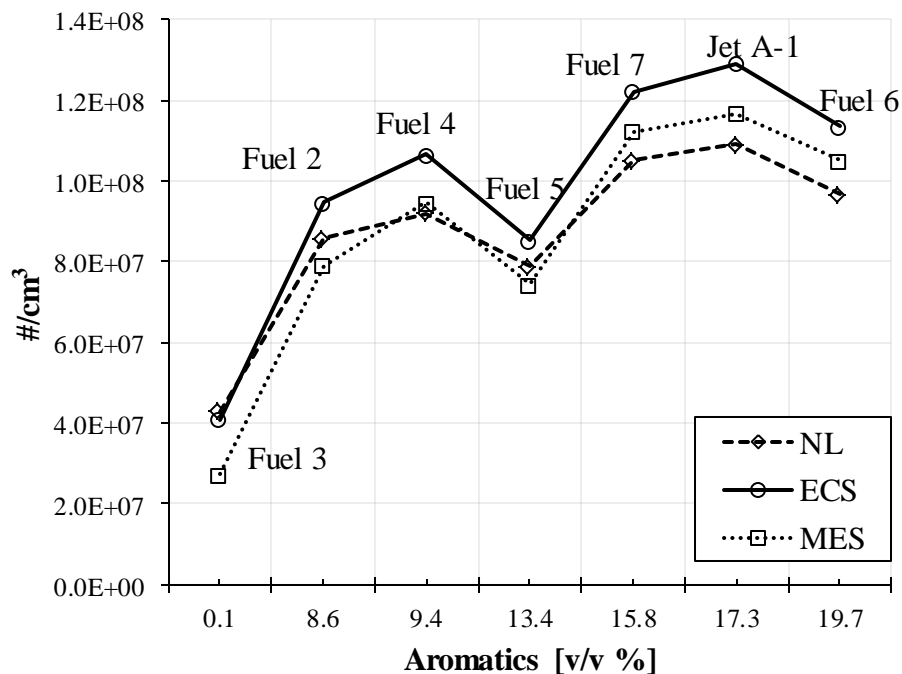


Figure 4-12: Particle number concentration for fuels 2 - 7 and Jet A-1

Jet A-1 which has the second highest aromatic concentration by volume has the highest particle number concentration for all three engine power settings. In

addition it can also be observed that the conventional Jet A-1 has the second highest density. Fuel 3 which contains no aromatic shows the lowest particle number concentration for all three engine power setting. Fuel 5 is the next fuel with the lowest particle number concentration despite containing 13.4% percent by volume of aromatics compared to Fuel 2 and Fuel 4 which both contain 8.6 and 9.4 percent by volume of aromatics. Meanwhile Fuel 5 has the lowest density of all the fuels tested. Also observed, is the difference in the particle number concentration between Jet A-1 and Fuel 6. Jet A-1 produces a higher particle number concentration despite its aromatic content by percentage volume being marginally lower than Fuel 6 aromatic content.

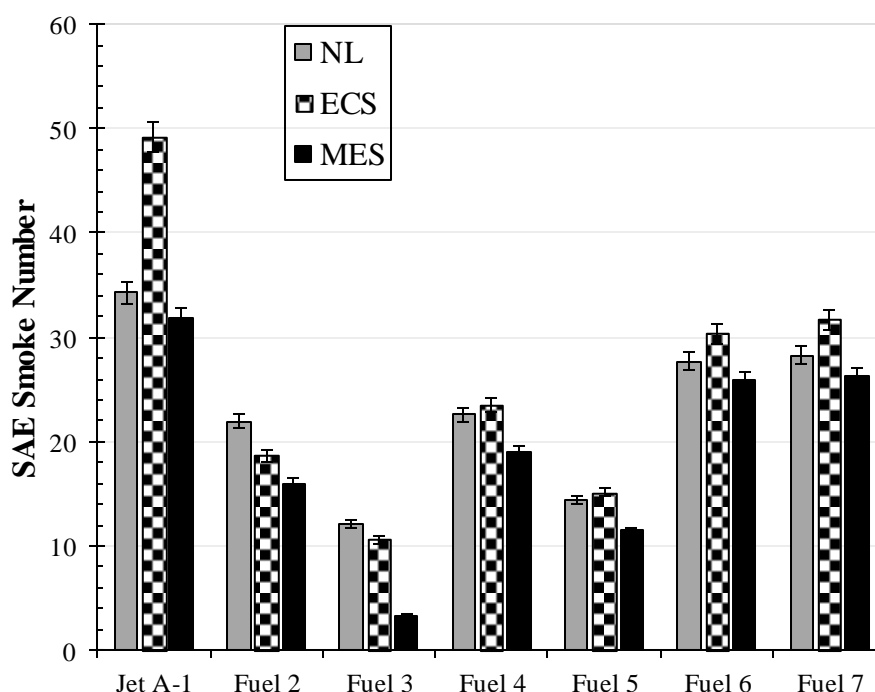


Figure 4-13: SAE smoke number for fuels 2-7 and Jet A-1

Figure 4-14 shows the geometric mean diameter of the each of the fuels at the three engine test points. It shows similar trend as observed with the particle number concentration and smoke number at each engine power setting. Overall the GMD is highest and lowest at NL and MES engine power settings respectively. Jet A-1 shows the highest particle sizes while PM emission from Fuel 3 which is composed of negligible aromatic exhibits the lower particle sizes. Despite Fuel 6 containing more aromatic than Jet A-1 (19.7% compared to Jet A-1 17.3%) the particle sizes are lower. Similar trend can be observed between Fuel 4

and Fuel 5. Fuel 4 contains lower aromatic by volume compared to Fuel 5 but the particle matter sizes are larger than PM emission from Fuel 5.

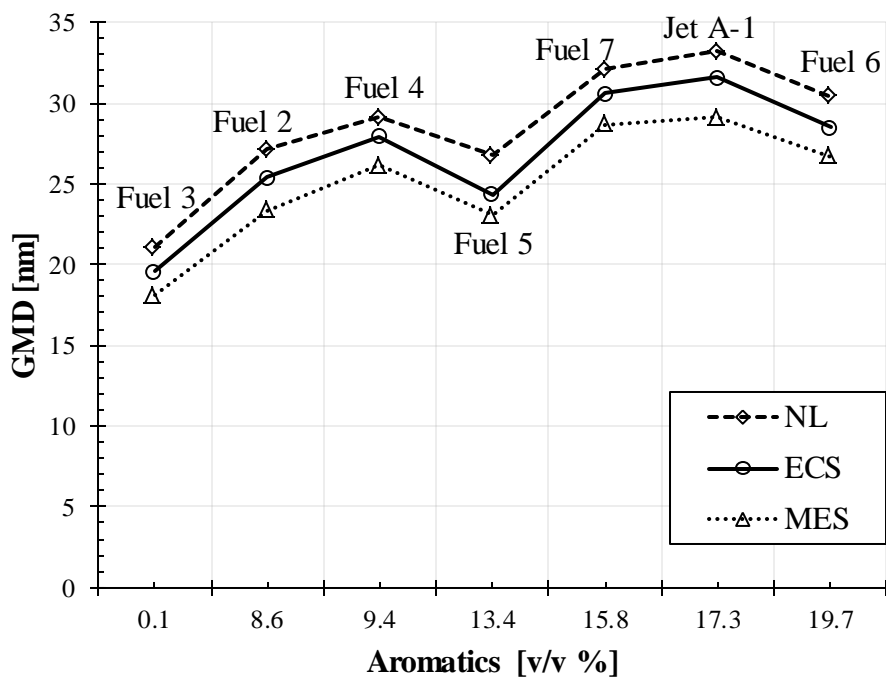


Figure 4-14: Geometric mean diameter for fuels 2-7 and Jet A-1

4.3.5 Discussion

From the hydrocarbon speciation of the fuels (Appendix C), the lower particle number concentration emitted and geometric mean diameter observed between Fuel 5 and Fuel 4 and Fuel 6 and Fuel 7, can be attributed to the aromatic species present rather than the volume. Firstly, Fuel 7 contains 11% by weight of benzocycloparaffins in contrast Fuel 6 which contain none with its aromatic content being of alky benzene type which in total are 18.6% against 13.8% by weight for Fuel 7. Thus, Fuel 7 generally contains aromatic that are denser and characteristically having a higher sooting threshold. Likewise, the same explanation can be given to the observed higher PM number concentration and geometric mean diameters observed for Fuel 4 compared to Fuel 5. Thus the observed feature suggests the rate determining steps to arrive at naphthalene (see section 2.1.1) are much faster for the fuels with multi-ring aromatic or benzocycloparaffins compared to alkyl benzenes to allow more time for particle growth by coalescence.

4.4 Characteristics of Particulate Emission from Different Aromatic Species

This section describes the test carried out to determine the relationship between fuel aromatic species and PM emission characteristics using a small scale premix burner. If doping of a low level aromatic content fuels were necessary to create different PM emission from the gas turbine test engine used in this thesis, one of the challenges would be the choice of aromatic species. As seen in the previous section there is no specificity about the impact of individual species on the PM emissions. To this end, a pre-mix burner has been used to compare the particle emission characteristics of a range of aromatic species blend with a baseline fuel with, zero aromatic content. The PM emissions generated are analysed using a laser induced incandescence instrument (Atrium LII300) to measure the refractory carbon concentration and the primary particle size distribution.

4.4.1 Experimental Details

4.4.1.1 The Premix Burner

The full description of the premix burner as detailed by Carrier et al [148] and modified by Lucas et al [149] is summarized as follows. The Premix Burner is a stand-alone soot generating burner based on vaporisation of premixed fuel in a controlled manner for ignition to generate flames. A small quantity fuel is added at a controlled flow rate to a hot air supply, and then vaporised to create an inflammable mixture. The flow rate of the air and fuel can be controlled to create rich or lean flame carbon formation. Although the laminar premixed burner flame study appears to be far from the reality of the turbulent phenomena happening with a turbine at high pressures, it provides an ideal platform to conduct fundamental premix combustion experiments.

The premix burner is a makeup of a number of individual glass sections assembled together as shown in Figure 4-15. At the core of the glass assembly is the shallow cylindrical vaporisation chamber, a riser comprising a mixing column and burner jet, and a protective glass chimney. By using glass construction, events

occurring within the burner; in particular, the accumulation of any fuel residues in the vaporisation chamber can be directly observed.

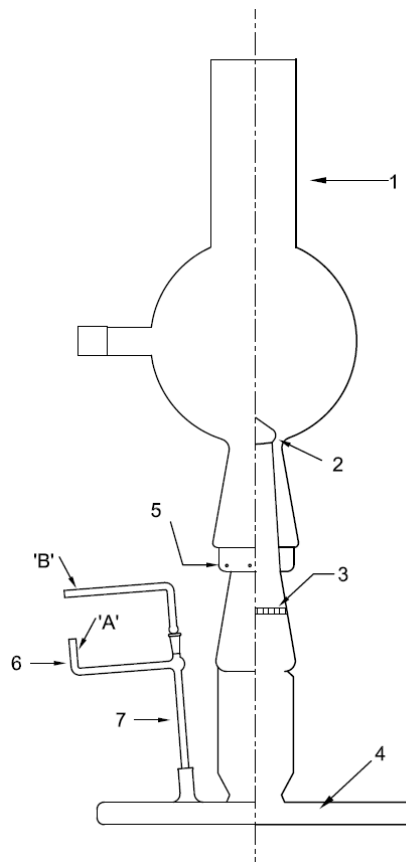


Figure 4-15: Schematic of Premixed Burner Assembly – 1, burner globe with side arm; 2, flame jet; 3, gas mixing baffle; 4, vaporisation chamber; 5, secondary air entrainment port; 6, fuel injector; air via 'A', test fuel via 'B', 7, test fuel capillary [148]

The vaporisation chamber is placed on a suitable hotplate. Also, placed on the hot plate is the air supply line of steel material coiled round the vaporisation chamber to produce the required hot air. Once at the required equilibrium temperature, fuel is injected into the vaporisation chamber with the continuous supply of air. Fuel is fed through a capillary tube seated inside a larger diameter glass tube, through which air is supplied. To avoid intermittent fuel flow through the capillary the test fuel is pumped into the capillary using a syringe pump that is capable of delivering extremely small volumes of liquid. The essence of co-annular supply is to enable heat exchange between the fuel and the heated air prior to its injection into the vaporisation chamber. This enables quick vaporisation of the fuel and air mixture. Also, the capillary terminates at an optimum distance above the chamber

base to aid instantaneous flash vaporisation of the fuel to be carried away by the surrounding air stream. The resulting mixture travels through the riser and the presence of an intermediates baffle ensure fully intimate mixing, prior to ignition by simply holding a flame over the top of the burner. The whole assembly is contained in an aluminium box which ensures that a uniform temperature and a draft free environment are maintained in the vicinity of the burner.

4.4.1.2 Test Fuels

Four aromatic species were investigated as listed in Table 4-3 with their chemical structures described. The aromatic species are not burnt directly but blended with a multi component surrogate fuel which contains decane, undecane, dodecane, tridecane and tetradecane. Two different percentage quantities by volume: 8% and 15% of the aromatic was blended with the surrogate jet fuel. In total 10 fuels have been tested including petroleum Jet A-1 and the surrogate jet fuels.

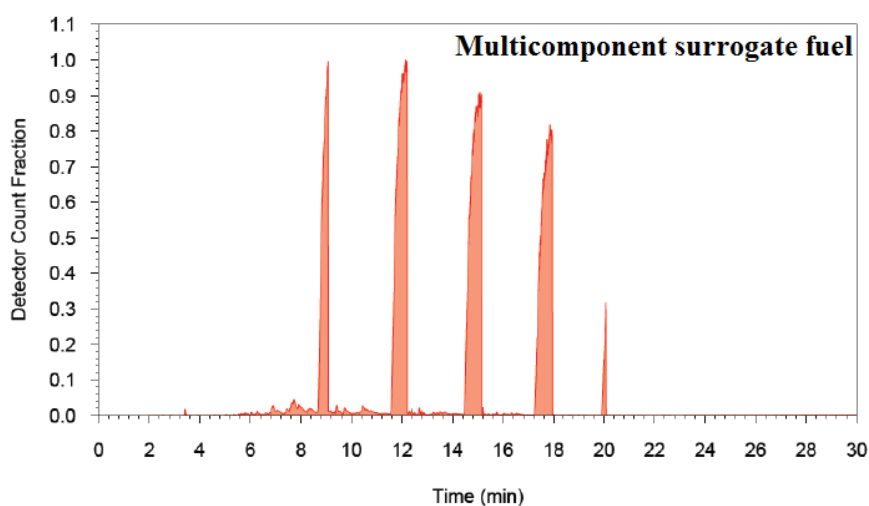
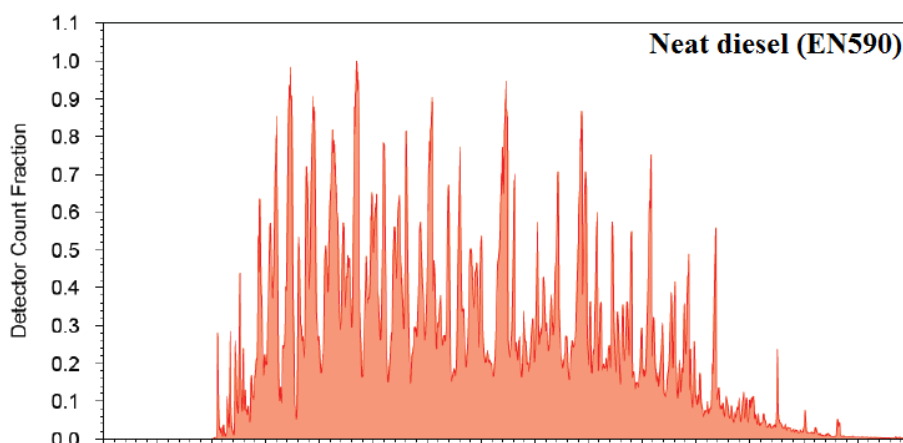
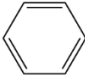
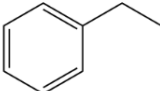
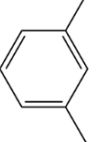
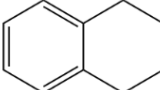


Figure 4-16: Gas chromatography and mass spectroscopy comparing diesel and the multicomponent surrogate fuel [150].

Table 4-3 Properties of Aromatics used in Experiments

Aromatic	Chemical Formula	Molecular Volume (cm^3/mol)	Molecular Mass (g/mol)	Chemical Structure
Benzene	C_6H_6	52.9	78.11	
Ethyl Benzene	$C_6H_5C_2H_5$	122.8	106.17	
m-Xylene	$C_6H_4(CH_3)_2$	123.3	106.16	
Tetralin	$C_{10}H_{12}$	136.6	132.2	

4.4.1.3 Burner Settings and Sampling System

One premix burner set point was used to investigate the test fuels. To determine the set point, the surrogate fuel was used since it would produce the least PM emission concentration as it does not contain aromatic. Therefore the aim was to achieve a rich mixture where the flame would be stable and the PM emission from the surrogate fuel would be detectable by the soot analyser. Accordingly, the operating condition set points are as follows: air flowrate of 1 l/min and fuel pump flow rate set at 27 ml/hr . Because of the offset of the syringe pump, the true value of the fuel flowrate when correct according to the premix burner manual [149] is 21.64 ml/hr . To ensure the quality of the results, contaminations between the test fuels was avoided within the fuel capillary by completely burning a syringe filled with the fuel under investigation to flush out traces of any previous test fuels before commencing testing for the fuel. The heating plate was set to 540 °C and the heating tape wrapped around the gas mixing baffle was set to 200 °C.

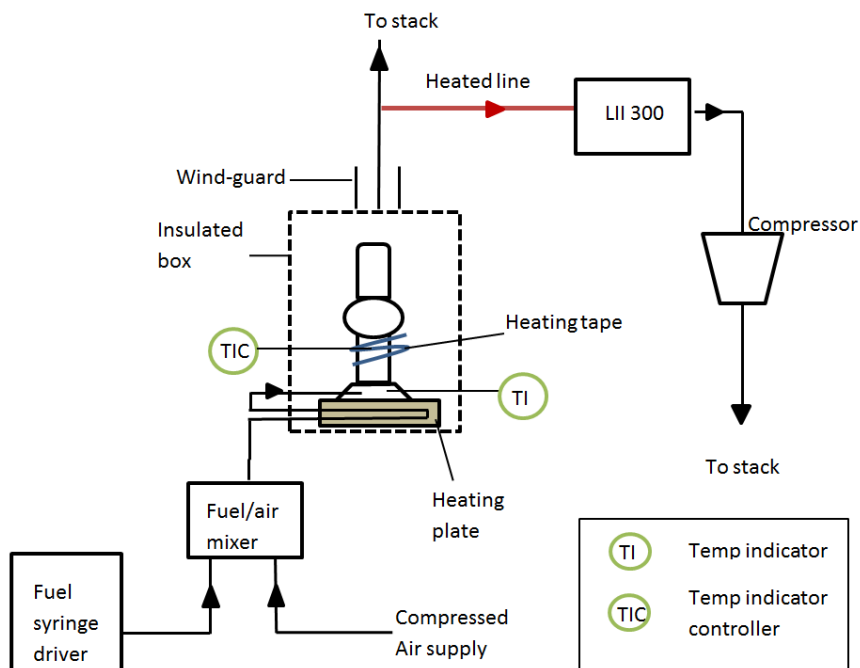


Figure 4-17: The premixed burner schematic [151]

The resulting effluent gas from the burner is extracted and transported through a one metre heated line that has an 8 mm inner diameter and directly connected to the PM emission analyser. The extraction location of heated lined probe inlet is located 5 cm above the top vent of the aluminium casing. The particle measurement system used is an Atrium LII300 described in section 3.1.2. It was used to measure the PM mass concentration and primary particle sizes. The analyser extract exhaust sample using an external pump placed downstream of the analyser at a flowrate of 8 litres per minute.

4.4.2 Results

4.4.2.1 Soot mass concentration

Figure 4-18 shows the soot mass concentration of the 100% surrogate fuel and Jet A-1 with error bars accounting for uncertainty of LII300 at $\pm 2\%$ [152]. From the figure it is clear that the PM concentration emitted compared to the conventional Jet A-1 fuel is negligible. Meanwhile Figure 4-19 showing the PM mass concentration of the fuel blends demonstrated the impact of aromatics in fuel. Comparing both figures it is clear that with blending of the surrogate fuel with any of the aromatic species there is a significant increase in the soot emitted.

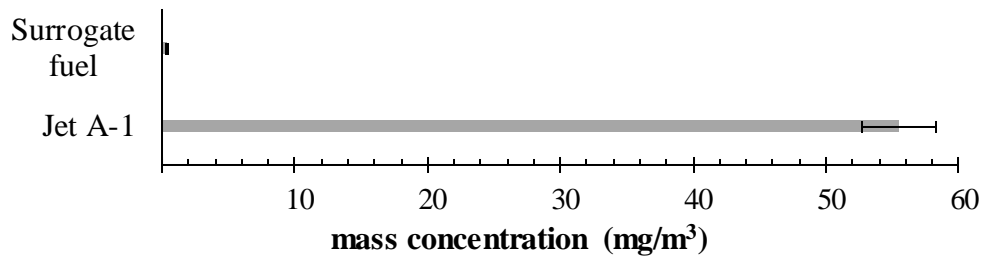


Figure 4-18: Soot mass concentration of the 100% surrogate fuel and Jet A-1

In the case of 15% tetralin blend the soot concentration produced is 48 times the concentration of soot concentration in the effluent gas from the surrogate. This restates the significance of the aromatic content in terms of particulate matter emissions and underlines the importance of aromatic selection towards particulate emission reduction from combustion.

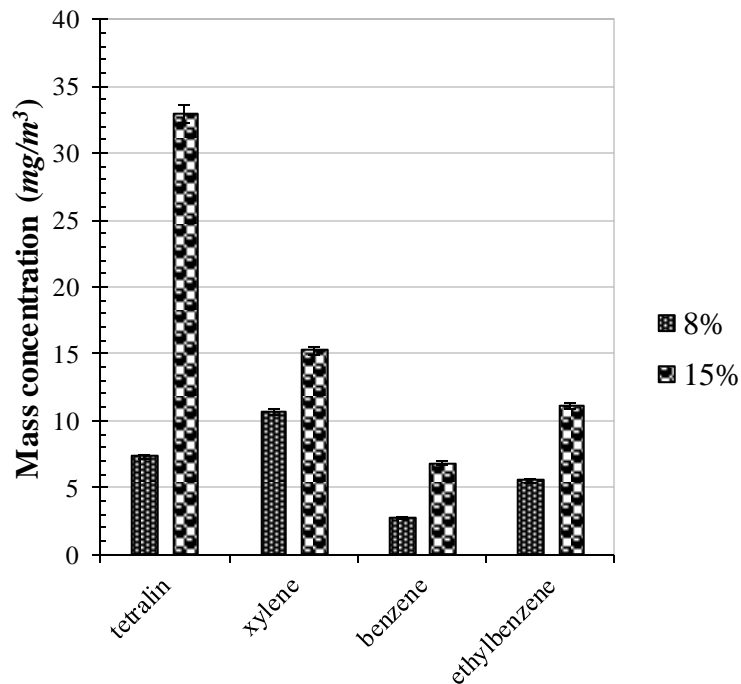


Figure 4-19: Soot mass concentrations emitted from blends of the surrogate fuel with aromatic blends

Comparing the soot concentration between the blends, benzene performs best in terms of low soot concentration followed by ethyl benzene and then xylene with for both 8% and 15% blends. Tetralin has significant high soot concentration for the 15% blend compared to the other aromatic specie blend at 15% but a lower

soot concentration can be observed for the 8% blend compared to the xylene. The most likely cause of this observation is that tetralin at 8% blend is interacting differently with the multi component surrogate fuel compared to been 15% in the fuel. The 100% surrogate fuel and benzene blend perform as expected with respect to each other and the other aromatics as described by Calcote et al. [37].

4.4.2.2 Soot particle size

Figure 4-20 shows the particle mean diameters emitted by the test fuels with error bars to account for uncertainty in the LII300 at $\pm 2\%$ as stated by the manufacturer [134]. The primary particle size detected varied for each additive used with tetralin emitting the largest particles with a mean diameter of 31.2 nm for the 15% blend with the surrogate fuel.

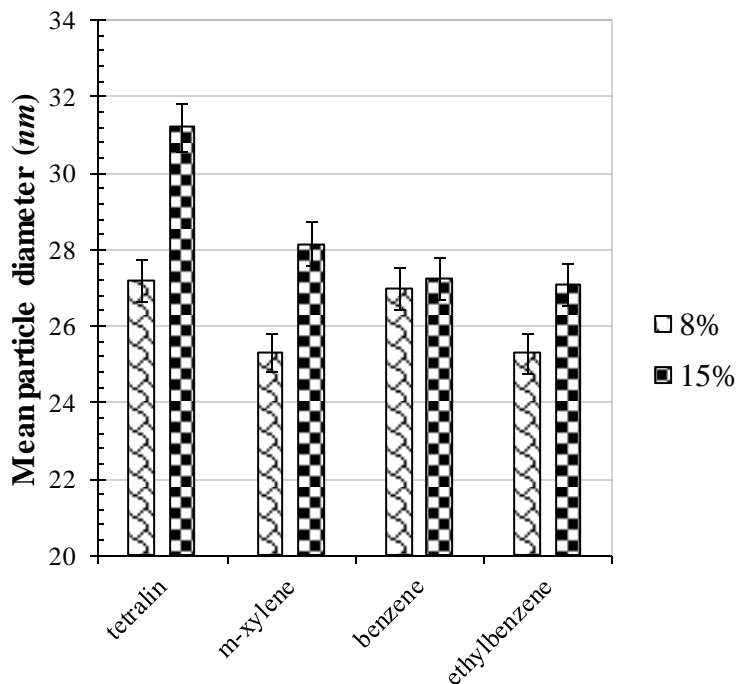


Figure 4-20: Mean primary particle diameter emitted by blends of the surrogate fuel and aromatic specie

Overall, the particle size for the 100% conventional Jet A-1 fuel is largest and significantly higher than particle size produced by the 100% surrogate fuel. The particle size for the 15% tetralin blend has similar size characteristics to the 100% Jet A-1 fuel. Compared to the 100% surrogate fuel, the particle sizes for the 15% aromatic blends are generally significantly larger than the particles exhibited by the 100% surrogate fuel. For the 8% aromatic blends the particle sizes for xylene

and ethylbenzene blends are within the particle size range for the 100% surrogate fuel all showing approximately 25 nm particle size diameter. However, significantly higher mean particle sizes can be observed between the 8% tetralin and benzene blends and the 100% surrogate fuel. The 8% tetralin and benzene blend show particle sizes of approximately 27 nm compared to the 25 nm observed for the 100% surrogate fuel. Also, unlike the lower mass concentration exhibited by the 8% tetralin blend compared to the 8% m-xylene blend, the particle sizes of the 8% tetralin blend are larger.

4.4.3 Discussion

The surrogate fuel alone shows low soot formation as expected as it lies on the alkane line shown in Figure 2-3. Benzene performed as expected with soot emission a lot higher than the paraffinic surrogate but less than the other aromatics with additional side chains and less carbons. The sooting concentrations observed between the fuels are in agreement with the TSI and YSI are in agreement with published literature [37] and [38]. However, mass concentration for the 8% tetralin blend compared to 8% xylene blend disagrees with the TSI and YSI. Meanwhile with respect to the mean particle size of the particulate emitted tetralin shows a higher particle size than the xylene mean particle size for the 8% blends.

These results bring into focus the chemical mechanisms that lead to the formation of the particles and also the physical particle growth mechanism. Experiments to determine the sooting indices of TSI and YSI were implemented using methane as the base fuel with the hydrocarbon of interest as the dopant or were combusted alone. This is different from the approach adopted in this experiment. Though the surrogate fuel contains no aromatics, it contains a range of iso-alkanes which may be dominating the interaction with 8% of tetralin effectively thus lowering mass concentration produced. Thus, with the corresponding large particle size also in perspective, it suggests that the presence of tetralin at 8% in the fuel plays an active role in the growth of the particles than the formation of the particle.

4.5 The APU PM Size Verification

This section of the thesis describes the test conducted to verify the particle size of the APU without having a pre-classifier upstream of the PM measurement instruments. As stated in section 2.3, despite information that the gas turbine PM emission from are less than one micron in size, majority of the testing on which this hypotheses is based have used a one micron pre classifier up stream of the PM analyser. This is largely due to the instrument limitation on the particle sizes which it can measure. For this testing an optical particle counter (OPC) instrument which covers a wider range of the particle sizes was deployed. The following sub sections describe the fuel composition, experimental apparatus, test matrix, and the emissions data obtained.

4.5.1 Experimental Details

4.5.1.1 Instrumentation

The OPC deployed for this study is GRIMM Model MiniWRAS 1.371. It combines optical particle counting and electrical mobility in order to cover a wide particle size range from 10 *nm* to 25 μm . In total the size range are grouped into 40 size classes. It uses the optical particle detection technique to detect particles greater than 200 *nm* and up to 25 microns while with the electrical detection technique it measures particles less than 200 *nm* down to 10 *nm*. As detailed by the particle sizing instrument manufacturer – GRIMM, the MiniWRAS 1.371 optical spectrometer and electrical detection are calibrated independently and performed annually. For the optical spectrometer, NIST-certified monodisperse PSL particles were used while electrical detection section was calibrated using a reference Faraday cup electrometer.

Figure 4-21 is a schematic of the optical chamber of the instrument. Sample gas drawn into the instrument at a rate of 1.2 litres per minutes is first subject to light scattering analysis in the optical chamber and subsequently electrical mobility after the particles are ionized using the Faraday cup electrometer. The particle size is proportional to the intensity of the detected scattered light signal, wherein the scattered light intensity is influenced not only by the particle size and refractive index, the particle shape and the orientation of the particle in the measurement

volume. The instrument has limitation of the particle concentration and also a maximum sample temperature of $40\text{ }^{\circ}\text{C}$ which are below the characteristics of the test engine PM emissions. These restrictions are addressed in the next section.

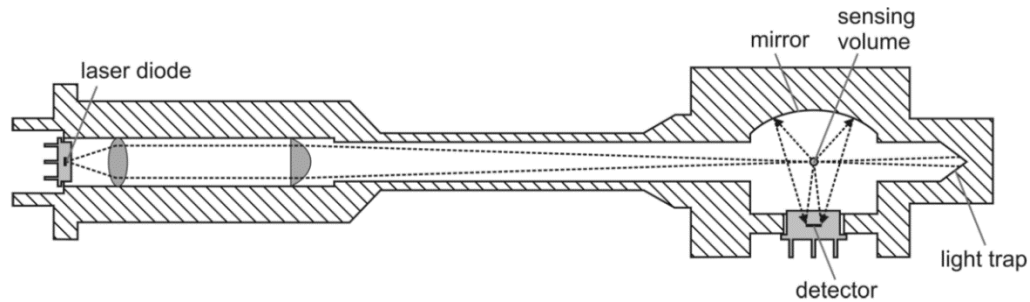


Figure 4-21: Laser measuring chamber of the optical particle counter

4.5.1.2 Sampling System

Figure 4-22 shows a schematic of the sampling system used to transport exhaust sample to the PM instruments. As shown in the diagram the exhaust gas is extracted and transferred through an 8 m heated sample line to a two way inlet flow junction with the outlet connected to a valve and a two way splitter downstream. Through the second inlet of the flow junction, metered nitrogen flow is introduced into the system. The nitrogen serves a dual purpose; purge of the 8 m heated line during engine start-up which requires closure of the connecting valve between the two way junction exit and two way splitter; and dilution during sampling. As noted in the previous section some of the restrictions of the instrument which needed to be considered in the sampling system design include the exhaust sample temperature and PM concentration. These concerns have been proven to be addressed with dilution without having an impact on the particle contained in the exhaust samples. Connected to the 3-way flow splitter is a 4 m unheated sample line connected to an aerosol flow control from which a 1 m unheated sample line connects the OPC. The purpose of the aerosol flow control is to ensure that the exhaust sample flow rate to the instrument was equal to or less than 1.2 litres per minute. The other exit of the two way splitter was connected to LII300 for the sole purpose of setting up the dilution ratio by using it as a real-time detector to monitor the PM sample concentration.

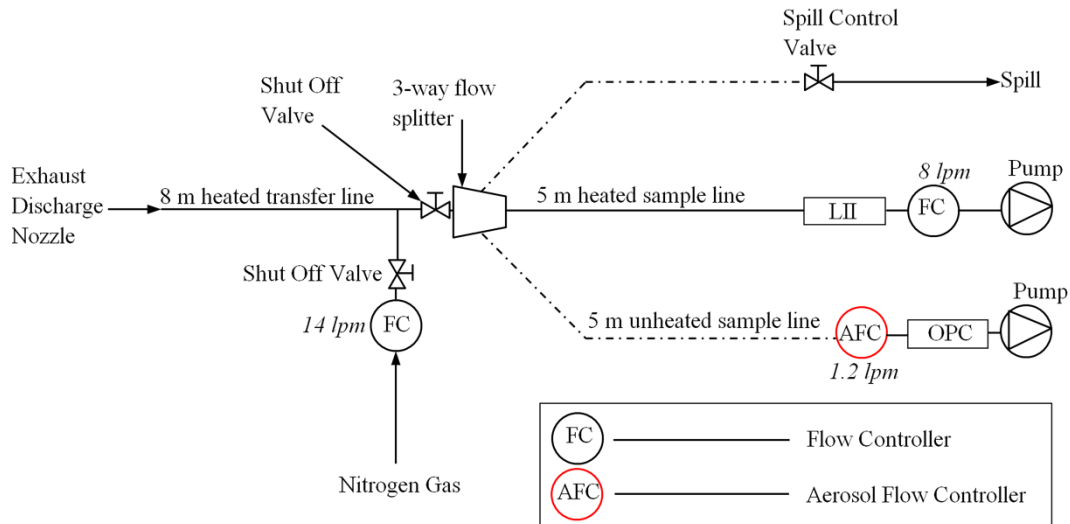


Figure 4-22: The design for the OPC sampling system

4.5.1.3 Experiment Procedure

The PM emission was investigated whilst burning diesel at the NL, ECS and MES engine power settings. Prior to engine start and during start, the OPC and the LII300 were isolated using the valve between the two way flow junction and splitter so that the 8 m heated sample line was purged with nitrogen to avoid exhaust sample deposits on the surface of the extraction nozzle and inside the transfer line. On attaining the engine set point the isolation valve was opened with subsequent sampling using the LII300 while the OPC remaining on standby. With the flow meter downstream of the bottled nitrogen used the exhaust sample was diluted until the sample concentration measurement with the LII300 was 1 mg/m^3 deemed suitable for measurement with the OPC. Next, the OPC measurement was initiated. The corresponding flowrate at which nitrogen was introduced to dilute the exhaust sample was to 14 lpm which implies that the dilution ratio of 14:9.2 as the total exhaust sample flow from the extraction point from the exhaust was 9.2 lpm (sum of the LII300 flow rate and the OPC flowrate).

4.5.1.4 Results and Discussion

Figure 4-23 to Figure 4-25 shows the number-size distributions distribution for the different engine power settings as measured by using the OPC.

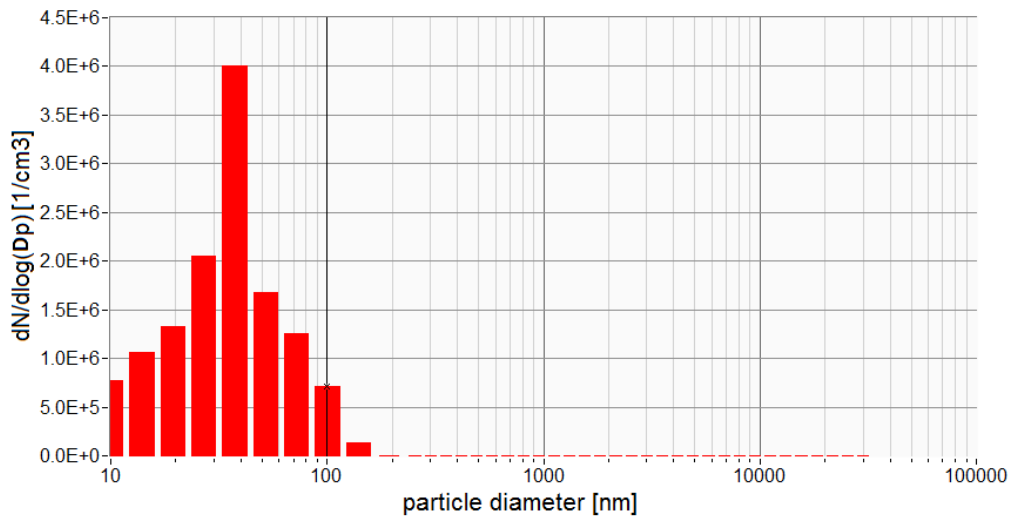


Figure 4-23: Particle number distribution for NL engine power setting burning diesel

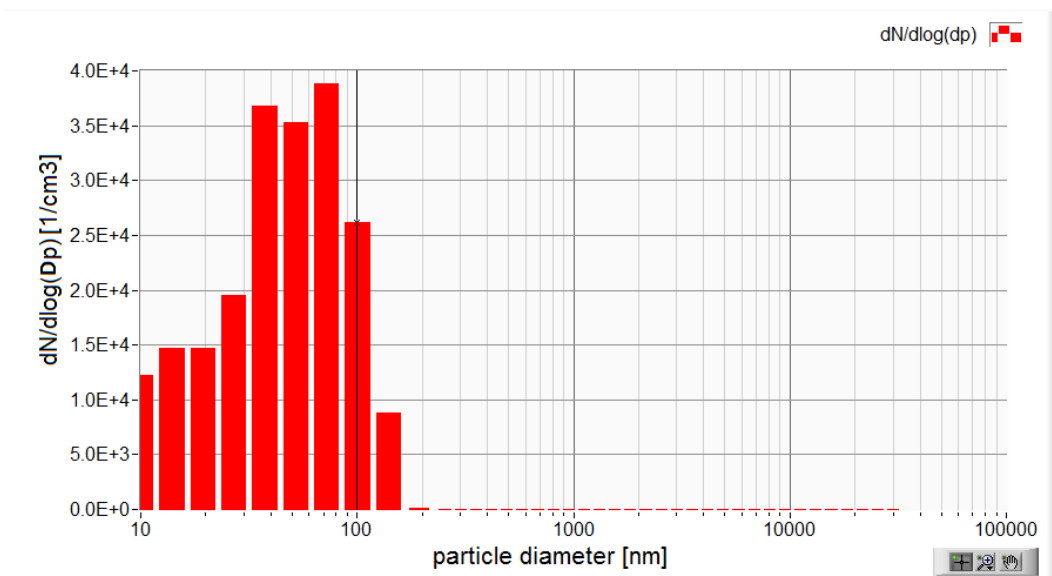


Figure 4-24: Particle number distribution for ECS engine power setting burning diesel

Across the three figures it can be observed that the majority of the particles counted are less than 1000 nm in size. This is in agreement with the scientific opinion (within SAE E31) that suggests that the individual particle matter that make up the particle emission from a gas turbine PM emission are well between the 1- 1000 nm in size.

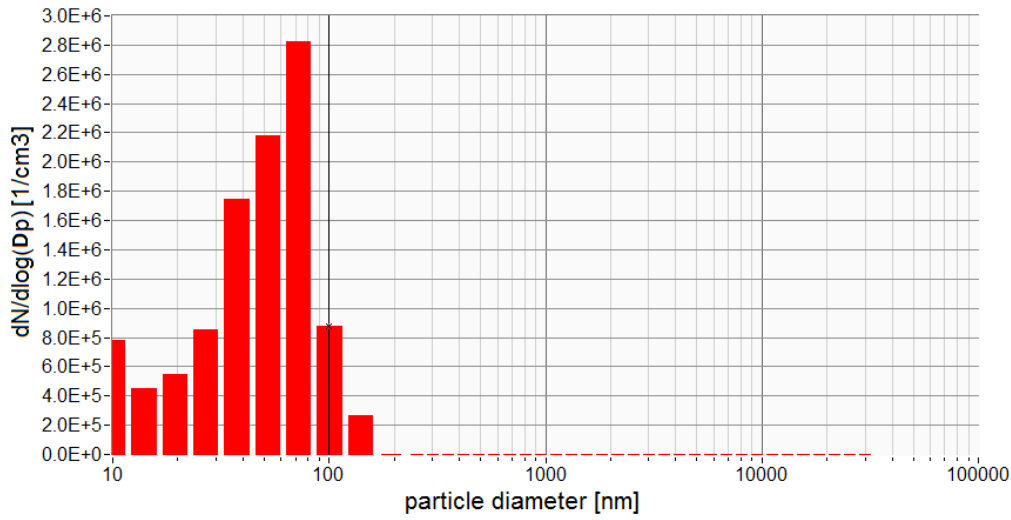


Figure 4-25: Particle number distribution for MES engine power setting burning diesel 50.5

Using a unit density to generate the mass from the particle measurement performed by the OPC as given in Figure 4-26 then it can be seen that more than 99% of mass is measured within the 1000nm cut-off point. The relatively large particle which makes up the remaining less one percent of the mass is insignificant to skew the mass data.

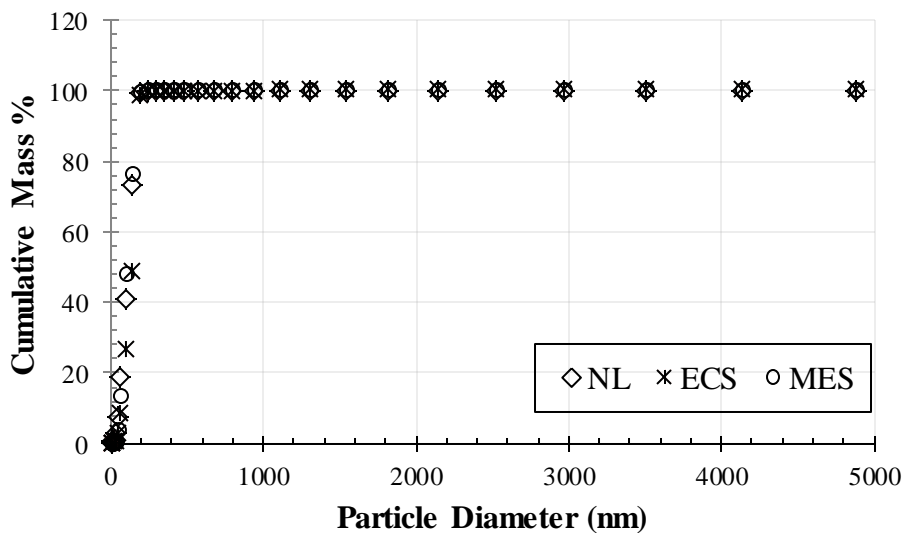


Figure 4-26: Cumulative Mass undersize plots for OPC data

4.6 Chapter Summary

In summary, this chapter covered the preliminary tests aimed at closing some knowledge gaps valuable in making decision on the best approach to achieve the goal of the thesis. The experiments covered include;

1. Engine performance and certification gas emissions
2. Traverse test
3. PM emission concentration correlation with fuel aromatic content
4. Characteristics of particulate emission from different aromatic species
5. Verification of test engine particle size distribution.

The following conclusion has been reached from the data about the performance and emissions characteristics of the APU.

1. The gaseous emissions from the APU; CO, NO_x and THC between the Jet A-1 and diesel were marginally different.
2. There is a significant spatial variation in the PM emission profile across the exit plane with better representative measurement achievable between point A and B as indicated in Figure 4-8.
3. Alternative fuels from alcohol to Jet (Fuel 4), catalytic hydrothermolysis (Fuel 7) and blends of cellulose - aromatic and SPK (Fuel 6) including a 50:50 blend of HEFA and Jet A-1 (Fuel 2) which all meet the current ASTM international specifications show a reduced particle number emissions and size compared to the conventional Jet A-1. Fuel 2 shows the lowest reduction in PM number-based emissions with a reduction of ~32% compared to the conventional Jet A-1 emissions.
4. The aromatic volume content as well as the species present in fuel influence PM production rate and the physical characteristics of the PM produced. There is no relationship between the influence on the PM production rate and the particle diameter of the PM produced. At 15% presence by volume, tetralin having the highest sooting propensity produced significantly larger particle diameters in correspondence to the high particle mass concentration. In contrast at 8% by volume in the fuel, the particle mass concentration

produced from tetralin is significantly lower than m-xylene but with larger particle diameter.

5. The engine particle matter emission size distribution is less than one micron meter as demonstrated with an optical particle counter (OPC) which has a particle size range of from 10 *nm* to 35 μm .

5 Test Matrix, Fuel Composition and Density Functions of the Particle Emissions from the APU Burning the Test Fuels

This chapter covers details of the test matrix including information about the property of the fuels burnt to produce representative industrial gas turbines PM emissions with the APU. It also covers the details of the work conducted to determine the density of the gas turbine particle emissions burning the selected test fuels using a combination of differential mobility analyser (DMA) to classify particle sizes based on their electrical mobility and a centrifugal particle mass analyser (CPMA) to measure the mass to charge ratio of the classified particle.

5.1 Test Matrix

Table 5-1 shows a summary of the test matrix. The table contains a list of the selected test fuels, engine power setting and repeats considered sufficient to generate representative particle emission concentrations from gas turbines. The test matrix is considered sufficient to generate data points to inter compare the PM instruments of interest based on the knowledge gained from the preparatory tests, fuel availability and operation cost.

Table 5-1 Experimental test points

Fuel Type	Engine Load Condition	Repeats
Jet A-1	NL	2
	ECS	2
	MES	2
Diesel	NL	2
	ECS	2
	MES	2
LACF	NL	-
	ECS	-
	MES	-

5.2 Fuel Composition

Table 5-2 summarizes the composition of the selected fuels for the experiment. The test fuels include a low aromatic content fuel (LACF) produced by the Fischer-Tropsch from a natural gas feedstock and shale, a commercial aviation fuel (Jet A-1), and petroleum diesel. Data for Jet A-1 and the LACF have been provided from laboratory measurement, while the diesel fuel properties were taken from EN590:2009 [144] except where otherwise referenced. The primary difference between the LACF and the Jet A-1 fuel is that it does not contain sulphur and aromatic content. Also, the molecular weight range is lowest for the LACF with diesel containing heavier hydrocarbons compared to both Jet A-1 and LACF.

Table 5-2 Selected Fuel Properties

Property	Unit	Jet A-1	Diesel	LACF
Density at 15 °C	<i>kg/m³</i>	802	820 - 845	730
Aromatic Content	<i>%vol</i>	19.2	24.0[153]	≤13
H/C ratio	<i>mol/mol</i>	1.899	1.797[137]	2.2
Viscosity	<i>cSt</i>	3.420	2.000 – 4.500	0.859
Sulphur	<i>mg/kg</i>	370	≤10	-

5.3 Effective Density Functions of the Particle Emissions from the APU Burning the Intended Test Fuels

This section describes the experiments performed to establish the power law relationship necessary to evaluate particle emissions mass concentrations from the DMS500 instrument in real-time. As detailed in section 2.8.2 to convert the number-size distribution measurement of the DMS500 either in real-time or off-line into a mass concentration a mass mobility exponent (fractal dimension) and the scaling constant are required from the power law relationship (equations 2-1 & 2-2). To establish the power law relationship, the PM emissions from the engine were classified according to sizes and further classified based on mass using DMA and CPMA respectively with a condensation particle counters downstream serving as a detector.

5.3.1 Instrumentation

Models of the specific instrument of the DMA-CPMA-CPC system are as follows; Differential Mobility Analyser (DMA; TSI, Model 3081, TSI Inc., St. Paul, USA)–Centrifugal Particle Mass Analyser (CPMA; Cambustion Ltd., Cambridge, UK)–Condensation Particle Counter (CPC; TSI, Model 3775; TSI Inc., St. Paul, USA) system.

5.3.1.1 Differential Mobility Analyser (DMA)

Figure 5-1 is a schematic of the DMA employed (model 3081 electrostatic classifier and model 3080 DMA, TSI Inc., Shoreview, USA). It comprises of three major's components; an inlet impactor, a neutralizer, and an electrostatic classifier. The impactor is the first components of the instrument in contact with the exhaust sample. Its purpose is to ensure that particles greater than one micron in size are cut off from flowing downstream. Next to the impactor is the neutralizer (model 3077, TSI Inc., Shoreview, USA) which applies uniform electrical charges on the particles and then the electrostatic classifier. Inside the classifier the user specified sizes are separated based on their electrical mobility. Accordingly, only the user selected particle size exit the instrument.

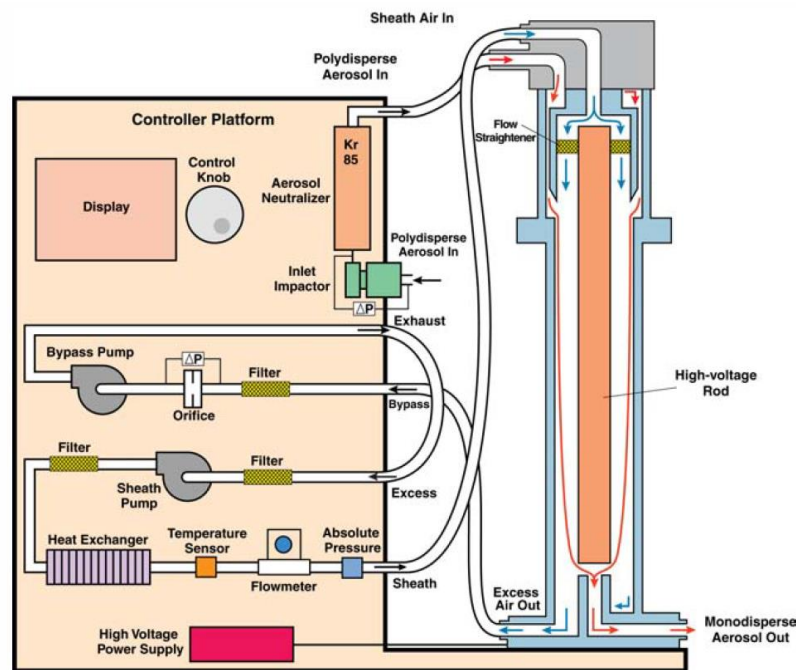


Figure 5-1: Schematic of A Differential Mobility Analyser [45]

5.3.1.2 Centrifugal Particle Mass Analyser (CPMA)

Figure 5-2 shows a schematic of the CPMA. It uses opposing electrical and centrifugal force fields to classify aerosol particles [105] based on mass. It achieves classification by using two concentric cylinders with a variable potential difference between them, which can be operated at the same or different speeds. If the cylinders operate at different speeds, it sets up a stable centrifugal/electric field across the classification region. This enables particles which have a higher mass: charge ratio than that selected to precipitate on the outer cylinder. Particles which have a lower mass: charge ratio than that selected precipitate on the inner cylinder while, particles which have the selected mass: charge ratio, follow a trajectory through the classifier. Thus, it is used to select mass based monodisperse aerosol.

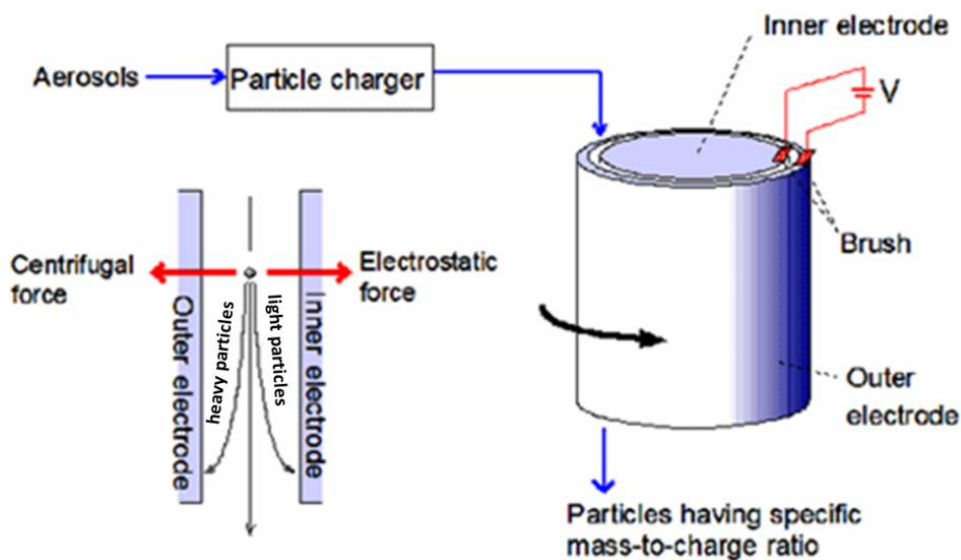


Figure 5-2: Schematic of A Centrifugal Particle Mass Analyser [106]

5.3.1.3 Condensation Particle Counter (CPC)

The CPC deployed for this testing is a Model 3775 manufactured by TSI. Able to detect particle as low as 4 nm, it operates by growing particles to sizes detectable when passed through a lighted viewing volume where the scattered light pulses are collected by a photodetector. The particle enlargement happens in two phases. As the exhaust gas enters the CPC at a constant flow rate, it is passed through an alcohol saturation chamber kept at 35 °C, thus saturating the particles in the exhaust gas sample. The particles are directed into a condensation chamber. The

chamber is kept at 10 °C, and under reduced pressure to create a supersaturated atmosphere making the alcohol droplets attached to the particles during saturation to condense onto the particles causing them to grow to detectable spheres of about 12 μm regardless of their initial diameters. Now large and uniform, the particles are directed to the path of an optical light which results in scattered light rays (Figure 5-3) which create electrical pulses subsequently translated to particle count.

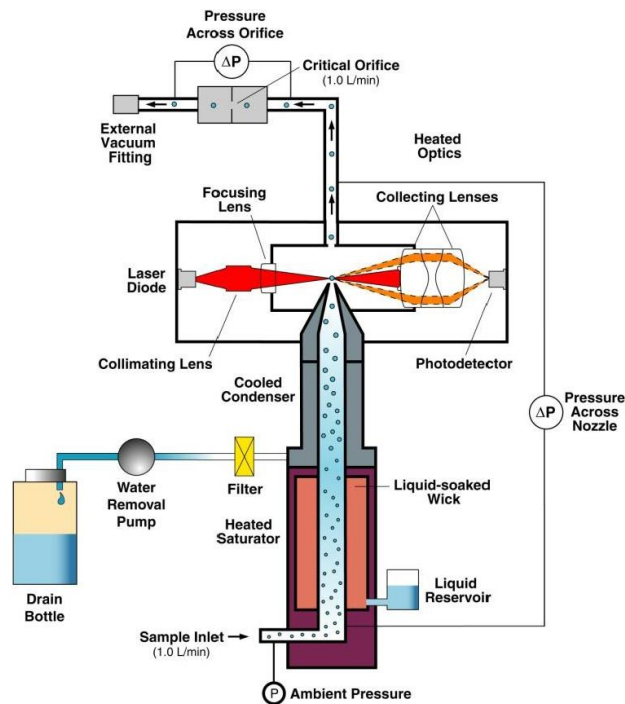


Figure 5-3: Schematic of a Condensation Particle Counter (CPC)

5.3.2 Sample System

Figure 5-4 shows a schematic of the sampling system used to transport exhaust sample to the PM instruments. The sampling system adopted parts of the emission certification regulations in the “Society of Automotive Engineers, Aerospace Information Report 6241” [131] and the United States Environmental Protection Agency (US EPA) Method 5I [27]. A borosilicate glass single probe designed in accordance with US EPA method 5I with a nominal internal diameter of 14.1 mm was used to continuously extract the APU exhaust samples to the PM instruments. The probe was positioned parallel to the exhaust gas flow and approximately 0.5 m downstream of the engine exhaust nozzle to ensure that fresh and non-aged exhaust were extracted. Directly attached to the probe was a stainless steel

sampling line with a nominal internal diameter of 8 mm which ran 8m from the probe to a two way splitter from which the exhaust samples is distributed to a Differential Mobility Spectrometer (DMS500) developed manufactured by Cambustion Ltd. and a DMA-CPMA-CPC system. The purpose of the DMS500 is to justify the range of the particle sizes scanned for the resulting particle emission from the different fuels and engine test conditions

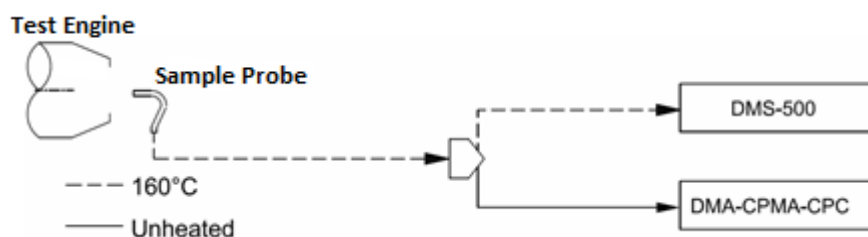


Figure 5-4: Schematic of Sampling System

The exhaust through the 8 m sample line directly connected to the probe was left undiluted but kept heated to 160 °C including the two way splitter. The connecting sample lines between the splitter and the instrument were 5m in length. For the connecting sample line that supplies the DMA-CPMA-CPC system, it was unheated and the exhaust sample undiluted as the sample was left to cool down to meet the instrument exhaust sample temperature requirement. The exhaust sample to the DMS500 was heated to 160 °C and diluted by a factor of 60 using zero grade nitrogen. Dilution was in two parts and controlled from the DMS software interface. Primary dilution was at the point exhaust sample are transferred from the splitter to the DMS500 heated sample line and a second dilution was inside the DMS500 using a rotating disc diluter.

5.3.2.1 Experiment Procedure

A minimum of four particle mass distributions have been evaluated with the DMA-CPMA-CPC for each of the test points. In general, the mass distributions of the particle sizes evaluated were less than 400 nm. These values are justified by the particle size distributions results of the DMS500 in next section. Basically, the DMA was used to select monodisperse aerosol particles of a desired electrical mobility size from the exhaust sample which were further classified by the CPMA. The selected sizes ranged between 30 and 450 nm in diameter. Using the particle mass charge ratio, the CPMA generates a mass spectral density fitted with

a log-normal distribution. The mode mass spectral density is selected as the particle mass of the DMA-classified particles. The duration for one DMA-CPMA-CPC scan, is on the average of 6 minutes but dependent on the resolution of the scan and initial estimate of the mass of the DMA single particles transferred to the CPMA, thus the engine run for each test point after engine stabilisation was a minimum of 24 minutes.

5.3.2.2 Test Fuels and Engine Power Settings

The test fuels include a low aromatic content fuel (LACF) produced by the Fischer-Tropsch from a natural gas feedstock, a commercial aviation fuel (Jet A-1), and petroleum diesel as presented in Table 5-2. Two engine powers setting have been investigated using the fuel flow as an indicator of the engine power. Table 5-3 lists the nominal values for Exhaust Gas Temperature (EGT), and Fuel flow rate achieved for the engine power settings. The engine power settings investigated are; no load (NL) which is the same as the engine idle condition and environmental cooling system conditions (ECS). For the NL conditions, the three test fuels have been investigated while only Jet A-1 was burnt at the ECS engine power setting which has been previously reported [128, 130, 154] to produce the highest smoke number when burning Jet A-1 fuel.

Table 5-3 Nominal APU Operating Conditions

Fuel	Engine Power Setting	Exhaust Gas Temperature (°C)	Fuel flow rate (g/s)	RPM
Jet A-1	NL	303	18.52	41663
LACF	NL	297	17.51	41414
Diesel	NL	305	19.17	41745
Jet A-1	ECS	406	24.67	41120

5.3.3 Results and Discussion

Figure 5-5 is a graph of the effective density expressed in kg/m^3 and the corresponding PM size using power regression model defined in equation 2-3 and Overall, the particle densities range between $220 kg/m^3$ and $1900 kg/m^3$. The graph show that the effective density is constant as a function of particle size as the

effective density can be observed to reduce with an increase in particle size. For instance, a particle size of 30 nm produced with LACF as the test fuel shows an effective density is 1900 kg/m³ while a particle size of 220 nm shows an effective density of 330 kg/m³. The graphs also shows no significant difference between the of NL and ECS engine power setting data for Jet A-1. The power regression model (equation 2-3) fit to the combined data of NL and BL produces a regression factor (R²) of 0.90. However there is a significant difference between the electrical mobility particle size and effective density data for three test fuels.

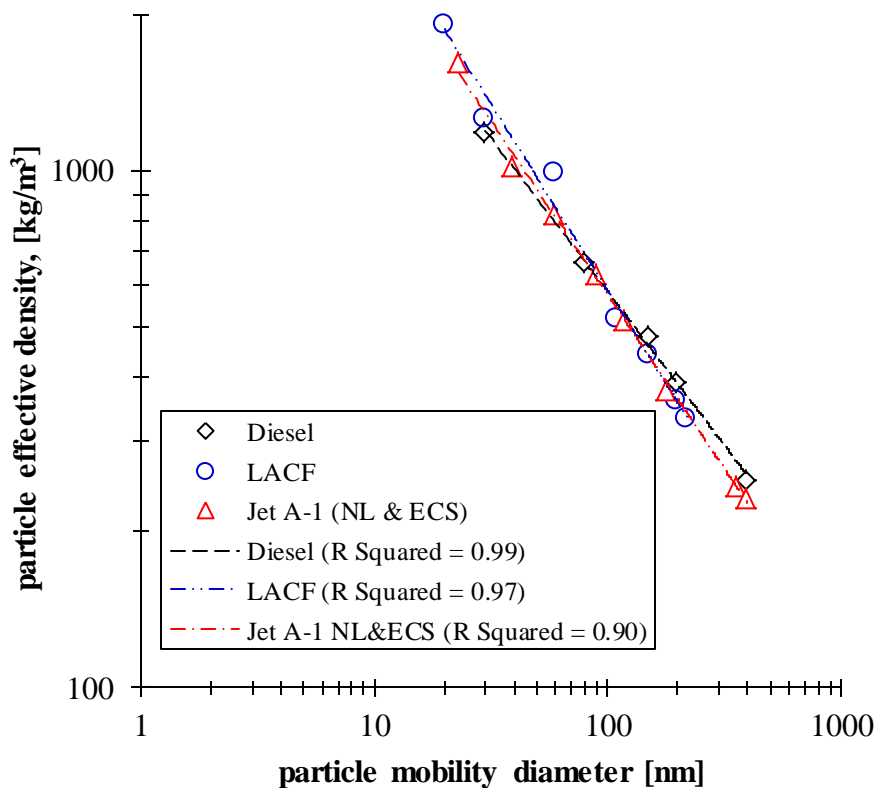


Figure 5-5: Power law trend lines of the effective densities and the corresponding mobility diameter.

To show the observed differences Table 5-4, is a comparison of specific electrical mobility particle sizes and corresponding effective densities for diesel and LACF fuel. For electrical mobility particle diameters of 150 and 200 nm, lower corresponding effective densities can be observed for LACF compared to diesel. Meanwhile, the corresponding effective density for a particle with electrical mobility diameter of 30 nm is higher for LACF produced particle emission compared to diesel.

Table 5-4 Results of effective densities of the same particle sizes from diesel and LACF

Fuel	size (nm)	Density (kg/m ³)
Diesel	30	1181.28
	150	475.91
	200	387.94
LACF	30	1259.09
	150	437.99
	200	358.10

Table 5-5 shows the correlation derived for each of the fuels containing mobility-prefactor and fractal dimension (see section 2.3). An increased mass-mobility prefactor can be observed from 1.39×10^{-3} for LACF to 8.5×10^{-3} and 57×10^{-3} for Jet A-1 and diesel respectively. Similarly, LACF fuel has the lowest mass fractal dimension compared to Jet A-1 and diesel with a value of 2.20 compared to 2.31 and 2.42 for Jet A-1 and the diesel respectively. The fractal dimensions are similar to values obtained by Park et al. [155] for a diesel and gas turbine engine at different engine loads. The significance of the fractal dimension is the information it gives about the structure of the particle. The higher fractal dimension observed for diesel particle emissions suggests the individual particles contains more voids compared to the particles emitted burning Jet A-1 and LACF and therein is the rationale for the observed variation in densities detailed in Table 5-2.

Table 5-5 Power law functions for all the test points including the overall functions for the test fuels at NL and the overall function for Jet A-1 at NL and BL.

Fuel	Engine Power Setting	Power Law Fit	Units
LACF	NL	$\rho_{eff} = 0.00139d_m^{(2.20-3)}$	kg/m ³
Diesel	NL	$\rho_{eff} = 0.0570d_m^{(2.42-3)}$	kg/m ³
Jet A-1	NL & ECS	$\rho_{eff} = 0.0085d_m^{(2.31-3)}$	kg/m ³

Diesel contains a wider spectrum of hydrocarbons including heavy hydrocarbon compared to Jet A-1 and LACF and expectedly produces more volatile species as a result of incomplete combustion. The volatile species which transform with time to CPM from the engine adsorb or condense on the solid particulate emissions and suggested [111] they fill up the voids in the solid particles instead of growing the size. The result is an increased mass of the particle but not the size. Consequently, the observed higher particle density observed for individual particle sizes of 150 and 200 *nm* from diesel compared to LACF generated particulate matter suggest that the voids are filled up with condensed particulate matter. In contrast the lower particle density observed for the 30 *nm* suggests that the voids unlike the larger particle are left empty which is expected because the larger particles have larger surface area to attract the condensation of the volatile particulate matter.

5.4 Chapter Summary

This chapter detailed the experimental matrix and the property of the test fuels to produce representative particle emission generated by industrial gas turbines to investigate the correlation between real-time PM instruments and gravimetric measurements. Also covered in the chapter is the experiment to determine the two important parameter required to convert the DMS 500 particle size distribution measurement namely; mobility prefactor and fractal dimension, to mass concentration from electrical mobility particle size and the corresponding mass relationship. Importantly, the experiment showed that there is no significant difference in the fit of the effective density and mobility size plot with respect to the engine operating conditions. This was evident as the combined power fit to the electrical mobility particle size and corresponding mass plot of particle emission generated burning JetA-1 at the NL and ECS engine power condition shows a correlation of 0.90. The implication is that the necessary parameters (fractal dimension and prefactor) obtained for the NL engines condition and required to convert the particle size distribution measured using the DMS500 instrument are sufficient to determine the total mass per volume concentration for the particle emissions for all the engine operating conditions.

6 Experimental Procedure

The goal of this chapter is to describe in detail the experimental and result analysis procedures. Thus, it first describes the configuration of the PM instruments aimed at improving response time, standard temperature and pressure correction and measurement precision. Section 6.1.2 details the step by step pre-test procedures including the gravimetric sampling train set-up; smoke meter and NIOSH 5040 clean filter analysis. This section also covers the equipment's start-up, the sequence in which the instrument sampling started and how the sample acquisition duration was evaluated. The chapter then proceeds to detail the sample recovery procedure, preservation and transportation to National Physics Laboratory in the case of the gravimetric and NIOSH 5040 sampling methods. Finally, detailed descriptions of the data processing for each of the PM instruments and data quality indicator are presented.

6.1 Equipment Configuration

6.1.1 Laser-Induced Incandescence

The Artium LII300 was operated and data acquired using the touch screen interface on the front panel of the instrument. It was configured as detailed in SAE AIR 6241 [131] accordingly the default parameter setting were reviewed. First the instrument was configured to use an external pump with the flowrate restricted to 8 *lpm* ($0.008 \text{ m}^3/\text{min}$) using an external flow controller. The automatic optimization of the photomultiplier gain voltage and neutral density filter were enabled and the laser rate set at 20 *Hz*. By selecting the automatic optimisation gains the instrument continuously monitors peak signal amplitudes and uses that information to select the optimum gain. Also important was the sampling cell temperature set at 160 °C to tally with the transfer line temperature set points. The standard temperature and pressure button (STP) was enabled with temperature (0 °C) and pressure (1 *atm*/4.696 *psia*/101.325 *kPa*) such that data displayed in real-time and logged were STP corrected.

6.1.2 Fourier Transform Infrared Spectrometer

The Thermo Scientific FTIR was operated and data acquired remotely from a computer with RESULT integration software installed. Some factory device parameter settings were reviewed to improve the signal-to-noise ratio of the measurement and thus increase the sensitivity while also recognising that sampling duration is premium. Consequently the total collection time, number of scans per spectrum, and resolution were adjusted. The number of scans per spectrum was adjusted to 15, while the resolution was set at 0.5 cm^{-1} and the total collection time set at 3600 *secs*. The number of scans determines the scans coded to produce each spectrum or interferogram. The resolution measures how well closely spaced peaks in a spectrum are differentiated while the total collection time parameter determines the length in seconds of the phase of data collection.

6.1.3 DMS500

The DMS500 was remotely operated and data acquired using a computer with a DMS500 user interface installed. First, the biomodal.dmd calibration file was loaded while the output logged to file was left in the default mode to report the total number concentration data. The sample averaging was set to “4” to reduce the frequency response of the instrument to 800 *ms* in a bid to improve noise and sensitivity and reduces the size of data files. Next the temperature set point for the heated line that directly connects the DMS500 was adjusted to 160 °C as it is directly controlled from the DMS500. Also the DMS500 controls the dilution of exhaust samples advancing to the instrument as detailed in section 3.2. As the DMS500 implements a two stage dilution system, for sampling which required dilution, the 1st and 2nd dilution factor were set at 5 and 12 in the user interface meaning a total dilution factor of 60. The total dilution factor is simply the product of 1st and 2nd dilution factor. For sampling which required no dilution as with the samples directed through a Nafion dryer to the DMS500, the 1st and 2nd dilution factors in the user interface were set to 1. Another important setting to ensure proper functioning of the instrument was the adjustment of the sample flow to the required 8 *slpm* ($0.008\text{ m}^3/\text{min}$). The instrument uses calibrated flow restrictors to control the flowrate which was changed on a trial and error basis until the desired flow, monitored on the software user interface was achieved.

6.1.4 Gravimetric Sample Train

The gravimetric sampling train is manually operated, thus the necessary readouts were recorded by hand. Outside the filter and impinger set-up as described in section 3.1.1, the two main parameters configured before operating the sampling train include, the heated box temperature which was set at 160 °C and the sampling flowrate set at 17 *lpm* (0.017 m^3/m). The sample flow rate was set and controlled using the valves (coarse and fine) in the sampling console while the front side of the dual-column 250-*mm* manometer was used to monitor the flow by observing the orifice reading (ΔH) on the manometer. To note the orifice reading (ΔH) on the manometer corresponding to 17 *lpm* (0.017 m^3/m), timed blank test runs (i.e. experiments performed with the sampling system on without the test engine running, so that no new particulates were entering the sampling system) were performed while using the fine valve to adjust the flow and a volume flow through the sampling through calculated from the difference in the initial and final volume dry gas meter and the end of the test. It was important to note the (ΔH) on the manometer that corresponds to 17 *lpm* (0.017 m^3/m) so that at the start of 17 *lpm* (0.017 m^3/m) flowrate is achieved immediately at the start of the gravimetric sampling. To ensure that the (ΔH) on the manometer that corresponds to 17 *lpm* (0.017 m^3/m) was accurate two technicians were asked to independently verify the flowrate implementing the blank test procedure and achieved results within 1%.

6.1.5 Smoke Meter

The Richard Oliver Smoke Meter deployed for the smoke number sample collection is manually operated and involves no data logging. As stated in section 3.1.5 the smoke meter is pre-set such that the unit achieves SAE ARP 1179 requirement. Thus, the instrument was checked to ensure that the configuration was still intact by ensuring that the exhaust flow rate through the filter is 14 *lpm* (0.014 m^3/m) at the external filter block temperature setting of 160 °C.

6.1.6 NIOSH 5040

Key configuration of the NIOSH 5040 sampling system was the heated box that housed the filter holder. This was set at 160 °C while the Aalborg mass flow

controller downstream of the filter holder to measure the flowrate at ambient conditions was set at 5 *lpm* ($0.005 \text{ m}^3/\text{m}$). As specified in the SAE AIR 6241 report [131] the filter papers used for this method is the 47-mm pre-baked quartz filters (Tissuequartz™ 2500 QAT-UP, from Pall Corporation Catalog #7202).

6.2 Pre-test Procedures

6.2.1 Sampling Media Preparation

6.2.1.1 Preparation of Gravimetric Sampling Train

The follow procedure was performed each measurement day for the gravimetric sampling train:

1. Ensure that the pre weighed blank quartz filter as received from National Physics Laboratory (NPL) is properly sealed in glass petri dishes with individual identification.
2. Prepare each set of impingers for a sampling run.
 - a) Knockout Impingers (impinger 1): Empty
 - b) Back-up impinger (impinger 2): Empty
 - c) Impinger 3: 100 *ml* of de-ionized water
 - d) Impinger 4: 200 *g* of silica gel
3. Weigh each impinger to the nearest 0.5 *g* and record initial weights on a field data sheet.
4. Assemble the impingers in the cold box with U-tubes, Double “L” adapter, and the sample case/umbilical adapter, using clips.
5. Using tweezers place the tared filter in the filter holder. Check the filter for tears after placement, and centre on the filter support. Assemble the filter holder and tighten the clamps around the filter holder to prevent leakage around the O ring;
6. Connect the filter holder in the hot box to the gravimetric sampling train exhaust sample heated supply line ball joint and to the “L” Adapter using ball joint clamps. Close the hot box doors and fasten shut
7. Place crushed ice and a little water around the impingers.

6.2.1.2 Preparation of Smoke Meter and NIOSH 5040 Filters

The preparation of Whatman #4 filter paper used for the smoke number analysis simply involved measurement of the absolute reflectance (R_w) using the reflectometer detailed in section 3.1.5. For NIOSH 5040 sampling, the filters required no further preparations apart from the pre baking stated in section 6.1.6.

6.2.2 Equipment start-up

The follow procedure was performed at the start of each measurement day:

- Turn on heated line controllers as well as heater tapes.
 - wait 1 hour to reach stable set point temperatures
- Turn on power for gravimetric sampling system to allow electronics to warm up and turn on hot box heater after preparing the sampling train as detailed in section 6.2.1.1. Make periodic checks and adjustments to ensure the desired temperatures. Check all thermocouple connections by dialling through each selection and noting ambient or heated temperatures.
- Using tweezers place the NIOSH filter in the filter holder. Check the filter for tears after placement, and centre on the filter support. Assemble the filter holder and tighten the clamps around the filter holder to prevent leakage around the O ring.
- Turn on the NIOSH 5040 hot box heater.
- Ensure the isolation valves for the NIOSH 5040 and gravimetric sampling trains are shut.
- Turn on the smoke meter to heat up.
- Turn on power for LII300 to allow warm up and to initiate sample cell heating and then start sampling with the LII.
- Turn on pumps and MFC for LII and make-up air to induce flow through the sample lines to assist with line heat up and temperature stabilisation.
- Turn on power for the DMS500.
 - it takes 20 minutes to warm up
- Purge FTIR sample cell with research grade nitrogen (< 10 ppm total contaminants) for 15 minutes.
- Fill FTIR liquid nitrogen reservoir while purging sample cell.

- Collect background spectrum for FTIR once nitrogen purge is complete.
- While some elements could be performed in parallel, overall the full start-up procedure took 1.5 hours.

6.2.3 Sample Acquisition

The follow procedure was performed when the heated line temperatures are close to set points prior to every sample acquisition for each test:

- Open the sampling system spill valve.
- Close the sampling system isolation valve.
- Open the nitrogen cylinder and open the purge valve.
- Start the engine and allow it to reach the desired steady state condition.
- Close the spill valve and immediately open the sampling system isolation valve.
- Shut the nitrogen purge valve.
- Wait for the LII300 real-time reading to stabilize.
- Start sampling with the DMS 500, FTIR and Gas analysers.
- Start gravimetric and NIOSH 5040 sampling. This step requires at least two people as the NIOSH 5040 sampling pump, isolation valve, gravimetric isolation valve, pump, timer and coarse valve all need to be opened at the same time. Failure to open valves simultaneously can lead to water in the third gravimetric impinger flooding the CPM filter.
- Record the time at which the gravimetric and NIOSH 5040 sampling was started.
- Start smoke meter sampling.
- Make periodic checks and adjustments to ensure the desired temperatures and flowrates especially for the gravimetric unit. Also for the gravimetric unit check all thermocouple connections by dialling through each selection and noting ambient or heated temperatures. In addition monitor the temperature of the ice and water around the impingers.
- Sampling should be stopped in the following manner. Stop gravimetric and NIOSH 5040 sampling by returning valves to positions before experiment started. Note the time and stop all other instrument except the

LII300 and the balance pump. Stop the engine. Wait 5 minutes and then stop the LII300 sampling and balance pump.

6.2.3.1 Sample Acquisition Duration

The total sampling time for each engine test run is largely dependent on the filter based PM measurement method with the highest ratio of target PM mass catch to the exhaust sample flowrate through the filter. In basic terms the sampling time of the filter based method is a function of the concentration and flow rate through the filters which is expressed mathematically as presented in equation 6.1. However this excludes the SAE Smoke Number technique as it requires 16.2 kg of exhaust gas per square metre of filter area instead of a target PM mass deposit on the filter as required for the gravimetric and NIOSH 5040 methods. Despite the fact that the response time of the real-time instruments (LII300, DMS500, and FTIR) not being dependent PM concentration in the exhaust samples and the transfer flow rates to the instruments, adequate amount of data needs to be recorded to attain an acceptable measurement precision as variations in the data are likely, thus real-time data is averaged over the same time period as the gravimetric filter.

$$T = \frac{M(mg)}{\gamma(mg/m^3) \times \bar{Q} (m^3/min)} \quad 6-1$$

Where;

- T = Sampling time
- \bar{Q} = Sampling volume flow rate
- γ = Exhaust PM mass concentration
- M = Expected sample catch

Among the filter based instruments, the gravimetric sampling train would largely determine the sampling time for each test point as it has the highest target PM mass catch to the exhaust sample flowrate ratio. Typically the gravimetric method expects a target filter sample catch of 3 mg of particulate per filter sample for the method 5I section. However, after inquiries with the National Physics Laboratory (NPL) it was established that a sample loading of 600 μg for the gravimetric filters, substantially less than the 3 mg can be weighed with a high degree of accuracy. For the NIOSH 5040 sampling, SAE AIR 6241[131] suggests a particle

load of at least $2 \mu\text{g}/\text{cm}^2$ per filter sample which means a filter mass load of $23.9 \mu\text{g}$ for a sample area of 11.95 cm^2 . As an illustration for the gravimetric sampling train, assuming the particle concentration of the test engine exhaust gas is $2000 \mu\text{g}/\text{m}^3$, a target filter loading of $600 \mu\text{g}$ while maintaining a sample flow rate of 17 lpm ($0.017 \text{ m}^3/\text{m}$) through the gravimetric sampling train as contained in the sampling system design would require 1060 sec . The sample times for possible particulate concentration levels in the test matrix are summarised in Table 6-1

Table 6-1 Test duration for four sample concentration levels

Particulate Concentration ($\mu\text{g}/\text{m}^3$)	Test Duration (s)	Test Duration (hrs)
500	4240	1.20
1000	2120	0.60
2000	1060	0.30
6000	360	0.10

The flow rate used in the experiments for gravimetric (17 lpm) is below the maximum allowable for the filters and thus shorter sampling times are theoretically possible. In Table 6-2, the sampling times for the gravimetric is recalculated for assumed flow rate of 50 lpm - the upper practical limit over the filters. It also shows the sampling time for NIOSH 5040 filter measurements using the 5 lpm to achieve a target loading of $23.9 \mu\text{g}$. Also included as a reference are the response times for LII300, DMS500, FTIR and SAE Smoke Number.

Table 6-2: Sampling times for a flow rate of 50 lpm across the gravimetric and EC/OC filters

Diagnostic	Sample time (s) as function of soot mass concentration:			
	$50 \mu\text{g}/\text{m}^3$	$200 \mu\text{g}/\text{m}^3$	$800 \mu\text{g}/\text{m}^3$	$2000 \mu\text{g}/\text{m}^3$
gravimetric	14400	3600	900	360
EC/OC	5736	1434	358	143
SAE SN	~36			
LII	0.05			
DMS500	0.8			
FTIR	15			

6.3 Sample Recovery, Preservation and Transportation

For the instruments that involve capture of PM samples with a filter, the filter sample recovery is a critical process as sample loss can occur (bias results low due to sampler errors) or contamination can be introduced (bias results high). This is the case for the smoke meter, NIOSH 5040 and gravimetric PM measurement procedure. To reduce the chance of sample loss or contamination occurring clean filters tweezers were used to remove the filter from the filter holders and immediately placed and sealed in the corresponding petri dish container.

6.3.1 Method 202 Liquid Content Recovery

As required by the US EPA method 202 the CPM liquid contents were recovered and the component parts rinsed in the following order for each test.

1. The liquids in the dropout and the backup impingers' if there is, were quantitatively transferred into a clean 500 ml (500 cm^3) amber glass bottle with PTFE cap seals. The bottle were labelled with test identification and CPM bottle #1;
2. The dropout and the backup impingers', condenser and all connecting glass components between the FPM filter and the CPM filter were rinsed twice with water and added to CPM bottle #1 with a mark of the liquid level on the bottle;
3. Next are organic rinses of dropout and the backup impingers', condenser and all connecting glass components between the FPM filter and the CPM filter. The rinses are recovered into a bottle labelled with test identification and CPM bottle #2 with a mark of the liquid level on the bottle. The organic rinse proceeds first with acetone and then two rinses with hexane.
4. At the end of the testing campaign, 200 ml (200 cm^3) of the deionized water, acetone and hexane was directly transferred from the wash bottle used for sample recovery placed in a clean, leak proof container labelled with test identification as reagent blanks.

6.3.2 Transportation

Transportation of the PM samples to an offsite laboratory (National Physics Laboratory) for analysis is one of the crucial aspects implementing the gravimetric method and the NIOSH 5040. Thus, to ensure that the samples were not compromised during postage they were properly sealed and packaged such that they remained in an upright position at all times during posting.

6.4 Post-Test Laboratory Procedures

6.4.1 PM Gravimetric Analysis

The gravimetric samples were sent to NPL for analysis. For the 47 mm quartz filter samples the weighing was in accordance with the procedure described by method 5I protocol. Accordingly, the filter samples were conducted to the same pre-treatment procedure (heat treatment/cooling/desiccation followed by timed weighing and extrapolation to ‘time zero’). For the method 202, the samples and blank reagents were extracted, evaporated and weighed to the constant weight criteria as contained in the method 202 document. Details of the analytical procedure are summarised in the flow chart as contained in Appendix D.

6.4.2 Analysis of Organic and Elemental Carbon

Like the gravimetric filter samples the NIOSH 5040 filter samples were sent to National Physics Laboratory for OC and EC carbon analysis. Speciation of the elemental carbon (EC) from organic carbon (OC) was performed using a thermal-optical analyser (see section 2.5.3.1.1) with timed heating ramps and “cool-down” cycles. As contained in the report provided by NPL, the samples were analysed according to NPL’s ISO17025 [156] accredited in-house procedures QPAS/B/561 following the “NIOSH-like” temperature profile as contained in PD CEN/TR 16243:2011[157] and as recommended in the SAE AIR 6241 [131]. Figure 6-1 is an illustration of the heat cycles produced by the calculation software contained within a thermal-optical analyser showing the split between the OC and EC content of a filter sample.

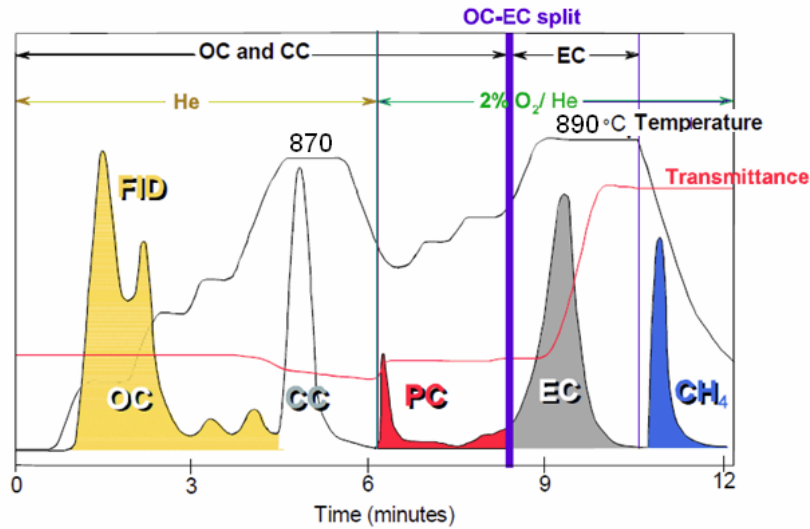


Figure 6-1: Illustration of a thermogram for filter sample containing organic carbon (OC), carbonate carbon (CC), and elemental carbon (EC). PC is pyrolytically generated carbon. The curves indicated with the OC, CC, PC, EC, and CH₄ labels are CH₄ concentrations being measured by a flame ionization detector (FID). The final peak is the methane calibration peak [59]

6.4.3 Smoke Number

The smoke filter samples were analysed in-house. After each test the absolute reflectance (R_s) of the filter samples were analysed using the reflectometer detailed in section 3.1.5. Subsequently, the individual smoke number (SN') were calculated using equation 6.2 having first determined the absolute reflectance of clean filter material (R_w) prior to testing – see section 6.2.1.2.

$$SN' = 100 \left[1 - \frac{R_s}{R_w} \right] \quad 6.2$$

Where:

R_s = absolute reflectance of the sample spot

R_w = absolute reflectance of clean filter material.

6.5 Data Post Processing

Particle emission concentration measurements expressed as mg/m^3 and ppm for gas phase species form the basis of correlation between the PM instruments. For instruments like DMS 500, LII300 and FTIR instruments which log multiple data over the duration of the test run a single representative determined as the average correlate the gravimetric and EC/OC data for the same run. Consequently, this

section details the data post processing requirements for computing average concentrations for each these instrument. In the cases of gravimetric and NIOSH 5040 details of the STP correction is described. Overall, there are no blank tests correction as the blank tests (i.e. experiments performed with the sampling system on without the test engine running, so that no new particulates were entering the sampling system) performed using the LII300 and the gaseous analysers produced virtually no particulate mass artefacts. Also described in this section are the data quality indicators (DQI).

6.5.1 Method 5I and Method 202

For each method 5I filter sample, NPL reported mass of the samples (M_{5i}) captured while for the method 202 samples the masses of organic CPM (M_{O-202}) inorganic CPM components (M_{i-202}) were reported. Consequently, the volume concentration (γ) of the gravimetric measurements is calculated by dividing the reported masses by the total exhaust volume corrected to STP (0°C, 101.325 kPa) ($V_{m\ std}$) through the gravimetric sampling train during the sampling period as expressed in equations 6-2 and 6-3.

$$\gamma = \frac{M}{V_{m\ std}} \quad 6-2$$

$$V_{m\ std} = \frac{(0.3592)(V_m) \left(P_b + \frac{\Delta H}{13.6} \right) (Y_d)}{(273 + T_m)} \quad 6-3$$

Where:

- P_b = barometric pressure (*mm.Hg*)
- T_m = average dry gas meter temperature (°C)
- V_m = volume of gas sample through the dry gas meter at meter conditions (m^3)
- Y_d = gas meter correction factor (dimensionless)
- ΔH = average pressure drop across meter box orifice (*mm.H₂O*)
- 0.3592 = conversion factor T_{std}/P_{std} (*K/mm.Hg*)
- 13.6 = conversion from *mm.H₂O* to *mm.Hg*
- 273 = °C to K conversion constant

6.5.2 NIOSH 5040

For each filter sample, NPL reported the masses of EC, OC and TC collected on the quartz fibre filters in $\mu\text{g}/\text{cm}^2$. To express the results as mg/m^3 , the values in $\mu\text{g}/\text{cm}^2$ are multiplied by the filter area and divided by the total exhaust volume that passed through the filter during the sampling period as presented in equations 6-4 to 6-6. The volume is the product of the flowrate reported by the flow controller and the total sampling time measured using the counter on the data logger for the gravimetric sampling instrument. The flow rate reported by the flow controller was not recorded as a function of time, therefore the average flow rate was assumed to be equal to the set point flow rate. The volume flowrate was first corrected to STP (0 °C, 101.325 kPa) as the flow was measured at ambient temperature and pressure.

$$\gamma_{EC} = \frac{M_{EC}A_F}{\bar{Q}\Delta t} \quad 6-4$$

$$\gamma_{OC} = \frac{M_{OC}A_F}{\bar{Q}\Delta t} \quad 6-5$$

$$\gamma_{TC} = \frac{M_{TC}A_F}{\bar{Q}\Delta t} \quad 6-6$$

Where;

γ_{EC} = mass concentration of EC ($\mu\text{g}/\text{m}^3$)

γ_{OC} = mass concentration of OC ($\mu\text{g}/\text{m}^3$)

γ_{TC} = mass concentration of OC ($\mu\text{g}/\text{m}^3$)

M_{EC} = mass of EC per unit area of filter ($\mu\text{g}/\text{cm}^2$)

M_{OC} = mass of OC per unit area of filter ($\mu\text{g}/\text{cm}^2$)

A_F = exposed filter area (cm^2)

(\bar{Q}) = sample flow rate through the filter (*slpm*)

Δt = sampling time (min)

6.5.3 DMS500 Data Analysis

The DMS500 user interface displays the number-weighted particle mobility diameter (D_p) distribution expressed as size spectral density in $dN/d\log D_p$ ($/cm^3$) in real-time. Though the interface is programmed to also calculate the total number concentration (which is an integration size spectral density over the measured size range) in real-time this can only be assessed when the logged and calculated data are exported to Microsoft excel file. In the Microsoft software the Combustion DMS Utilities v 6.1 – an Add-In Microsoft Excel macro was used to analyse the data. With the DMS utility, the total particle mass concentration GMD and GSD of the particle size distribution are calculated. The DMS utility makes provision to input the mass mobility exponent, D_{me} , and scaling constant, C , as derived in chapter five using the power law relationship as described in equation 2-3 for each fuel to derive the mass spectral density expressed as $dM/d\log D_p$ of each size class. The total mass concentration is therefore calculated by integrating the mass spectral density in $dM/d\log D_p$ (fg/cm^3).

6.5.4 Laser-Induced Incandescence Measurements

The post processing of the LII300 data simply required extraction of the data from the LII 300 unit into a USB where it was assessed using an AIMS program (standalone version: 4.1). From the AIM program (standalone version: 4.1) the mass concentrations data logged during the period of each test run was exported into a Microsoft Excel where the average was calculated. Thus, the single value obtained to represents the measurement for the test run.

6.5.5 Fourier Transform Infrared Spectrometry

The Thermo Fischer IGS FTIR reports gas species concentrations in terms of parts per million (*ppm*). These values do not vary as a function of temperature and pressure. During a given test run, the FTIR instrument completed multiple spectral scans from which various species are determined. The concentrations determined for each scan are stored as a CNC file. The data from all test conditions and runs were imported into Microsoft Excel and for each test run and each species, a mean and standard deviation was determined from the multiple data scans to represent specie concentration.

6.5.6 Smoke Number

In accordance with the ARP SAE 1179D [81] the smoke number (SN) reported for each of the test run is the arithmetic average of the individual smoke number (SN') values of three samples that agree within ± 3 smoke numbers.

6.6 Calculation of Data Quality Indicator

A data quality indicator is a parameter that describes the quality attribute of the measurement and test campaign in general. Two data quality indicators have been analysed as presented in chapter 7. Firstly is a summary of the data collected that are available for analysis per instrument known as completeness. Completeness is the percentage of acceptable collected data available for analysis. It is expressed as contained in equation 6-8. The second data quality indicator is an expression of the accuracy of the PM measurements. As there is generally no established reference for particle emissions at the time of the experiments, it was impossible to determine the accuracy of the individual instruments. Therefore the accuracy of the instrument is expressed in terms of precision. Precision is the closeness of agreement between a set of replicate measurements under stipulated conditions and expressed as percent relative standard deviation (RSD) as stated in equation 6-7. In the result plots in chapter 7 these are represented as error bars to indicate +/- one relative standard deviation.

$$RSD = \left(\frac{S}{\bar{x}_r} \right) * 100 \quad 6-7$$

Where;

S = standard deviation of replicate measurements

\bar{x}_r = average of replicate measurement

$$\%Completeness = \left(\frac{\text{Amount of Valid Data Collected}}{\text{Intended Collectable Data}} \right) * 100 \quad 6-8$$

6.7 Chapter Summary

This chapter detailed the developed standard operating procedures (SOP) of the instruments, the sampling system and the data processing as implemented in this thesis. First, the chapter describes the configuration of the PM instruments as used

in experiments. Based on the configurations a detailed procedure for preparing the instruments is described and a subsequent step by step operation procedure for the sampling system which is estimated to take about 1.5 hours before testing. Importantly, the chapter described how the test durations was determined without compromising the accuracy of the results especially with regards to the gravimetric method. The test duration largely depends on the target catch of the gravimetric method 5I filter sample which was reduced from 3 *mg* as contained in the method 5I document to 600 μg after consultation with National Physics Laboratory where the gravimetric filter samples were analysed.

The chapter also covered details of the data processing procedure for each of the instrument. In general the PM results were corrected to STP and presented in mg/m^3 except for the FTIR and gaseous instrument measurements which were presented in *ppm*. For the FTIR, DMS500 and LII300 an average of the data logged during the period sampling represented the measurements for each test run. In a similar manner the SN for each test is the average (in accordance with the ARP SAE 1179D [81] of the individual smoke number of the smoke samples collected.

Details of the calculation of two key data quality indicators were also described. The completeness of the intended tests expressed as a percent of acceptable data collected for each of the measurement instrument. The second data quality indicator expresses the accuracy of each of the measurement determined as the precision of the measurement instruments and indicated in the charts presented in chapter 7 as +/- one relative standard deviation.

7 Results and Discussions

This chapter covers the analysis of the results of the correlation study of the real-time PM measurement instrument with US EPA gravimetric method 5I and 202. However, before the correlations are presented this chapter gives a summary of the test campaign and the results (see section 6.6). Following the summary is a master summary of each of the raw data and filter sample collected from various PM instruments. Analysis and repeatability of both the engine power setting and the exhaust emission are presented in this chapter. Repeatability of the PM instruments and the validity of the measurements are also analysed.

7.1 Summary of Tests Completed

Table 7-1 presents a tabulated summary of the collected data during the experimental campaign. An overview of the test summary shows that over 95 percent of the intended measurements with the PM measurement instruments deployed for the experiment were achieved during the test points. FID readings were taken for all the test points. For test points 10, results for the method 202, LII and NIOSH 5040 are not available due to issues with either instrument malfunction or filter damage as in the case of method 202. Similarly, issues experienced with the gravimetric sampling kit meant the method 5I, 202 and NIOSH samples were not acceptable. The NIOSH 5040 test results for test point 21, is invalid as a result of leaks through the filter holder which was not properly fastened, however this was certified not to have affected the readings of the other instruments as the NIOSH 5040 pump still pulled PM samples on the filter. For the DMS500 80 percent completeness was recorded in total with and without a Nafion dryer in place. The majority of the test point had repeats, thus the effect of less than 5% instrument failure points is not considered as significant.

Table 7-1 Available Data

Test	Test Fuel	Engine Setting	5I	202	EC/OC	LII	DMS500	FID	FTIR	Smoke Meter
1	LACF	NL	✓	✓	✓	✓	✓	✓	✓	✓
2	LACF	NL	✓	✓	✓	✓	✓	✓	✓	✓
3	LACF	ECS	✓	✓	✓	✓	✓	✓	✓	✓
4	LACF	MES	✓	✓	✓	✓	✓	✓	✓	✓
5	Jet A-1	NL	✓	✗	✗	✗	✓	✓	✓	✗
6	Jet A-1	NL	✓	✓	✓	✓	✓	✓	✓	✓
7	Jet A-1	NL	✓	✓	✓	✓	✓	✓	✓	✓
8	Jet A-1	ECS	✓	✓	✓	✓	✓	✓	✓	✓
9	Jet A-1	ECS	✓	✓	✓	✓	✓	✓	✓	✓
10	Jet A-1	ECS	✓	✓	✓	✓	✓	✓	✓	✓
11	Jet A-1	MES	✓	✓	✓	✓	✗	✓	✓	✓
12	Jet A-1	MES	✓	✓	✓	✓	✓	✓	✓	✓
13	Jet A-1	MES	✗	✗	✗	✓	✗	✓	✓	✗
14	Diesel	NL	✓	✓	✓	✓	✓	✓	✓	✓
15	Diesel	NL	✓	✓	✓	✓	✓	✓	✓	✓
16	Diesel	NL	✓	✓	✗	✓	✓	✓	✓	✓
17	Diesel	ECS	✓	✓	✓	✓	✓	✓	✓	✓
18	Diesel	ECS	✓	✓	✓	✓	✓	✓	✓	✓
19	Diesel	ECS	✓	✓	✓	✓	✗	✓	✓	✓
20	Diesel	MES	✓	✓	✓	✓	✓	✓	✓	✓
21	Diesel	MES	✓	✓	✓	✓	✓	✓	✓	✓
22	Diesel	MES	✓	✓	✓	✓	✗	✓	✓	✓

Note:

- LACF* – Low Aromatic Content Fuel
- NL* – No Load (Idle)
- ECS* – Environmental Cooling System Engine Power setting
- MES* – Main Engine Start

7.2 Result

7.2.1 Method 5I

Figure 7-1 shows the pictures of samples of method 5I filters from LACF and diesel fuel of the MES engine operating conditions respectively. From the pictures it is clear that there is a difference in the amount of particles captured by the filters. This observation is interesting given that for the LACF fuel the sample was collected for an hour in contrast to the diesel fuel which was collected for 20 minutes. This difference can be attributed to the difference in the aromatic contents of the fuels [37, 38]. In general the particle loading of the filters ranged from 0.1 to 2.7 mg. National Physics Laboratory expressed no concerns about the filter loading thus indicating that these were good filter loadings for gravimetric analysis.

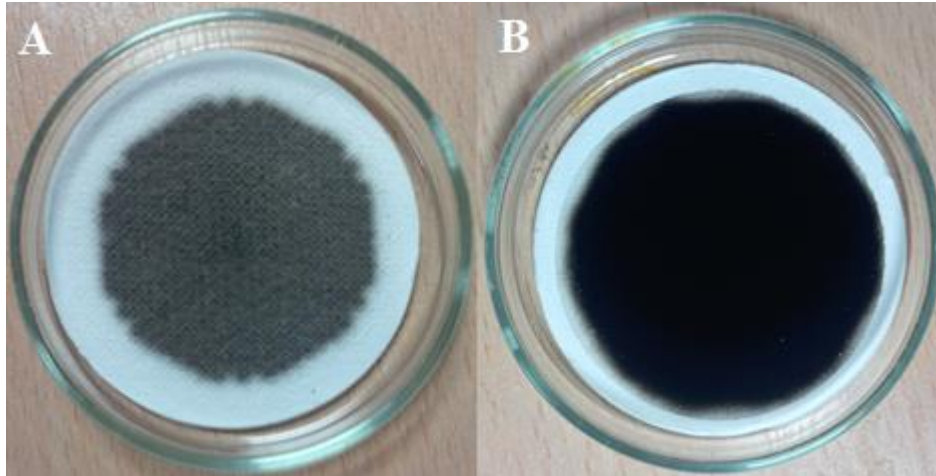


Figure 7-1: Examples of Method 5I filter samples. Picture A – engine run with LACF fuel at MES power setting and picture B – engine run with diesel fuel at MES power setting.

7.2.2 Method 202

Figure 7-2 are images of the method 202 filter samples of the engine at MES operating condition from LACF and diesel fuel respectively. Unlike the method 5I filters, these filters were not pre-weighed and post weighed after capturing the sample as the analytical process is different to method 5I as described in section 6.4.1. Nevertheless, the images demonstrate the efficiency of the method 5I filter in capturing the filterable particles in the exhaust stream as there are no visible particles on filters thus; no visible distinction to tell which fuel was burnt.

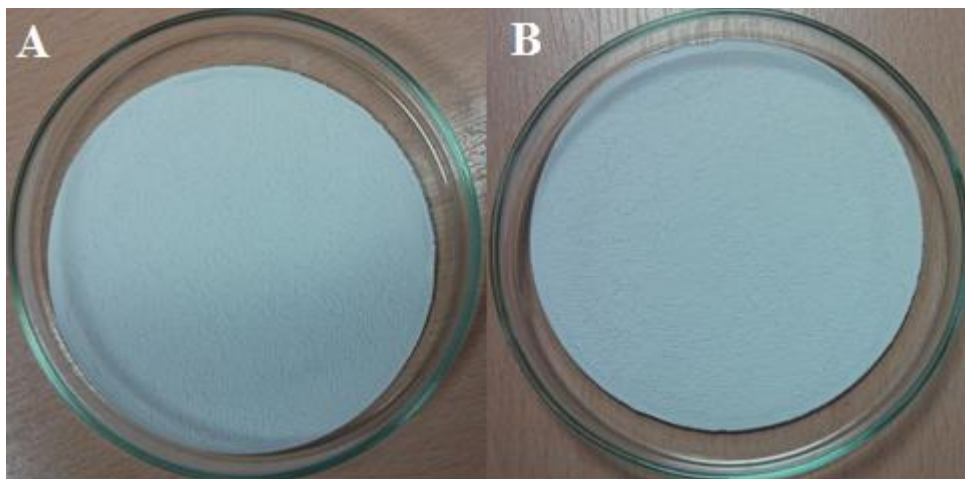


Figure 7-2: Examples of Method 202 filter samples. Picture A – engine run with LACF fuel at MES power setting and picture B – engine run with diesel fuel at MES power setting.

7.2.3 Laser-Induced Incandescence

Figure 7-3 is an example snap shot of real-time data of the LII measurements. It shows that the concentration of the exhaust was usually stable for the duration of the test runs. The LII was set to average data at a rate of 20-Hz rate. The red dots in the snap shot represent the single shot data, and the black line is a 1-Hz running average of the single shot data. Variations in the concentration did not exceed 10%.

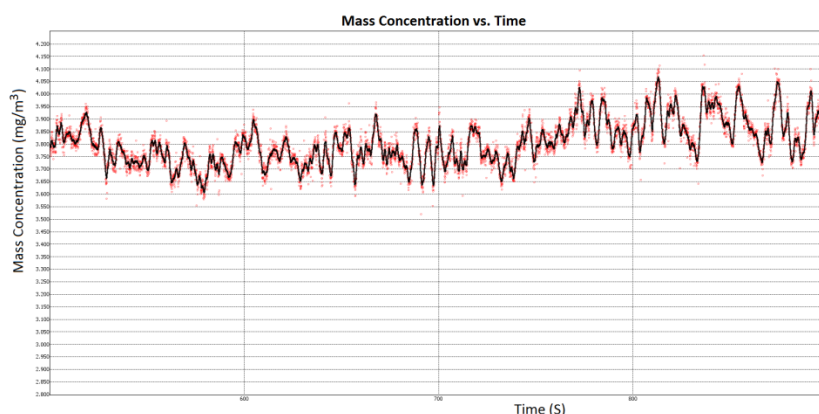


Figure 7-3: LII mass concentration measurement for Test point 15

7.2.4 NIOSH 5040 EC/OC

Figure 7-4 are images of particulate loading of the NIOSH 5040 EC/OC filters papers for test point 14 and 4 respectively. The particle loading ranged from 17.1 to 70.9 $\mu\text{g}\cdot\text{cm}^{-2}$. NPL certified the loading to be good for the analysis of the total carbon content of the samples.

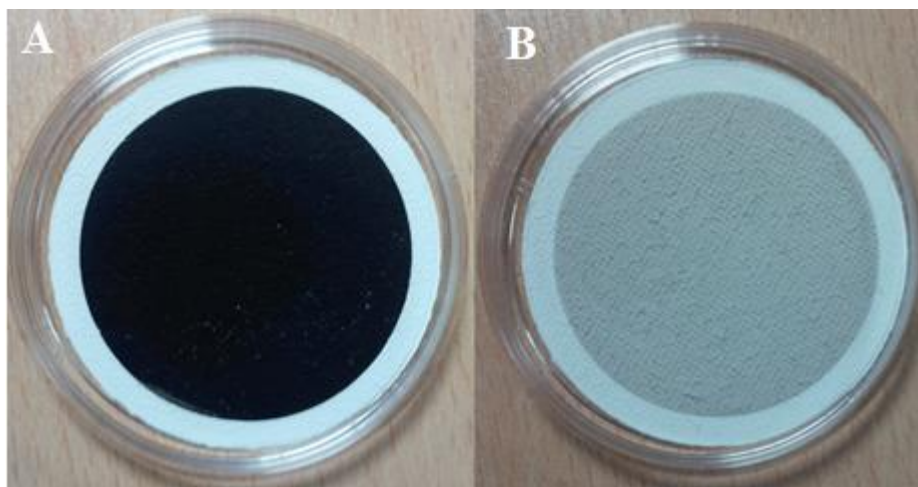


Figure 7-4: Example of sample deposits for NIOSH 5040. Picture A – engine run with diesel fuel at MES power setting and picture B – engine run with LACF fuel at MES power setting.

7.2.5 Differential Mobility Spectrometer DMS500

As discussed previously in section 2.5.2 the DMS500 is a size distribution instruments. Figure 7-5 is a snap shot of the three dimensional animation size-number distribution spectrum of test point 15 to show the stability of the PM sample during the duration of the test.

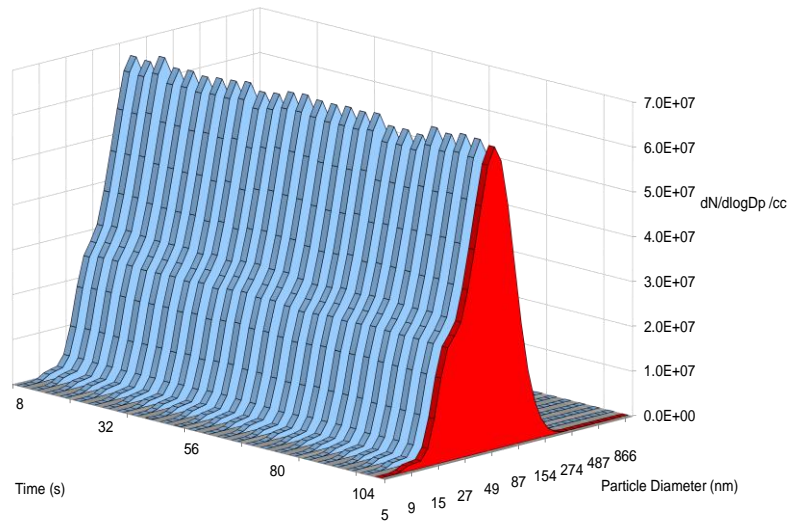


Figure 7-5: DMS500 three dimensional animation spectrum

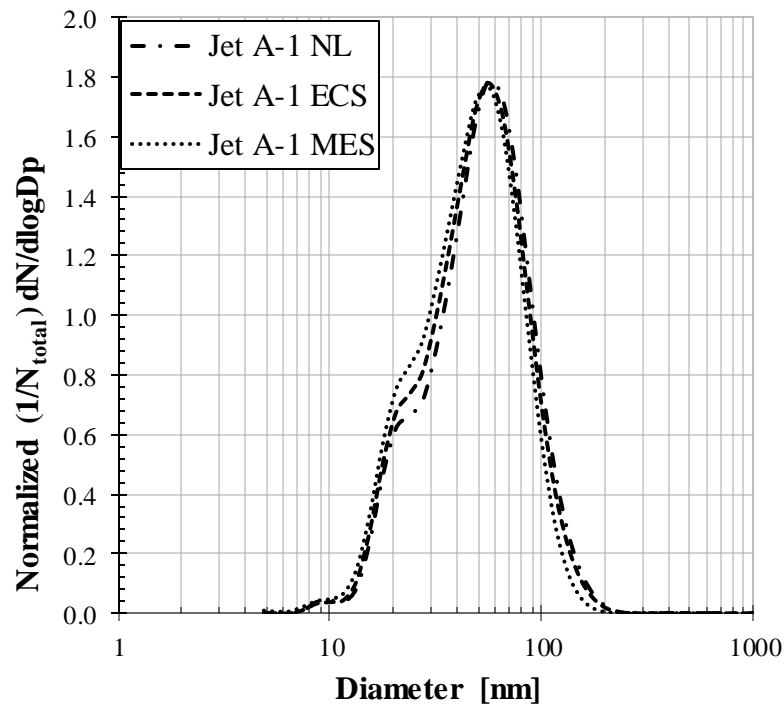


Figure 7-6: Showing the DMS500 size distribution for the engine power setting for Jet A-1

Figure 7-6 shows the normalized number-size distributions representation of engine power setting for Jet A-1 fuel. The distributions have two peak points suggesting the presence of two modes in the range of 15-25 nm and 45-55 nm for the test points.

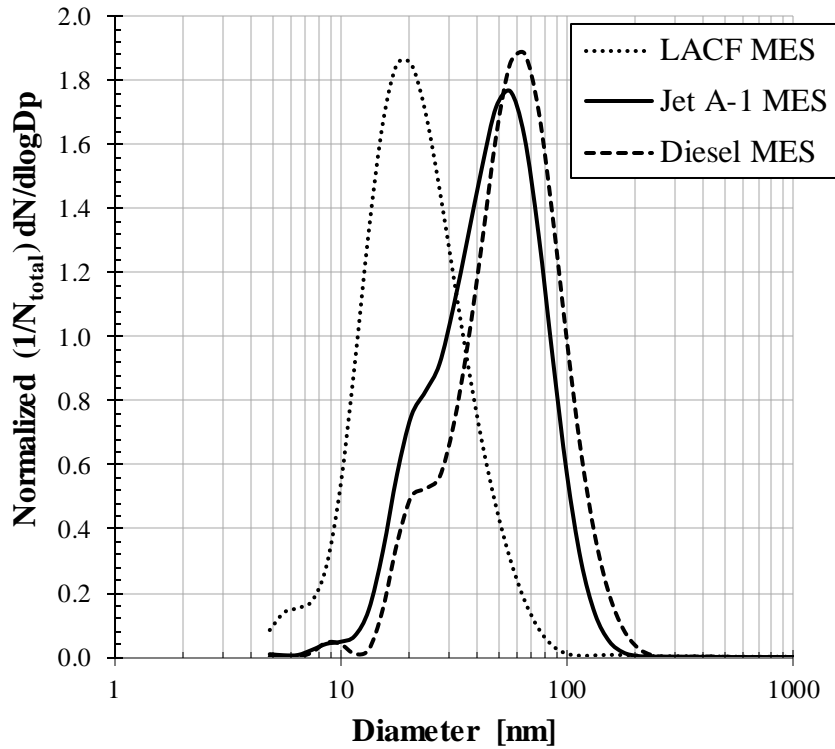


Figure 7-7: DMS500 size distribution of the test fuels at the MES engine condition for the three test fuels

Figure 7-7 shows the distribution of each of the test fuel at the MES engine condition. For the Jet A-1 and diesel fuels two modes can be observed while only one mode can be observed for the LACF fuel. It can also be observed that the LACF particle sizes tend to be smaller in size with particles from diesel exhibiting the largest particle sizes. The implication is that the LACF fuel contains more nuclei mode particle which suggests that the particles are mostly condensable particles. This observation can be attributed to the presence and lack of aromatics in the fuel. As described in section 2.1 the formation process of particle matter during combustion involves the formation of aromatics. Thus for fuels which contains aromatics there is a higher aromatic seed formation rate thus have more time for the particles to grow in size during combustion. Figure 7-8 which shows the un-normalised size distributions for the fuels at the MES power setting suggest

that further growth as a result of coagulation within the sample line resulting in the larger particle measured for diesel and Jet A1 respectively. This can be deduced from the increased particle number and size from the LACF to Jet A-1 fuel and then to diesel fuel.

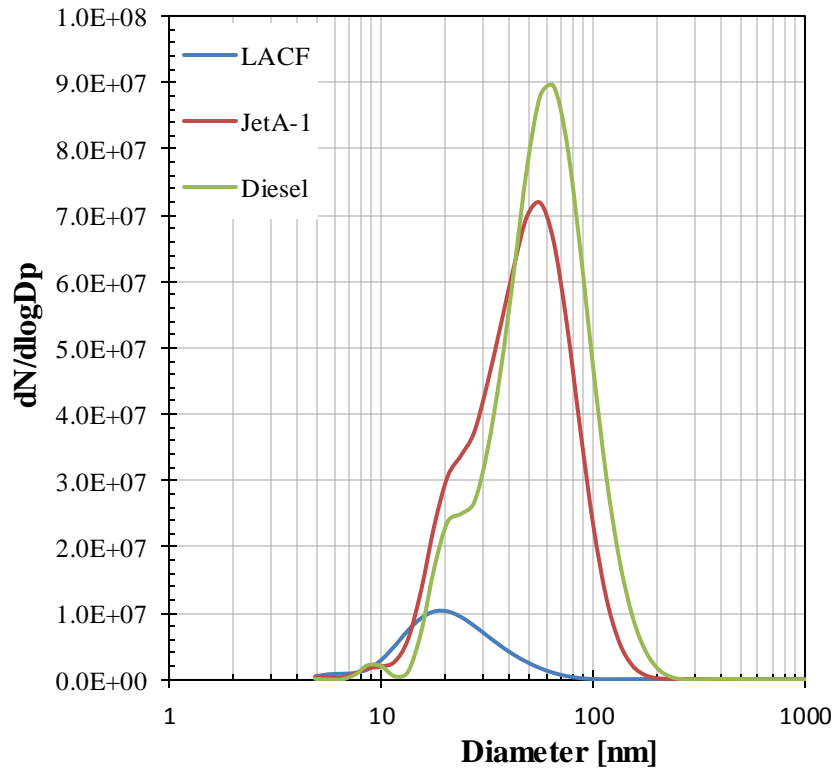


Figure 7-8: Un-normalised DMS500 size distribution of the test fuels at the MES engine condition for the three test fuels

Further information about the particle emissions can be observed by plotting graphs of the geometric mean particle diameter (GMD) and geometric standard deviation against engine set points as shown in Figure 7-9 and Figure 7-10 respectively for the three fuels tested in the APU. Of the three test fuels, diesel shows the largest GMD across the engine power setting. The GMDs range are as follows; Jet A-1 from 49.38 to 43 *nm* for; diesel from 52 to 55; and approximately 42 to 21 *nm* for LACF. This is consistent with the observation during the AAFEX experimental campaign [43] using the same engine type. Figure 7-10 shows the geometric standard deviation (GSD) of the particle size distribution. Overall, the GSDs range from ~ 1.69 to 1.87 depending both on EGT and fuel. For diesel, the

GSDs were substantially larger ranging from about 1.72 to 1.87 depending on EGT with the variation predominantly between the repeat NL power conditions.

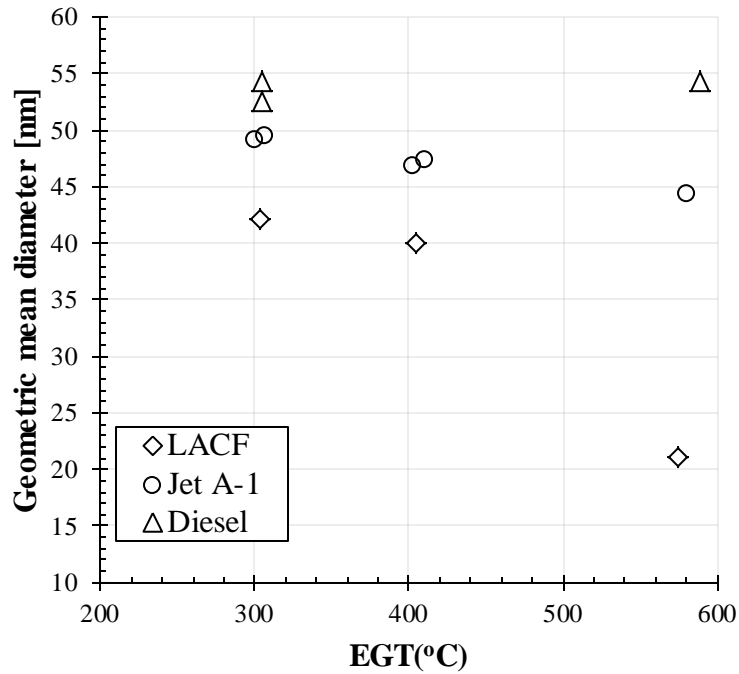


Figure 7-9: Geometric mean particle diameter

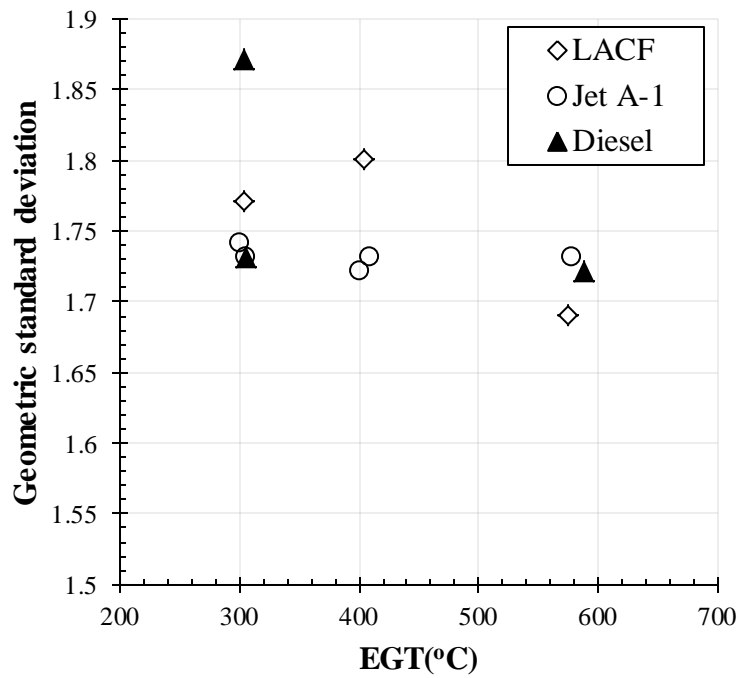


Figure 7-10: Geometric standard deviation

7.2.6 Smoke Meter

Figure 7-11 is a Whatman No 4 filter paper sample for LACF (test point 4) and diesel (test point 17) test fuels at the NL engine test points. Less visible or light absorbing material can be observed on the filter paper from the LACF combustion compared to the filter sample from diesel. This observation is similar to the previous work done by Khandelwal et al [130].

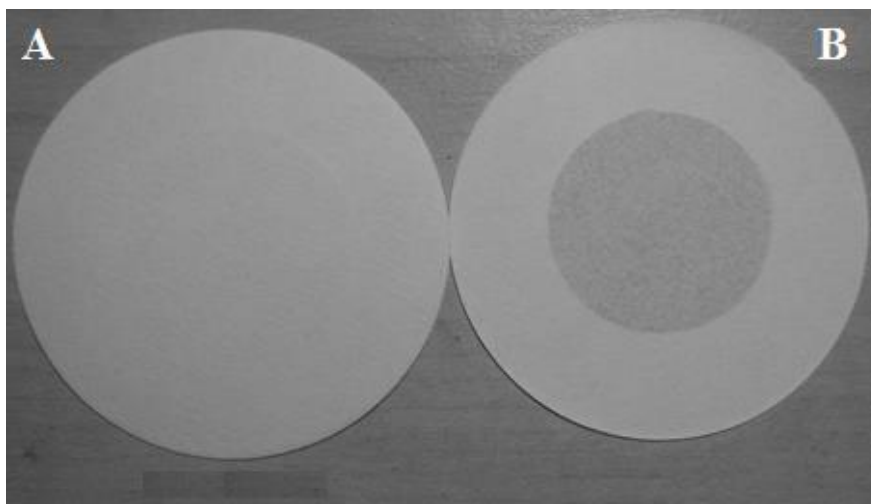


Figure 7-11: Example of sample deposits for Smoke Meter filter papers. Picture A – engine run with LACF fuel (Test 4) and picture B – engine run with diesel fuel (Test 17).

7.2.7 FTIR

The FTIR acquisition was started just after the start of the sample acquisition in the sample lines and runs to just after the end of the sample acquisition run time.

7.3 Repeatability of Engine Operating Conditions and Corresponding Emissions

7.3.1 Engine operating point check

To repeat a gas turbine engine operation at a specific condition depends on many parameters which are outside the scope of this study. Nevertheless, an accurate measurement of the engine power setting is important as the uncertainty in the data analysed is subject to repeatability of the engine operating condition for each test fuel as listed in section 5.1. Thus an assessment of the operating point helps identify the test runs that should be cautiously treated. To compare the engine operating parameters Table 7-2 presents the average fuel flow rates and RPM at

the various power conditions of 3 repeats. The values demonstrate reasonable consistent engine power setting for the experimental test points. From a different view point the engine fuel consumption is directly related to engine power output, in this case the exhaust gas temperature which has been used as an indication of the power setting of the engine. The test engine NL power setting is an automatic pre-set condition (idle) while the ECS and MES were achieved by changing the EGT which was constant for all the fuels tested. Accordingly, Figure 7-12 is a plot of the fuel flow rate data for the three types of fuels tested against the exhaust gas temperature. The linear correlation expression of the three plots demonstrates the consistency of the engine as the equations are identical. This suggests that despite the difference in the hydrogen and carbon ratio of the fuels the fuel consumption of the engine was not impacted which can be attributed to the similarity in the calorific values of the fuels.

Table 7-2: Average APU parameters

Test Fuels	Fuel Flow (g/s)			RPM		
	NL	ECS	MES	NL	ECS	MES
LACF	17.89	24.54	30.97	41550	41346	40588
Jet A-1	18.52	24.68	32.27	41601	41120	40683
Diesel	19.17	25.43	33.21	41745	41400	40864

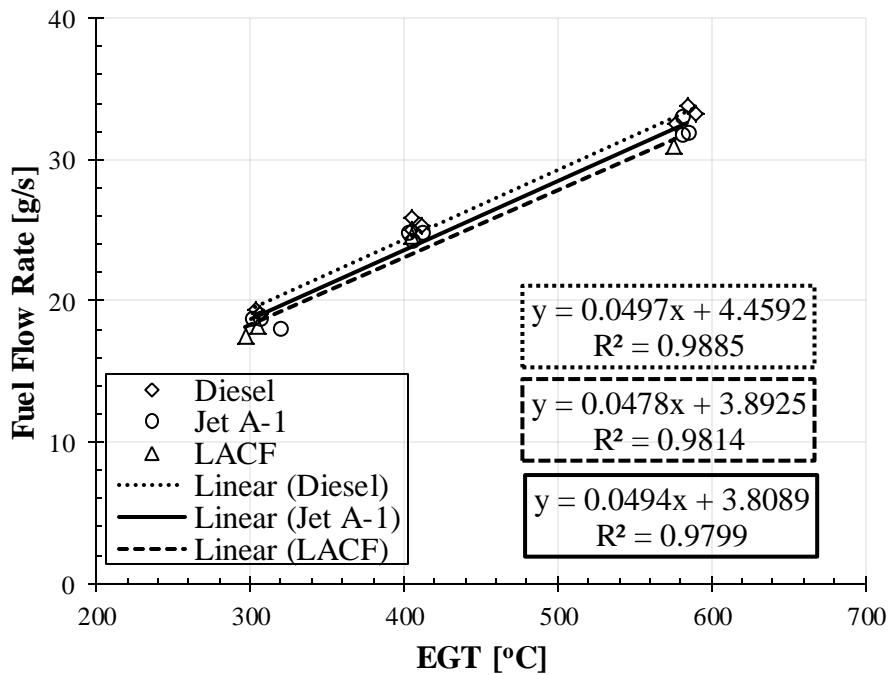


Figure 7-12: Correlation between fuel consumption and the engine exhaust gas temperature.

7.3.2 Variability of Engine Operating Parameters and Gaseous Emissions

Figure 7-13 and Figure 7-14 shows the percentage variability of engine parameters and gaseous emission of the test Jet A-1 and diesel from the engine power setting repeats as determined using the relative standard deviation (see section 6.6). In general the variation of the engine fuel flow and the exhaust gas temperature is less than two percent. This demonstrates that during the different days of testing the engine was very stable which is an important condition to be met, for the study of the correlation between the particle instruments. The CO, THC and CO₂ emissions variability is less than 13% for the Jet A-1 and diesel fuels across the engine power setting which is considered high compared with the fuel flow variation. The possibilities for the observed discrepancy include the weather condition and activities happening around the engine air inlet. For instance the APU fuel tank is situated close to the air inlet while other combustion activities must have been happening on site and unfortunately were not evaluated during this experiment.

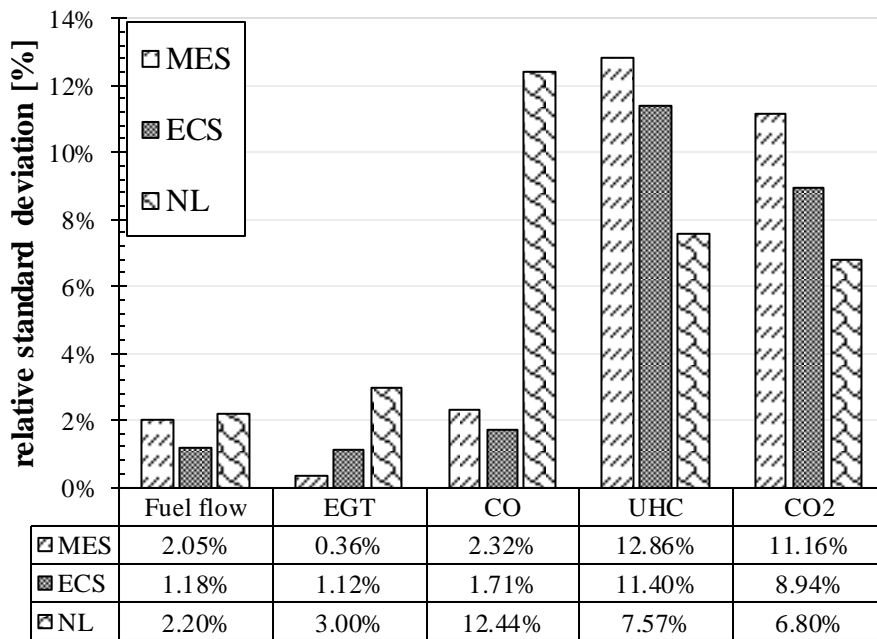


Figure 7-13: Relative standard deviation of the engine parameters and gaseous emissions for Jet A-1

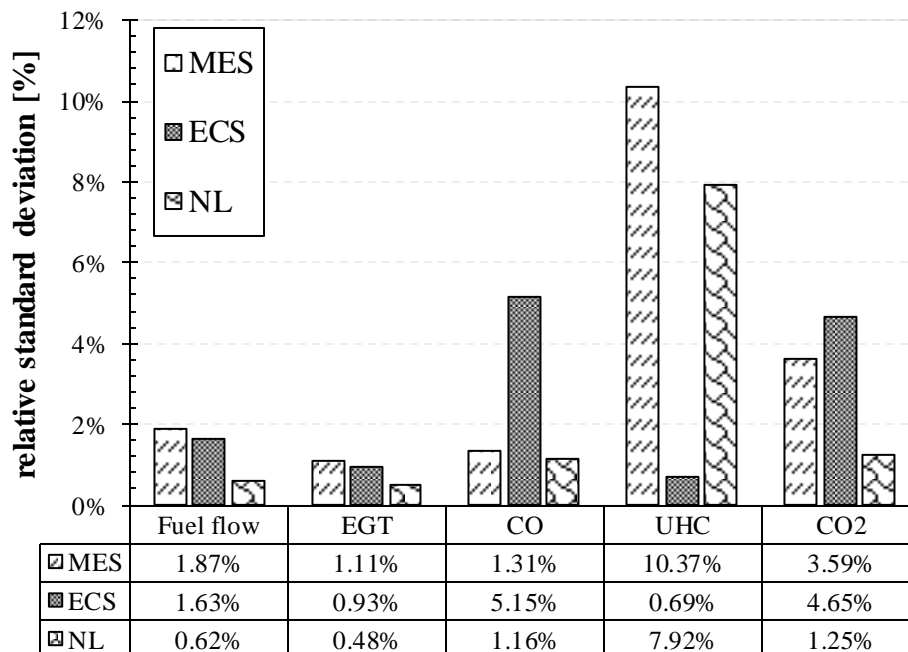


Figure 7-14: Relative standard deviation of the engine parameters and gaseous emissions for diesel

7.3.3 PM Instrument Repeatability of the Engine PM Emissions

Figure 7-15 and Figure 7-16 shows the uncertainty of the PM instruments expressed as one relative standard deviation for the three engine operating conditions. The variability of most of the instruments is within the range of 15%

or better with the exception of the method 202 total CPM results. Apart from the Jet A-1 fuel at the MES engine power setting the variation of the Method 5I is less than 10 percent. The variation for NIOSH 5040, range between 10 and 18 percent with the exception of the ECS power setting for Jet A-1. For the FTIR the variation of the THC is presented in the figures. It is generally less than 10 percent except for diesel fuel burnt at the NL engine power setting. Method 202 data show a fairly poor repeatability which is not surprising as previously described in section 2.4. It shows a variability as high as 140% and as low as 29%. As noted in section 2.3.1 and observed in Figure 2-8 very high variability was also experienced for the field testing reported [40]. Thus, the high variability is not unexpected. Further details of the variability of the organic and inorganic components of the method 202 data are discussed in section 7.7.

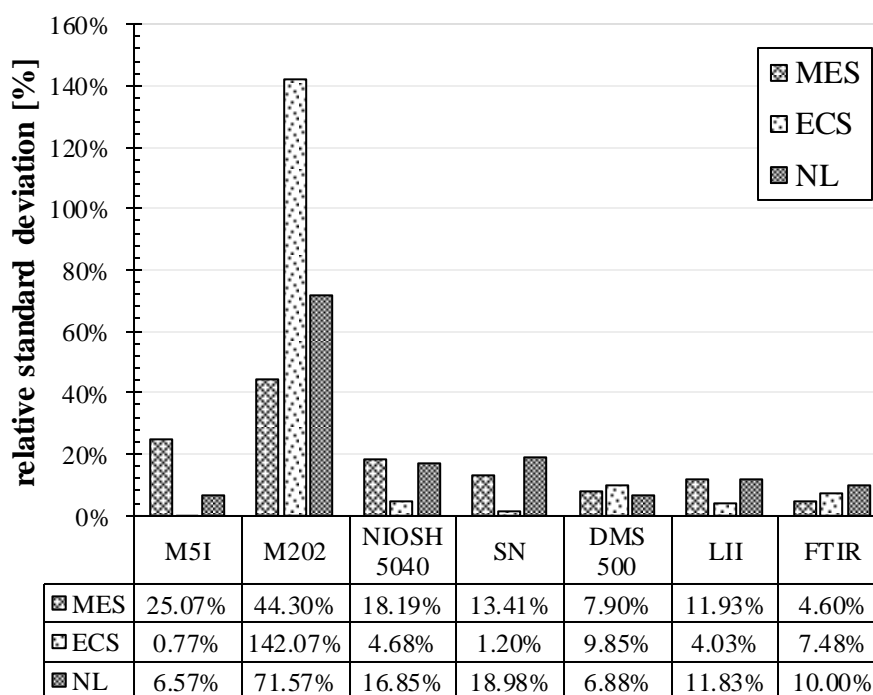


Figure 7-15: Relative standard deviation of the engine parameters / gaseous emissions for Jet A-1

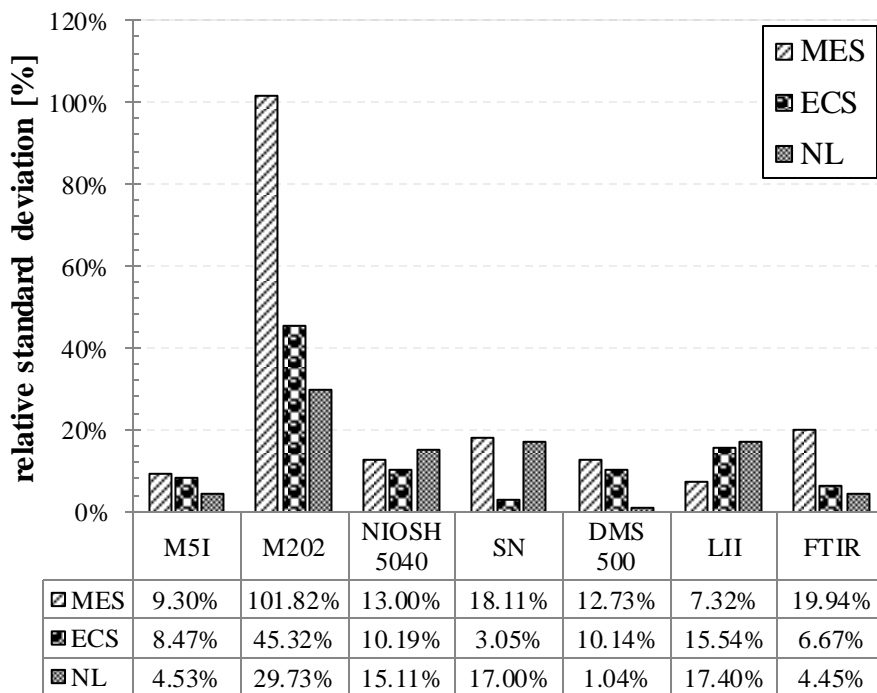


Figure 7-16: Relative standard deviation of the engine parameters / gaseous emissions for diesel

7.4 Validity of the PM Instruments Measurements

The objective of this section is to check the validity of the data collected by verifying the results with established outcomes of PM emissions from a gas turbine. For instance it is expected that the results of instruments that measure only elemental carbon or that speciate the elemental carbon emission should record an equal or lower mass when compared with instruments that measure total mass. Accordingly, Figure 7-17 compares the absolute values of the absolute values as measured with NIOSH 5040 and USA EPA method 5I. The figure shows on the average the total carbon concentration as measured with NIOSH is lower or equal to the mass concentration measured with method 5I except for the diesel MES condition which has a large difference. This difference can be attributed to human error including leaks due to filter holder not properly placed and timing of the flows which were experienced for this set of experiments. Thus, the exhaust volume through the filters sample flow used to calculate the mass concentration is high compared to the filter catch. The absolute values of the elemental carbon concentration as measured by NIOSH 5040 and LII300 in Figure 7-18 shows that the results are virtually equal considering the variability as represented with the error bars. However, the systematic lower LII readings can

be attributed to the manual EC split in addition to the loading of the filters which were generally heavy than usual for NIOSH 5040 analysis. Details of the correlation between the NIOSH 5040 and LII300 are discussed in section 7.5.1.

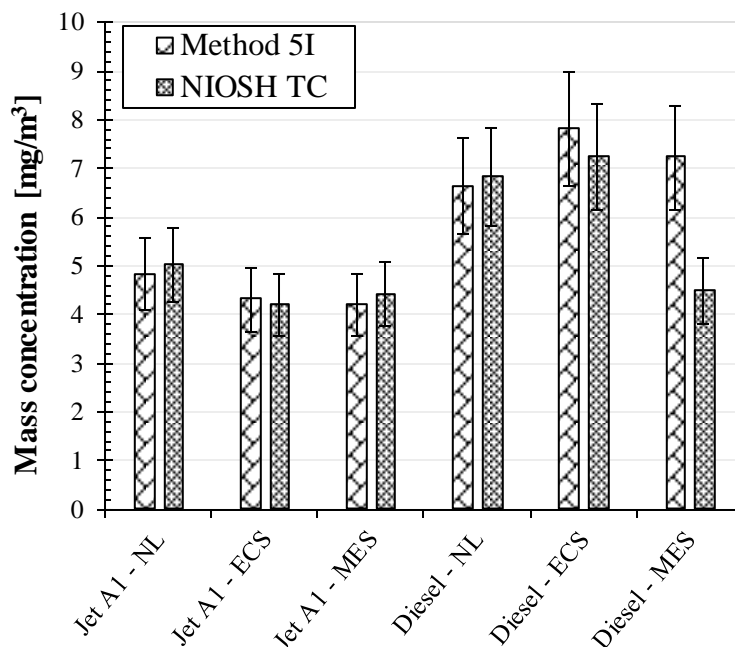


Figure 7-17: Absolute values of total mass and total carbon concentration measured using method 5I and NIOSH 5040 respectively

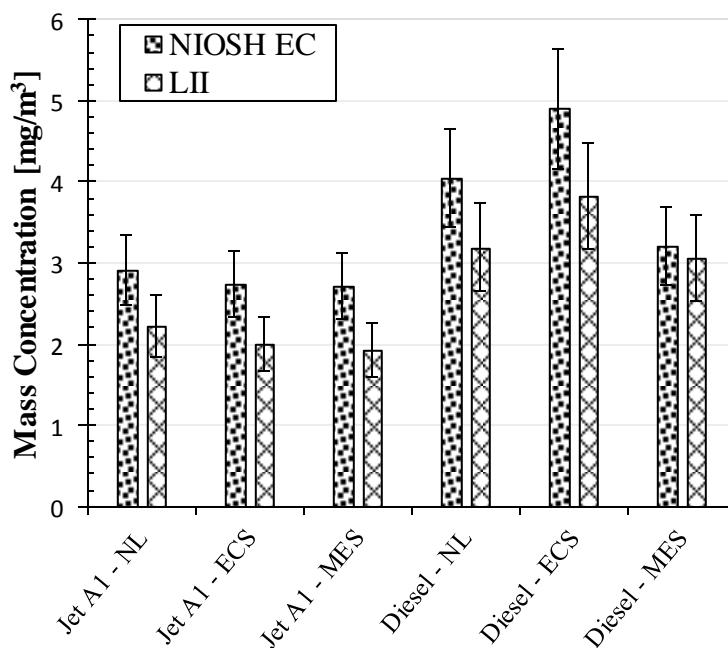


Figure 7-18: Absolute values of elemental carbon concentration measured using NIOSH 5040 and LII300.

7.5 Correlation between FPM Instruments

In this section the mass concentration of the LII300, DMS500 and NOISH 5040 are inter compared and also compared to the US EPA method 5I results. The results include error bars which are one standard deviation of the repeats test conditions expressed in percentage as detailed in section 7.3.3. The trends of the plots are forced through zero as the analysers read zero with HEPA air with the linear relationship and the R square indicated on the graphs. Also presented alongside the graphs are the regression statistics which includes the t Stat, P-values, intercept and x coefficients from the multi linear regression analysis. The P-values gives the significance of the linear equation established between the instruments. Values ≤ 0.001 indicate that the equation is statistically significant.

7.5.1 NIOSH 5040 Comparison

Figure 7-19 compares the LII300 results and elemental carbon contents of NIOSH 5040. The figure show an overall $R^2 = 0.99$ across all test conditions. For the prediction of NIOSH 5040 elemental carbon, the relationship is very near to 1:1 with LII300 estimates 20% lower than the NIOSH 5040 values.

Table 7-3: Multiple linear regression analysis of the relation between NIOSH5040 Elemental Carbon and LII mass concentrations.

	Multiple R	R Square	Adjusted R Square	Standard Error
	0.99403	0.98810	0.98736	0.13514
	Coefficients	Standard Error	t Stat	P-value
Intercept	-0.1390	0.0734	-1.8932	0.0766
x	0.8007	0.0220	36.4565	0.0000
Equation	$y = 0.8007x - 0.139$			

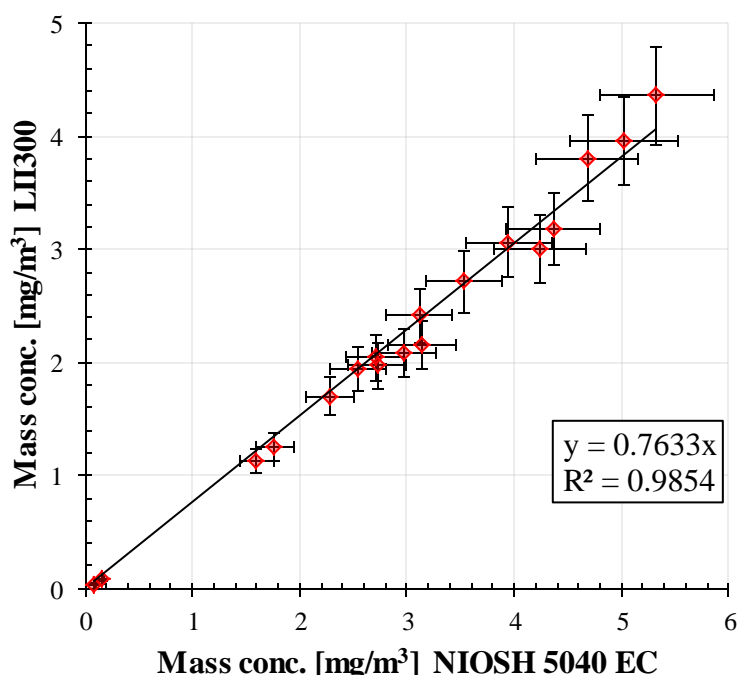


Figure 7-19: Correlation between LII300 and NIOSH 5040 EC

Figure 7-20 shows the correlation between the total carbon (TC = EC+OC) concentration measured by NIOSH 5040 EC/OC and the filterable mass concentration as measured by method 5I. A high correlation ($R^2 = 0.89$) can be observed between the two instrument. The associating linear equation show that the NIOSH 5040 results under predicts method 5I total mass concentration by 12%. This near 1:1 relation across the wide range of concentrations (0.12 mg/m^3 to 8.57 mg/m^3), suggests that the chemical components of the method 5I sample are majorly elemental and organic carbon.

Table 7-4: Multiple linear regression analysis of the relation between NIOSH5040 Total Carbon and Method 5I mass concentrations.

	Multiple R	R Square	Adjusted R Square	Standard Error
	0.9486	0.8998	0.8931	0.7004
	Coefficients	Standard Error	t Stat	P-value
Intercept	0.4079	0.3896	1.0470	0.3117
x	0.8204	0.0707	11.6037	0.0000
Equation	$y = 0.8204x + 0.4079$			

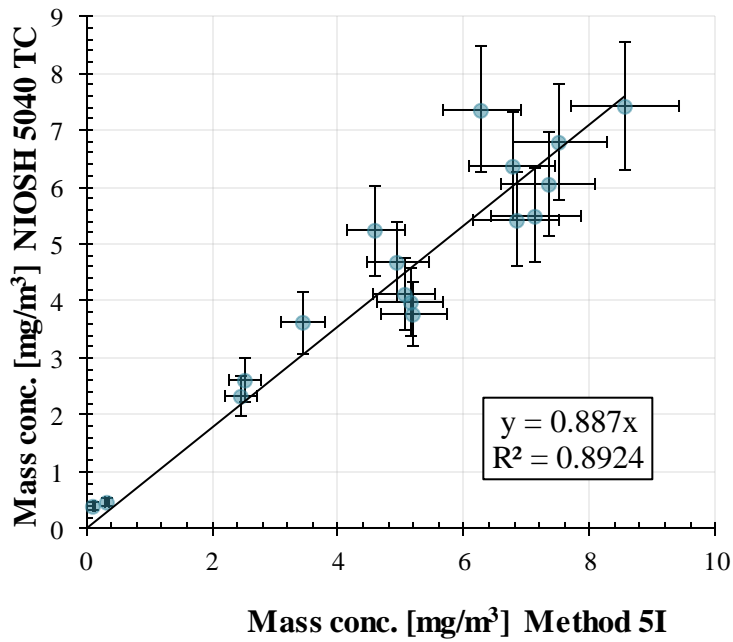


Figure 7-20: Correlation between Method 5I and NIOSH 5040 TC

Looking at the fuel data separately as shown in Figure 7-21, better correlation can be observed for the LACF compared to diesel to Jet A-1 data respectively. Jet A-1 have high level of sulphur compared to LACF and diesel and thus could be attributed to the remaining 12% by which the NIOSH TC under predicts the method 5I values.

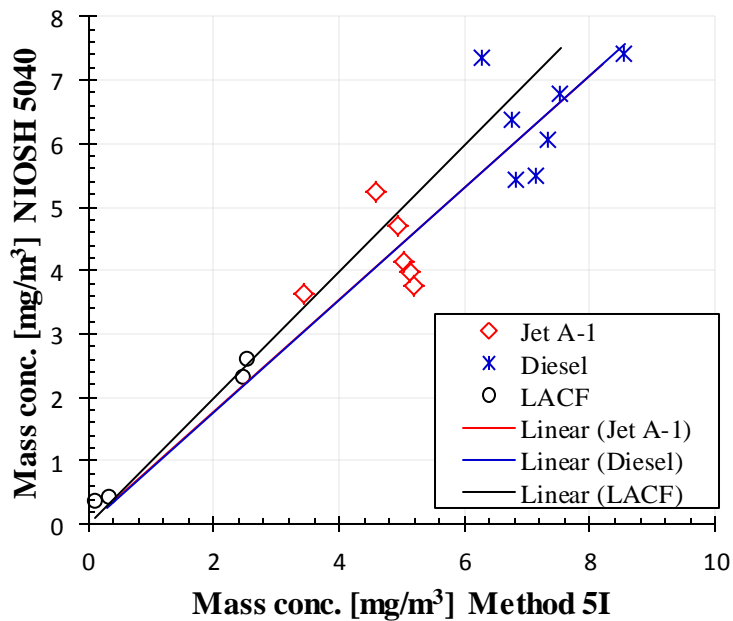


Figure 7-21: Correlation between Method 5I and NIOSH 5040 TC showing the fuel data separately.

7.5.1.1 Discussion - NIOSH 5040 Comparison

Total carbon measured by NIOSH 5040 showed a near one to one relationship as it predicts 90% of the FPM as measured by US EPA method 5I. The significance of this relationship is that the US EPA method 5I gas turbine PM sample capture is mostly carbon in nature. Meanwhile, the LII showed a very good correlation and predicts over 80% of the EC component of the NIOSH 5040 measurements. These instruments also formed the basis on which the validity of the instrument measurements was checked. A 100% prediction of the method 5I measurement was not expected using the aforementioned instruments as the method 5I filter is also capable of capturing traces of inorganic components in the exhaust that could be the consequence of chemical compound in the fuel or atmospheric air from which the engine draws its oxidant.

7.5.2 DMS500 Comparisons

This section compares the mass concentration of the DMS500 data without the Nafion dryer in place with the mass concentrations of method 5I total mass concentration and NIOSH 5040 total carbon measurements. To convert the particle number size parameters which the DMS500 typically measures, into mass concentration the density functions derived in chapter 5 of this thesis was used. Also comparisons are made with the DMS500 derived mass concentration from unit density commonly assumed for particle emissions.

7.5.2.1 Unit Density Derived Mass Concentration without Nafion Dryer in Place

Figure 7-22 is a plot of the DMS500 mass concentration derived from the application of unit density against method 5I mass concentration. It shows that the DMS500 estimates of mass concentration using a unit density are 1.5 times the mass concentration as measured using method 5I despite the good correlation ($R^2 = 0.93$). A similar trend can be observed for the NIOSH 5040 total carbon concentration plot in Figure 7-23.

Table 7-5: Multiple linear regression analysis of the relation between DMS500 mass concentration [No Nafion Dryer (Unit Density)] and Method 5I mass concentrations.

	Multiple R	R Square	Adjusted R Square	Standard Error
	0.9154	0.8380	0.8200	1.5740
	Coefficients	Standard Error	t Stat	P-value
Intercept	-0.2349	1.1743	-0.2000	0.8459
x	1.6860	0.2471	6.8236	0.0001
Equation	$y = 1.686x - 0.2349$			

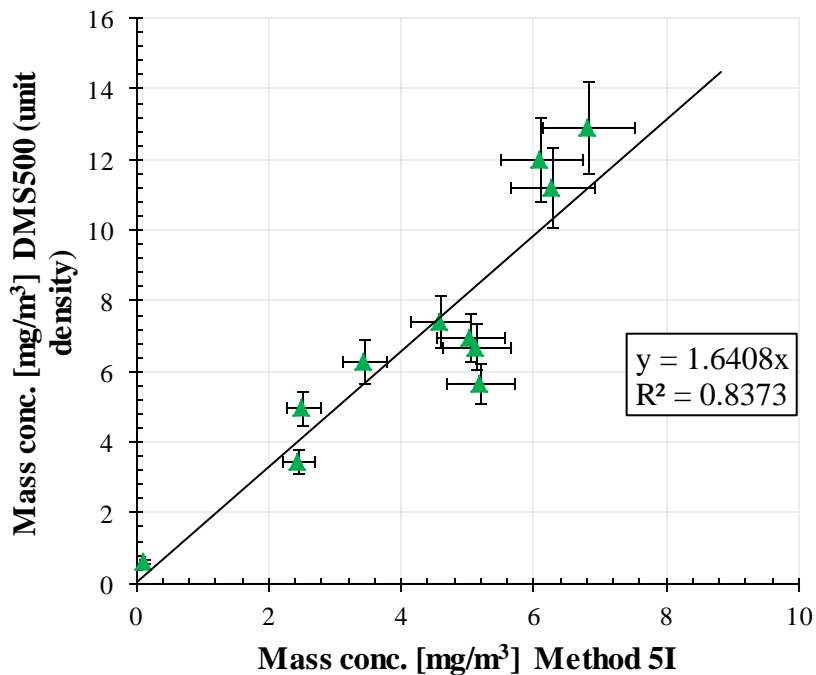


Figure 7-22: Correlation between DMS500 mass concentration [No Nafion Dryer (Unit Density)] and Method 5I

Table 7-6: Multiple linear regression analysis of the relation between NIOSH 5040 TC and DMS500 mass concentration [No Nafion Dryer (Unit Density)] mass concentrations.

	Multiple R	R Square	Adjusted R Square	Standard Error
	0.9128	0.8332	0.8123	1.5227
	Coefficients	Standard Error	t Stat	P-value
Intercept	0.0632	1.1413	0.0554	0.9572
x	1.6837	0.2664	6.3211	0.0002
Equation	$y = 1.6837x + 0.0632$			

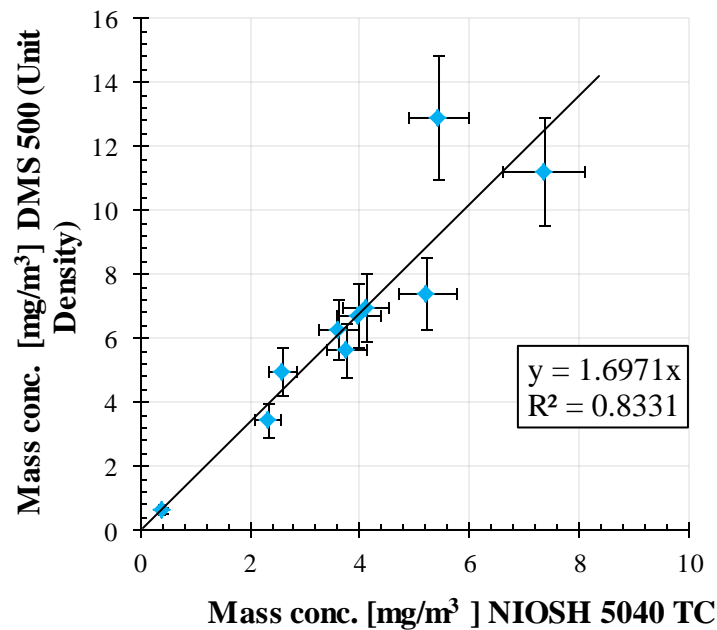


Figure 7-23: Correlation between NIOSH 5040 TC and DMS500 mass concentration [No Nafion Dryer (Unit Density)]

7.5.2.2 DMA/CPMA/CPC Density Derived Mass Concentration without Nafion Dryer in Place

Method 5I is compared to DMS500 mass concentration determined using the DMA/CPMA/CPC density functions obtained from the density experiments in chapter 5 as shown in Figure 7-24. It shows a good relationship between the DMS500 and method 5I ($R^2 = 0.87$) with a near 1:1 relationship with method 5I data as it with 11% of method 5I. In Figure 7-25 the same DMS500 data is compared with the NIOSH 5040 total carbon concentration. The plot shows a better quality of fit ($R^2 = 0.92$) and within 8% of NIOSH TC data compared with the method 5I correlation. The DMS500 mass concentration determined using experimental derived densities shows a significant predictability of the method 5I results compared to the DMS500 mass concentration determined from a unit density. Thus, the use of size to measure mass if effective density is also measured shows great promise.

Table 7-7: Multiple linear regression analysis of the relation between DMS500 mass concentration [No Nafion Dryer (DMA/CPMA/CPC Density)] and Method 5I mass concentrations.

	Multiple R	R Square	Adjusted R Square	Standard Error
	0.9356	0.8753	0.8614	0.7409
	Coefficients	Standard Error	t Stat	P-value
Intercept	-0.1553	0.5527	-0.2810	0.7851
x	0.9244	0.1163	7.9479	0.0000
Equation	$y = 0.9244x - 0.1553$			

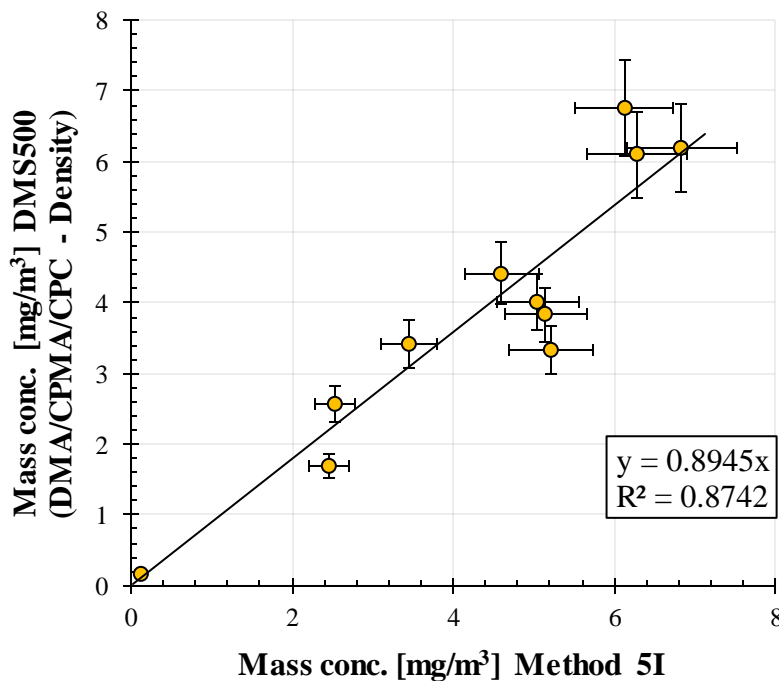


Figure 7-24: Correlation between DMS500 mass concentration [No Nafion Dryer (DMA/CPMA/CPC Density)] and Method 5I

Table 7-8: Multiple linear regression analysis of the relation between DMS500 mass concentration [No Nafion Dryer (DMA/CPMA/CPC Density)] and NIOSH 5040 TC mass concentrations.

	Multiple R	R Square	Adjusted R Square	Standard Error
	0.9599	0.9214	0.9116	0.5468
	Coefficients	Standard Error	t Stat	P-value
Intercept	-0.0251	0.4098	-0.0613	0.9526
x	0.9266	0.0956	9.6872	0.0000
Equation	$y = 0.9266x - 0.0251$			

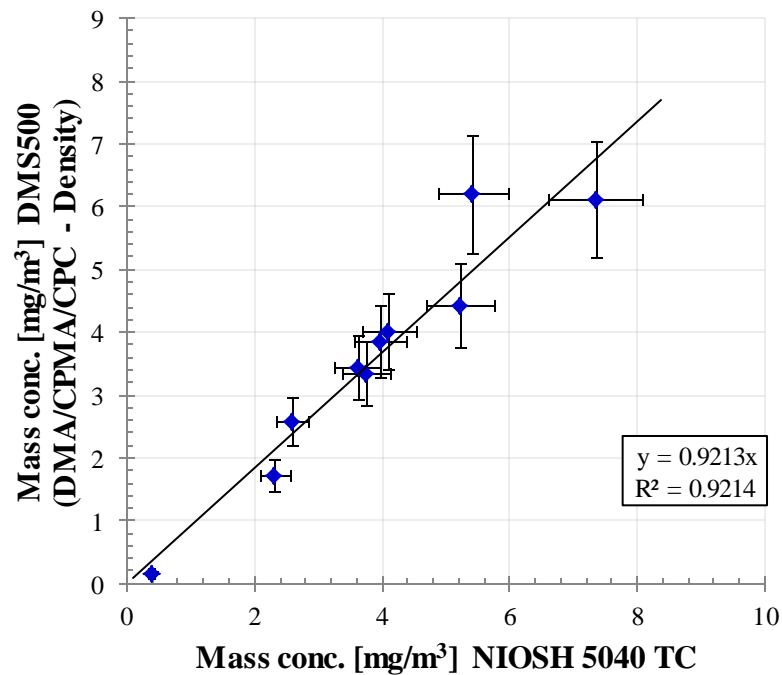


Figure 7-25: Correlation between DMS500 mass concentration [No Nafion Dryer (DMA/CPMA/CPC Density)] and NIOSH 5040 TC

7.5.3 DMS500 with Nafion Dryer

This section correlates the DMS500 mass concentration exhaust samples passed through a Nafion dryer with the method 5I and NIOSH 5040 total carbon. The DMS500 mass concentration has been determined using the effective densities from the DMA-CPMA-CPC instrumentation as described in chapter 5. The plots in Figure 7-26 and Figure 7-27 show a good quality of fit but a poor prediction of both the total mass concentration from method 5I and the NIOSH 5040 total carbon content respectively. As contained in the equation in the graph the DMS500 used this way can only directly predict nearly 30% of the method 5I measurement. This suggests particle losses and transformation must have occurred within the Nafion dryer considering the high predictability observed in the previous sub section.

Table 7-9: Multiple linear regression analysis of the relation between DMS500 mass concentration [Nafion Dryer (DMA/CPMA/CPC Density)] and Method 5I mass concentrations.

	Multiple R	R Square	Adjusted R Square	Standard Error
	0.9758	0.9522	0.9479	0.1855
	Coefficients	Standard Error	t Stat	P-value
Intercept	0.2038	0.1055	1.9323	0.0795
x	0.2893	0.0195	14.8063	0.0000

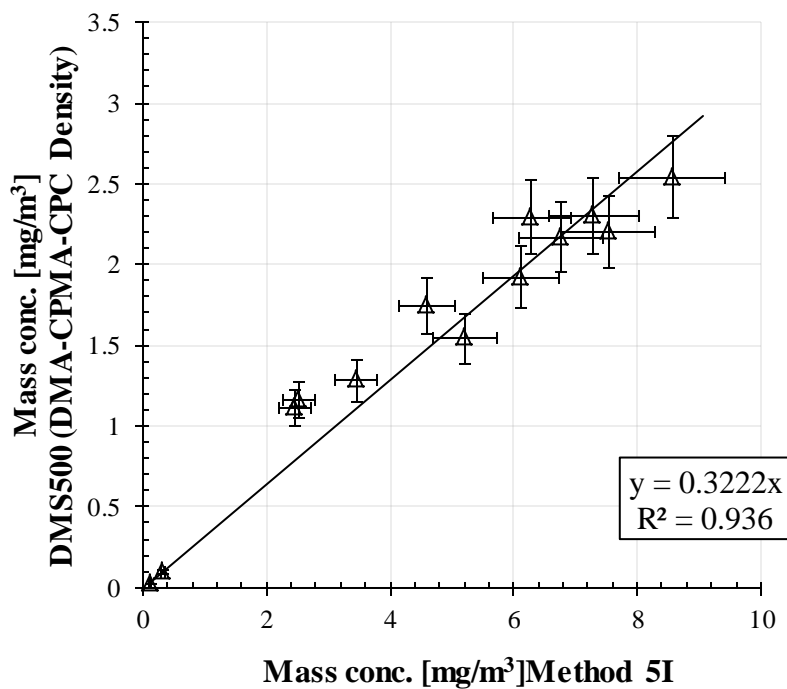


Figure 7-26: Correlation between DMS500 mass concentration [Nafion Dryer (DMA/CPMA/CPC Density)] and Method 5I

Table 7-10: Multiple linear regression analysis of the relation between NIOSH 5040 TC and DMS500 mass concentration [Nafion Dryer (DMA/CPMA/CPC Density)] mass concentrations.

	Multiple R	R Square	Adjusted R Square	Standard Error
	0.9805	0.9615	0.9572	0.1750
	Coefficients	Standard Error	t Stat	P-value
Intercept	0.1268	0.1039	1.2202	0.2534
x	0.3185	0.0213	14.9823	0.0000

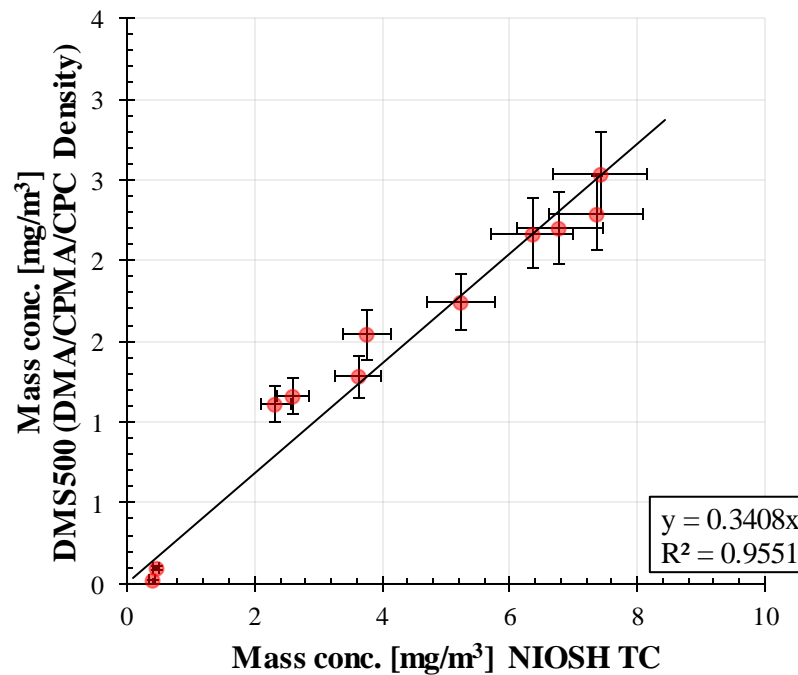


Figure 7-27: Correlation between NIOSH 5040 TC and DMS500 mass concentration [Nafion Dryer (DMA/CPMA/CPC Density)]

7.5.4 Comparisons between the Various DMS500 Mass Concentration

This section makes a comparison between the various DMS500 mass concentrations. First, Figure 7-28 is a plot comparing the absolute values of the DMS500 mass concentration derived using the unit density and the DMA-CPMA-CPC obtained density functions. From the plot it is apparent that the DMS500 unit density derived mass concentrations are nearly twice the mass concentration evaluation from the DMA-CPMA-CPC density- as shown in chapter 5. In Figure 7-29 the DMS500 mass concentration derived using the DMA-CPMA-CPC density for the exhaust sample with and without being passed through Nafion dryer is compared. The graph shows that the results of the case were the exhaust sample is not passed through a Nafion dryer is near double the results passing the exhaust through a Nafion dryer. This confirms that there is a substantial particle loss within the Nafion dryer which at this time have not been quantified thus not in agreement with earlier discussion for GDI engines in section 2.7.1.1 which suggested they were minimal.

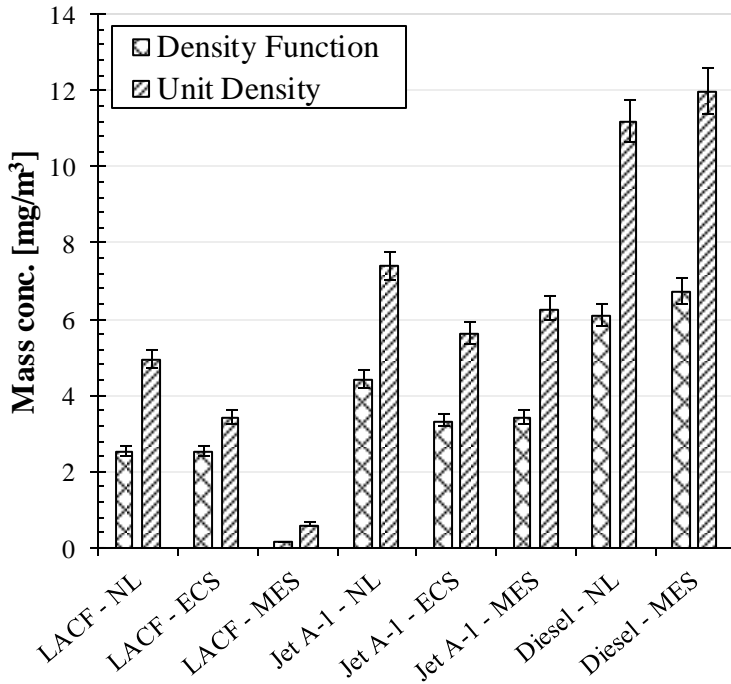


Figure 7-28: DMS 500 mass concentrations without Nafion dryer, derived from experimental density function and unit density

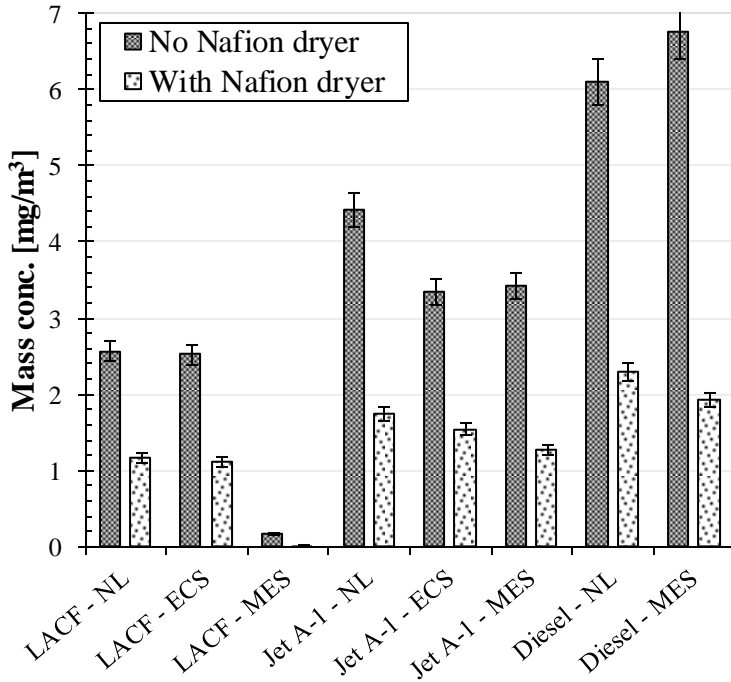


Figure 7-29: DMS 500 mass concentrations derived from experimental density function with and without Nafion dryer in place

Figure 7-30 shows that in addition to the particle losses observed in Figure 7-29, a massive particle transformation can be observed. The particle sizes are larger for the case with Nafion dryer compared to the case with no Nafion dryer in place.

This suggests that coagulation of the particles is happening inside the Nafion dryer which is similar to the observation made by Durdina et al [110].

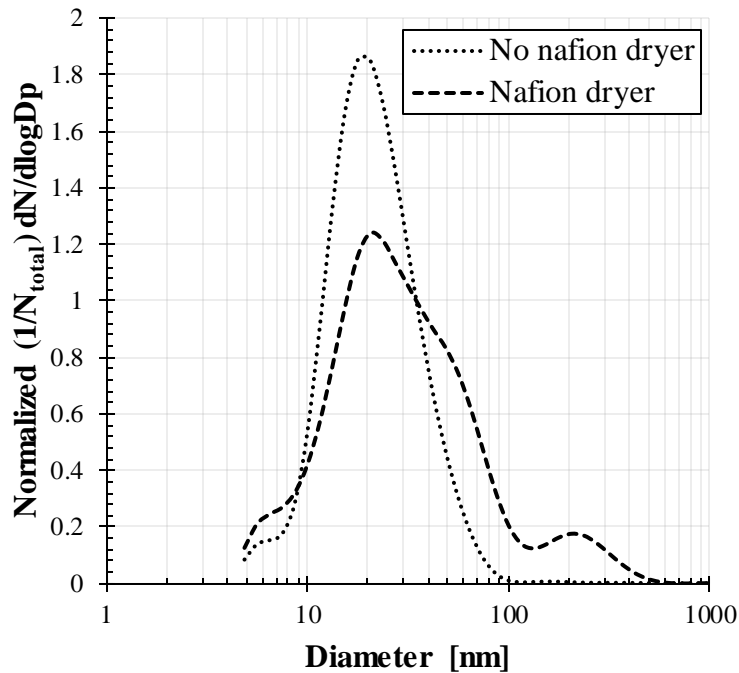


Figure 7-30: Particle size distribution of LACF at MES engine power setting with and without Nafion dryer

The other hypothesis investigated to determine the mass concentration from the DMS500 include;

1. The application of a Nafion dryer instead of dilution to reduce the vapour content of the exhaust to avoid instrument damage.
2. The assumption of unit density to particle-number size derived mass concentration.

Though good correlation is observed for the first case mentioned above, the predictability of the gravimetric measurement is observed to be poor as only 30% of the gravimetric result is predicted. The implication of this is that a portion of the particles are lost within the Nafion dryer tubes considering the difference in the mass concentration as observed in Figure 7-29. Meanwhile Figure 7-30 is an evidence of the substantial transformation the exhaust particle have undergone within inside the Nafion dryer more likely preferential loss of smaller particles. Therefore, offline corrections of the data would be required before reasonable predictability can be attained contrary to the goal this research work to establish

real-time predictability. In case 2, the DMS500 over predicts the mass concentration measured using US EPA method 5I. This observation confirms the flaw in assuming a unit density as observed in many literatures [43, 80, 93, 94].

7.6 Smoke Number Comparisons

In Figure 7-31 the concentration of black carbon in the exhaust is plotted against the corresponding smoke numbers for LACF, Jet A-1 and diesel over the NL, ECS and MES engine power settings. The uncertainty in the SN is approximately $\pm 10\%$ as determined from the three samples collected for each of the test points well within ± 3 SN accuracy. The black carbon concentrations represented in the plot are the elemental carbon measurement with the NIOSH 5040 which have both been described as referring to solid carbon deposits (see section 1.4.1) contained in the exhaust. The experimental data from this study is correlated using the power law over the range of measured smoke numbers which range from 7 to 21 while the carbon concentration range from 1.59 to $4.68\text{mg}/\text{m}^3$. The SN- C_{EC} correlation is

$$C_{BC} = 0.199(SN)^{1.03}$$

Included in Figure 7-31 are plots of black carbon concentration estimates generated using the correlations derived by Stettler et al [125] and First Order Approximation version 3 (FOA3) endorsed by ICAO [120] (see section 2.8.4). The two curves from Stettler et al [125] are: (1) the lower curve which represents the predictions of the mass concentration using the relationship developed for black carbon with a GMD of 60nm (2) the upper curve which represents the black carbon concentrations estimates using the relationship developed for gas turbine particle emission with GMD between $20 - 30\text{nm}$. The lowest curve are the black carbon estimates mass concentration from the ICAO FOA3 which have been reported to be developed using exhaust particle sizes ranging from $80 - 100\text{nm}$ [120]. The particle size range for this study is between 39 and 54nm (see Figure 7-9).

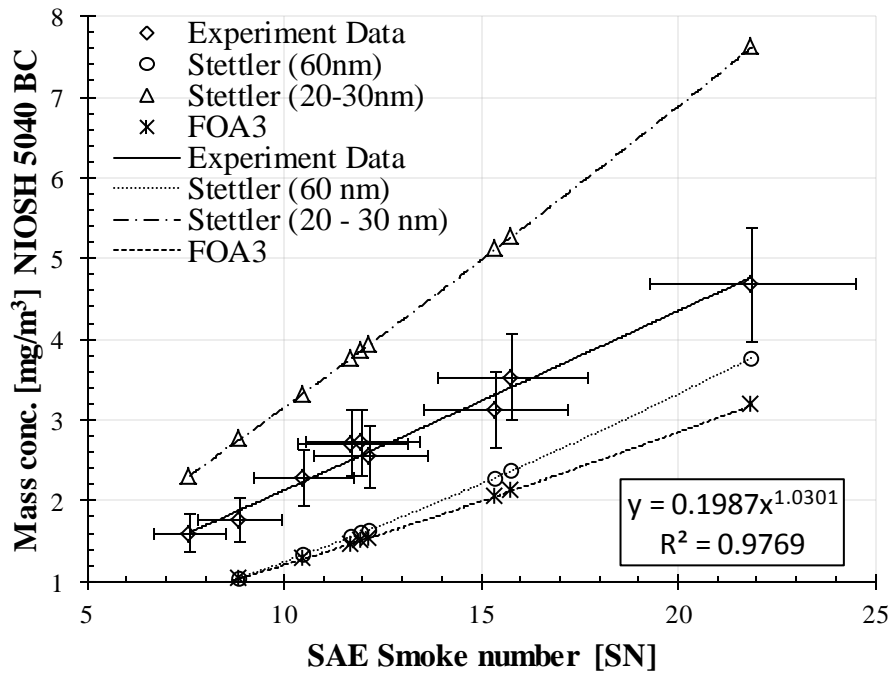


Figure 7-31: Black carbon mass concentration versus SAE Smoke number, comparing literature correlations with the data recorded in this study

For the SAE smoke number, there is a good relationship with the black carbon concentration as measured using NIOSH 5040 as shown in Figure 7-31. The interesting feature in the figure is the position of the plot compared to the black carbon concentration estimated from equations developed in previous work [120, 125]. The SN and corresponding mass concentration of this study falls between the 60 nm and 20 – 30 nm black carbon concentration estimates using equation developed by Stettler [125]. Meaning, the equation developed to estimate the black concentration based on the assumption that the turbine particle sizes are between 20 and 30 nm both under estimate and overestimate the black carbon concentration respectively. Lower estimate are recorded when the FAO3 endorsed by ICAO based on the particle sizes range 80 –100 nm [120]. With the particle mobility size for the Smoke Number of this study ranging between 39 and 54 nm, it implies that the relationship between black carbon mass concentration and SN is dependent on particle mobility diameter.

7.7 Condensable PM Data

In this section the condensable PM data as measured using method 202 is presented. Also as CPM are composed of organic and inorganic components, the THC measurement from FTIR and FID are presented and correlated with the organic components of the method 202 data. Although not all the medium molecular weight hydrocarbons that are true condensable particulate species are contained in the THC measurements. The FTIR was applied with the intention that some hydrocarbon species detectable by FTIR could be used to predict the organic and inorganic content of the particulate.

7.7.1 Method 202 Data

Figure 7-32 shows a plot of the absolute values of the total CPM, organic and inorganic components of method 202. For all the test point the organic component of the condensable are more than the inorganic concentration. In general the quality of the data is poor as the variability is very high and no discerning trend can observed with respect to changes in engine power settings. This is likely to be due to a combination of factors as this is not unexpected as described in sections 2.3.1. The high variability of measurement can be largely attributed to the organic components of the data.

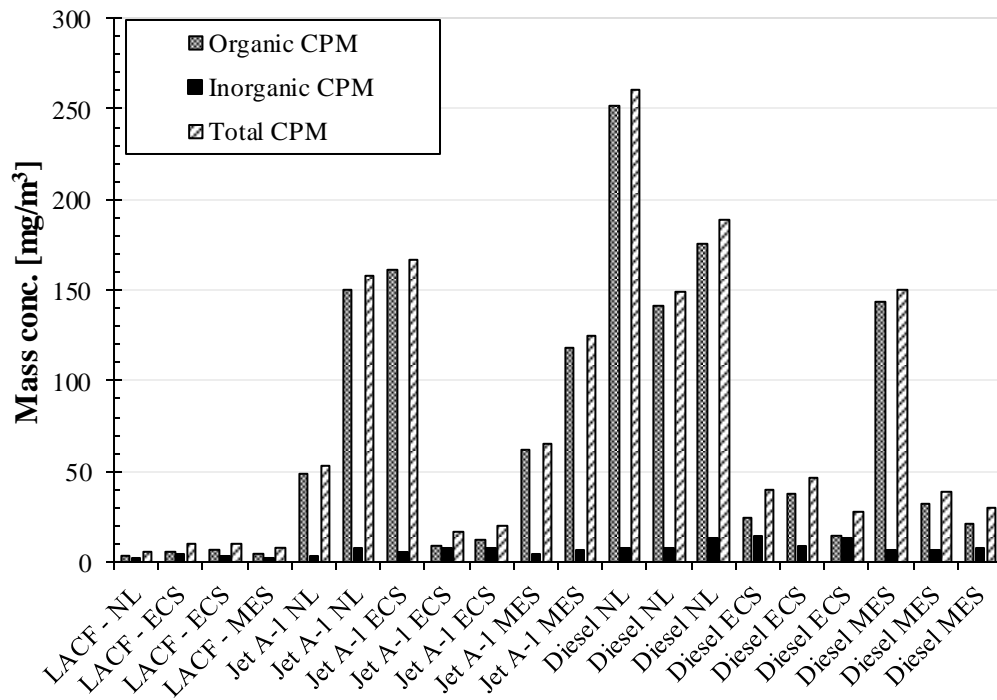


Figure 7-32: Method 202 data for Jet A-1 and diesel at the NL, ECS and MES gas turbine engine power settings.

To ensure that the sampling system has no impact on the method 202 variability, a smaller scale testing was done using a vehicle (FORD VAN) as the source of particle emission. The VAN was run at idle condition. The data as presented in Figure 7-33, shows a good repeatability despite the testing been carried out on different days.

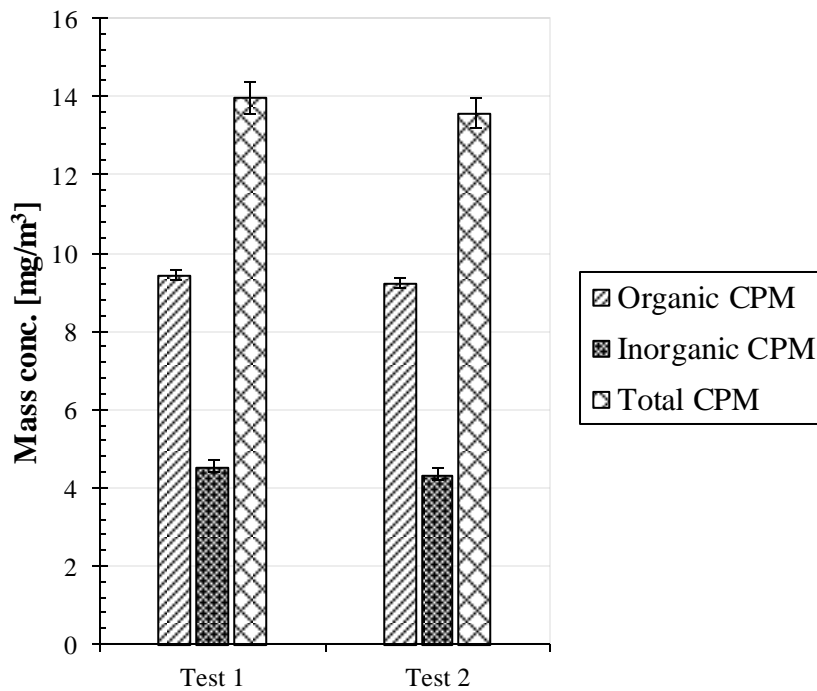


Figure 7-33: Method 202 data for the Van engine test at idle condition

7.7.2 FTIR and FID Data

Figure 7-34 present the THC measured using and the FID. The results are presented in the parts-per-million. The hydrocarbon data indicates that the FTIR THC has a similar pattern with the THC measurements of the FID. The THC is lower and highest at the NL and MES engine power setting respectively apart for the FTIR data at the ECS engine condition for Jet A-1. Despite the similar pattern the FTIR THC data for each engine power setting by a value up to 15 ppm.

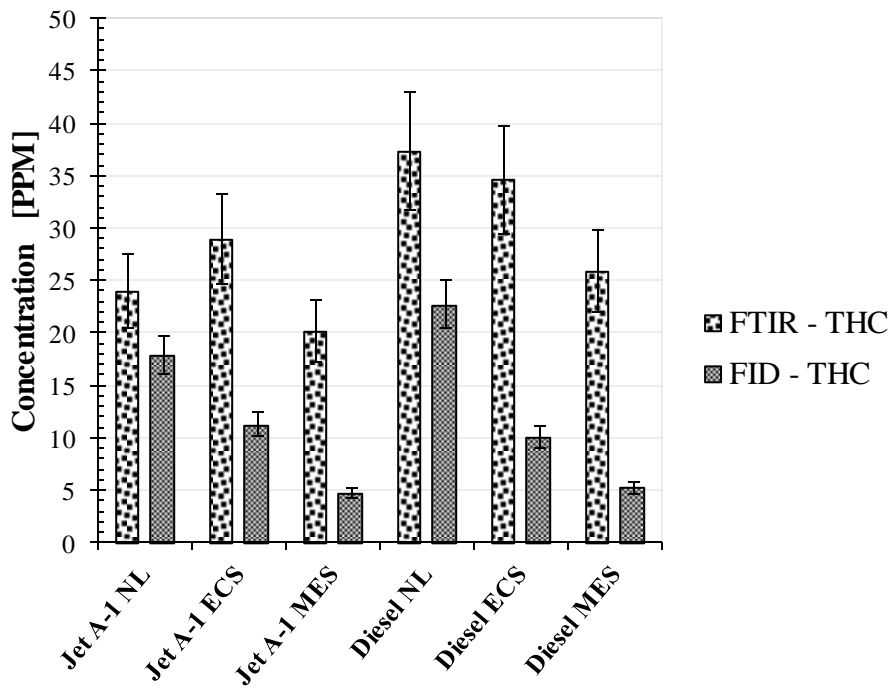


Figure 7-34: FTIR and FID THC emissions

7.7.3 Correlation between Method 202, FTIR and FID

Figure 7-35 to Figure 7-38 shows the correlation between the FTIR and FID with the corresponding fractions of method 202. First, Figure 7-35 is a plot of the inorganic gases measured with FTIR and the inorganic fraction of method 202. The FTIR inorganic gases are a summation of the ammonia and the oxides of nitrogen. The plot shows a poor correlation as the regression factor is 0.0717.

Table 7-11: Multiple linear regression analysis of the relation between Method 202 inorganic mass concentration and FTIR inorganic concentrations.

	Multiple R	R Square	Adjusted R Square	Standard Error
	0.2677	0.0717	0.0171	6.6165
	Coefficients	Standard Error	t Stat	P-value
Intercept	31.9181	3.5789	8.9183	0.0000
x	-0.5059	0.4416	-1.1457	0.2678

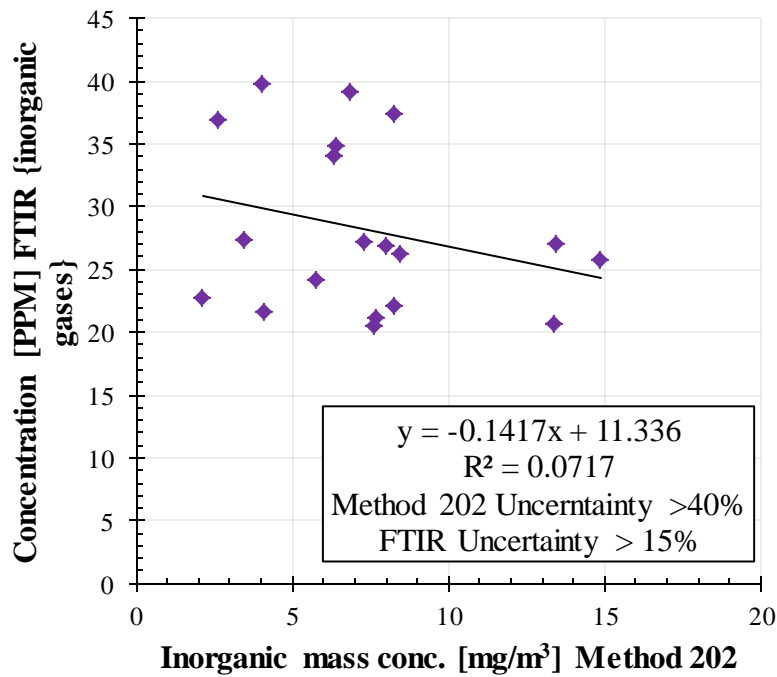


Figure 7-35: Correlation between Method 202 inorganic mass concentration and FTIR inorganic gas data

The correlation between the total hydrocarbon components as measured with FTIR and FID and carbon fraction of method 202 are presented in Figures 7-36 and 7-37. Poor agreement can generally be observed in these figures. However the FID show a better correlation ($R^2=0.36$) compared with the FTIR ($R^2=0.015$) measurement.

Table 7-12: Multiple linear regression analysis of the relation between Method 202 organic mass concentration and FTIR THC concentrations.

	Multiple R	R Square	Adjusted R Square	Standard Error
	0.1253	0.0157	-0.0390	6.4588
	Coefficients	Standard Error	t Stat	P-value
Intercept	28.9099	1.9732	14.6510	0.0000
x	0.0104	0.0194	0.5356	0.5988

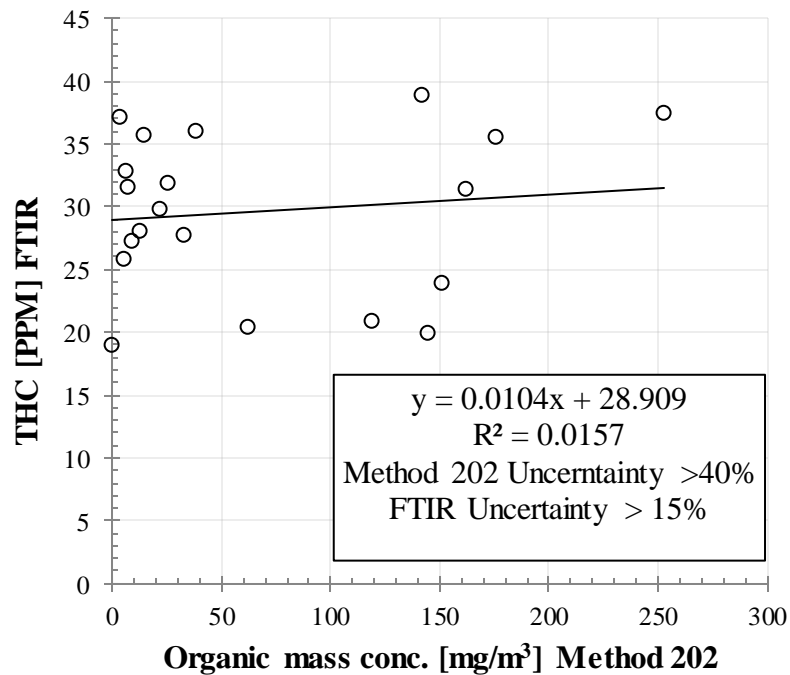


Figure 7-36: Correlation between Method 202 organic mass concentration and FTIR THC concentration

With the three engines power setting tested, it is expected as noted in chapter two and demonstrated in section 4.1.2.2 for this test engine that the hydrocarbon content changes with the engine power setting. This is also the case for the organic fractions of the condensable particulate. As a result, Figure 7-38 is a plot of the FID THC against the organic fraction of method 202. The FID results for THC show a distinct behaviour with the method 202 organic component. While the ECS test condition results in a very poor correlation the NL and MES engine power settings have reasonable correlations ($R^2 = 0.90$ and 0.87 , respectively) between THC and OC. However, constants in the linear equations are dramatically different, making it difficult to predict the total OC mass concentration based on THC from FID.

Table 7-13: Multiple linear regression analysis of the relation between Method 202 organic mass concentration and FID THC concentration.

	Multiple R	R Square	Adjusted R Square	Standard Error
	0.6022	0.3626	0.3272	5.3509
	Coefficients	Standard Error	t Stat	P-value
Intercept	7.9682	1.6791	4.7456	0.0002
x	0.0572	0.0179	3.2002	0.0050

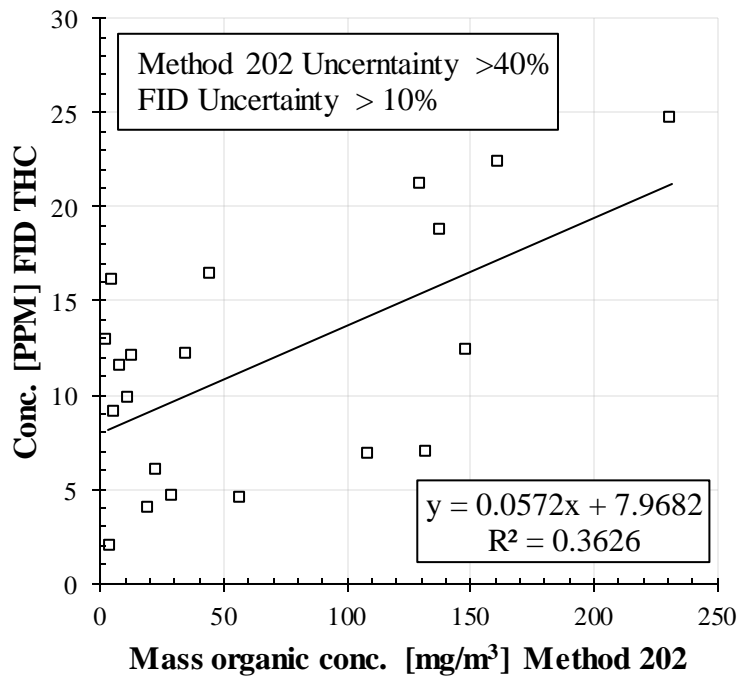


Figure 7-37: Correlation between Method 202 organic mass concentration and FID THC concentration

Table 7-14: Regression statistics of the relation between Method 202 organic mass concentration and FID organic gas emission for 3 engine power settings.

Regression Statistics		MES	ECS	NL	
Multiple R		0.9362	0.3688	0.9526	
R Square		0.8764	0.1360	0.9074	
Adjusted R Square		0.8456	-0.0368	0.8889	
Standard Error		0.7359	2.3703	1.3662	
		Coefficients	Standard Error	t Stat	P-value
MES	Intercept	2.8230	0.4835	5.8389	0.0043
	x	0.0342	0.0064	5.3267	0.0060
ECS	Intercept	9.8728	1.1195	8.8190	0.0003
	x	0.0169	0.0190	0.8871	0.4156
NL	Intercept	14.2913	0.8389	17.0352	0.0000
	x	0.0452	0.0065	7.0002	0.0009

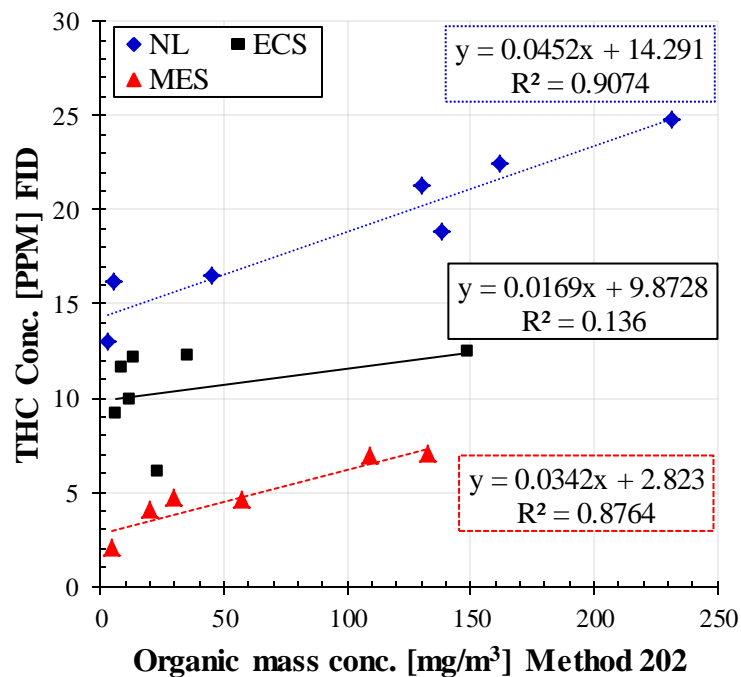


Figure 7-38: Correlation between Method 202 organic mass concentration and FID organic gas emission for 3 engine power settings

7.8 Chapter Summary

The PM instrument suite deployed for the analysis of the APU particulate matter emissions provided for the comparison of the US EPA regulatory method 5I and method 202 and also between the instruments. In summary;

- DMS500 derived mass concentration shows a very good correlation to the FPM mass concentration defined by US EPA Method 5I. DMS500 best correlates with US EPA method 5I FPM measurement of undiluted exhaust sample when a dilution factor of 60 is applied. Crucially, the conversion of the DMS500 particle size distribution measurement into mass concentration must be performed using experimentally derived effective densities.
- The correlation between SAE Smoke Number and the black carbon (BC) mass concentration depends on the particle mobility size BC emitted. The BC mass concentration predictive models established based on particle size of approximately 100 *nm* and 60 *nm* significantly underestimates the BC mass concentration for particles with sizes ranging between 38 and 50 *nm*. Likewise, there is significant over estimation using predictive models established based on particle size range of 20 *nm* - 30 *nm*.
- The FTIR did not correlate with the US EPA method 202 due to the high variability exhibited by both instrument. However, the correlation between the method 202 OC fractions and the FID THC suggest that correlations can be established. In addition, although the variability of the method 202 cannot be explained but rather guessed. However the repeatability demonstrated from the measurement CPM emissions from a FORD VAN, shows that the sampling system implemented in this study has no impact on the method 202 results.

8 Conclusions and Future Work

Increased interest in particulate matter emitted from gas turbines and the consequent progress in development of real-time PM measurement instrument are providing the need to ensure these new technologies are commensurate with the conventionally accepted gravimetric measurement protocols. Limited data however, exist on the complex relationships between these real-time instruments and the gravimetric protocol with respect to gas turbine particulates. The focus of this research was to determine the degree to which these real-time instruments correlate with the components fraction of the total PM mass, namely filterable particulate matter (FPM) and condensable particulate matter (CPM). Nevertheless, in this work some key knowledge gaps that were important to the setup and determination of the test procedure were bridged. Thus, this chapter summarises the key contribution to knowledge of this PhD and introduces recommendations for future work.

8.1 Contribution to Knowledge

A number of conclusions were reached as a result of the research. These conclusions are as follows:

- There is no single direct reading instrument available that can measure the total particle matter (FPM + CPM) as defined by the current gravimetric methods. However, there are individual instruments that can measure different components that make up PM emission. PM emission is chemically complex. A PM emission measurement strategy that requires the assembly of different instrumentation would be clumsy to implement especially as some of the chemical components are only present in traces. Thus, the best approach to develop correlations to the gravimetric reference method as shown in this thesis is to combine direct reading instruments that measure a majority of the components and those that simultaneously measure a number of traces of the component that make up the CPM.
- The sampling system as recommended in the SAE AIR 6241 is adequate for correlation study of real-time instrument with a gravimetric system

implementing both filterable particulate matter and condensable PM measurement without the need to dilute the system. Equally demonstrated is the handling of the water content section of the gravimetric kit in the sampling system as back pressures can easily cause water to flood the CPM filter and back-up impinger of the method 202 section which can lead to a repeat of experiment or skewed results.

- Aromatic species in gas turbine fuel influence the mass concentration and physical characteristics of the particle emitted but no relationship exists between their contribution towards particle production and physical property of the particle emitted. As the only aromatic present at 15% by volume in a surrogate fuel, tetralin which has a higher sooting threshold index compared to m-xylene produced significantly larger particle diameters in correspondence to the high particle mass concentration. In contrast at 8% by volume in the fuel, the particle mass concentration produced from tetralin is significantly lower than m-xylene but with larger particle diameter.
- Alternative fuels from alcohol to Jet (Fuel 4), catalytic hydrothermolysis (Fuel 7), blends of cellulose - aromatic and SPK (Fuel 6) and 50:50 blend of HEFA and Jet A-1 all show a reduced particle number emissions and size compared to the conventional Jet A-1. This can be attributed to the aromatic content and composition in the fuels. However, the 50:50 blends of HEFA and Jet A-1 which would meet current ASTM International specifications shows the lowest reduction in PM number-based emissions with a reduction of ~32% compared to the conventional Jet A-1 emissions.
- The particle size distribution of the test engine GTCP85CK series engine which is still presently in use as auxiliary power unit (APU) in aircraft agrees well with the expectations of current scientific opinion that aero gas turbine exhaust PM emission size (diameter) are less than 1000 nm in terms of number concentration.
- The effective density of individual particle sizes from the GTCP85CK engine, range between 1900 kg/m^3 and 220 kg/m^3 and generally decreased

with increasing mobility particle size. Likewise, the mass-mobility exponents range from 2.20 to 2.42 for engine depending on the fuel used. The mass-mobility exponents were similar to those obtained from diesel engines which range between 2.2 to 2.44 measured.

- The effective densities of PM with identical electrical mobility particle produced from different fuels vary. Diesel produced PM show a higher corresponding effective density for particles greater than 150 *nm* compared to Jet A-1 and LACF while the reverse can be observed for particles at the lower spectrum of the particle size distribution. The corresponding effective density for a particle with electrical mobility diameter of 30 *nm* is higher for LACF produced particle emission compared to diesel.
- This work has shown that there is no significant difference in the effective density and mobility size plot with respect to the engine operating conditions. This was evident as the combined power fit to the electrical mobility particle size and corresponding mass plot of particle emission generated from JetA-1 at the NL and ECS engine power condition shows a correlation of 0.90. The implication is that the necessary parameters (fractal dimension and prefactor) obtained for the NL engines condition and required to convert the particle size distribution measured using the DMS500 instrument are sufficient to determine the total mass per volume concentration for the particle emissions for all the engine operating conditions.
- This work has demonstrated that relationship between the black carbon mass concentration and SN is dependent on the particle mobility diameter. It has shown that the black carbon mass concentration of particle emissions with particle mobility size study ranging between 39 and 54 *nm* have a different correlation model to that proposed by Stettler [125] for 30 and 60 *nm* and that currently used in FOA3 [120].
- The research work has shown that there is a good correlation between the particle sizes derived mass concentration applying experimentally derived particle densities and the filterable particulate mass concentration measurement from a US EPA gravimetric procedure. This is achieved with

the particle sample distributed to the particle sizing instrument diluted by a factor of 60. The results are a ratio of 0.92 between the DMS500 derived mass and gravimetric mass determined for a gas turbine engine.

8.2 Future Work

Following the knowledge gained from this research there are a number of areas that require further study to advance the knowledge of gas turbine PM measurement as defined by the gravimetric procedures.

- Following the correlation between FPM fraction of the gravimetric protocol; and particle size instrument derived mass concentration using experimentally determined particle density. It would be interesting to investigate for gas turbine PM emissions, the impact of the difference of the lower temperature specification of the DMA-CPMA-CPC on derived mass concentration from particle size distribution instrument.
- Since there was no correlation between organic and inorganic fractions of Method 202 with FTIR THC and inorganic measurement as well as FID THC, it would be worthwhile repeating as in theory they should correlate. The lack of correlation between the instruments may be attributed to unexplained high variability with the Method 202. However, having certified that the Method 202 procedure as set up with the sampling system can produce repeatable results; it is suggested that experiments are performed on a combustor rig to investigate the correlation between Method 202 and FTIR or an aerosol mass spectrometer before experimenting with gas turbine particulate emissions.
- Tests with alternative liquid gas turbine fuels and gaseous fuels to develop a relationship between PM emissions density and fuel. This is important to build a correlation profile of PM emission concentration less than 2 mg/m^3 . The scope for future work around this subject should look at the testing of these fuel blends on full size engines such as an auxiliary power unit and field gas engine.
-

9 References

- [1] M. Mohr, U. Lehmann, and J. Rütter, "Comparison of mass-based and non-mass-based particle measurement systems for ultra-low emissions from automotive sources," *Environmental science & technology*, vol. 39, pp. 2229-2238, 2005.
- [2] D. Laskin, "The Great London Smog," *Weatherwise*, vol. 59, pp. 42-45, 2006/01/01 2006.
- [3] J. M. Samet, F. Dominici, F. C. Curriero, I. Coursac, and S. L. Zeger, "Fine Particulate Air Pollution and Mortality in 20 US Cities, 1987–1994," *New England journal of medicine*, vol. 343, pp. 1742-1749, 2000.
- [4] H.-E. Wichmann and A. Peters, "Epidemiological evidence of the effects of ultrafine particle exposure," *Philosophical Transactions of the Royal Society of London. Series A: Mathematical, Physical and Engineering Sciences*, vol. 358, pp. 2751-2769, 2000.
- [5] G. Polichetti, S. Cocco, A. Spinali, V. Trimarco, and A. Nunziata, "Effects of Particulate Matter (PM10, PM2.5 and PM1) on The Cardiovascular System," *Toxicology*, vol. 261, pp. 1-8, 2009.
- [6] J. De Hartog, G. Hoek, A. Peters, K. Timonen, A. Ibaldo-Mulli, B. Brunekreef, *et al.*, "Effects of Fine and Ultrafine Particles on Cardiorespiratory Symptoms in Elderly Subjects with Coronary Heart Disease The ULTRA Study," *American Journal of Epidemiology*, vol. 157, pp. 613-623, 2003.
- [7] M. C. Chang and G. C. England, "Development of Fine Particulate Emission Factors And Speciation Profiles For Oil And Gas-Fired Combustion Systems Update: Critical Review Of Source Sampling And Analysis Methodologies For Characterizing Organic Aerosol And Fine Particulate Source Emission Profiles - Final Report," American Petroleum Institute, 2004.
- [8] D. W. Dockery, "Health Effects of Particulate Air Pollution," *Annals of Epidemiology*, vol. 19, pp. 257-263, 2009.
- [9] D. W. Dockery, C. A. Pope, X. Xu, J. D. Spengler, J. H. Ware, M. E. Fay, *et al.*, "An Association between Air Pollution and Mortality in Six U.S. Cities," *New England Journal of Medicine*, vol. 329, pp. 1753-1759, 1993.

- [10] G. Oberdörster, Z. Sharp, V. Atudorei, A. Elder, R. Gelein, A. Lunts, *et al.*, "Extrapulmonary translocation of ultrafine carbon particles following whole-body inhalation exposure of rats," *Journal of Toxicology and Environmental Health Part A*, vol. 65, pp. 1531-1543, 2002.
- [11] F. J. Kelly and J. C. Fussell, "Size, source and chemical composition as determinants of toxicity attributable to ambient particulate matter," *Atmospheric Environment*, vol. 60, pp. 504-526, 12// 2012.
- [12] J. Heyder, "Deposition of Inhaled Particles in the Human Respiratory Tract and Consequences for Regional Targeting in Respiratory Drug Delivery," *Proceedings of the American Thoracic Society*, vol. 1, pp. 315-320, December 1, 2004 2004.
- [13] R. D. Brook and J. R. Brook, "A Road Forward to Improve Public Health," *Circulation*, vol. 123, pp. 1705-1708, 2011.
- [14] W. F. Rogge, L. M. Hildemann, M. A. Mazurek, G. R. Cass, and B. R. T. Simoneit, "Sources of fine organic aerosol. 4. Particulate abrasion products from leaf surfaces of urban plants," *Environmental Science & Technology*, vol. 27, pp. 2700-2711, 1993/12/01 1993.
- [15] D. A. Grantz, J. H. B. Garner, and D. W. Johnson, "Ecological Effects of Particulate Matter," *Environment International*, vol. 29, pp. 213-239, 2003.
- [16] B. Freedman, "1 - The Ecological Effects Of Pollution, Disturbance, and Other Stresses," in *Environmental Ecology (Second Edition)*, ed San Diego: Academic Press, 1995, pp. 1-10.
- [17] S. W. Lee, "Fine particulate matter measurement and international standardization for air quality and emissions from stationary sources," *Fuel*, vol. 89, pp. 874-882, 2010.
- [18] "Directive 2001/80/EC of the European Parliament and of the Council of 23 October 2001 on the limitation of emissions of certain pollutants into the air from large combustion plants " in *Official Journal of the European Union*. European Union, 2001.
- [19] "Directive 2010/75/EU of the European Parliament and of the Council of 24 November 2010 on industrial emissions (integrated pollution prevention and control)." European Union, 2010.
- [20] Environmental, Health, and Safety Guidelines for Thermal Power Plants, International Finance Corporation, 2008.

http://www.ifc.org/wps/wcm/connect/dfb6a60048855a21852cd76a6515b18/FINAL_Thermal%2BPower.pdf?MOD=AJPERES&id=1323162579734

- [21] Pollution Prevention and Abatement Handbook, WORLD BANK GROUP, 1998.
- [22] S. Webb, E. C. Group, N. R. C. T. R. Board, A. C. R. Program, and U. S. F. A. Administration, "Research Needs Associated with Particulate Emissions at Airports," Transportation Research Board, 9780309117395, 2008.
- [23] S. K. Friedlander, *Smoke, dust, and haze* vol. 198: Oxford University Press New York, 2000.
- [24] US EPA, "Air Quality Criteria for Particulate Matter Final Report," Washington, DC, , Oct 2004.
- [25] US EPA, "Method 5—Determination of Particulate Matter Emissions From Stationary Sources," 1996.
- [26] US EPA, "Method 17 - Determination of Particulate Matter Emissions From Stationary Sources," 1996.
- [27] US EPA, "Determination of Low Level Particulate Matter Emissions," *Method 5I*, 1999.
- [28] US EPA, "Dry impinger method for determining condensable particulate emissions from stationary sources," *Method 202*, 2010.
- [29] W. C. Hinds, *Aerosol technology: properties, behavior, and measurement of airborne particles*: Wiley, 1999.
- [30] D. B. Kittelson, "Engines and nanoparticles: a review," *Journal of Aerosol Science*, vol. 29, pp. 575-588, 1998.
- [31] D. Kittelson, T. Hands, C. Nicoklaus, N. Collings, V. Niemelä, and M. Twigg, "Mass Correlation of Engine Emissions with Spectral Instruments (2)."
- [32] K. T. Whitby, "The physical characteristics of sulfur aerosols," *Atmospheric Environment (1967)*, vol. 12, pp. 135-159, 1978.

- [33] J. B. Edwards, *Combustion: the formation and emission of trace species*: Ann Arbor Science Publishers, 1974.
- [34] Cambustion, "Engineer Training, DMS500 - Fast response particulate analyzer," *Power Point Presentation*, 2012.
- [35] H. Bockhorn, *Soot Formation in Combustion: Mechanisms and Models*: Springer London, Limited, 2011.
- [36] A. H. Lefebvre and D. R. Ballal, *Gas Turbine Combustion: Alternative Fuels and Emissions*: Taylor & Francis Group, 2010.
- [37] H. F. Calcote and D. M. Manos, "Effect of molecular structure on incipient soot formation," *Combustion and Flame*, vol. 49, pp. 289-304, 1983.
- [38] C. S. McEnally and L. D. Pfefferle, "Improved sooting tendency measurements for aromatic hydrocarbons and their implications for naphthalene formation pathways," *Combustion and Flame*, vol. 148, pp. 210-222, 3// 2007.
- [39] M. L. Botero, S. Mosbach, J. Akroyd, and M. Kraft, "Sooting tendency of surrogates for the aromatic fractions of diesel and gasoline in a wick-fed diffusion flame," *Fuel*, vol. 153, pp. 31-39, 8/1/ 2015.
- [40] L. A. Corio and J. Sherwell, "In-stack condensible particulate matter measurements and issues," *Journal of the Air & Waste Management Association*, vol. 50, pp. 207-218, 2000.
- [41] M. T. Timko, Z. Yu, T. B. Onasch, H. W. Wong, R. C. Miake-Lye, A. J. Beyersdorf, *et al.*, "Particulate Emissions of Gas Turbine Engine Combustion of a Fischer–Tropsch Synthetic Fuel," *Energy & Fuels*, vol. 24, pp. 5883-5896, 2010/11/18 2010.
- [42] R. L. Vander Wal, V. M. Bryg, and C.-H. Huang, "Insights into the combustion chemistry within a gas-turbine driven auxiliary power unit as a function of fuel type and power level using soot nanostructure as a tracer," *Fuel*, vol. 115, pp. 282-287, 1// 2014.
- [43] J. S. Kinsey, M. T. Timko, S. C. Herndon, E. C. Wood, Z. Yu, R. C. Miake-Lye, *et al.*, "Determination of the emissions from an aircraft auxiliary power unit (APU) during the Alternative Aviation Fuel Experiment (AAFEX)," *Journal of the Air & Waste Management Association*, vol. 62, pp. 420-430, 2012/04/01 2012.

- [44] E. Corporan, M. J. DeWitt, V. Belovich, R. Pawlik, A. C. Lynch, J. R. Gord, *et al.*, "Emissions Characteristics of a Turbine Engine and Research Combustor Burning a Fischer–Tropsch Jet Fuel," *Energy & Fuels*, vol. 21, pp. 2615-2626, 2007/09/01 2007.
- [45] A. Crayford, M. Johnson, R. Marsh, Y. Sevcenco, D. Walters, P. Williams, *et al.*, "SAMPLE III: Contribution to aircraft engine PM certification requirement and standard," *Second Specific Contract–Final Report for research project EASA*, 2010.
- [46] R. Marsh, A. Petzold, M. Johnson, M. Miller, Y. Sevcenco, D. Delhaye, *et al.*, "Study on sampling and measurement of aircraft particulate emissions SAMPLE – Final Report," Institute of Atmospheric Physics, DLR Oberpfaffenhofen, 82234 Wessling, Germany, EASA.2008.OP.13, October 2009.
- [47] US EPA, "Determination of PM₁₀ and PM_{2.5} emissions from stationary sources (constant sampling rate procedure)," *Method 201A*, 2010.
- [48] BSI, "Gas turbines - Exhaust gas emission - Part 1: Measurement and evaluation," *BS ISO 11042-1:1996*, 1996.
- [49] J. C. Chow, "Measurement methods to determine compliance with ambient air quality standards for suspended particles," *Journal of the Air & Waste Management Association*, vol. 45, pp. 320-382, 1995.
- [50] AIR QUALITY EXPERT GROUP, "Fine Particulate Matter (PM_{2.5}) in the United Kingdom," 2012.
- [51] P. H. McMurry, K. S. Woo, R. Weber, D.-R. Chen, and D. Y. Pui, "Size distributions of 3–10 nm atmospheric particles: Implications for nucleation mechanisms," *Philosophical Transactions of the Royal Society of London. Series A: Mathematical, Physical and Engineering Sciences*, vol. 358, pp. 2625-2642, 2000.
- [52] B. J. Turpin, J. J. Huntzicker, and S. V. Hering, "Investigation of organic aerosol sampling artifacts in the Los Angeles basin," *Atmospheric Environment*, vol. 28, pp. 3061-3071, 1994.
- [53] M. Katz and C. Chan, "Comparative distribution of eight polycyclic aromatic hydrocarbons in airborne particulates collected by conventional high-volume sampling and by size fractionation," *Environmental Science & Technology*, vol. 14, pp. 838-843, 1980.

- [54] H. Wang and W. John, "Characteristics of the Berner impactor for sampling inorganic ions," *Aerosol Science and Technology*, vol. 8, pp. 157-172, 1988.
- [55] M. D. McDannel, "*Measurement of Condensable Particulate Matter: A Review of Alternatives to EPA Method 202*," EPRI, Palo Alto, CA, TR-111327, 30-Sep-1998, 1998.
- [56] J. Richards, T. Holder, and D. Goshaw, "Optimized method 202 sampling train to minimize the biases associated with method 202 measurement of condensable particulate matter emissions," in *Air & Waste Management Association Hazardous Waste Combustion Specialty Conference. St. Louis, Missouri*, 2005.
- [57] P. Batchelor, "Functional Requirements - Real Time Particulate Matter (PM) Measurement Method," GTES11165 8th March 2014.
- [58] M. M. Maricq and H. Maldonado, "Directions for Combustion Engine Aerosol Measurement in the 21st Century," *Journal of the Air & Waste Management Association*, vol. 60, pp. 1165-1176, 2010/10/01 2010.
- [59] N. E. Carbon, "Method 5040," in *NIOSH Manual of Analytical Methods*, 1999.
- [60] J. M. Jaklevic, R. C. Gatti, F. S. Goulding, and B. W. Loo, "A .beta.-gauge method applied to aerosol samples," *Environmental Science & Technology*, vol. 15, pp. 680-686, 1981/06/01 1981.
- [61] C. Lu and A. W. Czanderna, *Applications of Piezoelectric Quartz Crystal Microbalances*: Elsevier Science, 1984.
- [62] H. Patashnick and E. G. Rupprecht, "Continuous PM-10 Measurements Using the Tapered Element Oscillating Microbalance," *Journal of the Air & Waste Management Association*, vol. 41, pp. 1079-1083, 1991/08/01 1991.
- [63] A. Charron, R. M. Harrison, S. Moorcroft, and J. Booker, "Quantitative interpretation of divergence between PM10 and PM2.5 mass measurement by TEOM and gravimetric (Partisol) instruments," *Atmospheric Environment*, vol. 38, pp. 415-423, 2004.
- [64] H. Hauck, A. Berner, B. Gomiscek, S. Stopper, H. Puxbaum, M. Kundi, *et al.*, "On the equivalence of gravimetric PM data with TEOM and beta-attenuation measurements," *Journal of Aerosol Science*, vol. 35, pp. 1135-1149, 2004.

- [65] Centre for Atmospheric Chemistry. (2012, 10 March 2016). *DIFFERENTIAL MOBILITY ANALYZER*. Available: <http://www.cac.yorku.ca/differential-mobility-analyzer/>
- [66] (10 March 2016). *Measurement Methods II. How to detect, collect and analyse aerosol particles*. Available: <http://fy.chalmers.se/OLDUSERS/molnar/lectures/Measurement%20Methods%20II.htm>
- [67] P. Kulkarni, P. A. Baron, and K. Willeke, *Aerosol Measurement*. US: John Wiley & Sons Inc, 2011.
- [68] W. J. Glantschnig and S.-H. Chen, "Light scattering from water droplets in the geometrical optics approximation," *Applied Optics*, vol. 20, pp. 2499-2509, 1981.
- [69] J. Agarwal and L. Fingerson, "Real-time aerodynamic particle size measurement with a laser velocimeter," *TSI Quarterly*, vol. 1, 1979.
- [70] T. M. Peters and D. Leith, "Concentration measurement and counting efficiency of the aerodynamic particle sizer 3321," *Journal of Aerosol Science*, vol. 34, pp. 627-634, 2003.
- [71] GRIMM, GRIMM Mini Wide Range Aerosol Spectrometer Mini - WRAS 1.371, Manual.
- [72] BSI, "Determination of particle size distribution — Differential electrical mobility analysis for aerosol particles," *BS ISO 15900:2009*, 2009.
- [73] BSI, "Aerosol particle number concentration — Calibration of condensation particle counters," *BS ISO 27891:2015*, 2015.
- [74] B. Y. Liu and D. Y. Pui, "A submicron aerosol standard and the primary, absolute calibration of the condensation nuclei counter," *Journal of Colloid and Interface Science*, vol. 47, pp. 155-171, 1974.
- [75] L. Rye, P. Lobo, P. I. Williams, I. Uryga-Bugajska, S. Christie, C. Wilson, *et al.*, "Inadequacy of Optical Smoke Measurements for Characterization of Non-Light Absorbing Particulate Matter Emissions from Gas Turbine Engines," *Combustion Science and Technology*, vol. 184, pp. 2068-2083, 2012/12/01 2012.
- [76] W. F. Northrop, S. V. Bohac, J.-Y. Chin, and D. N. Assanis, "Comparison of filter smoke number and elemental carbon mass from partially premixed low temperature combustion in a direct-injection

- diesel engine," *Journal of engineering for gas turbines and power*, vol. 133, p. 102804, 2011.
- [77] A. Hansen, H. Rosen, and T. Novakov, "The aethalometer—an instrument for the real-time measurement of optical absorption by aerosol particles," *Science of the Total Environment*, vol. 36, pp. 191-196, 1984.
- [78] A. Petzold and M. Schönlinner, "Multi-angle absorption photometry—a new method for the measurement of aerosol light absorption and atmospheric black carbon," *Journal of Aerosol Science*, vol. 35, pp. 421-441, 2004.
- [79] A. Petzold, H. Schloesser, P. J. Sheridan, W. P. Arnott, J. A. Ogren, and A. Virkkula, "Evaluation of multiangle absorption photometry for measuring aerosol light absorption," *Aerosol Science and Technology*, vol. 39, pp. 40-51, 2005.
- [80] A. Petzold, R. Marsh, M. Johnson, M. Miller, Y. Sevcenco, D. Delhaye, *et al.*, "Evaluation of Methods for Measuring Particulate Matter Emissions from Gas Turbines," *Environmental Science & Technology*, vol. 45, pp. 3562-3568, 2011/04/15 2011.
- [81] "Aircraft Gas Turbine Engine Exhaust Smoke Measurement " *SAE ARP1179D* 2011.
- [82] International Civil Aviation Organisation, "Environmental Protection Volume II — Aircraft Engine Emissions," *Annex 16*, 2008.
- [83] D. R. Snelling, G. J. Smallwood, R. A. Sawchuk, W. S. Neill, D. Gareau, W. L. Chippior, *et al.*, "Particulate Matter Measurements in a Diesel Engine Exhaust by Laser-Induced Incandescence and the Standard Gravimetric Procedure," *SAE Technical Paper*, vol. 01-3653, 1999.
- [84] F. Liu, D. R. Snelling, K. A. Thomson, and G. J. Smallwood, "Sensitivity and relative error analyses of soot temperature and volume fraction determined by two-color LII," *Applied Physics B*, vol. 96, pp. 623-636, 2009/09/01 2009.
- [85] F. A. Miller and C. H. Wilkins, "Infrared Spectra and Characteristic Frequencies of Inorganic Ions," *Analytical Chemistry*, vol. 24, pp. 1253-1294, 1952/08/01 1952.
- [86] M. R. Canagaratna, J. T. Jayne, J. L. Jimenez, J. D. Allan, M. R. Alfarra, Q. Zhang, *et al.*, "Chemical and microphysical characterization of ambient aerosols with the aerodyne aerosol mass spectrometer," *Mass Spectrometry Reviews*, vol. 26, pp. 185-222, 2007.

- [87] Y. A. Sevcenco, A. P. Crayford, R. Marsh, P. J. Bowen, M. N. Miller, and M. P. Johnson, "Evaluation of a Particulate Sampling Methodology From a Gas Turbine Exhaust Using Real-Time Size and Number Analysis at Simulated Aircraft Conditions," in *ASME Turbo Expo 2010: Power for Land, Sea, and Air*, Glasgow, UK, 2010, pp. 1113-1124.
- [88] H. Burtscher, "Physical characterization of particulate emissions from diesel engines: a review," *Journal of Aerosol Science*, vol. 36, pp. 896-932, 2005.
- [89] B. E. Anderson, A. J. Beyersdorf, C. H. Hudgins, J. V. Plant, K. L. Thornhill, E. L. Winstead, *et al.*, "Alternative Aviation Fuel Experiment (AAFEX)," NASA/TM-2011-217059, 2011.
- [90] Perma Pure LLC. Available: <http://www.permapure.com/products/gas-sample-dryers/pd-gas-dryers/>
- [91] A. Johansson, "DMS500 Dilution/Naifon Dryer," *Personal Communication*, 31/03/2014 2014.
- [92] G. Smallwood, K. Thomson, and D. Clavel, "Assessment Of Real-Time Instruments For Gravimetric Equivalent Measurement of PM – Phase I," MSS-BCM-2012-001, July 2012, 2012.
- [93] J. S. Kinsey, Y. Dong, D. C. Williams, and R. Logan, "Physical characterization of the fine particle emissions from commercial aircraft engines during the Aircraft Particle Emissions eXperiment (APEX) 1–3," *Atmospheric Environment*, vol. 44, pp. 2147-2156, 2010.
- [94] P. Lobo, D. E. Hagen, and P. D. Whitefield, "Comparison of PM Emissions from a Commercial Jet Engine Burning Conventional, Biomass, and Fischer–Tropsch Fuels," *Environmental Science & Technology*, vol. 45, pp. 10744-10749, 2011/12/15 2011.
- [95] D. Hagen, P. Whitefield, J. Paladino, M. Trueblood, and H. Lilenfeld, "Particulate sizing and emission indices for a jet engine exhaust sampled at cruise," *Geophysical Research Letters*, vol. 25, pp. 1681-1684, 1998.
- [96] E. Corporan, A. Quick, and M. J. DeWitt, "Characterization of Particulate Matter and Gaseous Emissions of a C-130H Aircraft," *Journal of the Air & Waste Management Association*, vol. 58, pp. 474-483, 2008/04/01 2008.
- [97] P. H. McMurry, X. Wang, K. Park, and K. Ehara, "The Relationship between Mass and Mobility for Atmospheric Particles: A New Technique

- for Measuring Particle Density," *Aerosol Science and Technology*, vol. 36, pp. 227-238, 2002/01/01 2002.
- [98] W. Kelly and P. McMurry, "Measurement of Particle Density by Inertial Classification of Differential Mobility Analyzer–Generated Monodisperse Aerosols," *Aerosol Science and Technology*, vol. 17, pp. 199-212, 1992.
- [99] Y. Zhu, W. C. Hinds, S. Kim, and C. Sioutas, "Concentration and size distribution of ultrafine particles near a major highway," *Journal of the Air & Waste Management Association*, vol. 52, pp. 1032-1042, 2002.
- [100] P. F. DeCarlo, J. G. Slowik, D. R. Worsnop, P. Davidovits, and J. L. Jimenez, "Particle Morphology and Density Characterization by Combined Mobility and Aerodynamic Diameter Measurements. Part 1: Theory," *Aerosol Science and Technology*, vol. 38, pp. 1185-1205, 2004/01/01 2004.
- [101] J. P. Symonds, K. S. J. Reavell, J. S. Olfert, B. W. Campbell, and S. J. Swift, "Diesel soot mass calculation in real-time with a differential mobility spectrometer," *Journal of Aerosol Science*, vol. 38, pp. 52-68, 2007.
- [102] Y. Li, J. Xue, K. Johnson, T. Durbin, M. Villela, L. Pham, *et al.*, "Determination of Suspended Exhaust PM Mass for Light-Duty Vehicles," *SAE Technical Paper*, vol. 2014-01-1594, 2014.
- [103] X. Li-Jones, P. F. Penko, S. Williams, and C. Moses, "Gaseous and Particle Emissions in the Exhaust of a T700 Helicopter Engine," in *ASME Turbo Expo 2007: Power for Land, Sea, and Air*, 2007, pp. 395-411.
- [104] T. B. Onasch, J. T. Jayne, S. Herndon, D. R. Worsnop, R. C. Mlake-Lye, I. P. Mortimer, *et al.*, "Chemical Properties of Aircraft Engine Particulate Exhaust Emissions," *Journal of Propulsion and Power*, vol. 25, pp. 1121-1137, 2009/09/01 2009.
- [105] K. Ehara, C. Hagwood, and K. J. Coakley, "Novel method to classify aerosol particles according to their mass-to-charge ratio—aerosol particle mass analyser," *Journal of Aerosol Science*, vol. 27, pp. 217-234, 1996.
- [106] J. S. Olfert and N. Collings, "New method for particle mass classification—the Couette centrifugal particle mass analyzer," *Journal of Aerosol Science*, vol. 36, pp. 1338-1352, 11// 2005.

- [107] L. Durdina, B. T. Brem, M. Abegglen, P. Lobo, T. Rindlisbacher, K. A. Thomson, *et al.*, "Determination of PM mass emissions from an aircraft turbine engine using particle effective density," *Atmospheric Environment*, vol. 99, pp. 500-507, 12// 2014.
- [108] T. J. Johnson, J. S. Olfert, J. P. R. Symonds, M. Johnson, T. Rindlisbacher, J. J. Swanson, *et al.*, "Effective Density and Mass-Mobility Exponent of Aircraft Turbine Particulate Matter," *Journal of Propulsion and Power*, vol. 31, pp. 573-582, 2015/03/01 2015.
- [109] M. Abegglen, L. Durdina, B. T. Brem, J. Wang, T. Rindlisbacher, J. C. Corbin, *et al.*, "Effective density and mass–mobility exponents of particulate matter in aircraft turbine exhaust: Dependence on engine thrust and particle size," *Journal of Aerosol Science*, vol. 88, pp. 135-147, 10// 2015.
- [110] L. Durdina, B. Brem, M. Abegglen, P. Lobo, T. Rindlisbacher, K. Thomson, *et al.*, "Determination of PM mass emissions from an aircraft turbine engine using particle effective density," *Atmospheric Environment*, vol. 99, pp. 500-507, 2014.
- [111] T. J. Johnson, J. S. Olfert, J. P. Symonds, M. Johnson, T. Rindlisbacher, J. J. Swanson, *et al.*, "Effective density and mass-mobility exponent of aircraft turbine particulate matter," *Journal of Propulsion and Power*, vol. 31, pp. 573-582, 2015.
- [112] M. Abegglen, L. Durdina, B. Brem, J. Wang, T. Rindlisbacher, J. Corbin, *et al.*, "Effective density and mass–mobility exponents of particulate matter in aircraft turbine exhaust: Dependence on engine thrust and particle size," *Journal of Aerosol Science*, vol. 88, pp. 135-147, 2015.
- [113] K. Park, D. B. Kittelson, and P. H. McMurry, "A closure study of aerosol mass concentration measurements: comparison of values obtained with filters and by direct measurements of mass distributions," *Atmospheric Environment*, vol. 37, pp. 1223-1230, 2003.
- [114] Z. Liu, J. Swanson, D. B. Kittelson, and D. Y. Pui, "Comparison of methods for online measurement of diesel particulate matter," *Environmental science & technology*, vol. 46, pp. 6127-6133, 2012.
- [115] C. D. Cappa, D. A. Lack, J. B. Burkholder, and A. Ravishankara, "Bias in filter-based aerosol light absorption measurements due to organic aerosol loading: Evidence from laboratory measurements," *Aerosol Science and Technology*, vol. 42, pp. 1022-1032, 2008.

- [116] D. L. Champagne, "Standard measurement of aircraft gas turbine engine exhaust smoke," in *ASME 1971 International Gas Turbine Conference and Products Show*, 1971, pp. V001T01A088-V001T01A088.
- [117] J. Stockham and H. Betz, "Study of visible exhaust smoke from aircraft jet engines," DTIC Document, 1971.
- [118] S. Girling, C. Hurley, J. Mitchell, and A. Nichols, "Development and characterization of a smoke generator for the calibration of aerosol emissions from gas turbine engines," *Aerosol science and technology*, vol. 13, pp. 8-19, 1990.
- [119] International Civil Aviation Organization, "Airport Air Quality Guidance Manual," *Doc 9889*, 2011.
- [120] R. L. Wayson, G. G. Fleming, and R. Iovinelli, "Methodology to estimate particulate matter emissions from certified commercial aircraft engines," *Journal of the Air & Waste Management Association*, vol. 59, pp. 91-100, 2009.
- [121] G. Ratliff, C. Sequeira, I. Waitz, M. Ohsfeldt, T. Thrasher, M. Graham, *et al.*, "Aircraft Impacts on Local and Regional Air Quality in the United States," *PARTNER Project*, vol. 15, 2009.
- [122] S. Arunachalam, B. Wang, N. Davis, B. H. Baek, and J. I. Levy, "Effect of chemistry-transport model scale and resolution on population exposure to PM 2.5 from aircraft emissions during landing and takeoff," *Atmospheric environment*, vol. 45, pp. 3294-3300, 2011.
- [123] J. I. Levy, M. Woody, B. H. Baek, U. Shankar, and S. Arunachalam, "Current and Future Particulate - Matter - Related Mortality Risks in the United States from Aviation Emissions During Landing and Takeoff," *Risk Analysis*, vol. 32, pp. 237-249, 2012.
- [124] M. Woody, B. H. Baek, Z. Adelman, M. Omary, Y. F. Lam, J. J. West, *et al.*, "An assessment of Aviation's contribution to current and future fine particulate matter in the United States," *Atmospheric environment*, vol. 45, pp. 3424-3433, 2011.
- [125] M. E. J. Stettler, J. J. Swanson, S. R. H. Barrett, and A. M. Boies, "Updated Correlation Between Aircraft Smoke Number and Black Carbon Concentration," *Aerosol Science and Technology*, vol. 47, pp. 1205-1214, 2013/11/01 2013.

- [126] J. S. Kinsey, *Characterization of emissions from commercial aircraft engines during the Aircraft Particle Emissions eXperiment (APEX) 1 to 3*: Office of Research and Development, US Environmental Protection Agency, 2009.
- [127] P. F. DeCarlo, J. R. Kimmel, A. Trimborn, M. J. Northway, J. T. Jayne, A. C. Aiken, *et al.*, "Field-deployable, high-resolution, time-of-flight aerosol mass spectrometer," *Analytical chemistry*, vol. 78, pp. 8281-8289, 2006.
- [128] P. Lobo, S. Christie, B. Khandelwal, S. G. Blakey, and D. W. Raper, "Evaluation of Non-volatile Particulate Matter Emission Characteristics of an Aircraft Auxiliary Power Unit with Varying Alternative Jet Fuel Blend Ratios," *Energy & Fuels*, 2015/10/16 2015.
- [129] J. Heland and K. Schäfer, "Determination of major combustion products in aircraft exhausts by FTIR emission spectroscopy," *Atmospheric Environment*, vol. 32, pp. 3067-3072, 9/1/ 1998.
- [130] B. Khandelwal, E. Ubogu, M. Akram, S. Blakey, and C. W. Wilson, "Experimental analysis on emission production and performance of stressed 100% SPK, stressed Fully Formulated Synthetic Jet Fuel and Jet A-1 in a small gas turbine engine," in *Proceedings of the 11th International Energy Conversion Engineering Conference, San Jose, CA, USA*, 2013, pp. 14-17.
- [131] "Procedure for the Continuous Sampling and Measurement of Non-Volatile Particle Emissions from Aircraft Turbine Engines," *SAE AIR6241*, 2013.
- [132] APEX INSTRUMENTS INC, "Isokinetic Source Sampler (500-Series Models) - Opearator's Manual," 2008.
- [133] J. Reimann, S. A. Kuhlmann, and S. Will, "2D aggregate sizing by combining laser-induced incandescence (LII) and elastic light scattering (ELS)," *Applied Physics B*, vol. 96, pp. 583-592, 2009/09/01 2009.
- [134] Artium Technologies Inc, "LII 300 User Manual," 2011.
- [135] T. C. Lieuwen and Vigor Yang, *Gas Turbine Emissions*: Cambridge University Press, 2013.
- [136] "Introduction to Fourier Transform Infrared Spectrometry," Thermo Nicolet, 2001.

- [137] L. J. Rye, "The Influence of Alternative Fuel Composition on Gas Turbine Combustion Performance," Mechanical Engineering Sheffield, 2012.
- [138] "Procedure for the Continuous Sampling and Measurement of Gaseous Emissions from Aircraft Turbine Engines," *SAE ARP1256D*, 2011.
- [139] R Burrows and L Rye, " "Audit Procedures for Gas Analysis Instruments, R/120643-11-1," University of Sheffield, 2010.."
- [140] "Procedure for the Analysis and Evaluation of Gaseous Emissions from Aircraft Engines," *SAE ARP1533B*, 2013.
- [141] D. W. Boone, W. I. Shoup, and D. G. Furst, "Exhaust Emissions Test - Airesearch Aircraft Propulsion and Auxiliary Power Gas Turbine Engines," Airesearch Manufacturing Company of Arizona, GT- 8747 R, 1971.
- [142] Prem Lobo, Philip D. Whitefield, Donald E. Hagen, Lucas J. Rye, Simon Blakey, Christopher W. Wilson, *et al.*, "*SAE E31 Methodology Development and Associated PM Emissions Characteristics of Aircraft APUs burning Conventional and Alternative Aviation Fuels*," Partnership for AiR Transportation Noise and Emissions Reduction An FAA/NASA/Transport Canadasponsored Center of Excellence, PARTNER-COE-2011-005, July 2011.
- [143] J. S. Kinsey, M. T. Timko, S. C. Herndon, E. C. Wood, Z. Yu, R. C. Miake-Lye, *et al.*, "Determination of the Emissions from an Aircraft Auxiliary Power Unit (APU) during the Alternative Aviation Fuels EXperiment (AAFEX)," 2011.
- [144] "Automotive Fuels-Diesel Requirements and Test Methods," *EN 590*, 2009.
- [145] R. P. Howard, K. M. Stephens, P. D. Whitefield, D. E. Hagen, S. L. Achterberg, E. A. Black, *et al.*, "Interim Particulate Matter Test Method for the Determination of Particulate Matter from Gas Turbine Engines," DTIC Document, 2011.
- [146] ASTM International, "Standard Specification for Aviation Turbine Fuel Containing Synthesized Hydrocarbons," *ASTM D7566*, 2015.
- [147] FAA Continuous Lower Energy - Emissions and Noise (CLEEN) Technologies Program, "Rolls-Royce Alternative Fuels Program – Laboratory Test of Candidate Fuels," FAA Report Number: DOT/FAA/AEE/2015-03, 2015.

- [148] D. M. Carrier and R. J. Wetton, *Prediction of combustion performance of aviation kerosines using a novel premixed flame technique* vol. 110. New York, N, ETATS-UNIS: American Society of Mechanical Engineers, 1988.
- [149] L. Rye, "Premixed Burner Instructions," 2010.
- [150] E. Alborzi, S. Blakey, T. Keane, and A. Meijer, "Construction of a Reduced Chemical Kinetic Mechanism for Petroleum Diesel Autoxidation," Low Carbon Combustion Centre, University of Sheffield.
- [151] T. Davies, "The relationship between aromatics and soot formation and the selection of aromatics for novel aviation fuels," M Eng, Mechanical Engineering, University of Sheffield, 2015.
- [152] Artium Technologies Inc, "LII 300 Brochure."
- [153] S. Martin, G. Kraaij, T. Ascher, P. Baltzopoulou, G. Karagiannakis, D. Wails, *et al.*, "Direct steam reforming of diesel and diesel–biodiesel blends for distributed hydrogen generation," *International Journal of Hydrogen Energy*, vol. 40, pp. 75-84, 1/5/ 2015.
- [154] S. Roy and B. Khandelwal, "Comparison of Gaseous Emissions between Jet A-1 and Severely Hydro-Processed Jet Fuel from Conventional sources," in *13th International Energy Conversion Engineering Conference*, ed: American Institute of Aeronautics and Astronautics, 2015.
- [155] K. Park, D. B. Kittelson, and P. H. McMurry, "Structural Properties of Diesel Exhaust Particles Measured by Transmission Electron Microscopy (TEM): Relationships to Particle Mass and Mobility," *Aerosol Science and Technology*, vol. 38, pp. 881-889, 2004/09/01 2004.
- [156] "General requirements for the competence of testing and calibration laboratories," *BS EN ISO/IEC 17025:2005*, 2005.
- [157] "Ambient air quality. Guide for the measurement of elemental carbon (EC) and organic carbon (OC) deposited on filters," *PD CEN/TR 16243:2011*, 2011.

Appendix A: Analysers Interference analysis

Analyser performance specifications (ARP1256C)

Criteria	Limit
Zero Drift	Less than $\pm 1\%$ of full scale in 1 hr
Span Drift	Less than $\pm 1\%$ of full scale in 1 hr
Noise	Less than $\pm 1\%$ of full scale
Linearity	Within $\pm 1\%$ of full scale

Measured interference factors

Effect	Analyser	Value	ARP Limit	Units
CO ₂ on CO (L)	NDIR (CO)	-5.67E-6	-0.0002	Mole CO/mole CO ₂
H ₂ O on CO (M)	NDIR (CO)	0	-0.00002	Mole CO/mole H ₂ O
O ₂ on CO ₂ (J)	NDIR (CO ₂)	0.1850	0.1	% reading/%O ₂
CO ₂ on NO (L)	CLD (NO)	0.0572	0.05	% reading/%CO
H ₂ O on NO (M)	CLD (NO)	0.1145	0.1	% reading/%H ₂ O
Converter eff. (n)	CLD (NO _x)	95.19	>95	%

Analyser linearity (R2) and noise (% full scale)

Analyser	Gas	Linearity (R2)	Noise (%f.s)
Binos 1000 (NDIR)	CO	0.9999	0.041
	CO ₂	0.9999	0.124
Signal 3000 (FID)	UHC	1	1.249
Eco Physical (CLA)	NO	0.9999	0.005
	NO _x	0.9999	0.467
ADC (MAG)	O ₂	0.9999	0.305

Analysers drift (% full scale)

Analyser	Gas	Zero (% f.s)	Span (% f.s)
Binos 1000 (NDIR)	CO	0.402	0.547
	CO ₂	0.331	0.622
Signal 3000 (FID)	UHC	-	-
Eco Physical (CLA)	NO	0.099	1.779
	NO _x	0.197	1.671
ADC (MAG)	O ₂	0.957	1.311

Appendix B: Full details of Engine Gaseous Emission concentration

Jet A-1 Results

<i>AFR (wet)</i>	<i>Neff (%)</i>	<i>CO2 (%)</i>	<i>CO (ppm)</i>	<i>O2 (%)</i>	<i>THC (ppmC)</i>	<i>NO (ppm)</i>	<i>NO2 (ppm)</i>	<i>NOx (ppm)</i>
Data Points for Condition 1								
129.0	98.7	1.6	273.0	18.4	74.9	10.3	8.6	18.9
129.7	98.8	1.6	265.0	18.4	71.6	11.1	7.9	19.0
130.2	98.8	1.6	263.0	18.4	69.7	10.8	8.1	18.9
130.4	98.8	1.6	260.0	18.4	69.2	11.2	7.8	19.1
130.7	98.8	1.6	259.0	18.4	68.7	11.3	7.8	19.1
Data Points for Condition 2								
74.1	99.5	2.7	308.0	16.7	0.0	14.5	19.0	33.4
74.1	99.5	2.7	309.0	16.7	0.0	14.7	18.7	33.4
74.3	99.5	2.7	309.0	16.7	0.0	14.9	18.5	33.4
74.5	99.5	2.7	309.0	16.7	0.0	14.3	18.8	33.1
74.6	99.5	2.7	308.0	16.7	0.0	14.6	18.9	33.4
Data Points for Condition 3								
54.0	99.7	3.7	262.0	15.2	0.0	12.7	33.8	46.6
53.9	99.7	3.8	262.0	15.2	-0.0	13.1	33.5	46.5
54.1	99.7	3.7	261.0	15.2	0.0	13.4	33.2	46.7
54.0	99.7	3.8	263.0	15.2	0.0	13.3	33.1	46.4
54.1	99.7	3.7	264.0	15.2	0.0	12.9	33.3	46.1

Emission Index

<i>AFR (wet)</i>	<i>CO2</i>	<i>CO</i>	<i>THC</i>	<i>NO</i>	<i>NOx</i>
Data Points for Condition 1					
129.0	3172.0	34.8	4.7	1.8	4.0
129.7	3174.0	33.9	4.6	1.7	4.0
130.2	3175.0	33.8	4.5	1.7	4.0
130.4	3176.0	33.4	4.4	1.6	4.0
130.7	3176.0	33.4	4.4	1.6	4.0
Data Points for Condition 2					
74.1	3170.0	22.6	0.0	2.3	4.0
74.1	3170.0	22.7	0.0	2.2	4.0
74.3	3170.0	22.8	0.0	2.2	4.0
74.5	3170.0	22.8	0.0	2.3	4.0
74.6	3170.0	22.8	0.0	2.3	4.1
Data Points for Condition 3					
54.0	3171.0	14.1	0.0	3.0	4.1
53.9	3170.0	14.1	0.0	3.0	4.1
54.1	3171.0	14.1	0.0	3.0	4.1
54.0	3170.0	14.2	0.0	2.9	4.1
54.1	3170.0	14.2	0.0	3.0	4.1

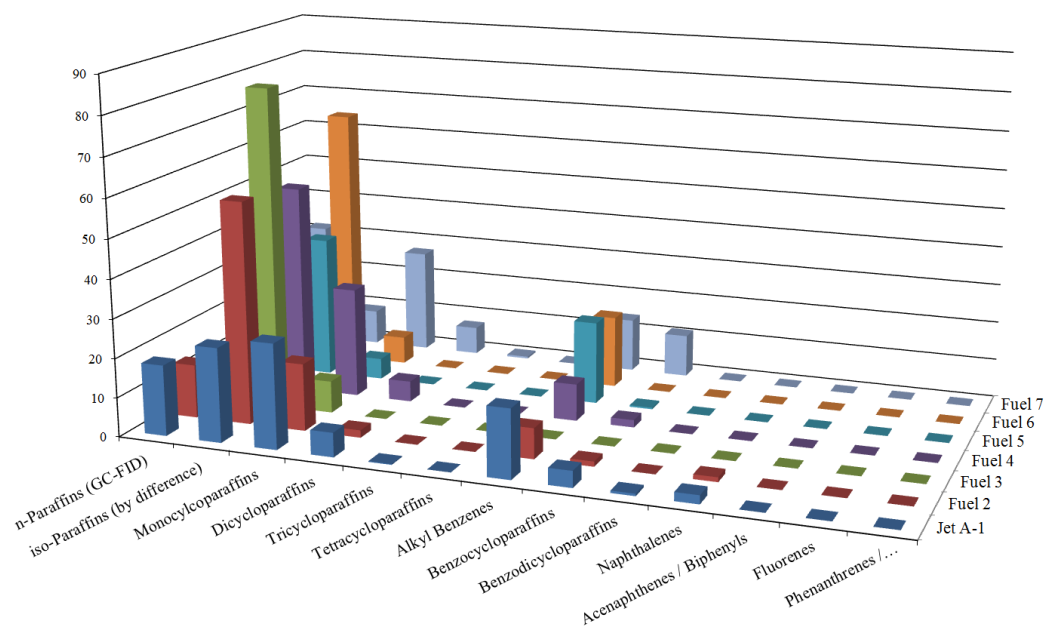
Diesel Results

<i>AFR</i> (wet)	<i>Neff</i> (%)	<i>CO2</i> (%)	<i>CO</i> (ppm)	<i>O2</i> (%)	<i>THC</i> (ppmC)	<i>NO</i> (ppm)	<i>NO2</i> (ppm)	<i>NOx</i> (ppm)
Data Points for Condition 1 (Idle Cold)								
122.2	98.7	1.7	318.0	18.2	74.4	8.6	10.8	19.4
123.0	98.7	1.7	310.0	18.3	71.3	9.4	10.0	19.3
123.7	98.7	1.6	305.0	18.3	70.9	9.4	10.0	19.4
123.8	98.7	1.6	304.0	18.3	72.5	9.9	9.5	19.5
123.9	98.7	1.6	304.0	18.3	72.9	10.0	9.4	19.4
Data Points for Condition 2								
71.5	99.4	2.8	373.0	16.5	3.0	12.7	21.3	34.0
71.7	99.4	2.8	374.0	16.5	3.0	13.1	20.9	34.0
71.7	99.4	2.8	375.0	16.5	3.0	13.6	20.3	33.9
71.8	99.4	2.8	376.0	16.5	3.0	12.8	21.2	33.9
71.9	99.4	2.8	377.0	16.5	3.0	12.6	21.2	33.9
Data Points for Condition 3								
51.2	99.6	3.9	337.0	14.9	0.0	13.2	35.5	48.7
51.4	99.6	3.9	340.0	14.9	0.0	13.4	35.0	48.4
51.4	99.6	3.9	338.0	14.9	0.0	13.8	34.7	48.5
51.6	99.6	3.9	339.0	14.9	-0.0	13.4	35.0	48.4
51.7	99.6	3.9	338.0	14.9	-0.0	13.7	34.8	48.5

Emission Index

<i>AFR</i> (wet)	<i>CO2</i>	<i>CO</i>	<i>THC</i>	<i>NO</i>	<i>NOx</i>
Data Points for Condition 1 (Idle Cold)					
122.2	3163.0	38.4	4.5	2.1	3.8
123.0	3165.0	37.6	4.3	2.0	3.9
123.7	3166.0	37.2	4.3	2.0	3.9
123.8	3166.0	37.2	4.4	1.9	3.9
123.9	3166.0	37.1	4.4	1.9	3.9
Data Points for Condition 2					
71.5	3162.0	26.4	0.1	2.5	4.0
71.7	3162.0	26.6	0.1	2.5	4.0
71.7	3162.0	26.7	0.1	2.4	4.0
71.8	3162.0	26.8	0.1	2.5	4.0
71.9	3162.0	26.9	0.1	2.5	4.0
Data Points for Condition 3					
51.2	3164.0	17.2	0.0	3.0	4.1
51.4	3164.0	17.4	0.0	3.0	4.1
51.4	3164.0	17.3	0.0	2.9	4.1
51.6	3164.0	17.5	0.0	3.0	4.1
51.7	3164.0	17.4	0.0	2.9	4.1

Appendix C: Speciation Analysis of Main Hydrocarbon Types



Appendix D: Method 202 Sample Processing Flow Chart

